Connecting Cellular Redox State and Community Behavior in *Pseudomonas aeruginosa* PA14

Chinweike Okegbe

Submitted in partial fulfillment of the

requirements for the degree of

Doctor of Philosophy

in the Graduate School of Arts and Sciences

COLUMBIA UNIVERSITY

2016

ABSTRACT

Connecting Cellular Redox State and Community Behavior

in *Pseudomonas aeruginosa* PA14

Chinweike Okegbe

Redox chemistry is the basis for biological energy generation and anabolism. Redox conditions also serve as critical cues that modulate the development of many organisms. Roles for redox chemistry in the control of gene expression have been well characterized in multicellular eukaryotes, where oxygen availability in particular is a major developmental cue. As a gaseous metabolic substrate, oxygen becomes limiting as cellular communities grow, and can act as an indicator of aggregate size or developmental stage. In many of these cases, there are dedicated sensory and signal transduction networks that link oxygen and other redox signals to changes in gene expression and morphogenesis.

The opportunistic pathogen *Pseudomonas aeruginosa,* like many species of microbes, forms multicellular structures called biofilms. Cells in biofilms can assume physiological states that differ from cells grown in well-mixed, homogeneous liquid cultures. They often exhibit increased resistance to environmental stresses and antibiotics, rendering biofilm physiology an important focus in the study of microbial pathogens. Biofilm development and architecture are tuned by environmental conditions. In turn, growth and survival in the community, and the specific structure of that community, give rise to internal microenvironments that are experienced by cells within a biofilm. Mechanisms that tune biofilm developmental programs in response to redox conditions are not well understood. This is due to challenges presented by most popular laboratory models of biofilm formation, which are not amenable to perturbation, characterization at the microscale, or high-throughput screening or analysis.

In this thesis, I describe a standardized colony morphology assay for the study of *P. aeruginosa* PA14 biofilm development and use this model to address fundamental questions about the relationships between electron acceptor availability, biofilm cell physiology, and the regulation of biofilm morphogenesis. In the colony morphology assay, PA14 grows as ~1cm-diameter biofilms on agar-solidified media under controlled conditions, and displays a developmental pattern that is predictably influenced by changes in redox conditions. Microscale heterogeneity in chemical ecology can be profiled using microelectrodes, and the effects of specific mutations on development can be rigorously tested through high-throughput screening and the application of metabolic assays directly to biofilm samples. Prior to the work described here, application of the colony morphology assay had revealed that endogenous redox-active antibiotics called phenazines influence PA14 biofilm development such that defects in phenazine production promote colony wrinkling and the formation of a distinct wrinkle pattern. As phenazines can act as alternate electron acceptors for cellular metabolism, this provided an early clue to the role of redox conditions in determining biofilm architecture.

The introduction to this thesis (**Chapter 1**) provides an overview of observations in *P. aeruginosa* and other microbes, drawing parallels between the physiology of colony biofilm development across phylogeny and highlighting specific preliminary studies that hint at redox-sensing mechanisms and signaling pathways that drive community morphogenesis. The associated **Appendix A** examines the effects of CORM-2, a synthetic compound that releases the respiratory poison carbon monoxide, on *P. aeruginosa* biofilm development. The inhibitory effects of CORM-2 are ameliorated by reducing agents and increased availability of electron donors for *P. aeruginosa* metabolism.

Chapter 2 describes the foundational characterization of the *P. aeruginosa* PA14 colony morphology assay model, which showed that colony wrinkling is invoked under high intracellular NADH levels and electron acceptor-limiting conditions, suggesting that it is an adaptive strategy to increase access to electron acceptor. The associated **Appendices B and**

C describe (i) a mathematical modeling approach demonstrating that wrinkle geometry is indeed optimized for efficient access to electron acceptors, and (ii) a study investigating the effects of phenazine antibiotics on the multicellular development of a eukaryotic microbe.

Chapter 3 details the identification and characterization of a candidate mediator of the multicellular response to electron acceptor availability in PA14 called RmcA. RmcA contains domains that have been implicated in redox-sensitive developmental control in eukaryotic systems and domains that modulate intracellular levels of cyclic di-GMP (c-di-GMP). C-di-GMP is an important secondary messenger that controls social behaviors, including the secretion of factors required for colony biofilm structure formation, in diverse bacteria. RmcA thus bridges the gap between sensing of redox signals and colony morphogenesis. **Appendix D** outlines my approaches to purification and attempts to crystallize this and one other protein contributing to PA14 redox-driven colony morphogenesis. Finally, **Appendix E** describes the role of another protein that modulates c-di-GMP in response to metabolite-dependent signaling and physiological effects during interactions between *P. aeruginosa* and the fungus *C. albicans*. Together, the findings presented in this thesis have expanded our knowledge about the role that redox chemistry plays in biofilm development.

TABLE OF CONTENTS

FIGURES

TABLES

ACKNOWLEDGEMENTS

In 2010, I began my time as a PhD candidate. Over the past six years, I completed the research presented in this dissertation. This work could not have been accomplished without the help of many entities.

First and foremost I would like to thank God for the strength to carry on with the various demands of graduate school and to keep pushing through the many good and difficult times.

A heartfelt thank you to my advisor, Dr. Lars Dietrich. Thank you for taking a chance on the naive kid “fresh out of college” and allowing me to join your lab from its beginning. It has been a tremendous privilege to grow under your tutelage and I’m grateful your support and guidance through both the ups and downs of graduate school.

Thank you to Dr. David Recinos, Dr. Matthew Sekedat and Dr. Hassan Sakhtah, who were my first lab mates and helped get the Dietrich Lab up and running in the Fall of 2010. I enjoyed the early days setting up all the new equipment as they arrived as well the numerous conversations and drinks we shared.

Thank you to my wonderful colleagues over the years. To Dr. Alexa Price-Whelan, Dr. Diana Morales, Jeanyoung Jo, Yu-cheng Lin, Anastasia Benderbury, William Cole and Lisa Khal, thank you for providing genuine camaraderie and thoughtful discussions along the way.

Thank you to all my excellent undergraduate research assistants particularly Blanche Fields and Zwoisy Mears-Clarke. I consider myself extremely fortunate to have worked with you. Many thanks for all the laughs as well. It certainly kept the things going smoothly.

A big Thank you to Victor Wong, Dr. Chi Wang, Dr. Farhad Forouhar and Dr. Tristan Coady for your immense help with ALL my biochemistry questions. You made me comfortable learning techniques I had no experience with and were always there to assist me with troubleshooting equipment and protocols.

Thank you to my thesis committee members, Dr. John Hunt, and Dr. Carol Prives, for the constructive feedback and intellectual support through out my PhD. To my defense committee, thank you in advance for your consideration and mercy.

Thank you to the admin staff of the Fairchild 500 and 600 offices as well as the Dean's office, particularly Sarah Kim, Jaya Santosh, Adelia Gulliver-Niles, Al Rodriguez, Thomas Tarduongo, Harold Ansah and Rebecca Hirade. Your help in processing lab orders, class registration, reimbursements and stipends cannot be overstated.

Thank you to custodians Leo and David for your company and conversations during my several late night "shifts" in the lab

Thank you to the HHMI Gilliam Fellowship for Advanced Graduate Study for funding me throughout the duration of PhD.

Finally, thank you to my dear parents, siblings and friends too numerous to mention. You definitely had no idea what I was up to whenever I said "I'm going to work" but you have provided me with unwavering support through the years and you all serve as a constant source of motivation.

DEDICATION

I dedicate this thesis to my brother and best friend Oladapo “Mr. Dapson” Atitebi. You were a major reason I accepted my offer from Columbia because I knew that our friendship and bond would be a great support and anchor especially with moving to the “big city”. My first few years living in New York were smooth because of you and this helped A LOT with settling into my graduate school work. I wish you could be here to see me complete the journey just as you saw me start it. I cannot thank you enough for your support.

CHAPTER 1

Introduction and Background

This chapter is adapted from two review articles that I co-wrote:

1. Okegbe C, Sakhtah H, Sekedat MD, Price-Whelan A, Dietrich LEP:

Redox eustress: roles for redox-active metabolites in bacterial signaling and behavior.

Antioxidants & Redox Signaling 2012, 16:658–667.

2. Okegbe C, Price-Whelan A, Dietrich LEP:

Redox-driven regulation of microbial community morphogenesis.

Current Opinion in Microbiology 2014, 18:39–45.

In this introduction, I integrate elements from each review that are relevant to the studies described in my thesis. I have also elaborated on some topics addressed in the reviews to provide additional context for my thesis work.

1-1 REDOX CHEMISTRY IN BACTERIAL PHYSIOLOGY AND BEHAVIOR

As the energy that fuels life is derived from electron transfer reactions, redox chemistry is a fundamental feature of every known metabolism that supports life. Strong reductants and oxidants are thought to have enabled the origin of life and the evolution of complex life forms, respectively (Fig. 1-1). While the energy provided by redox chemistry is required for life, unchecked redox activity and changes in electron availability alter the intracellular redox state and are a common source of intracellular damage. Organisms have therefore evolved well-studied mechanisms that allow them to cope with, avoid or combat potentially destructive fluctuations in redox potential that can compromise protein function and the stability of nucleic acids and lipids. In characterizing these mechanisms, researchers in many fields have traditionally focused on the high metabolic activity or exposure to strong oxidants that can generate toxic, enzyme-damaging species [1,2]. However, biologists are uncovering cases where organisms utilize unusually redox-active compounds for functions such as signaling and survival, which are not directly part of metabolism during active growth. They are also finding that compounds that are often viewed as toxins due to their high level of redox activity in some cells play roles that facilitate communication and/or survival in others, and that their effects may vary qualitatively as a function of concentration. These findings emphasize the context- and organism-dependent effects of compounds that participate in redox chemistry *in vivo*.

Traditionally, certain redox-active compounds have been categorized as “stressors” because they stimulate protective responses, without which organisms of interest would not be able to survive in the molecule’s presence. The term “stressor” originated with the work of Hans Selye, a physiologist who, in the late 1930s, devised the concept of the “stress response” during his work examining recovery from harsh treatments in rats [3]. This work established a paradigm increasingly applied by biologists describing responses to environmental stimuli. Although Selye recognized that the response to a stressor can be positive (“eustress”) or negative

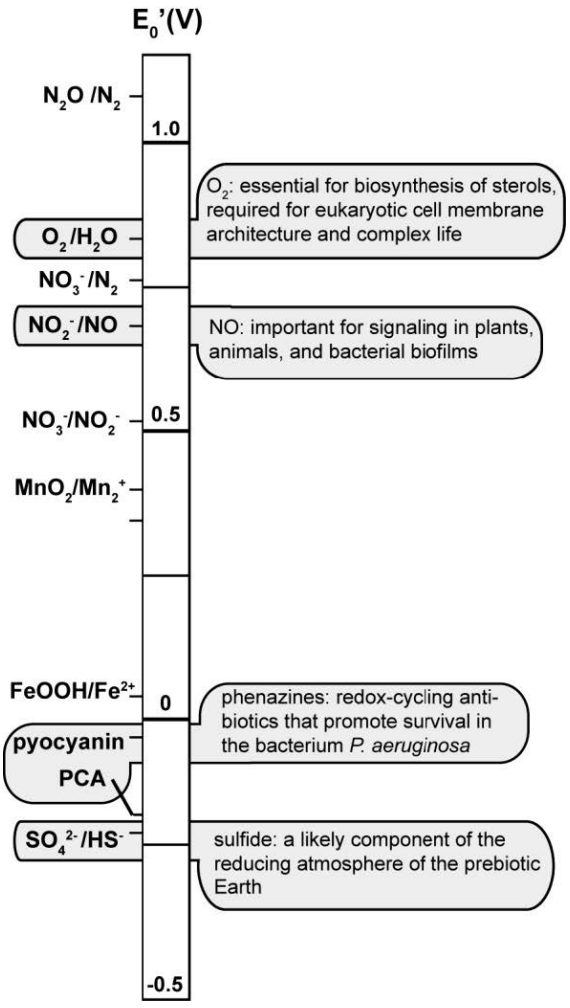

Figure 1-1. Redox chemistry is essential for life. Selected redox couples with major roles in biological chemistry are shown organized according to their redox potentials. Major events and responses associated with these couples are listed. Source: Okegbe *et al Antioxidants & Redox Signaling., 2012*

("distress"), this dual nature of stress is often overlooked [4]. The word "stress" typically has a negative connotation, and agents that induce pathology in a particular biological context are often treated categorically as negative stressors. However, the mechanisms that have evolved to respond to these signals do not always bear the hallmarks of "distress". In these cases, the organism is not negatively affected by exposure to the stressor.

Stress has been defined as a "threat to homeostasis" [5]. This definition was originally applied in the context of animal physiology and psychology, but can also apply to responses to stimuli in bacteria. An abstract representation of this concept is depicted in Fig. 1-2. An organism maintaining homeostasis, with respect to parameters such as metabolic flux and internal pH, is depicted as a ball sitting on a plateau. When the organism is exposed to a stressor that causes

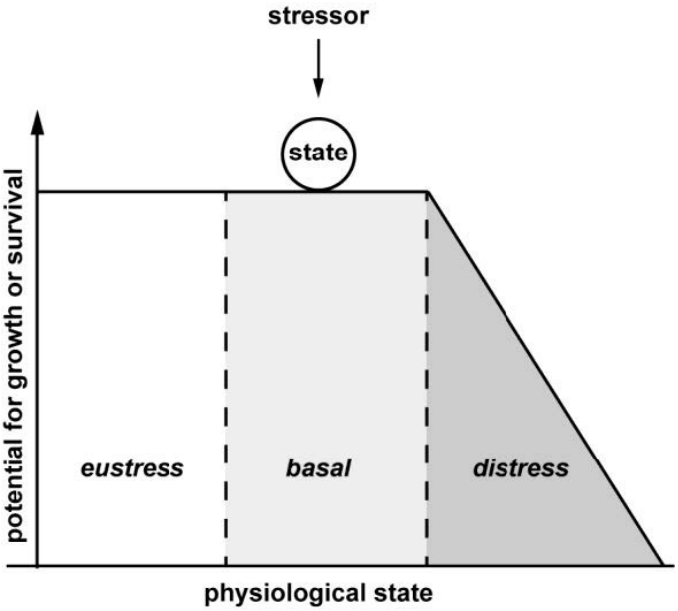

Figure 1-2. The influence of stressors on physiology. The normal functional state of a biological system can be likened to a ball on a plateau. Endogenous and exogenous stressors can push the ball to the edge of the precipice, but biological systems are robust and actively maintain the functional state. This sometimes requires the organism to transition to a new, qualitatively different functional state, as can occur when the stressor is a source of eustress. Source: Okegbe *et al Antioxidants & Redox Signaling., 2012*

distress, it can no longer maintain a functional physiological state, and this is represented as the ball rolling down the slope. However, when the organism is exposed to a stressor that causes eustress, it enters a qualitatively different physiological state, but still maintains homeostasis. This is represented as a different area atop the same hill.

There are several examples of sensing mechanisms and stimuli involved in eustress in the form of bacterial survival and development. These examples concern molecules that are typically referred to as “redox-active metabolites.” This is a misleading term, because most of the compounds produced during metabolism are technically “redox-active” in the sense that they readily undergo enzyme-mediated redox transformations within the cell, but the majority of these are unlikely to cause stress. Despite this, biologists use this term for compounds that are unusually reactive and therefore more likely to cause damage in the form of irreversible reactions that inactivate enzymes or the generation of additional reactive species. Some of these molecules are also called “redox-cycling compounds” because they enter the cell in a relatively harmless state, but are readily reduced by endogenous enzymes and catalyze downstream reactions producing highly-reactive toxic species (Fig. 1-3). These downstream reactions are oxidizing and regenerate the original compound, which can again react with the

endogenous enzyme and continuously cycle between reductant and oxidant. I will adhere to convention and refer to unusually redox-active metabolites as simply “redox-active” or “redox-cycling” compounds, as their high level of redox activity is what distinguishes them from the myriad redox couples present within the cell. However, although these terms carry negative connotations, our use of them does not imply that these compounds are universal sources of distress. In specific contexts, their effects on bacterial physiology are neutral or beneficial. They can transition the organism to a physiological state that is different from the default, but still conducive to survival and community development (Fig. 1-2).

1-2 MICROBIAL MULTICELLULARITY

Most bacteria are able to aggregate into multicellular communities called biofilms [6-9]. The formation of biofilms is an active process that involves the coordinated action of billions of bacterial cells encased in excreted matrices. This mode of growth is a strategy that is employed by bacteria to ward off challenging environmental stimuli such as nutrient depletion or the presence of antibiotics, detergents, or other potentially harmful environmental insults [10,11]. Although the mechanisms that govern biofilm formation can differ between species and even between strains of the same species, it seems to be an adaptation common to most bacterial species for surviving in hostile environments .

Biofilms can form on any type of surface and under diverse conditions in the laboratory and in the wild. This ability poses a huge clinical concern due to biofilm formation in the host during various infections (e.g., in lungs, burn wounds, or urinary tracts and on teeth or skin) [12-15] or on equipment and medical devices such as catheters and implantations [16-19]. In the wild, biofilms tend to consist of multiple microbial species and may represent a strategy to compete for scarce resources. Still, there are instances where biofilms are beneficial and confer advantages to the host organism– biofilms of *Actinobacteria* on the backs of ants provide protection from fungal and protozoan pathogens [20], while *P. chlororaphis* biofilms on roots protect plants from invaders [21].

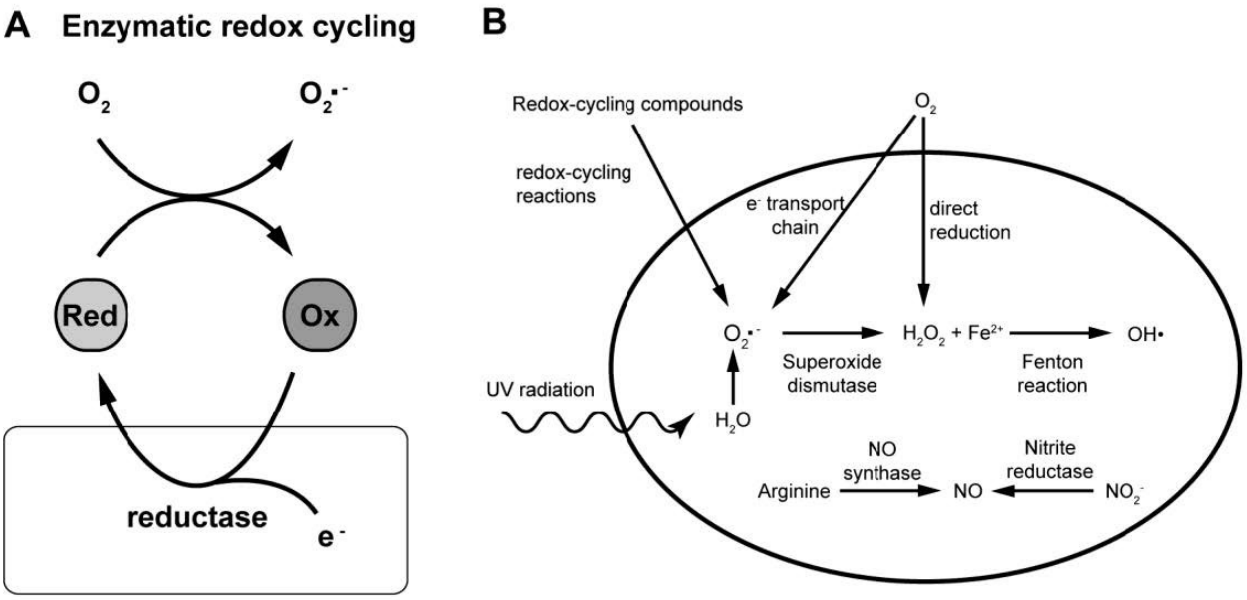

Figure 1-3. (A,B) The distinction between "redox-active" and "redox-cycling" metabolites. The term "redox-active metabolite" typically refers to compounds that do not participate constructively in primary metabolism during growth. These compounds react with metabolites, nucleic acids, proteins, and/or lipids without the aid of enzymes. The term "redox-cycling metabolite" is used to describe compounds that enter the cell in an oxidized state, participate in enzyme-mediated redox transformations to become reduced, then react with other substrates without the aid of enzymes. Source: Okegbe *et al Antioxidants & Redox Signaling., 2012*

Biofilms have complex architectures and chemical compositions. In static cultures, biofilms grow at air-gel interfaces, forming colonies, or at air-liquid interfaces, forming pellicles [22]. Probably as long as these culture techniques have been in use, microbiologists have marveled at the elaborate morphologies, visible to the naked eye, that are often formed by such communities [23]. The wrinkled structures of rugose colonies and pellicles have strikingly similar appearances in phylogenetically disparate organisms. Wrinkle-forming organisms that have become models for the study of biofilm morphogenesis include representatives from the genera *Bacillus* [24-28], *Candida* [29,30], *Escherichia* [31,32], *Pseudomonas* [33-38], *Rhodospirillum* [39], Saccharomyces [40-42], *Salmonella* [43], *Serratia* [44] *Vibrio* [45-48] and members of the phylum *Actinobacteria* [49,50] (Fig. 1-4). Regardless of species, the defining feature of a biofilm is the self-produced matrix, which is composed of polysaccharides,

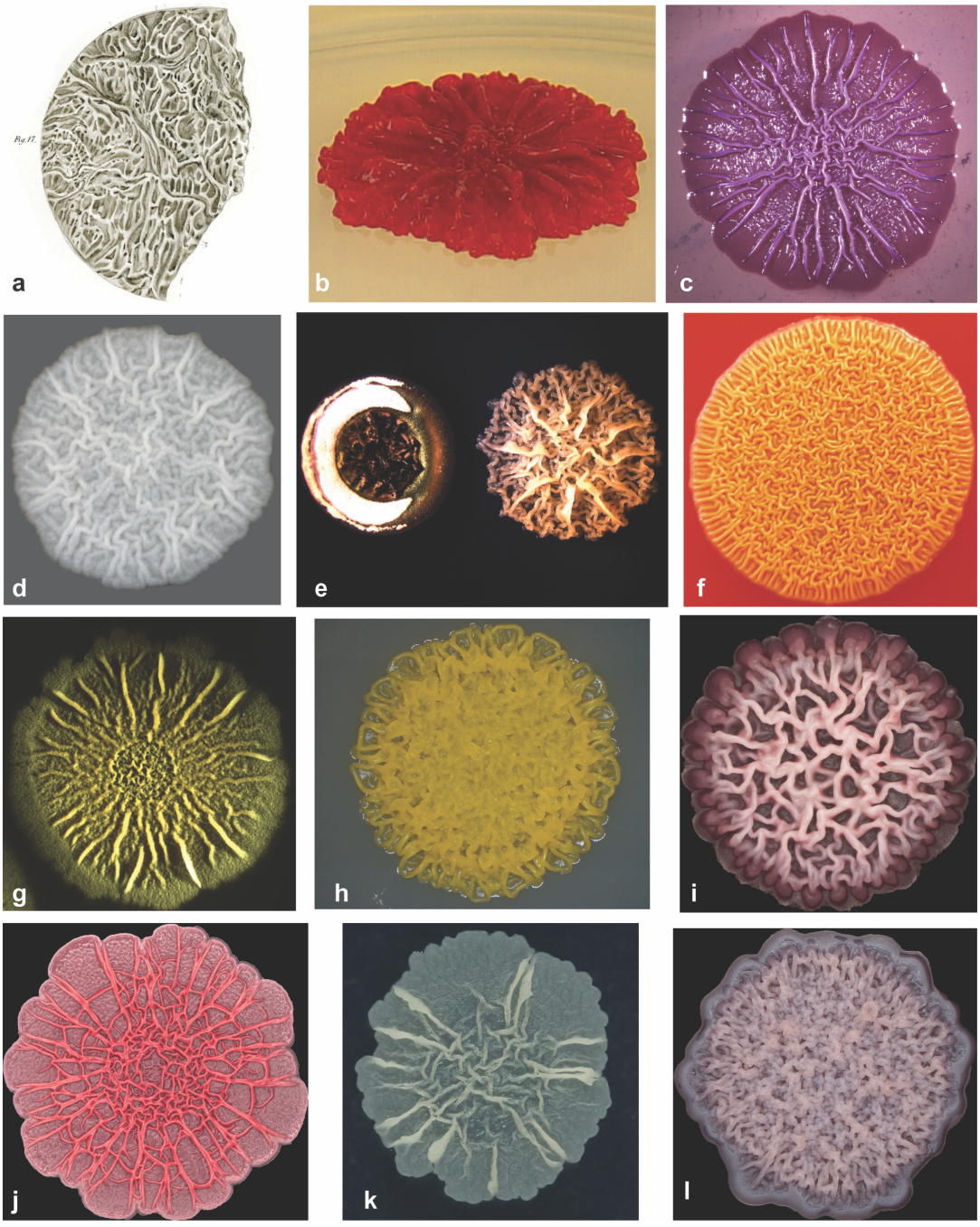

Figure 1-4. Wrinkled morphologies are formed by diverse microbial communities at the interface with air. (**a**): *Coccobacteria septic* pellicle (T. Billroth, 1874). (**b**): Cyst-forming *Rhodospirillum centenum* (J. Berleman and C. Bauer). (**c**) *Escherichia coli* K-12 derivative AR3110 (R. Hengge). (**d**) *Saccharomyces cerevisiae* SK1 (C. Sison, B. Miller, and L. Dietrich). (**e**) *Streptomyces coelicolor* M145 (left) and Amycolatopsis sp. AA4 (right) (M. Traxler and R. Kolter). (**f**) *Serratia marcescens* strain CHASM, isolated from a backyard compost heap (R. Shanks). (**g**) *Bacillus subtilis* NCIB3610 (M. Cabeen and R. Losick). (**h**) *Pseudomonas oryzihabitans*, isolated from a bench in Riverside Park, New York, NY (S. Jordan and L. Dietrich). (**i**) *Candida albicans* (D. Morales and D. Hogan). (**j**) *Pseudomonas aeruginosa* PA14 Δ*phz* mutant (D. Murphy and L. Dietrich). (**k**) *Mycobacterium smegmatis* (A. Balachandran and G. Hatfull). (**l**) *Vibrio cholerae* rugose colony variant (N. Fong, F. Yildiz, and H. Sakhtah). Source: Okegbe *et al Current Opinion in Microbiology., 2014*

proteins, and extracellular DNA [25,51-56].

Biofilms harbor metabolically heterogenous populations of cells that experience gradients of resources. This leads to distinct populations of cells that occupy various niches within the biofilm [57,58]. A well-studied gradient in biofilms is that of oxygen, which is characterized by high levels at the top of the biofilm exposed to the atmosphere or flowing liquid medium and low levels at the bottom of the biofilm where oxygen cannot reach [59,60]. Oxygen gradients in biofilms not only affect metabolism and survival of resident cells [61,62], but also their behavior and community morphogenesis. Multicellular communities can cope with the threat of redox imbalance through the utilization of redox-active metabolites as alternate electron acceptors or structural modulation that increases access to oxygen for cells in the community [63-66] (Chapter 2, Appedix B).

This thesis describes the physiological characterization of biofilms formed by the opportunistic pathogen *Pseudomonas aeruginosa* PA14, grown primarily in a standardized assay of colony morphogenesis. This biofilm model system is amenable to perturbation, in situ profiling of chemical ecology, and high-throughput screening. I have leveraged this model in the application of mutational anlysis and quantitative techniques that measure intracellular redox state, levels of an intracellular secondary messenger, and production of biofilm matrix. The following sections of this introduction provide an overview of the conditions that influence, and mechanisms that control, biofilm development in *P. aeruginosa* and other bacteria with an emphasis on their relevance to colony biofilm morphogenesis.

1-3 PHENAZINES: REDOX-ACTIVE ANTIBIOTICS WITH ROLES IN SIGNALING AND METABOLISM

Bacteria produce both inorganic and organic redox-active metabolites (Fig. 1-5). Intermediates in the full reduction of molecular oxygen and nitrate can be produced both as side-products of essential metabolic reactions and by the activities of organic redox-cycling compounds. Despite their high reactivity and potential to damage protein cofactors, DNA, and cellular lipids

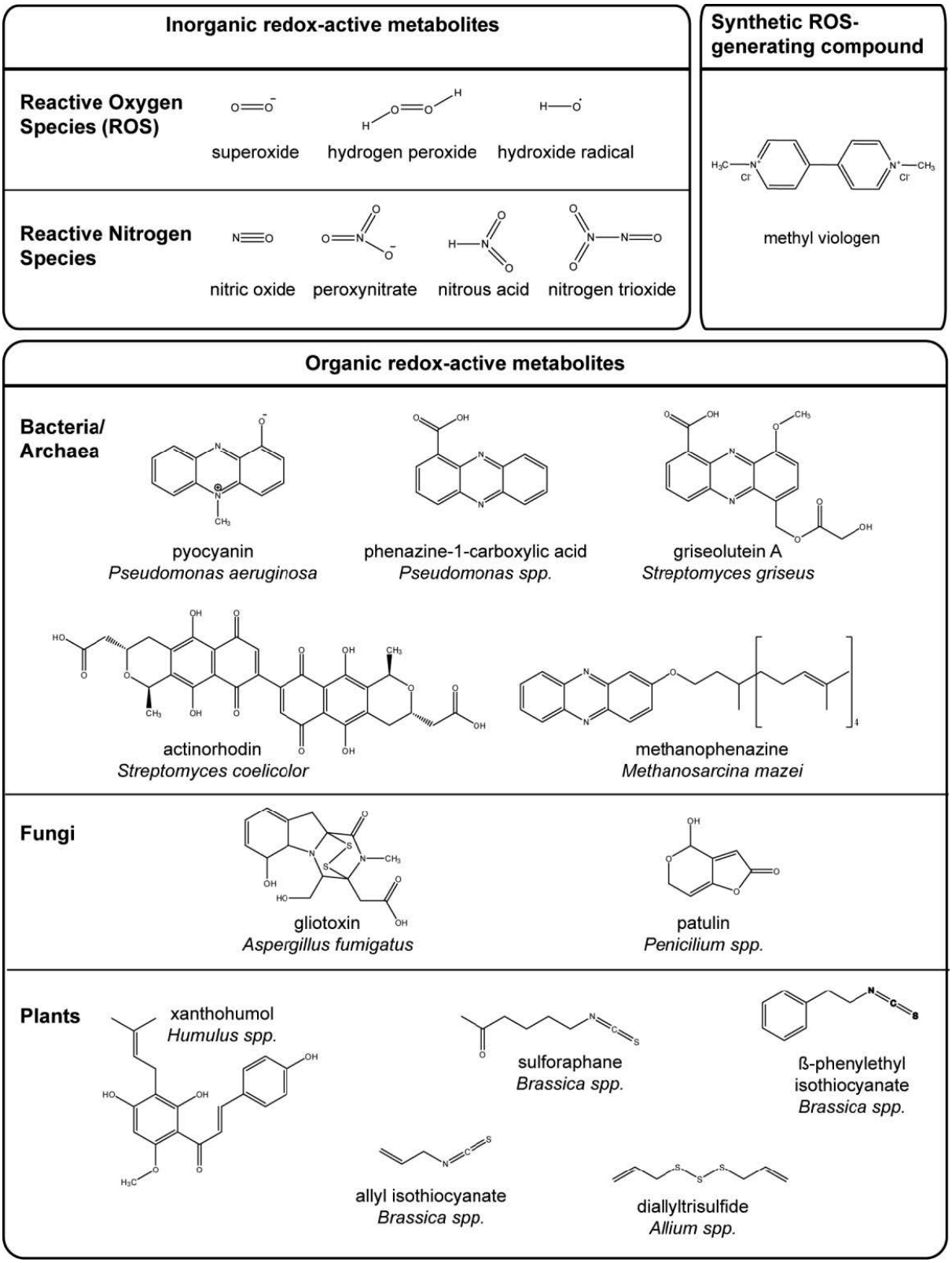

Figure 1-5. Examples of inorganic and organic redox-active metabolites. Source: Okegbe *et al Antioxidants & Redox Signaling., 2012*

[67], some of these compounds have been shown to serve signaling functions in a diversity of organisms.

Production of inorganic redox-active metabolites is more likely to occur during active growth. The production of redox-active organic compounds, however, is often growth phase- and condition-dependent, occurring in the stationary phase of the growth curve of a batch culture and during limitation for specific nutrients [57,68]. In fact, this is one of the properties that have lead to their categorization as “secondary metabolites.” Production of secondary metabolites is not directly required for the growth of microbes in laboratory batch cultures. Historically, the major functions ascribed to these compounds have been related to their antibiotic activity and competition between divergent microbes in soil.

Selman Waksman initiated the use of the term ‘antibiotic’ as a noun in the early 1940s when his team discovered that the small molecule streptomycin, isolated from the soil actinomycete *Streptomyces griseus*, was effective against tuberculosis [69]. At the time, the term was meant to describe any substance produced by a microbe that is antagonistic to microbial growth [70], but it has evolved to include all compounds that prevent the growth of microbes [71]. This definition implies that antibiotic-producing organisms excrete these compounds at levels high enough to kill competing microbes. In recent years, however, levels of canonical antibiotics in soil have been reported that are insufficient for biocidal activity, suggesting that sublethal effects of antibiotics are environmentally relevant. Indeed, many “antibiotics” have been shown to affect gene expression at subinhibitory concentrations [72]. It must therefore be considered that the primary roles for these stressors in bacteria are related to the survival of the producing organism rather than the killing of competing organisms. This interpretation puts a dramatic new spin on bacterial stress responses. In the next section, I will discuss the physiological roles that have been described for a class of antibiotics called phenazines.

Phenazines are redox-active, heterocyclic compounds produced by several genera of bacteria [73]. Their discovery dates back to the late 19th century when doctors noticed blue-tinted pus

secreted from purulent wounds in patients [74] and were able to isolate a blue phenazine from these secretions, which was named “pyocyanin”. Phenazines have long been categorized as antibiotics because their intracellular reduction and re-oxidation generates reactive oxygen species [75], leading to cell death in some organisms. Phenazine-producing bacteria are often able to tolerate high levels of phenazines, likely through the activities of superoxide dismutases. The archaeon *Methanosarcina mazei* produces a phenazine derivative with a long

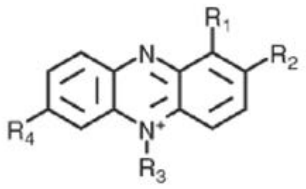

No	Name	R_1	R_2	R_3	R_4	K_{OW} ox	K_{OW} red	$E^{0\prime}$ (mV)
1	Aeruginosin A	COOH		CH_3	NH_2	−0.71	0.46	NA
2	Phenazine-1-carboxylic acid (PCA)	COOH				2.17	3.72	−177
3	Pyocyanin (PYO)	OH		CH_3		1.60	2.89	−172
4	2-Hydrozyphenazine-1-carboxylic acid (2-OHPCA)	COOH	OH			2.54	3.32	−34
5	Phenazine-1-carboxaminde	$CONH_2$				1.04	2.19	NA
6	1-Hydrozyphenazine (1-OHPHZ)	OH				1.81	2.35	−115

Figure 1-6. Chemical properties of phenazines produced by *P. aeruginosa*. The functional groups and the redox potentials at pH 7 are shown. Source: Price-Whelan *et al., Nat. Chem. Bio., 2006*

hydrophobic tail. This compound is not excreted, but rather resides in the cell membrane where it participates in methanogenic electron transport and plays a primary metabolic role [76]

Additional phenazines have been subsequently identified from culture supernatants as well as chronic *P. aeruginosa* infections [77,78]. Although most are biosynthetically derived from the yellow compound phenazine-1-carboxylic acid (PCA), they display a broad range of chemical structures, physical properties, and biological activities (Fig. 1-6). The best-studied phenazine biosynthetic pathways are encoded by the *phz* genes of pseudomonad species. These genes encode enzymes required for the biosynthesis of PCA, as well as modifying enzymes that derivatize the compound, producing pigments such as the blue pyocyanin, the greenish-yellow

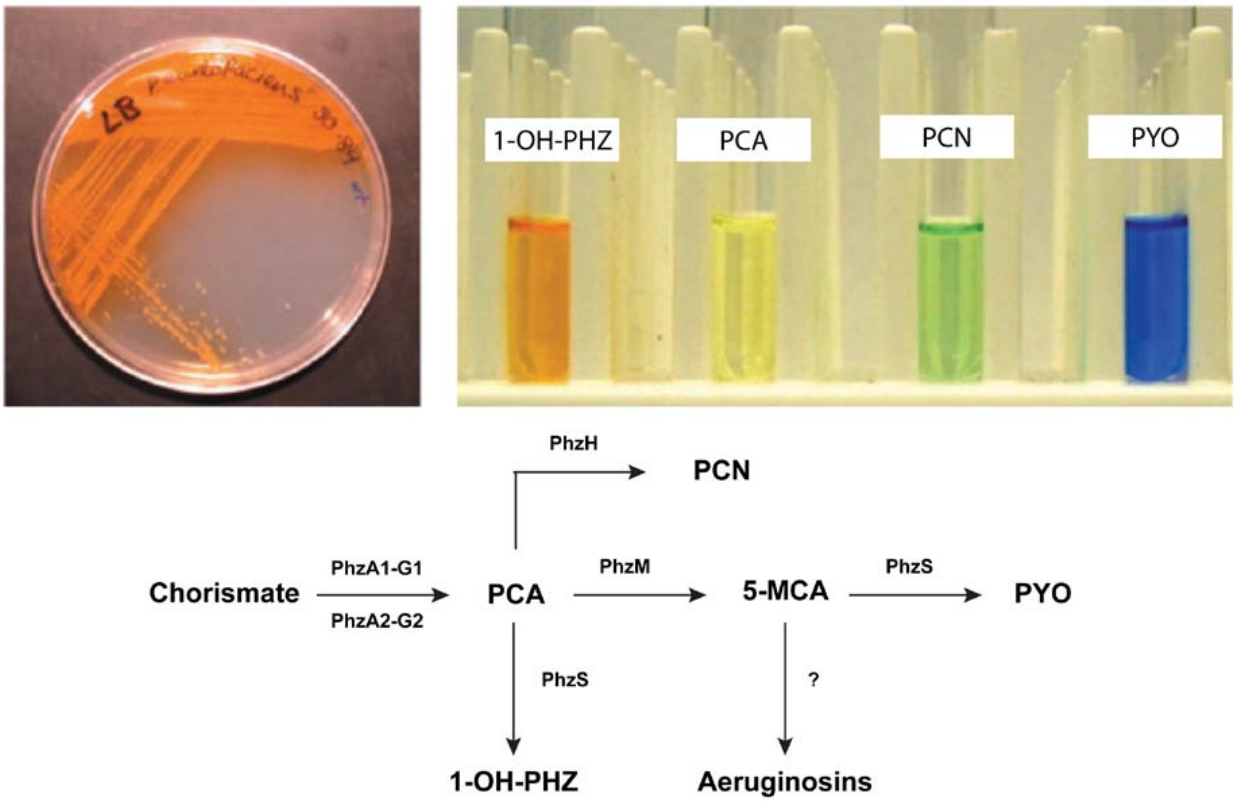

Figure 1-7. *P.seudomonads* produces a variety of colorful phenazines. Top left: Plate of a phenazine-producing soil isolate. Top right: solutions of individual phenazines. Bottom: Known and postulated steps in the *P. aeruginosa* phenazine biosynthetic pathway.Adapted from Price-Whelan *et al., Nat. Chem. Bio., 2006*

phenazine-1-carboxamide, and the orange 1-hydroxyphenazine (Fig. 1-7). Pyocyanin is probably the most notorious of these molecules, as lab cultures of many isolates of the pathogen *P. aeruginosa* owe their intense coloration to this pigment. It is also a common feature of patients with burn wound and lung infections due to the production of blue (pyocyanin-containing) pus and mucus [79].

The toxic, redox-cycling effects of bacterial phenazines in non-producing organisms are thought to facilitate competition for resources in the soil in cases of environmental isolates, and contribute to the pathogenicity of *P. aeruginosa*. However, these compounds also have effects that are beneficial for their producers. Natural phenazines can increase the bioavailability of

iron [80,81], transmit intercellular signals to coordinate gene expression across cell populations [82] and facilitate maintenance of intracellular redox homeostasis [83]. Here I will focus on the roles that phenazines play in respiration and redox balancing as well as their significance in the context of biofilm development in *P. aeruginosa* PA14.

1-3-1 Phenazines in respiration and redox balancing

Phenazine-producing bacteria catalyze the reduction of phenazines in addition to their biosynthesis. The most striking evidence of bacterial phenazine reduction can be observed in a standing *P. aeruginosa* culture, which will gradually turn from bright blue to bright yellow. This process occurs because pyocyanin exhibits a brilliant blue color in its oxidized state, but changes to colorless as it is reduced [84], while PCA is a faint yellow in its oxidized form, but turns bright yellow when it is reduced. This activity has also been demonstrated in oxygen-limited cultures of the bacterium *P. chlororaphis*, which can use its phenazine product, phenazine-1-carboxamide (PCN) to reduce extracellular iron oxides [85]. In the 1930s, Ernst Friedheim demonstrated that pyocyanin production promotes oxygen consumption in *P. aeruginosa* cell suspensions, and suggested that phenazines could act as electron carriers in respiratory or redox-balancing reactions. He would have been excited to learn that an unequivocal proof of his hypothesis can be found in the archaeon *M. mazei*, where the hydrophobic membrane-bound compound methanophenazine is required for the electron transport that ultimately powers ATP synthesis [76].

Methanophenazine is the only small organic pigment for which a direct role in respiration has been characterized. However, decades after Friedheim proposed that *P. aeruginosa* phenazines could react with “labile hydrogen” inside the bacterium, new studies have shown that phenazines facilitate intracellular redox balancing and survival. Planktonic cultures of phenazine-deficient *P. aeruginosa* mutants exhibit a higher NADH/NAD^+ ratio in stationary phase, suggesting that an inability to produce phenazines at the normal time point of their synthesis results in a reduced intracellular environment [83]. The NADH re-oxidation coupled

(directly or indirectly) to phenazine reduction may allow primary anabolic reactions to proceed under conditions where other terminal electron acceptors are unavailable, as is the case in dense, oxygen-limited stationary-phase cultures. Intriguingly, in anaerobic reactors containing electrodes poised at phenazine-reducing potentials, the phenazines pyocyanin, PCA, and 1-hydroxyphenazine promote survival of *P. aeruginosa* in the absence of any other electron acceptor [86]. The bacteria catalyze phenazine-mediated extracellular electron shuttling, using the electrodes as the terminal oxidant. It therefore appears that these secondary metabolites participate in reactions of primary metabolic significance under some conditions; the specific reactions that support bacterial survival in these cases remain to be identified.

1-3-2 Phenazines modulate community development

Many bacteria, including those that produce phenazines, frequently exist in nature not as unicellular organisms but within complex biofilm communities. Previous studies have established the presence of decreasing oxygen gradients in biofilms [62] and I have hypothesized that phenazines play an important role in balancing the redox state of cells within anoxic zones. Indeed, the effects of phenazine production or exposure on colony biofilm development produce dramatic macroscopic effects: wild-type colonies of *P. aeruginosa* PA14 are smooth and smaller than those of the phenazine-null mutant, which are highly wrinkled and spread over a larger surface area of the agar plate (Fig. 1-8). Although it has been established that bacterial cells in cultures and flow-cell biofilms can coordinate their gene expression, the ability for 10 billion bacterial cells to organize into a structure like the phenazine-null colony suggests that the mechanisms by which they do so are far more complex than previously appreciated, and probably involve both cell-cell communication and redox balancing. In addition to influencing homogenous cell populations like a bacterial colony, phenazines can also mediate interactions between heterogeneous cell populations. This is especially relevant in soil environments and during host infections, where phenazine-producers typically live in biofilms with a diversity of other species [85,87].

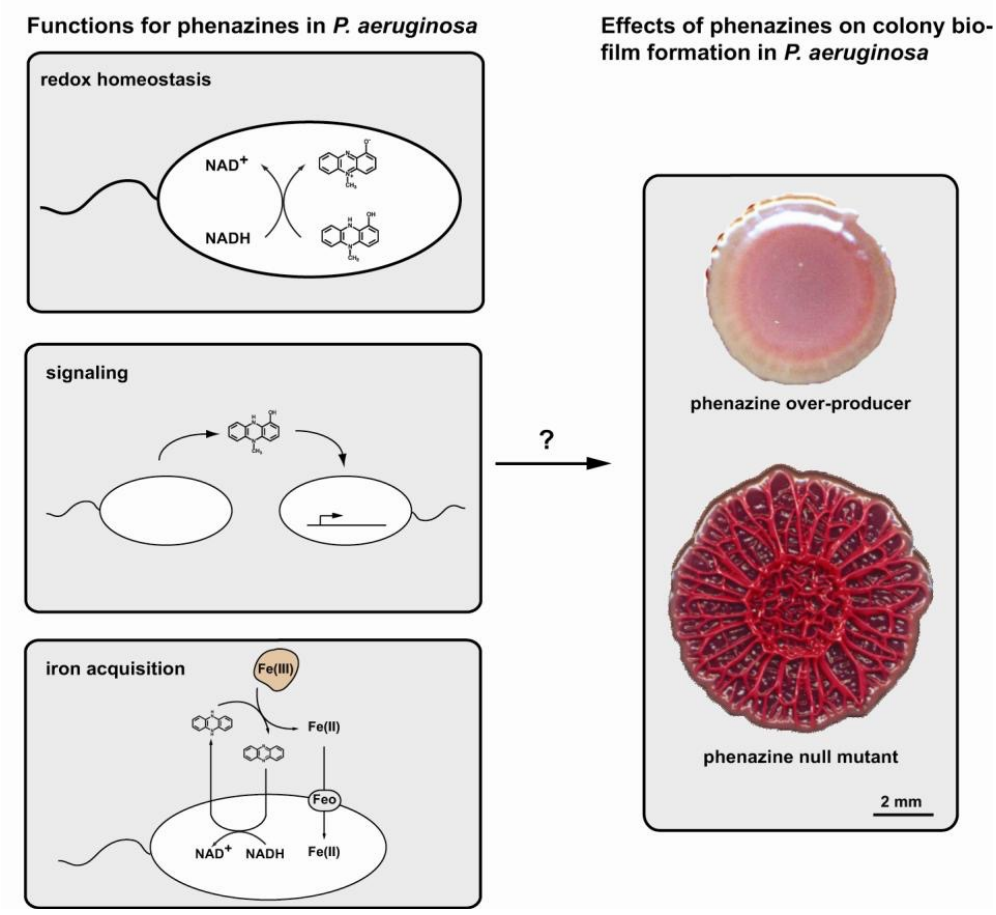

Figure 1-8. The physiological roles of phenazines. Phenazines play a role in iron acquisition, redox balancing, and signaling may contribute to the drastic morphological switch observed in phenazine-producing versus phenazine-null colony biofilms in *P. aeruginosa* PA14. Source: Okegbe et al Antioxidants & Redox Signaling., 2012

1-4 STRUCTURAL MODULATION AS A RESPONSE TO REDOX IMBALANCE

The molecular details, mechanics, and physiological relevance of structural development have been studied for many models of microbial multicellularity. Large bodies of work describe the signaling cascades that control motility and matrix production and thereby affect biofilm morphogenesis [31,33,38,48,88,89]. In *Bacillus subtilis* biofilms, nonuniform cell death has been observed to precede and was proposed to determine wrinkle pattern formation when mechanical forces, arising from colony growth, promote vertical buckling [90]. Results from an additional study in *B. subtilis* have suggested that wrinkles are actually channels that allow for

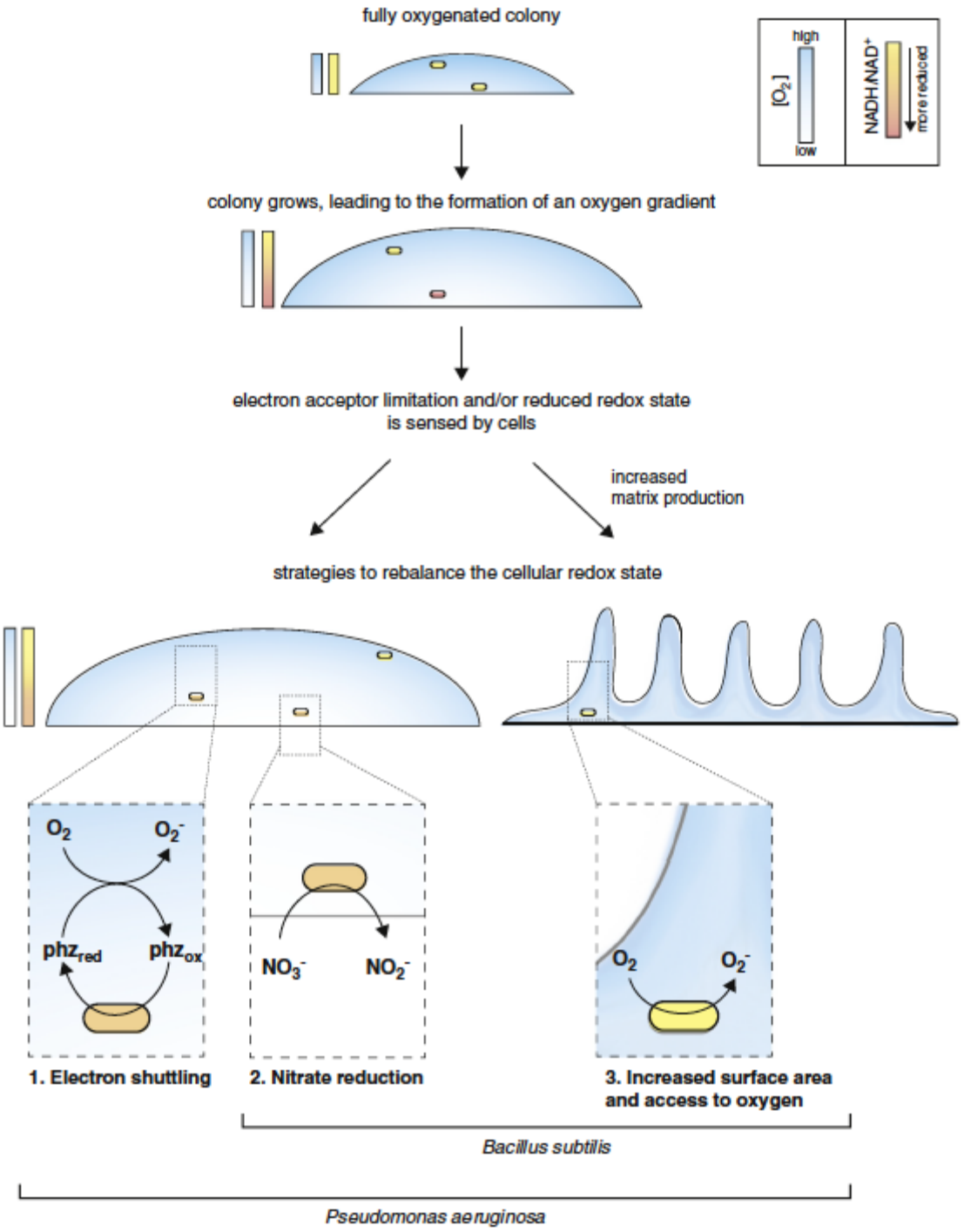

Figure 1-9. Strategies to achieve redox homestasis. Electron shuttling, nitrate reduction, and colony wrinkling are strategies that can support redox balancing, indicated by the NADH/NAD⁺ ratio, for microbes in biofilms. The model presented here is based on findings from two recent publications concerning colony morphogenesis in *P. aeruginosa* and *B. subtilis*; whether these strategies are employed in other microbial communities remains to be investigated. Source: Okegbe *et al Current Opinion in Microbiology., 2014*

enhanced liquid transport through the biofilm [91]. Despite these advances, for most models a thorough analysis of the response to environmental cues, and especially to changes in redox potential, have not been conducted. The significance of redox potential in determining biofilm morphology has only become apparent over the last few years with the examination of this relationship in *P. aeruginosa* and *B. subtilis*. Results from these studies suggest that colony wrinkling enhances access to oxygen and maintenance of redox homeostasis for bacteria in biofilms.

The elaborate wrinkles formed by colonies of some *P. aeruginosa* mutants became a focus of the Dietrich lab's work when it was discovered that the change in morphology--dramatically enhanced rugosity--that occurs when this organism is unable to produce antibiotics called phenazines [92,93]. Phenazines are redox-active and are reduced and excreted by *P. aeruginosa* [94]. Extracellularly, they react readily with oxidants and can be taken up by the bacteria once again, thus acting as mediators that facilitate extracellular electron transfer [95]. Such phenazine redox cycling can support survival when *P. aeruginosa* is incubated in suspension with no terminal electron acceptors other than an electrode poised to catalyze phenazine oxidation [86]. Work presented Chapter 2 of this thesis further investigates the role of colony wrinkling in increasing access to oxygen and enabling redox balancing under conditions of redox stress as experienced by the phenazine-null mutant (Fig. 1-9).

Whether colony wrinkling is a strategy for accessing oxygen in the diversity of rugose colony models that have been studied is still unknown. However, a recent publication by Kolodkin-Gal et al. indicates that this scenario does hold in the bacterium *B. subtilis* [63]. *B. subtilis* does not produce phenazines, but, as I have observed in *P. aeruginosa*, varying the atmospheric oxygen concentration modulates the extent of colony wrinkling. Furthermore, adding nitrate to the medium also decreases wrinkling. The effects of varying oxygen concentration and adding nitrate on both colony systems are consistent with the model that colony wrinkling is a readout for redox imbalance. Interestingly, different nitrate reductases appear to be involved in the

rugose-smooth morphological change that occurs when *P. aeruginosa* and *B. subtilis* are grown with nitrate in an aerobic atmosphere. While *P. aeruginosa* requires the periplasmic nitrate reductase Nap for smooth colony formation on nitrate, *B. subtilis* requires the membrane-assocated (respiratory), cytoplasmic nitrate reductase Nar. Nevertheless, these results suggest that for both *P. aeruginosa* and *B. subtilis*, wrinkling to enhance access to oxygen and utilization of nitrate (when available) are strategies for balancing the intracellular redox state during growth in biofilms (Fig. 1-9). In organisms where additional anaerobic metabolisms, such as fermentation, contribute to redox balancing, utilization of such strategies may support the survival of bacteria in anoxic biofilm regions [31].

Though many additional studies are required to investigate the physiological roles of wrinkling in the diverse microbes that adopt this colony morphology, intriguing findings across phylogeny point to a theme with respect to the roles of mediator compounds. In early work examining respiratory activity in both normal and malignant tissues, biologists observed that compounds such as phenazines increased respiration rates [96,97]. They theorized that such mediators could act as electron acceptors for cells experiencing oxygen limitation within tissues, then diffuse to aerobic zones for re-oxidation. Furthermore, upon observing that such electron acceptors are produced by certain species of bacteria, some authors also suggested that they could act as endogenous respiratory substrates [98]. It was only recently and with the increased appreciation that the biofilm lifestyle is a dominant mode of growth for many microorganisms that it became apparent that mediators could support redox balancing for their producing cells during residence in multicellular structures. Intriguingly, mutants of *Streptomyces coelicolor* A3(2) unable to produce the diffusible redox-active antibiotic actinorhodin form more rugose colonies than their wild-type parent, raising the possibility that pigment-dependent electron shuttling occurs in diverse organisms [92]. Microbes that do not produce mediators may be able to utilize diffusible redox-cycling compounds produced by other organisms in the environment to support redox balancing during multicellular growth. In this context it is interesting to note that phenazines induce a rugose-to-smooth morphotypic

transformation in colonies of the yeast *Candida albicans* [30] (and see Appendix C), though whether *C. albicans* communities can use phenazines for extracellular electron transfer and cellular redox balancing in biofilms is not known.

1-5 MECHANISMS LINKING REDOX SENSING TO COMMUNITY OUTPUT

Metabolism and redox chemistry are tightly linked as anabolic and catabolic processes involve reductive and oxidative reactions, respectively. However, the cellular redox balance is constantly threatened by changes in the availability of electron donors and acceptors and exposure to highly redox-active metabolites. It is monitored by a variety of sensors; some of these directly sense stressors, while others sense their effects on the cell. The latter type of sensor takes advantage of the redox properties of cofactors, such as iron-sulfur clusters, flavins, and hemes. These proteins can couple redox sensing to a variety of outputs, but in most cases they ultimately affect transcription [1,99].

Though redox sensors have been best studied as mechanisms for protecting the cells from distress, there is growing appreciation for the role that these sensors play in the coordination of neutral or positive responses to redox-active metabolites. These alternate responses occur because different functions for identical redox-sensing systems have evolved to meet the needs of specific organisms. Thus, two homologues of the same redox-sensing system that detect the same redox signal are linked with different outputs with opposing functions, such as coping mechanisms for distress (a.k.a. “stress responses”) in one organism versus developmental signaling in another. Two examples that illustrate this concept are (i) the nitric oxide (NO) sensor NsrR in *Escherichia coli* and *Neisseria meningitidis* and (ii) SoxR, a sensor for redox-cycling compounds in *E. coli* and *Pseudomonas aeruginosa*. Both NsrR and SoxR are transcriptional regulators that sense redox-active signals through iron-sulfur clusters [100-102].

1-5-1 NsrR: Stress response to NO vs. utilization of NO in primary metabolism

In *E. coli*, NsrR induces approximately 20 genes that mediate a response to the toxicity of NO including *hmp*, *nrfA* and *ytfE*. Hmp converts NO to nitrate in the presence of oxygen [103], NrfA converts nitrite to ammonium through an NO intermediate [104], and YtfE is involved in repairing iron-sulfur clusters that have been damaged by NO [105]. In this scenario, the regulon encodes mechanisms that enable the bacterium to cope with exposure to the redox-active compound, suggesting that NO has the potential to cause distress in *E. coli*. When the stress response is fully functional, however, redox homeostasis is maintained.

In a contrasting scenario, *N. meningitidis* NsrR regulates a smaller set of genes [106], including *aniA* and *norB*. AniA reduces nitrite to NO, which is further reduced by NorB to nitrous oxide. This was originally interpreted as a way for the bacterium to clear NO that is released from macrophages during infection [107]. However, these reactions can also enable the maintenance of redox homeostasis by allowing *N. meningitidis* to utilize NO as an electron acceptor. This function may support survival in the microaerobic environments it encounters during host infection, due to the abundance of mucus in the nasopharynx [104].

1-5-2 SoxR: A sensor of exogenous and endogenous redox-cycling compounds

SoxR is a well-established stress response regulator in *E. coli* that senses redox-cycling xenobiotics [82,92,108,109]. In *E. coli*, SoxR activates expression of the transcription factor SoxS, which in turn regulates the expression of more than one hundred genes [110]. The products of this regulon include transporters of redox-cycling agents and enzymes that detoxify the products of redox-cycling, including reactive oxygen species. Induction of the SoxRS regulon therefore represents a coping mechanism that protects from the toxicity of exogenous redox-cycling agents.

In non-enteric bacteria such as *P. aeruginosa*, the mechanism of sensing redox-cycling compounds is similar to that of *E. coli* SoxR, but the response is different. *P. aeruginosa* SoxR is activated by endogenously-produced phenazines [82], which bear structural similarity to

some of the compounds that activate *E. coli* SoxR. However, unlike the *E. coli* SoxRS system, *P. aeruginosa* SoxR induces transcription of a small set of genes, encoding two transporters and a monooxygenase [82,111]. Work from the Dietrich lab would suggest that the transporters are needed for the proper shuttling of phenazines [92]. Similar observations have been made in *Streptomyces coelicolor*, where the endogenous antibiotic actinorhodin and/or its biosynthetic precursors activate SoxR [92,108,112]. Similar to the case for *P. aeruginosa*, its regulon consists of a small set of genes, encoding transporters and oxygenase-type enzymes.

The sensors NsrR and SoxR are two examples of the transcription factors that respond to redox signals in a context-specific fashion. In *E. coli*, they provide effective means to ward off or recover from redox toxicity and allow bacteria to cope with exposure to these compounds. While these mechanisms merely facilitate tolerance to these compounds, there are also cases where these sensors allow bacteria to exploit the same compounds as metabolic substrates or signals controlling community development and morphogenesis.

1-5-3 Connecting redox to colony morphogenesis

The redox signals highlighted in the previous section– nitric oxide and phenazines, have been shown to play roles in biofilm development in *P. aeruginosa* [113,114]. In 2003, Webb and colleagues uncovered new roles for reactive oxygen and nitrogen species in cell lysis and cell dispersal from microcolony biofilms of *P. aeruginosa* growing in flow cells, where biofilms grow attached to a surface under a constant flow of liquid medium [115]. Soon after, the specific role of NO in biofilm development and dispersal was investigated. This work revealed that non-toxic levels of NO indicate to the colonies that environmental conditions are favorable for planktonic growth, signaling the biofilm communities to strategically disperse into individual cells [116]. NO acts via a signaling pathway to upregulate phosphodiesterase activity, leading to decreased intracellular levels of cyclic di-GMP (c-di-GMP) [113], an intracellular second messenger involved in bacterial switching from sessile to motile states. The role of c-di-GMP in biofilm development will be discussed in section 1-6 of this chapter. Work from the Dietrich lab

has showed how the different phenazines made by *P. aeruginosa* PA14 affect biofilm development. The redox potentials of phenazines are such that they can be easily reduced by the bacterial cell and react extracellularly with higher potential oxidants such as ferric iron and oxygen, acting as electron shuttles between the bacterium and an external substrate [80,117]. In short, phenazines allow survival in the deepest parts of the colony biofilm where oxygen and other usable electron acceptors are unavailable. Their absence therefore triggers colony wrinkling as a compensatory mechanism.

The effects of electron acceptor limitation on *P. aeruginosa* and *B. subtilis* colony biofilm morphogenesis suggest that regulatory proteins serve to sense redox conditions and regulate community behavior. In this section, I discuss what is already known about mechanisms of multicellular structure formation in these two species in the context of redox homeostasis.

In *P. aeruginosa* PA14, colony wrinkling requires the secretion of a polysaccharide called Pel [33]. Colonies formed by a double mutant unable to produce Pel polysaccharide or phenazines remain smooth and exhibit a reduced intracellular redox state that persists throughout colony development [64]. This finding suggests that the NADH/NAD^+ ratio, or another indicator of the cellular redox potential, is sensed by regulatory pathways that control features such as Pel polysaccharide production that then control colony wrinkling. In *B. subtilis*, a polysaccharide encoded by the *eps* genes and the amyloid protein TasA are major components of the matrix that are required for wild-type wrinkling [25]. Kolodkin-Gal et al. found that expression from the promoter controlling the *tapA-sipW-tasA* or "*tapA*" operon correlated with wrinkling in the context of varying oxygen and nitrate availability. Decreasing the concentration of $FeCl_3$ in the medium demonstrated a correlation between wrinkling, expression from P_{tapA}, and oxidation of the NAD(H) pool (decreased NADH/NAD^+). However, a time course was not conducted, so this study does not examine the possibility of a causative relationship between changes in the NADH/NAD^+ ratio and colony wrinkling. Production of the polysaccharide cellulose and curli fimbriae are required for rugosity in *E. coli* and *S. enterica Typhimurium* [31,118-120], and a

polysaccharide critical for rugosity has also been described for *Vibrio cholerae* [46,121]. Various stresses have been shown to affect the production of these components, though in most cases it is not clear whether redox imbalance is one of them. Interestingly, studies examining the effects of oxygen limitation on regulatory gene expression, and the abundance of NAD^+ in wild-type and matrix-deficient strains, in *Salmonella* suggest that colony development could both respond to and affect redox homeostasis in this organism [122,123].

If sensing of the internal redox state is directly related to initiation of wrinkling, what signal transduction pathways are mediating this response? In *B. subtilis*, a regulatory cascade, which proceeds via expression of the anti-repressor SinI, links matrix gene expression to the master regulator Spo0A. The phosphorylation state and activity of Spo0A is determined by a phosphorelay, and the histidine kinases KinA-E contribute phosphoryl groups to this relay [124]. Kolodkin-Gal et al. reported that wild-type colony wrinkling requires KinA-D. When expression from the sinI promoter (expected to correlate with tapA expression and wrinkling) was measured for various KinA-D single and double mutants, a kinA kinB double mutant showed the most dramatic decrease relative to the wild type. The colony phenotype of this double mutant closely resembled that of the wild type grown with 5 μM $FeCl_3$, where no wrinkling occurred during the incubation time used for the experiment. KinB is predicted to bind to the cell membrane. Immunoprecipitation experiments and mutational analyses suggested that KinB interacts with components of the electron transport chain, which may allow KinB to sense respiratory activity and transduce this information into a macroscopic response.

In contrast to KinB, KinA is not predicted to interact with the membrane. KinA contains three tandem PAS domains, motifs that often bind small molecule ligands. In organisms ranging from bacteria to plants and humans, PAS domains (discussed in section 1-7) have been shown to sense signals and parameters such as redox potential, oxygen availability, and light intensity through conformational changes or phosphorylation events [125]. Associated effector domains

on the same protein propagate this signal to downstream targets. The PAS-A and PAS-C domains of KinA were found to be necessary for wild-type levels of P_{sinI} activity and wrinkling. Through HPLC and mass spectrometry of extracts from purified KinA, NAD^+ was identified as a potential ligand for the PAS-A domain. This result suggests that KinA contributes to the morphological response to changes in iron levels and oxygen availability by sensing the effects of these environmental cues on the cellular NAD(H) pool [63].

Work from the Dietrich lab has also indicated a role for PAS domain-containing proteins in *P. aeruginosa* colony morphogenesis. To find the players involved in sensing and initiating the response to electron acceptor limitation in colonies, I screened a *P. aeruginosa* PA14 transposon mutant library for hyperwrinkled mutants. Focusing on proteins with predicted sensory and signal transduction roles, I hypothesized that the mutants hyperwrinkled due to an inability to relay information about intracellular redox state; i.e., they wrinkled to alleviate a redox stress that didn't exist. Several mutants representing PAS domain-containing proteins were found among the hyperwrinklers. These and additional studies, detailed in Chapter 3, suggest that one of these proteins affects Pel polysaccharide production by modulating levels of the ubiquitous second messenger c-di-GMP.

1-6 CYCLIC DI-GMP

Cyclic di-GMP (c-di-GMP) is a ubiquitous bacterial intracellular second messenger that was first described in 1987 by Moshe Benziman and colleagues at The Hebrew University of Jerusalem as an allosteric activator of cellulose synthase in the bacterium *Acetobacter xylinum* (now called *Gluconacetobacter xylinus*) [126,127]. In the years since this discovery, c-di-GMP has emerged as an important player modulating an array of processes such as biofilm formation, motility, virulence, cell cycle, and differentiation [128-133]. More recently, c-di-GMP was found to also regulate cellular differentiation in simple eukaryotes [134].

Genomic annotations predict that *P. aeruginosa* PA14 has 40 proteins with domains involved in c-di-GMP metabolism [135-137]. While the physiological roles of these particular proteins remain under-characterized, a great amount of effort has gone into elucidating the biochemistry of c-di-GMP synthesis, degradation and binding more generally. Domains with digunalyate cyclase (DGC) activity, involved in c-di-GMP synthesis, generally contain a characteristic Gly-Gly-Asp-Glu-Phe (G G D E F) sequence motif (i.e., the active site or "A-site") and are often referred to as "GGDEF domains". Domains with phosphodiesterase (PDE) activity, involved in

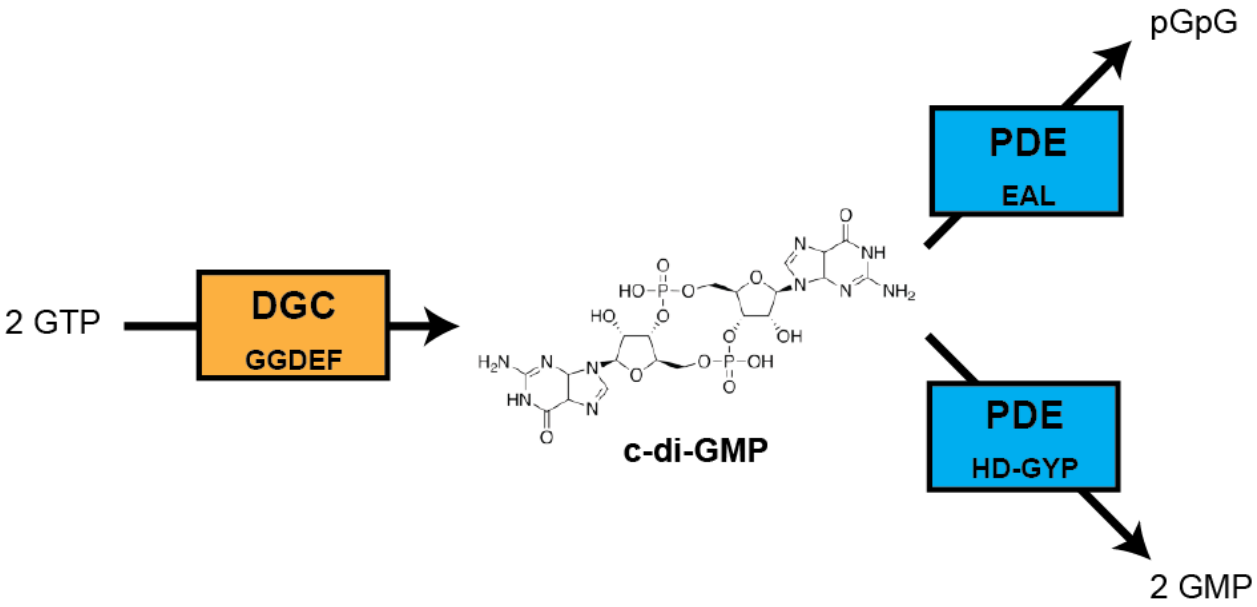

Figure 1-10. Cyclic di-GMP biosynthesis at a glance. One molecule of c-di-GMP (shown in center) is synthesized from two molecules of GTP by enzymes known as diguanylate cyclases (DGCs), which carry a conserved GGDEF domain. c-di-GMP can bedegraded by two families of phosphodiesterases (PDEs); those with an EAL domain linearize the molecule to produce pGpG, and proteins with an HD-GYP domain generate two molecules of GMP. Adapted from: Ha and O'Toole, *Microbiol Spectr., 2015*.

c-di-GMP hydrolysis, fall into two classes: (i) "EAL domains", with a highly conserved Glu-Ala/Val-Leu (E A/V L) active site motif, and (ii) "HD-GYP" domains, which have conserved His-Asp (HD) and Gly-Tyr-Pro (GYP) motifs that play roles in cofactor and substrate binding. Though these two types of PDE domains are both involved in c-di-GMP hydrolysis, they yield different products (Fig. 1-10). The terms described above can also be applied to domains that

structurally resemble GGDEF, EAL, and HD-GYP domains but actually contain a degenerate sequence in place of their canonical motifs.

1-6-1 Diguanylate cyclases

Diguanylate cyclases (DGC) synthesize c-di-GMP from 2 GTP molecules in a two-step process involving a 5'-pppGpG reaction intermediate [138]. DGC domains function as homodimers with dimerization occurring at the active site interface [139]. The active site or A site of DGC domains bind GTP using the first two Gly residues. Two Mg^{2+} or Mn^{2+} cations, which are coordinated to the fourth Glu residue are required for the phosphodiester bond to form. The third Asp or Glu residue is also used for cation coordination and is required for c-di-GMP synthesis [140] This third residue is often targeted in mutational studies of DGC domains. Overall, the GG(D/E)EF motif is predicted to have a ß-hairpin conformation [141]. Although the precise catalytic mechanism of DGC domain activity remains poorly understood, existing structural studies have proposed that the successful catalysis of c-di-GMP occurs when active homodimers are close enough. This would suggest that conformational arrangements dictated by sensory domains and feedback inhibition mechanisms control the formation of DGC homodimer complexes by isolating active sites at far enough distances to prevent unwanted c-di-GMP synthesis [140,142].

It is noteworthy that most c-di-GMP metabolizing enzymes are linked to sensory input domains at their N-terminus. Such sensory input domains include PAS (first discovered in Per, Arnt, and Sim proteins), GAF (found in cGMP-specific phosphodiesterases, adenylyl cyclases, and FhlA), and REC (RECeiver) domains [143,144]. These sensory domains sense cues or signals and initiate downstream processes and a desired output. A signal such as a residue phosphorylation event or cofactor oxidation/reduction causes a conformational change and subunit reorganization in the sensory input domains which brings the DGC domains in close enough proximity to catalyze c-di-GMP synthesis. This has been shown for the surface sensing protein WspR in *P. aeruginosa*. WspR has a REC-GGDEF domain architecture and is part of the

Wsp system, which is activated in response to growth on surfaces [145-147]. Structural studies reveal that the DGC domains are closer, and more capable of forming a catalytically competent homodimer, in the phosphorylated protein when compared to the nonphosphorylated protein. Similar results have been obtained for *Caulobacter crescentus* PleD [148] and *Borrelia burgdorferi*, Rrp1 [149].

Feedback inhibition in DGC domains occurs at the inhibitory (I) site. The conserved characteristic I-site motif is RxxD, where "x" is any residue and it is situated five amino acids upstream of the GG(D/E)EF motif. In spite of the sequence proximity of the I and A sites, they are located diametrically opposite to each other in the domain [148,150]. DGC activity is inhibited when the c-di-GMP dimers bind to the I-site. This locks the DGC domain in place and prevents the mobility of the DGC domain required for DGC homodimer formation.

1-6-2 Phosphodiesterases

There are two classes of phosphodiesterase activity: PDE-A, carried out by EAL domains, and PDE-B, carried out by HD-GYP domains (Fig. 1-10). Initial work on PDE-A activity, which hydrolyses c-di-GMP to produce the linear di-GMP molecule 5'-pGpG, was done by Benziman and colleagues, who purified predicted PDEs from *G. xylinus* and showed the these proteins were able to breakdown c-di-GMP. This activity required either two Mn2+ or Mg2+ cations [151,152] and was repressed by Ca2+. Several genetic and biochemical studies using PDEs from different organisms showed that EAL domains were required for c-di-GMP hydrolysis [153-155]. Interestingly, this reaction was c-di-GMP specific as other phosphoester- and phosphodiester-containing compounds tested, including cyclic AMP (cAMP), were unaffected.

Although EAL domains have been characterized as dimers and multimers in vitro [156,157] they are able to retain activity as monomers [154]. A number of studies have solved the structures of EAL domains [158-160] yielding insights into the catalytic mechanism. C-di-GMP present in the EAL domain during hydrolysis takes on an open conformation (Fig. 1-11) in contrast to the U-shape confirmation observed when c-di-GMP is in the I-site of DGC domains.

Studies in the BlrP1 protein from *Klebsiella pneumoniae* showed that the activity of the EAL domain proteins depends on the structure of a two-metal cation cluster in which the metals coordinate two water molecules, one of which is involved in a hydrolytic attack on a phosphoester bond of c-di-GMP. The Glu residue is required for cation coordination [158] and is conserved in all active EAL domains. BlrP1 has a BLUF-EAL architecture and its PDE-A activity is turned on in response to blue light [161,162], which causes conformational changes that stabilize the active site and EAL-EAL dimer interface.

HD-GYP domains belong to the HD domain superfamily of enzymes, which have been shown

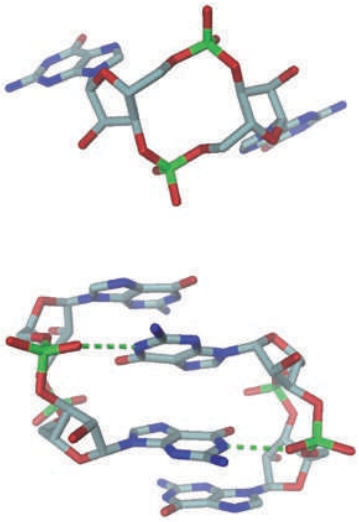

Figure 1-11. Three-dimensional structures of cyclic-di-GMP, showing one molecule in the the open conformation (top) or 2 molecules in the U-shaped conformation (bottom). Carbon atoms are shown in light blue, oxygen in red, nitrogen in deep blue and phosphorous in green. Reprinted by permission from Macmillan Publishers Ltd: *Nature Reviews Microbiology,* Schirmer and Jenal, copyright 2009

to catalyse phosphomonoesterase and phosphodiesterase reactions depending on their catalytic metal centre being mono- or binuclear respectively [137,144,163,164]. Initial studies investigating HD-GYP domain activity were done on RpfG from *Xanthomonas campestris.* RfpG complemented an EAL domain phosphodiesterase mutant and had c-di-GMP-specific activity when purified and expressed in *Pseudomonas aeruginosa* PAO. The main product of this activity was however not linear 5'pGpG but GMP [165], showing that, in contrast to PDE-A activity, PDE-B activity hydrolyzes c-di-GMP to two GMP molecules. Additional HD-GYP proteins from diverse genera such as *Pseudomonas* and *Borrelia* have since been characterized [137,166]. However, it remains an open question whether linearized 5'-pGpG, the

product of PDE-A activity, is an intermediate in HD-GYP activity. Furthermore, the biological significance of having different phosphodiesterase activities is yet to be fully understood.

1-6-3 Proteins with tandem DGC and PDE domains

It is interesting that the first DGCs and PDEs discovered by Benziman had tandem GGDEF - EAL domains [167]. Genome wide-studies have found that 33% of GGDEF domains and 67% of EAL domains are arranged in tandem with each other [168]. Given that DGC and PDE domains are known to function independently the significance of these tandem domain arrangements has remained an interesting but unanswered question. There are two main scenarios that may account for tandem arrangements: (1) Both domains are active but are regulated differentially by environmental signals; or (2) One domain is degenerate and functions to sequester the substrate for the active domain or downstream effectors.

Thus far, the scenario in which both domains are functional remains a very rare in occurrence among c-di-GMP metabolizing enzymes. Examples that have been characterized include *Rhodobacter sphaeroides* BphG1, *Mycobacterium smegmatis* MSDGC-1, *Vibrio parahaemolyticus* Src, and *Legionella pneumophila* LpL0329 [157] [169]. The activities of the latter two proteins have been shown to be influenced by conditional cues: Src exhibits DGC activity under normal conditions but switches to PDE activity during periods of high cell density [170], while Lpl03329 loses DGC activity upon phosphorylation of its REC domain [171]. GGDEF-HD-GYP tandems are rare especially when compared to GGDEF-EAL tandems. Although studies characterizing GGDEF-HD-GYP tandem proteins are scarce, it is expected that they function similarly to other well characterized GGDEF-EAL tandem proteins [140].

Structural studies coupled with site-directed mutagenesis have given the c-di-GMP field substantial insight and ability to predict DGC and PDE domains that are likely to be active or inactive. Proteins with degenerate motifs in their DGC or PDE domains are numerous. Genomic analyses predict that about 40% of GGDEF-EAL tandem proteins have mutations that abolish DGC activity compared to 13% with PDE-abolishing mutations. This suggests that DGC

domains are more likely to be degenerate in proteins with GGDEF and EAL domains arranged in tandem [168]. Indeed, there is little known about catalytically inactive EAL domains in such proteins. Further characterization of tandem proteins is needed to understand the intramolecular regulation of c-di-GMP metabolism and its roles in in bacterial physiology.

1-6-4 Regulation of biofilm development by c-di-GMP

Numerous studies characterizing the roles of c-di-GMP in *P. aeruginosa* social behaviors have led to a paradigm in which this organism is understood to grow in one of two states: (i) a sessile state associated with high c-di-GMP levels, polysaccharide excretion and biofilm formation, or (ii) a motile state associated with low c-di-GMP levels and a type of motility on semisolid surfaces called swarming [172-174] [140,175,176]. Mutants lacking proteins involved in c-di-GMP metabolism or binding tend to fall into one of these two phenotypic categories, though exceptions to this trend (i.e., mutants that overproduce polysaccharide yet exhibit robust swarming motility) have been described [181]. This section will focus on the role of c-di-GMP in regulating polysaccharide production, which is required for wrinkle structure formation in the colony biofilms and wild-type levels attachment to surfaces in static liquid culture models of biofilm formation.

In *P. aeruginosa* PA14, the primary model strain used in this work, Pel constitutes the major polysaccharide component of the matrix. Pel biosynthesis is regulated by c-di-GMP at the transcriptional level via FleQ and post-translational level via PelD. The transcriptional regulator FleQ promotes Pel transcription when bound to c-di-GMP [172]. When c-di-GMP is low or absent, FleQ complexes with FleN, an ATP-binding protein. This complex binds the Pel promoter region to bend the DNA and inhibit Pel transcription [173] (Fig. 1-12). It is speculated that the DGC WspR, upon activation through a phosphorylation event initiated by surface contact, provides the localized c-di-GMP pool used by FleQ for efficient transcriptional control [145,146]

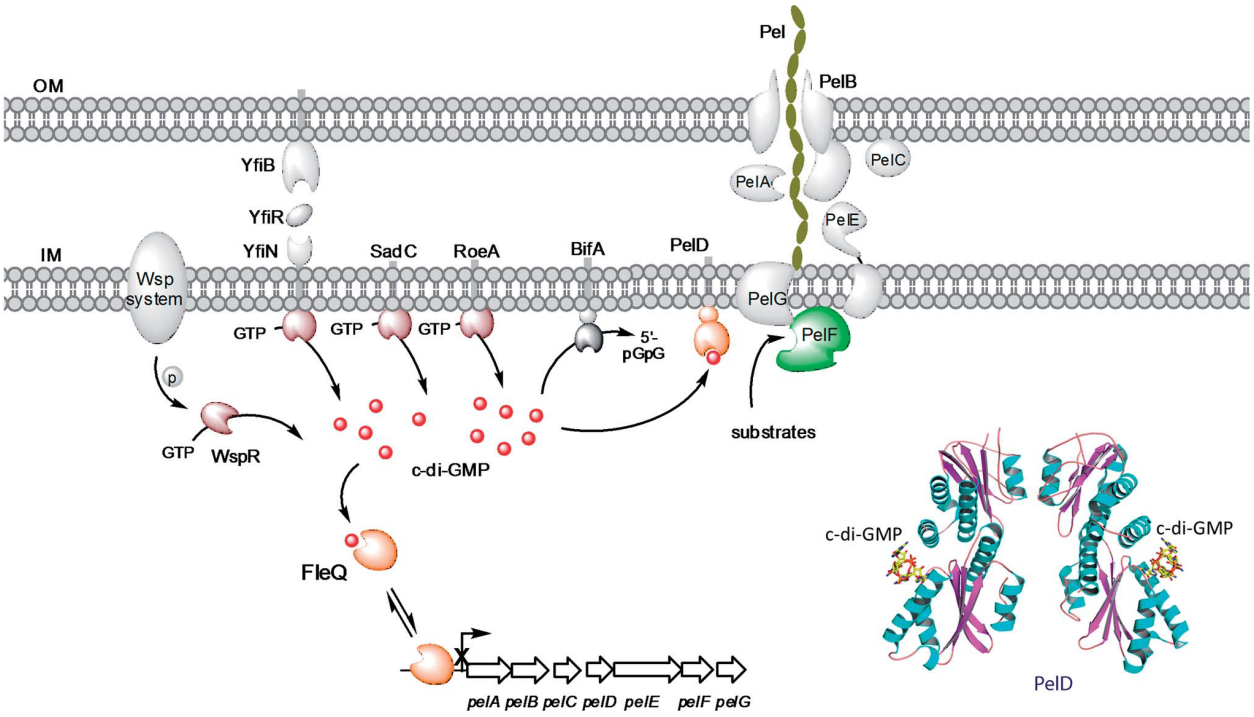

Figure 1-12. Cyclic-di-GMP-dependent regulation of Pel polysaccharide biosynthesis in *P. aeruginosa*. Reproduced from Liang, *Natural Product Reports., 2015*.permission of The Royal Society of Chemistry.

At the post-translational level, Pel biosynthesis is regulated by PelD, a c-di-GMP receptor with an I-site (RxxD) motif that is allosterically activated by c-di-GMP [177]. Mutation of the I-site motif, which leads to loss of c-di-GMP binding, results in an inability to form biofilms properly [177-179]. While the exact mechanism of PelD function is yet to be fully elucidated, DGCs and PDEs that tune the c-di-GMP level in response to environmental cues probably control Pel biosynthesis through PelD. The well-characterized DGCs RoeA and SadC and the PDE BifA have all been shown to regulate Pel production [180,181].

Biofilms that form on submerged surfaces can also disperse in response to environmental signals. Dispersal triggered by NO or glutamate has been attributed to a lowering of cellular c-di-GMP via the activity of the PDEs DipA and RbdA [182] [183,184]. Studies from Karen Sauer's group characterizing the role of c-di-GMP in dispersal have also described the protein BldA, which is required for biofilm dispersal and contains both PAS and chemotaxis-associated domains. Although BldA does not contain domains directly associated with c-di-GMP

metabolism, it appears to be cleaved when c-di-GMP levels are high [183,185,186]. DipA-dependent lowering of c-di-GMP levels inhibits BldA cleavage and allows dispersal to occur. Whether the PAS domains of BldA confer redox sensitivity and link redox conditions to the regulation of dispersal is not known.

1-7 PAS DOMAINS

PAS domains were initially discovered by sequence similarity between three proteins– **P**ER, **A**RNT and **S**IM—with roles in circadian regulation, the immune response, and cell development in complex eukaryotes [125,187,188] [189] [190] [191]. The first structure of a PAS domain was published in the late 90s and since then, structures of many more have improved our understanding of their cofactor binding and other features. PAS domains are usually about 100 residues in length [192,193] and have a characteristic five-stranded antiparallel beta sheet with alpha helices that form the ligand binding pocket on the beta sheet [187].

PAS domains are found in all domains of life [194,195] (Fig. 1-13) and are widely abundant in bacterial proteomes [196]. PAS domains are typically found in sensory and signal transduction proteins as they are able to sense a variety of signals such as redox potential, oxygen, light [195]. In order to sense such diverse signals, PAS domains are usually coordinated to ligands such as heme and flavins [125] which are often the site of signal sensing within these domains. Although some ligands that are bound to PAS domains are known, deciphering precisely what environmental stimuli and substrates are sensed by individual PAS domains is often challenging [125] because there is low primary sequence similarity between PAS domains although the three-dimensional structure is conserved [195,197]. However, for proteins with solved structures, the conserved 3-D fold of PAS domains has allowed the identification of cofactors and ligands because the residues in the ligand-binding pockets are usually conserved [125,198].

PAS domain-containing proteins often play critical roles in development and survival in specific environmental contexts. An example from complex eukaryotes is the well-studied PAS domain

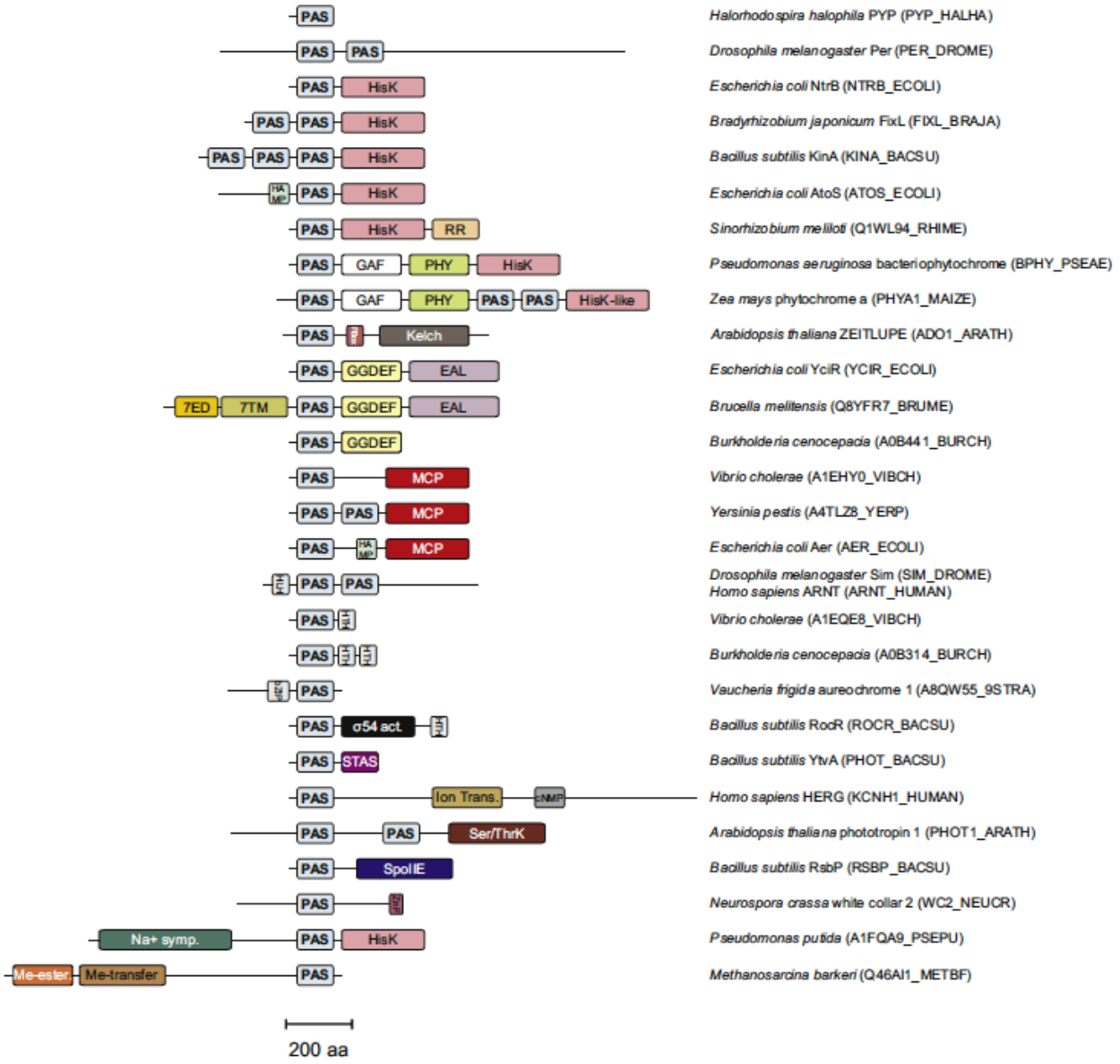

Figure 1-13. The diversity of PAS proteins. Examples of PAS-domain-containing proteins from all domains of life and their domain archtecture. PAS domains are usually linked to output domains, which can have diverse functions. Reprinted from Structure, 17(10), Möglich *et al,* Structure and Signaling Mechanism of Per-ARNT-Sim Domains, 1283-1294, copyright 2009, with permission from Elsevier

proteins Hypoxia Inducible Factor-1 (HIF-1), involved in tumor development. Rapidly growing cancer cells quickly outpace oxygen availability needed for survival and therefore must activate adaptive mechanisms such as angiogenesis and glucose metabolism to meet the increased demand for oxygen [199,200]. In bacteria, PAS domain-containing proteins have been implicated in an array of important cellular processes such as photosynthesis, circadian

regulation, biofilm formation, chemotaxis, sporulation, and nitrogen fixation [63,184,185,201-203]. Bacterial PAS domain-containing proteins can also harbor diverse

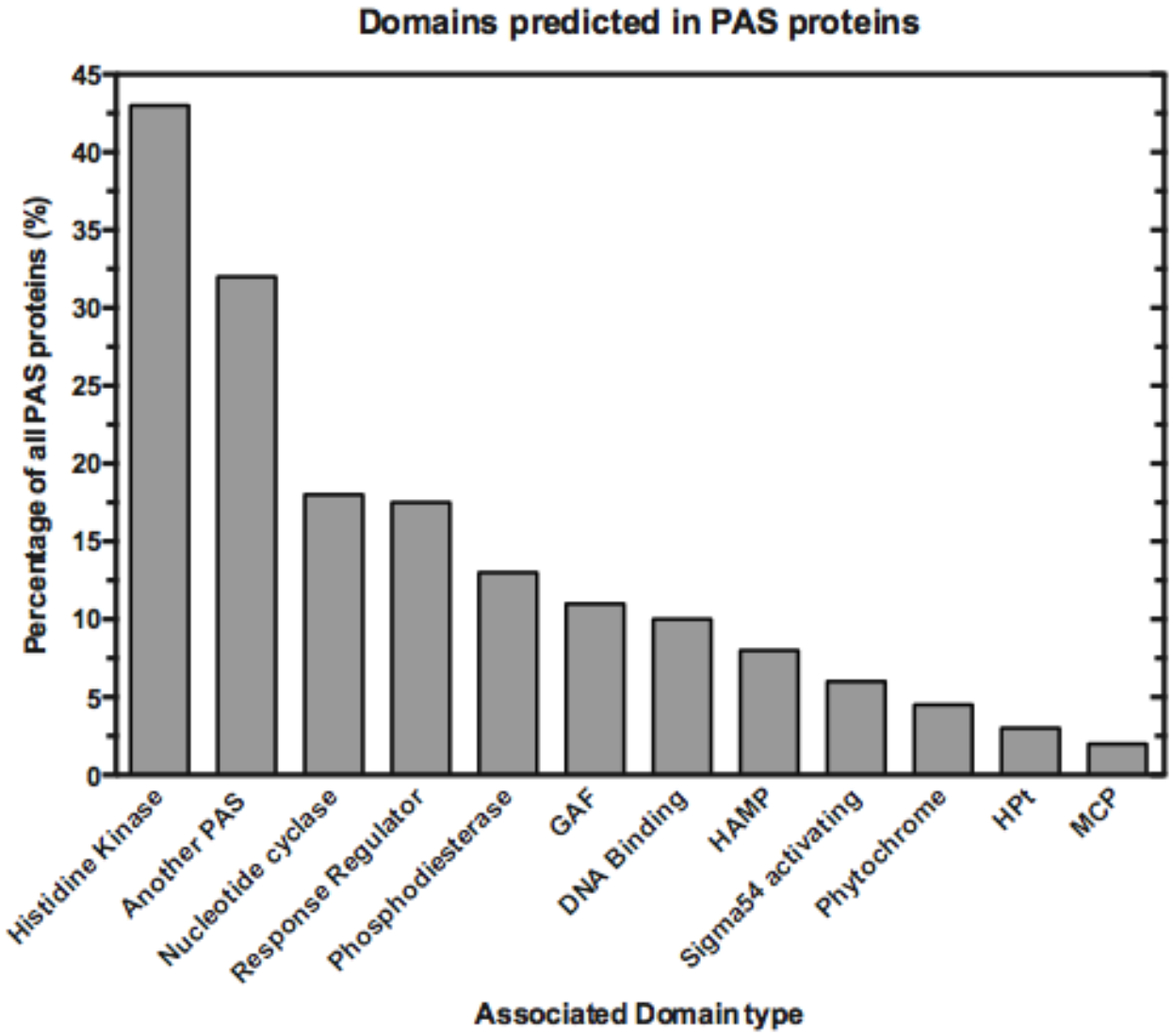

Figure 1-14. Predicted domains contained in bacterial PAS proteins. Most common domains associated with PAS proteins are associated with sensory input, transduction or output. Adapted from: Henry and Crosson, *Annu. Rev. Microbiol 2011.*

effector or output domains involved in phosphorylation, DNA-binding and cyclic-di-GMP metabolism [125] (Fig. 1-14). As such, PAS domains are crucial to sensory and signal transduction networks that allow bacteria to readily adapt to ever-changing and potentially harmful environmental conditions.

1-8 AIMS OF THIS WORK

Colony biofilms form captivating patterns that are strongly influenced by growth conditions. How do the billions of microscopic residents in these communities coordinate their activities to produce a macroscopic response? My thesis approaches this fundamental question through the application of diverse techniques to colony biofilms formed by the opportunistic pathogen *P. aeruginosa* PA14. PA14 colony biofilm architecture is dramatically altered by changes in redox conditions. While much is known about the molecular mechanisms underpinning biofilm structure formation, the relationships between conditions and morphological output, and the regulatory mechanisms that support these relationships, are not well understood. The work described in this thesis has been motivated by the following two aims:

Aim 1: Characterize the relationship between electron acceptor availability and colony biofilm development

This goal is addressed by the work presented in Chapter 2 and Appendices B and C. Chapter 2 describes the characterization of PA14 colony development under different redox regimes. Results from microelectrode-based profiling, measurement of cellular NADH/NAD^+ levels, fluorescence microscopy of colony thin sections, and mutant analyses support the conclusions that phenazines act as alternate electron acceptors to support the survival of cells in anoxic biofilm subzones and that redox imbalance is a major determinant of the colony developmental program in *P. aeruginosa* PA14. Indeed biofilm maturation is hampered by the presence of redox stressors like carbon monoxide (Appendix A), and mathematical modeling shown in Appendix B supports the hypothesis that the colony takes on optimal geometry and architecture to ensure survival in specific redox regimes. Finally, aspects of the influence of phenazines on PA14 biofilm development are paralleled in colonies formed by the fungus *Candida albicans* (Appendix C).

Aim 2: Determine the sensory link(s) between cues, such as altered redox conditions and environmental stressors, and colony biofilm morphogenesis

This goal is addressed in Chapter 3 and Appendix D, which describe the identification, characterization, and purification of PAS domain-containing redox sensors that regulate biofilm development through the modulation of c-di-GMP levels. An additional study characterizing the effects of *C. albicans*-produced ethanol, described in Appendix E, showed that it affects biofilm matrix production via the modulation of c-di-GMP levels.

Overall, this work has furthered our understanding of fundamental principles that govern PA14 community behavior and revealed mechanisms that allow this bacterium to respond to electron acceptor availability at the population level. These results show that in bacterial biofilms, as in multicellular eukaryotic organisms, electron acceptor availability influences and is influenced by collective structure and that cellular redox state is an important driver of community morphogenesis. The matrix-encased cells in bacterial biofilms, like those in complex multicellular eukaryotes, employ PAS-domain-dependent signaling cascades to mediate the community response to redox conditions. I predict that, as the role of relative electron donor and acceptor availability in shaping populations is determined for additional and diverse microbial species, the importance of redox chemistry, not just to metabolism but also to morphogenesis, in biology will continue to become all the more evident.

1-9 REFERENCES

1. Green J, Paget MS: Bacterial redox sensors. Nat Rev Micro 2004, 2:954–966.
2. Foyer C, Noctor G: Redox homeostasis and antioxidant signaling: A metabolic interface between stress perception and physiological responses. Plant Cell 2005, 17:1866–1875.
3. Selye H: A syndrome produced by diverse nocuous agents. Nature 1936, 138:32–32.
4. Selye H: Forty years of stress research: principal remaining problems and misconceptions. Can Med Assoc J 1976, 115:53–56.
5. Munck A, Guyre PM, Holbrook NJ: Physiological functions of glucocorticoids in stress and their relation to pharmacological actions. Endocr. Rev. 1984, 5:25–44.
6. Shapiro J: Bacteria as multicellular organisms. Sci. Am. 1988, [no volume].
7. STOODLEY P, Sauer K, Davies DG, Costerton JW: Biofilms as complex differentiated communities. Annu. Rev. Microbiol. 2002, 56:187–209.
8. Camilli A: Bacterial Small-Molecule Signaling Pathways. Science 2006, 311:1113–1116.
9. Shapiro JA: Thinking about bacterial populations as multicellular organisms. Annu. Rev. Microbiol. 1998, 52:81–104.
10. Branda SS, Vik Å, Friedman L, Kolter R: Biofilms: the matrix revisited. Trends in Microbiology 2005, 13:20–26.
11. Costerton JW, LEWANDOWSKI Z, Caldwell DE, Korber DR, Lappin-Scott HM: Microbial biofilms. Annu. Rev. Microbiol. 1995, 49:711–745.
12. Williams BJ, Dehnbostel J, Blackwell TS: Pseudomonas aeruginosa: host defence in lung diseases. Respirology 2010, 15:1037–1056.
13. Jackson K, Keyser R, Wozniak DJ: The role of biofilms in airway disease. Semin Respir Crit Care Med 2003, 24:663–670.
14. Nazzari E, Torretta S, Pignataro L, Marchisio P, Esposito S: Role of biofilm in children with recurrent upper respiratory tract infections. Eur. J. Clin. Microbiol. Infect. Dis. 2015, 34:421–429.
15. Cataldi M, Sblendorio V, Leo A, Piazza O: Biofilm-dependent airway infections: a role for ambroxol? Pulm Pharmacol Ther 2014, 28:98–108.
16. Stickler DJ, King JB, Winters C, Morris SL: Blockage of urethral catheters by bacterial biofilms. J. Infect. 1993, 27:133–135.
17. Holá V, Růzicka F: [Urinary catheter biofilm infections]. Epidemiol Mikrobiol Imunol 2008, 57:47–52.

18. Holling N, Lednor D, Tsang S, Bissell A, Campbell L, Nzakizwanayo J, Dedi C, Hawthorne JA, Hanlon G, Ogilvie LA, et al.: Elucidating the genetic basis of crystalline biofilm formation in Proteus mirabilis. Infect. Immun. 2014, 82:1616–1626.

19. Zegans ME, Becker HI, Budzik J, O'Toole G: The role of bacterial biofilms in ocular infections. DNA Cell Biol. 2002, 21:415–420.

20. Currie CR: A community of ants, fungi, and bacteria: a multilateral approach to studying symbiosis. Annu. Rev. Microbiol. 2001, 55:357–380.

21. Chin-A-Woeng TF, Bloemberg GV, Mulders IH, Dekkers LC, Lugtenberg BJ: Root colonization by phenazine-1-carboxamide-producing bacterium Pseudomonas chlororaphis PCL1391 is essential for biocontrol of tomato foot and root rot. Mol. Plant Microbe Interact. 2000, 13:1340–1345.

22. Merritt JH, Kadouri DE, O'Toole GA: Growing and analyzing static biofilms. Curr Protoc Microbiol 2005, Chapter 1:Unit 1B.1.

23. Billroth T: Untersuchungen über die Vegetationsformen von Coccobacteria septica und den Antheil, welchen sie an der Entstehung und Verbreitung der accidentellen …. 1874.

24. Branda SS, González-Pastor JE, Ben-Yehuda S, Losick R, Kolter R: Fruiting body formation by Bacillus subtilis. Proc. Natl. Acad. Sci. U.S.A. 2001, 98:11621–11626.

25. Romero D, Aguilar C, Losick R, Kolter R: Amyloid fibers provide structural integrity to Bacillus subtilis biofilms. Proceedings of the National Academy of Sciences 2010, 107:2230–2234.

26. Branda SS, González-Pastor JE, Dervyn E, Ehrlich SD, Losick R, Kolter R: Genes involved in formation of structured multicellular communities by Bacillus subtilis. Journal of Bacteriology 2004, 186:3970–3979.

27. Kearns DB, Chu F, Branda SS, Kolter R, Losick R: A master regulator for biofilm formation by Bacillus subtilis. Mol Microbiol 2005, 55:739–749.

28. Aguilar C, Vlamakis H, Guzman A, Losick R, Kolter R: KinD is a checkpoint protein linking spore formation to extracellular-matrix production in Bacillus subtilis biofilms. MBio 2010, 1:e00035–10–e00035–10.

29. Martinez JP, Gil ML, Casanova M, Lopez-Ribot JL, Garcia De Lomas J, Sentandreu R: Wall mannoproteins in cells from colonial phenotypic variants of Candida albicans. J. Gen. Microbiol. 1990, 136:2421–2432.

30. Morales DK, Grahl N, Okegbe C, Dietrich LEP, Jacobs NJ, Hogan DA: Control of Candida albicans Metabolism and Biofilm Formation by Pseudomonas aeruginosa Phenazines. MBio 2013, 4.

31. Serra DO, Richter AM, Hengge R: Cellulose as an Architectural Element in Spatially Structured Escherichia coli Biofilms. Journal of Bacteriology 2013, 195:5540–5554.

32. DePas WH, Hufnagel DA, Lee JS, Blanco LP, Bernstein HC, Fisher ST, James GA, Stewart PS, Chapman MR: Iron induces bimodal population development by Escherichia coli. Proceedings of the National Academy of Sciences 2013, 110:2629–2634.

33. Friedman L, Kolter R: Genes involved in matrix formation in Pseudomonas aeruginosa PA14 biofilms. Mol Microbiol 2004, 51:675–690.

34. Ueda A, Wood TK: Connecting quorum sensing, c-di-GMP, pel polysaccharide, and biofilm formation in Pseudomonas aeruginosa through tyrosine phosphatase TpbA (PA3885). PLoS Pathog 2009, 5:e1000483.

35. Colvin KM, Irie Y, Tart CS, Urbano R, Whitney JC, Ryder C, Howell PL, Wozniak DJ, Parsek MR: The Pel and Psl polysaccharides provide Pseudomonas aeruginosa structural redundancy within the biofilm matrix. Environmental Microbiology 2012, 14:1913–1928.

36. Ma L, Conover M, Lu H, Parsek MR, Bayles K, Wozniak DJ: Assembly and development of the Pseudomonas aeruginosa biofilm matrix. PLoS Pathog 2009, 5:e1000354.

37. Parsek MR, Tolker-Nielsen T: Pattern formation in Pseudomonas aeruginosa biofilms. Current Opinion in Microbiology 2008, 11:560–566.

38. Colvin KM, Gordon VD, Murakami K, Borlee BR, Wozniak DJ, Wong GCL, Parsek MR: The pel polysaccharide can serve a structural and protective role in the biofilm matrix of Pseudomonas aeruginosa. PLoS Pathog 2011, 7:e1001264.

39. Berleman JE, Hasselbring BM, Bauer CE: Hypercyst mutants in Rhodospirillum centenum identify regulatory loci involved in cyst cell differentiation. Journal of Bacteriology 2004, 186:5834–5841.

40. Voordeckers K, De Maeyer D, van der Zande E, Vinces MD, Meert W, Cloots L, Ryan O, Marchal K, Verstrepen KJ: Identification of a complex genetic network underlying Saccharomyces cerevisiae colony morphology. Mol Microbiol 2012, 86:225–239.

41. Kuthan M, Devaux F, Janderová B, Slaninová I, Jacq C, Palková Z: Domestication of wild Saccharomyces cerevisiae is accompanied by changes in gene expression and colony morphology. Mol Microbiol 2003, 47:745–754.

42. Granek JA, Magwene PM: Environmental and genetic determinants of colony morphology in yeast. Plos Genet 2010, 6:e1000823.

43. Römling U, Sierralta WD, Eriksson K, Normark S: Multicellular and aggregative behaviour of Salmonella typhimurium strains is controlled by mutations in the agfD promoter. Mol Microbiol 1998, 28:249–264.

44. Shanks RMQ, Lahr RM, Stella NA, Arena KE, Brothers KM, Kwak DH, Liu X, Kalivoda EJ: A Serratia marcescens PigP homolog controls prodigiosin biosynthesis, swarming

motility and hemolysis and is regulated by cAMP-CRP and HexS. PLoS ONE 2013, 8:e57634.

45. Yildiz FH, Visick KL: Vibrio biofilms: so much the same yet so different. Trends in Microbiology 2009, 17:109–118.

46. Yildiz FH, Schoolnik GK: Vibrio cholerae O1 El Tor: identification of a gene cluster required for the rugose colony type, exopolysaccharide production, chlorine resistance, and biofilm formation. Proc. Natl. Acad. Sci. U.S.A. 1999, 96:4028–4033.

47. Liu X, Beyhan S, Lim B, Linington RG, Yildiz FH: Identification and characterization of a phosphodiesterase that inversely regulates motility and biofilm formation in Vibrio cholerae. Journal of Bacteriology 2010, 192:4541–4552.

48. Fong JCN, Yildiz FH: The rbmBCDEF gene cluster modulates development of rugose colony morphology and biofilm formation in Vibrio cholerae. Journal of Bacteriology 2007, 189:2319–2330.

49. Traxler MF, Seyedsayamdost MR, Clardy J, Kolter R: Interspecies modulation of bacterial development through iron competition and siderophore piracy. Mol Microbiol 2012, 86:628–644.

50. Nguyen KT, Willey JM, Nguyen LD, Nguyen LT, Viollier PH, Thompson CJ: A central regulator of morphological differentiation in the multicellular bacterium Streptomyces coelicolor. Mol Microbiol 2002, 46:1223–1238.

51. Ryder C, Byrd M, Wozniak DJ: Role of polysaccharides in Pseudomonas aeruginosa biofilm development. Current Opinion in Microbiology 2007, 10:644–648.

52. Peterson BW, van der Mei HC, Sjollema J, Busscher HJ, Sharma PK: A distinguishable role of eDNA in the viscoelastic relaxation of biofilms. MBio 2013, 4:e00497–13.

53. Purish LM, Asaulenko LG, Abdulina DR, Vasil'ev VN, Iutinskaia GA: [Role of polymer complexes in the formation of biofilms by corrosive bacteria on steel surfaces]. Prikl. Biokhim. Mikrobiol. 2012, 48:294–301.

54. Barnhart MM, Chapman MR: Curli biogenesis and function. Annu. Rev. Microbiol. 2006, 60:131–147.

55. Dueholm MS, Petersen SV, Sønderkær M, Larsen P, Christiansen G, Hein KL, Enghild JJ, Nielsen JL, Nielsen KL, Nielsen PH, et al.: Functional amyloid in Pseudomonas. Mol Microbiol 2010, 77:1009–1020.

56. Arciola CR, Campoccia D, Ravaioli S, Montanaro L: Polysaccharide intercellular adhesin in biofilm: structural and regulatory aspects. Front Cell Infect Microbiol 2015, 5:7.

57. Fraleigh SP, Bungay HR: Modelling of nutrient gradients in a bacterial colony. J. Gen. Microbiol. 1986, 132:2057–2060.

58. Blackstone NW: Metabolic gradients: a new system for old questions. Curr. Biol. 2008, 18:R351–3.

59. Schobert M, Tielen P: Contribution of oxygen-limiting conditions to persistent infection of Pseudomonas aeruginosa. Future Microbiol 2010, 5:603–621.

60. Stewart PS, Franklin MJ: Physiological heterogeneity in biofilms. Nat Rev Micro 2008, 6:199–210.

61. Werner E, Roe F, Bugnicourt A, Franklin MJ, Heydorn A, Molin S, Pitts B, Stewart PS: Stratified growth in Pseudomonas aeruginosa biofilms. Applied and Environmental Microbiology 2004, 70:6188–6196.

62. Xu KD, Stewart PS, Xia F, Huang CT, McFeters GA: Spatial physiological heterogeneity in Pseudomonas aeruginosa biofilm is determined by oxygen availability. Applied and Environmental Microbiology 1998, 64:4035–4039.

63. Kolodkin-Gal I, Elsholz AKW, Muth C, Girguis PR, Kolter R, Losick R: Respiration control of multicellularity in Bacillus subtilis by a complex of the cytochrome chain with a membrane-embedded histidine kinase. Genes Dev. 2013, 27:887–899.

64. Dietrich LEP, Okegbe C, Price-Whelan A, Sakhtah H, Hunter RC, Newman DK: Bacterial community morphogenesis is intimately linked to the intracellular redox state. Journal of Bacteriology 2013, doi:10.1128/JB.02273-12.

65. Okegbe C, Sakhtah H, Sekedat MD, Price-Whelan A, Dietrich LEP: Redox eustress: roles for redox-active metabolites in bacterial signaling and behavior. Antioxidants & Redox Signaling 2012, 16:658–667.

66. Okegbe C, Price-Whelan A, Dietrich LEP: Redox-driven regulation of microbial community morphogenesis. Current Opinion in Microbiology 2014, 18:39–45.

67. Imlay JA: How oxygen damages microbes: oxygen tolerance and obligate anaerobiosis. Adv Microb Physiol 2002, 46:111–153.

68. Pomposiello PJ, Demple B: Global adjustment of microbial physiology during free radical stress. Adv Microb Physiol 2002, 46:319–341.

69. Schatz A, Bugie E, Waksman SA: Streptomycin, a substance exhibiting antibiotic activity against gram-positive and gram-negative bacteria. 1944. 2005.

70. Waksman SA: What Is an Antibiotic or an Antibiotic Substance? Mycologia 1947, 39:565.

71. Hadacek F, Bachmann G, Engelmeier D, Chobot V: Hormesis and a Chemical Raison D'être for Secondary Plant Metabolites. Dose Response 2011, 9:79–116.

72. Davies J, Spiegelman GB, Yim G: The world of subinhibitory antibiotic concentrations. Current Opinion in Microbiology 2006, 9:445–453.

73. Mavrodi von DV, Peever TL, Mavrodi von OV, Parejko JA, Raaijmakers JM, Lemanceau P, Mazurier S, Heide L, Blankenfeldt W, Weller DM, et al.: Diversity and Evolution of the Phenazine Biosynthesis Pathway. Appl. Environ. Microbiol. 2010, 76:0.

74. Mentel M, Ahuja EG, Mavrodi DV, Breinbauer R, Thomashow LS, Blankenfeldt W: Of two make one: the biosynthesis of phenazines. Chembiochem 2009, 10:2295–2304.

75. Jacob C, Jamier V, Ba LA: Redox active secondary metabolites. Current Opinion in Chemical Biology 2011, 15:149–155.

76. Abken HJ, Tietze M, Brodersen J, Bäumer S, Beifuss U, Deppenmeier U: Isolation and characterization of methanophenazine and function of phenazines in membrane-bound electron transport of Methanosarcina mazei Gö1. Journal of Bacteriology 1998, 180:2027–2032.

77. Fothergill JL, Panagea S, Hart CA, Walshaw MJ, Pitt TL, Winstanley C: Widespread pyocyanin over-production among isolates of a cystic fibrosis epidemic strain. BMC Microbiol. 2007, 7:45.

78. Leisinger T, Margraff R: Secondary metabolites of the fluorescent pseudomonads. Microbiol. Rev. 1979, 43:422–442.

79. Wilson R, Sykes DA, Watson D, Rutman A, Taylor GW, Cole PJ: Measurement of Pseudomonas aeruginosa phenazine pigments in sputum and assessment of their contribution to sputum sol toxicity for respiratory epithelium. Infect. Immun. 1988, 56:2515–2517.

80. Wang Y, Newman DK: Redox reactions of phenazine antibiotics with ferric (hydr)oxides and molecular oxygen. Environ Sci Technol 2008, 42:2380–2386.

81. Wang Y, Wilks JC, Danhorn T, Ramos I, Croal L, Newman DK: Phenazine-1-carboxylic acid promotes bacterial biofilm development via ferrous iron acquisition. Journal of Bacteriology 2011, 193:3606–3617.

82. Dietrich LEP, Price-Whelan A, Petersen A, Whiteley M, Newman DK: The phenazine pyocyanin is a terminal signalling factor in the quorum sensing network of Pseudomonas aeruginosa. Mol Microbiol 2006, 61:1308–1321.

83. Price-Whelan A, Dietrich LEP, Newman DK: Pyocyanin alters redox homeostasis and carbon flux through central metabolic pathways in Pseudomonas aeruginosa PA14. Journal of Bacteriology 2007, 189:6372–6381.

84. Friedheim E, Michaelis L: Potentiometric study of pyocyanine. Journal of Biological Chemistry; 1931.

85. Hernandez ME, Kappler A, Newman DK: Phenazines and other redox-active antibiotics promote microbial mineral reduction. Applied and Environmental Microbiology 2004, 70:921–928.

86. Wang Y, Kern SE, Newman DK: Endogenous phenazine antibiotics promote anaerobic survival of Pseudomonas aeruginosa via extracellular electron transfer. Journal of Bacteriology 2010, 192:365–369.

87. Pierson LS, Pierson EA: Metabolism and function of phenazines in bacteria: impacts on the behavior of bacteria in the environment and biotechnological processes. Appl. Microbiol. Biotechnol. 2010, 86:1659–1670.

88. Da Re S, Ghigo J-M: A CsgD-independent pathway for cellulose production and biofilm formation in Escherichia coli. Journal of Bacteriology 2006, 188:3073–3087.

89. Giglio KM, Fong JC, Yildiz FH, Sondermann H: Structural basis for biofilm formation via the Vibrio cholerae matrix protein RbmA. Journal of Bacteriology 2013, doi:10.1128/JB.00374-13.

90. Asally M, Kittisopikul M, Rué P, Du Y, Hu Z, Cagatay T, Robinson AB, Lu H, Garcia-Ojalvo J, Süel GM: Localized cell death focuses mechanical forces during 3D patterning in a biofilm. Proceedings of the National Academy of Sciences 2012, 109:18891–18896.

91. Wilking JN, Zaburdaev V, De Volder M, Losick R, Brenner MP, Weitz DA: Liquid transport facilitated by channels in Bacillus subtilis biofilms. Proceedings of the National Academy of Sciences 2013, 110:848–852.

92. Dietrich LEP, Teal TK, Price-Whelan A, Newman DK: Redox-active antibiotics control gene expression and community behavior in divergent bacteria. Science 2008, 321:1203–1206.

93. Mavrodi DV, Blankenfeldt W, Thomashow LS: Phenazine compounds in fluorescent Pseudomonas spp. biosynthesis and regulation. Annu Rev Phytopathol 2006, 44:417–445.

94. Price-Whelan A, Dietrich LEP, Newman DK: Rethinking “secondary” metabolism: physiological roles for phenazine antibiotics. Nat Chem Biol 2006, 2:71–78.

95. Hernandez ME, Newman DK: Extracellular electron transfer. Cell. Mol. Life Sci. 2001, 58:1562–1571.

96. Friedheim EA: The effect of pyocyanine on the respiration of some normal tissues and tumours. Biochem. J. 1934, 28:173–179.

97. Barron ES: THE CATALYTIC EFFECT OF METHYLENE BLUE ON THE OXYGEN CONSUMPTION OF TUMORS AND NORMAL TISSUES. J. Exp. Med. 1930, 52:447–456.

98. Swan GA: The Chemistry of Heterocyclic Compounds, Phenazines. 1957.

99. Bauer C, Elsen S, Bird T: Mechanisms for redox control of gene expression. Annu. Rev. Microbiol. 1999, 53:495–523.

100. Tsaneva IR, Weiss B: soxR, a locus governing a superoxide response regulon in Escherichia coli K-12. Journal of Bacteriology 1990, 172:4197–4205.

101. Greenberg JT, Monach P, Chou JH, Josephy PD, Demple B: Positive control of a global antioxidant defense regulon activated by superoxide-generating agents in Escherichia coli. Proc. Natl. Acad. Sci. U.S.A. 1990, 87:6181–6185.

102. Tucker NP, Hicks MG, Clarke TA, Crack JC, Chandra G, Le Brun NE, Dixon R, Hutchings MI: The Transcriptional Repressor Protein NsrR Senses Nitric Oxide Directly via a [2Fe-2S] Cluster. PLoS ONE 2008, 3:–.

103. Kim SO, Orii Y, Lloyd D, Hughes MN, Poole RK: Anoxic function for the Escherichia coli flavohaemoglobin (Hmp): reversible binding of nitric oxide and reduction to nitrous oxide. FEBS Lett. 1999, 445:389–394.

104. Tucker NP, Le Brun NE, Dixon R, Hutchings MI: There's NO stopping NsrR, a global regulator of the bacterial NO stress response. Trends in Microbiology 2010, 18:149–156.

105. Justino MC, Almeida CC, Teixeira M, Saraiva LM: Escherichia coli di-iron YtfE protein is necessary for the repair of stress-damaged iron-sulfur clusters. J. Biol. Chem. 2007, 282:10352–10359.

106. Heurlier K, Thomson MJ, Aziz N, Moir JWB: The nitric oxide (NO)-sensing repressor NsrR of Neisseria meningitidis has a compact regulon of genes involved in NO synthesis and detoxification. Journal of Bacteriology 2008, 190:2488–2495.

107. Stevanin TM, Moir JWB, Read RC: Nitric oxide detoxification systems enhance survival of Neisseria meningitidis in human macrophages and in nasopharyngeal mucosa. Infect. Immun. 2005, 73:3322–3329.

108. Cruz Dela R, Gao Y, Penumetcha S, Sheplock R, Weng K, Chander M: Expression of the Streptomyces coelicolor SoxR regulon is intimately linked with actinorhodin production. Journal of Bacteriology 2010, 192:6428–6438.

109. Gu M, Imlay JA: The SoxRS response of Escherichia coli is directly activated by redox-cycling drugs rather than by superoxide. Mol Microbiol 2011, 79:1136–1150.

110. Pomposiello PJ, Bennik MH, Demple B: Genome-wide transcriptional profiling of the Escherichia coli responses to superoxide stress and sodium salicylate. Journal of Bacteriology 2001, 183:3890–3902.

111. Palma M, Zurita J, Ferreras JA, Worgall S, Larone DH, Shi L, Campagne F, Quadri LEN: Pseudomonas aeruginosa SoxR does not conform to the archetypal paradigm for SoxR-dependent regulation of the bacterial oxidative stress adaptive response. Infect. Immun. 2005, 73:2958–2966.

112. Shin J-H, Singh AK, Cheon D-J, Roe J-H: Activation of the SoxR regulon in Streptomyces coelicolor by the extracellular form of the pigmented antibiotic actinorhodin. Journal of Bacteriology 2011, 193:75–81.

113. Barraud N, Schleheck D, Klebensberger J, Webb JS, Hassett DJ, Rice SA, Kjelleberg S: Nitric oxide signaling in Pseudomonas aeruginosa biofilms mediates phosphodiesterase activity, decreased cyclic di-GMP levels, and enhanced dispersal. Journal of Bacteriology 2009, 191:7333–7342.

114. Van Alst NE, Picardo KF, Iglewski BH, Haidaris CG: Nitrate sensing and metabolism modulate motility, biofilm formation, and virulence in Pseudomonas aeruginosa. Infect. Immun. 2007, 75:3780–3790.

115. Webb JS, Thompson LS, James S, Charlton T, Tolker-Nielsen T, Koch B, Givskov M, Kjelleberg S: Cell death in Pseudomonas aeruginosa biofilm development. Journal of Bacteriology 2003, 185:4585–4592.

116. Barraud N, Hassett DJ, Hwang S-H, Rice SA, Kjelleberg S, Webb JS: Involvement of nitric oxide in biofilm dispersal of Pseudomonas aeruginosa. Journal of Bacteriology 2006, 188:7344–7353.

117. Muller M: Scavenging of neutrophil-derived superoxide anion by 1-hydroxyphenazine, a phenazine derivative associated with chronic Pseudomonas aeruginosa infection: relevance to cystic fibrosis. Biochim. Biophys. Acta 1995, 1272:185–189.

118. Serra DO, Richter AM, Klauck G, Mika F, Hengge R: Microanatomy at cellular resolution and spatial order of physiological differentiation in a bacterial biofilm. MBio 2013, 4:e00103–13.

119. Zogaj X, Nimtz M, Rohde M, Bokranz W, Römling U: The multicellular morphotypes of Salmonella typhimurium and Escherichia coli produce cellulose as the second component of the extracellular matrix. Mol Microbiol 2001, 39:1452–1463.

120. Römling U, Rohde M, Olsén A, Normark S, Reinköster J: AgfD, the checkpoint of multicellular and aggregative behaviour in Salmonella typhimurium regulates at least two independent pathways. Mol Microbiol 2000, 36:10–23.

121. Srivastava D, Hsieh M-L, Khataokar A, Neiditch MB, Waters CM: Cyclic di-GMP inhibits Vibrio cholerae motility by repressing induction of transcription and inducing extracellular polysaccharide production. Mol Microbiol 2013, doi:10.1111/mmi.12432.

122. Gerstel U, Römling U: Oxygen tension and nutrient starvation are major signals that regulate agfD promoter activity and expression of the multicellular morphotype in Salmonella typhimurium. Environmental Microbiology 2001, 3:638–648.

123. White AP, Weljie AM, Apel D, Zhang P, Shaykhutdinov R, Vogel HJ, Surette MG: A global metabolic shift is linked to Salmonella multicellular development. PLoS ONE 2010, 5:e11814.

124. Vlamakis H, Chai Y, Beauregard P, Losick R, Kolter R: Sticking together: building a biofilm the Bacillus subtilis way. Nature Publishing Group 2013, 11:157–168.

125. Henry JT, Crosson S: Ligand-Binding PAS Domains in a Genomic, Cellular, and Structural Context. Annu. Rev. Microbiol. 2011, 65:261–286.

126. ROSS P, MAYER R, BENZIMAN M: Cellulose biosynthesis and function in bacteria. Microbiol. Rev. 1991, 55:35–58.

127. Wolfe AJ, Visick KL, Microbiology ASF: The second messenger cyclic Di-GMP. Washington, DC : ASM Press; 2010.

128. D'Argenio DA, Miller SI: Cyclic di-GMP as a bacterial second messenger. Microbiology (Reading, Engl.) 2004, 150:2497–2502.

129. Jenal U: Cyclic di-guanosine-monophosphate comes of age: a novel secondary messenger involved in modulating cell surface structures in bacteria? Current Opinion in Microbiology 2004, 7:185–191.

130. Jenal U, Malone J: Mechanisms of cyclic-di-GMP signaling in bacteria. Annu. Rev. Genet. 2006, 40:385–407.

131. Römling U, Gomelsky M, Galperin MY: C-di-GMP: the dawning of a novel bacterial signalling system. Mol Microbiol 2005, 57:629–639.

132. Römling U, Amikam D: Cyclic di-GMP as a second messenger. Current Opinion in Microbiology 2006, 9:218–228.

133. Tamayo R, Pratt JT, Camilli A: Roles of cyclic diguanylate in the regulation of bacterial pathogenesis. Annu. Rev. Microbiol. 2007, 61:131–148.

134. Chen Z-H, Schaap P: The prokaryote messenger c-di-GMP triggers stalk cell differentiation in Dictyostelium. Nature 2012, 488:680–683.

135. Kulasakara H, Lee V, Brencic A, Liberati N, Urbach J, Miyata S, Lee DG, Neely AN, Hyodo M, Hayakawa Y, et al.: Analysis of Pseudomonas aeruginosa diguanylate cyclases and phosphodiesterases reveals a role for bis-(3“-5”)-cyclic-GMP in virulence. Proc. Natl. Acad. Sci. U.S.A. 2006, 103:2839–2844.

136. Ha D-G, Richman ME, O'Toole GA: Deletion mutant library for investigation of functional outputs of cyclic diguanylate metabolism in Pseudomonas aeruginosa PA14. Applied and Environmental Microbiology 2014, 80:3384–3393.

137. Ryan RP, Lucey J, O'Donovan K, McCarthy Y, Yang L, Tolker-Nielsen T, Dow JM: HD-GYP domain proteins regulate biofilm formation and virulence in Pseudomonas aeruginosa. Environmental Microbiology 2009, 11:1126–1136.

138. ROSS P, WEINHOUSE H, ALONI Y, MICHAELI D, WEINBERGEROHANA P, MAYER R, BRAUN S, DEVROOM E, VANDERMAREL GA, VANBOOM JH, et al.: Regulation of Cellulose Synthesis in Acetobacter-Xylinum by Cyclic Diguanylic Acid. Nature 1987, 325:279–281.

139. Paul R, Abel S, Wassmann P, Beck A, Heerklotz H, Jenal U: Activation of the diguanylate cyclase PleD by phosphorylation-mediated dimerization. J. Biol. Chem. 2007, 282:29170–29177.

140. Römling U, Galperin MY, Gomelsky M: Cyclic di-GMP: the First 25 Years of a Universal Bacterial Second Messenger. Microbiol. Mol. Biol. Rev. 2013, 77:1–52.

141. Pei J, Grishin NV: GGDEF domain is homologous to adenylyl cyclase. Proteins 2001, 42:210–216.

142. Schirmer T, Jenal U: Structural and mechanistic determinants of c-di-GMP signalling. Nature Publishing Group 2009, 7:724–735.

143. Galperin MY: Bacterial signal transduction network in a genomic perspective. Environmental Microbiology 2004, 6:552–567.

144. Galperin MY, Nikolskaya AN, Koonin EV: Novel domains of the prokaryotic two-component signal transduction systems. FEMS Microbiol. Lett. 2001, 203:11–21.

145. Güvener ZT, Harwood CS: Subcellular location characteristics of the Pseudomonas aeruginosa GGDEF protein, WspR, indicate that it produces cyclic-di-GMP in response to growth on surfaces. Mol Microbiol 2007, 66:1459–1473.

146. Hickman JW, Tifrea DF, Harwood CS: A chemosensory system that regulates biofilm formation through modulation of cyclic diguanylate levels. Proc. Natl. Acad. Sci. U.S.A. 2005, 102:14422–14427.

147. De N, Navarro MVAS, Raghavan RV, Sondermann H: Determinants for the activation and autoinhibition of the diguanylate cyclase response regulator WspR. J. Mol. Biol. 2009, 393:619–633.

148. Wassmann P, Chan C, Paul R, Beck A, Heerklotz H, Jenal U, Schirmer T: Structure of BeF3- -modified response regulator PleD: implications for diguanylate cyclase activation, catalysis, and feedback inhibition. Structure 2007, 15:915–927.

149. Ryjenkov DA, Tarutina M, Moskvin OV, Gomelsky M: Cyclic diguanylate is a ubiquitous signaling molecule in bacteria: insights into biochemistry of the GGDEF protein domain. Journal of Bacteriology 2005, 187:1792–1798.

150. Chan C, Paul R, Samoray D, Amiot NC, Giese B, Jenal U, Schirmer T: Structural basis of activity and allosteric control of diguanylate cyclase. Proc. Natl. Acad. Sci. U.S.A. 2004, 101:17084–17089.

151. Salter EA, Wierzbicki A: The mechanism of cyclic nucleotide hydrolysis in the phosphodiesterase catalytic site. J Phys Chem B 2007, 111:4547–4552.

152. Rao F, Qi Y, Chong HS, Kotaka M, Li B, Li J, Lescar J, Tang K, Liang Z-X: The functional role of a conserved loop in EAL domain-based cyclic di-GMP-specific phosphodiesterase. Journal of Bacteriology 2009, 191:4722–4731.

153. Bobrov AG, Kirillina O, Perry RD: The phosphodiesterase activity of the HmsP EAL domain is required for negative regulation of biofilm formation in Yersinia pestis. FEMS Microbiol. Lett. 2005, 247:123–130.

154. Schmidt AJ, Ryjenkov DA, Gomelsky M: The ubiquitous protein domain EAL is a cyclic diguanylate-specific phosphodiesterase: enzymatically active and inactive EAL domains. Journal of Bacteriology 2005, 187:4774–4781.

155. Navarro MVAS, De N, Bae N, Wang Q, Sondermann H: Structural analysis of the GGDEF-EAL domain-containing c-di-GMP receptor FimX. Structure 2009, 17:1104–1116.

156. Rao F, Yang Y, Qi Y, Liang Z-X: Catalytic mechanism of cyclic di-GMP-specific phosphodiesterase: a study of the EAL domain-containing RocR from Pseudomonas aeruginosa. Journal of Bacteriology 2008, 190:3622–3631.

157. Tarutina M, Ryjenkov DA, Gomelsky M: An unorthodox bacteriophytochrome from Rhodobacter sphaeroides involved in turnover of the second messenger c-di-GMP. J. Biol. Chem. 2006, 281:34751–34758.

158. Barends TRM, Hartmann E, Griese JJ, Beitlich T, Kirienko NV, Ryjenkov DA, Reinstein J, Shoeman RL, Gomelsky M, Schlichting I: Structure and mechanism of a bacterial light-regulated cyclic nucleotide phosphodiesterase. Nature 2009, 459:1015–1018.

159. Minasov G, Padavattan S, Shuvalova L, Brunzelle JS, Miller DJ, Baslé A, Massa C, Collart FR, Schirmer T, Anderson WF: Crystal structures of YkuI and its complex with second messenger cyclic Di-GMP suggest catalytic mechanism of phosphodiester bond cleavage by EAL domains. J. Biol. Chem. 2009, 284:13174–13184.

160. Tchigvintsev A, Xu X, Singer A, Chang C, Brown G, Proudfoot M, Cui H, Flick R, Anderson WF, Joachimiak A, et al.: Structural insight into the mechanism of c-di-GMP hydrolysis by EAL domain phosphodiesterases. J. Mol. Biol. 2010, 402:524–538.

161. Gomelsky M, Hoff WD: Light helps bacteria make important lifestyle decisions. Trends in Microbiology 2011, 19:441–448.

162. Gomelsky M, Klug G: BLUF: a novel FAD-binding domain involved in sensory transduction in microorganisms. Trends Biochem. Sci. 2002, 27:497–500.

163. Galperin MY, Koonin EV: Divergence and convergence in enzyme evolution. J. Biol. Chem. 2012, 287:21–28.

164. Bellini D, Caly DL, McCarthy Y, Bumann M, An S-Q, Dow JM, Ryan RP, Walsh MA: Crystal structure of an HD-GYP domain cyclic-di-GMP phosphodiesterase reveals an enzyme with a novel trinuclear catalytic iron centre. Mol Microbiol 2013, 91:26–38.

165. Ryan RP, Fouhy Y, Lucey JF, Crossman LC, Spiro S, He Y-W, Zhang L-H, Heeb S, Cámara M, Williams P, et al.: Cell-cell signaling in Xanthomonas campestris involves an HD-GYP domain protein that functions in cyclic di-GMP turnover. Proc. Natl. Acad. Sci. U.S.A. 2006, 103:6712–6717.

166. Sultan SZ, Pitzer JE, Boquoi T, Hobbs G, Miller MR, Motaleb MA: Analysis of the HD-GYP domain cyclic dimeric GMP phosphodiesterase reveals a role in motility and the enzootic life cycle of Borrelia burgdorferi. Infect. Immun. 2011, 79:3273–3283.

167. Tal R, Wong HC, Calhoon R, Gelfand D, Fear AL, Volman G, MAYER R, ROSS P, Amikam D, WEINHOUSE H, et al.: Three cdg operons control cellular turnover of cyclic di-GMP in Acetobacter xylinum: genetic organization and occurrence of conserved domains in isoenzymes. Journal of Bacteriology 1998, 180:4416–4425.

168. Seshasayee ASN, Fraser GM, Luscombe NM: Comparative genomics of cyclic-di-GMP signalling in bacteria: post-translational regulation and catalytic activity. Nucleic Acids Res. 2010, 38:5970–5981.

169. Bharati BK, Sharma IM, Kasetty S, Kumar M, Mukherjee R, Chatterji D: A full-length bifunctional protein involved in c-di-GMP turnover is required for long-term survival under nutrient starvation in Mycobacterium smegmatis. Microbiology (Reading, Engl.) 2012, 158:1415–1427.

170. Ferreira RBR, Antunes LCM, Greenberg EP, McCarter LL: Vibrio parahaemolyticus ScrC modulates cyclic dimeric GMP regulation of gene expression relevant to growth on surfaces. Journal of Bacteriology 2008, 190:851–860.

171. Levet-Paulo M, Lazzaroni J-C, Gilbert C, Atlan D, Doublet P, Vianney A: The atypical two-component sensor kinase Lpl0330 from Legionella pneumophila controls the bifunctional diguanylate cyclase-phosphodiesterase Lpl0329 to modulate bis-(3“-5”)-cyclic dimeric GMP synthesis. J. Biol. Chem. 2011, 286:31136–31144.

172. Hickman JW, Harwood CS: Identification of FleQ from Pseudomonas aeruginosa as a c-di-GMP-responsive transcription factor. Mol Microbiol 2008, 69:376–389.

173. Baraquet C, Murakami K, Parsek MR, Harwood CS: The FleQ protein from Pseudomonas aeruginosa functions as both a repressor and an activator to control gene expression from the pel operon promoter in response to c-di-GMP. Nucleic Acids Res. 2012, 40:7207–7218.

174. Jyot J, Dasgupta N, Ramphal R: FleQ, the major flagellar gene regulator in Pseudomonas aeruginosa, binds to enhancer sites located either upstream or atypically downstream of the RpoN binding site. Journal of Bacteriology 2002, 184:5251–5260.

175. Ha D-G, O'Toole GA: c-di-GMP and its Effects on Biofilm Formation and Dispersion: a Pseudomonas Aeruginosa Review. Microbiol Spectr 2015, 3.

176. Caiazza NC, Merritt JH, Brothers KM, O'Toole GA: Inverse regulation of biofilm formation and swarming motility by Pseudomonas aeruginosa PA14. Journal of Bacteriology 2007, 189:3603–3612.

177. Lee VT, Matewish JM, Kessler JL, Hyodo M, Hayakawa Y, Lory S: A cyclic-di-GMP receptor required for bacterial exopolysaccharide production. Mol Microbiol 2007, 65:1474–1484.

178. Whitney JC, Colvin KM, Marmont LS, Robinson H, Parsek MR, Howell PL: Structure of the cytoplasmic region of PelD, a degenerate diguanylate cyclase receptor that

regulates exopolysaccharide production in Pseudomonas aeruginosa. J. Biol. Chem. 2012, 287:23582–23593.

179. Li Z, Chen J-H, Hao Y, Nair SK: Structures of the PelD cyclic diguanylate effector involved in pellicle formation in Pseudomonas aeruginosa PAO1. J. Biol. Chem. 2012, 287:30191–30204.

180. Kuchma SL, Brothers KM, Merritt JH, Liberati NT, Ausubel FM, O'Toole GA: BifA, a cyclic-Di-GMP phosphodiesterase, inversely regulates biofilm formation and swarming motility by Pseudomonas aeruginosa PA14. Journal of Bacteriology 2007, 189:8165–8178.

181. Merritt JH, Ha D-G, Cowles KN, Lu W, Morales DK, Rabinowitz J, Gitai Z, O'Toole GA: Specific control of Pseudomonas aeruginosa surface-associated behaviors by two c-di-GMP diguanylate cyclases. MBio 2010, 1.

182. Yoon SS, Hennigan RF, Hilliard GM, Ochsner UA, Parvatiyar K, Kamani MC, Allen HL, DeKievit TR, Gardner PR, Schwab U, et al.: Pseudomonas aeruginosa Anaerobic Respiration in Biofilms. Dev. Cell 2002, 3:593–603.

183. Sauer K, Cullen MC, Rickard AH, Zeef LAH, Davies DG, Gilbert P: Characterization of nutrient-induced dispersion in Pseudomonas aeruginosa PAO1 biofilm. Journal of Bacteriology 2004, 186:7312–7326.

184. Roy AB, Petrova OE, Sauer K: The phosphodiesterase DipA (PA5017) is essential for Pseudomonas aeruginosa biofilm dispersion. Journal of Bacteriology 2012, 194:2904–2915.

185. Morgan R, Kohn S, Hwang S-H, Hassett DJ, Sauer K: BdlA, a chemotaxis regulator essential for biofilm dispersion in Pseudomonas aeruginosa. Journal of Bacteriology 2006, 188:7335–7343.

186. Petrova OE, Sauer K: Dispersion by Pseudomonas aeruginosa requires an unusual posttranslational modification of BdlA. Proceedings of the National Academy of Sciences 2012, 109:16690–16695.

187. Möglich A, Ayers RA, Moffat K: Structure and signaling mechanism of Per-ARNT-Sim domains. Structure 2009, 17:1282–1294.

188. Gu YZ, Hogenesch JB, Bradfield CA: The PAS superfamily: sensors of environmental and developmental signals. Annu. Rev. Pharmacol. Toxicol. 2000, 40:519–561.

189. Reddy P, Jacquier AC, Abovich N, Petersen G, Rosbash M: The period clock locus of D. melanogaster codes for a proteoglycan. Cell 1986, 46:53–61.

190. Moura-Alves P, Faé K, Houthuys E, Dorhoi A, Kreuchwig A, Furkert J, Barison N, Diehl A, Munder A, Constant P, et al.: AhR sensing of bacterial pigments regulates antibacterial defence. Nature 2014, 512:387–392.

191. Nambu JR, Lewis JO, Wharton KA, Crews ST: The Drosophila single-minded gene encodes a helix-loop-helix protein that acts as a master regulator of CNS midline development. Cell 1991, 67:1157–1167.

192. Herrmann S, Ma Q, Johnson MS, Repik AV, Taylor BL: PAS domain of the Aer redox sensor requires C-terminal residues for native-fold formation and flavin adenine dinucleotide binding. Journal of Bacteriology 2004, 186:6782–6791.

193. McIntosh BE, Hogenesch JB, Bradfield CA: Mammalian Per-Arnt-Sim proteins in environmental adaptation. Annu. Rev. Physiol. 2010, 72:625–645.

194. Möglich A, Ayers RA, Moffat K: Addition at the molecular level: signal integration in designed Per-ARNT-Sim receptor proteins. J. Mol. Biol. 2010, 400:477–486.

195. Taylor BL, Zhulin IB: PAS domains: internal sensors of oxygen, redox potential, and light. Microbiol. Mol. Biol. Rev. 1999, 63:479–506.

196. Ulrich LE, Koonin EV, Zhulin IB: One-component systems dominate signal transduction in prokaryotes. Trends in Microbiology 2005, 13:52–56.

197. Vreede J, van der Horst MA, Hellingwerf KJ, Crielaard W, van Aalten DMF: PAS domains. Common structure and common flexibility. J. Biol. Chem. 2003, 278:18434–18439.

198. Xie Z, Ulrich LE, Zhulin IB, Alexandre G: PAS domain containing chemoreceptor couples dynamic changes in metabolism with chemotaxis. Proceedings of the National Academy of Sciences 2010, 107:2235–2240.

199. Semenza GL: Hypoxia-inducible factor 1: oxygen homeostasis and disease pathophysiology. Trends Mol Med 2001, 7:345–350.

200. Ravi R, Mookerjee B, Bhujwalla ZM, Sutter CH, Artemov D, Zeng Q, Dillehay LE, Madan A, Semenza GL, Bedi A: Regulation of tumor angiogenesis by p53-induced degradation of hypoxia-inducible factor 1alpha. Genes Dev. 2000, 14:34–44.

201. Repik A, Rebbapragada A, Johnson MS, Haznedar JO, Zhulin IB, Taylor BL: PAS domain residues involved in signal transduction by the Aer redox sensor of Escherichia coli. Mol Microbiol 2000, 36:806–816.

202. Edgar RS, Green EW, Zhao Y, van Ooijen G, Olmedo M, Qin X, Xu Y, Pan M, Valekunja UK, Feeney KA, et al.: Peroxiredoxins are conserved markers of circadian rhythms. Nature 2012, 485:459–464.

203. Little R, Slavny P, Dixon R: Influence of PAS domain flanking regions on oligomerisation and redox signalling by NifL. PLoS ONE 2012, 7:e46651.

Chapter 2

Bacterial Community Morphogenesis Is Intimately Linked to the Intracellular Redox State

Lars E. P. Dietrich, Chinweike Okegbe, Alexa Price-Whelan, Hassan Sakhtah, Ryan C. Hunter, Dianne K. Newman

Data within published in Journal of Bacteriology 2013

Author contributions:

H.S. contributed the thin sections and analysis in Figures 2-2 A-G and 2-7, G. Squyres contributed colony images in Figure 2-5 A, A.P-W. contributed complement strain in Figure 2-8. C.O.contributed all remaining experiments.

2-1 ABSTRACT

Many microbial species form multicellular structures comprising elaborate wrinkles and concentric rings, yet the rules govern- ing their architecture are poorly understood. The opportunistic pathogen *Pseudomonas aeruginosa* produces phenazines, small molecules that act as alternate electron acceptors to oxygen and nitrate to oxidize the intracellular redox state and that influence biofilm morphogenesis. Here, we show that the depth occupied by cells within colony biofilms correlates well with electron acceptor availability. Perturbations in the environmental provision, endogenous production, and utilization of electron acceptors affect colony development in a manner consistent with redox control. Intracellular NADH levels peak before the induction of colony wrinkling. These results suggest that redox imbalance is a major factor driving the morphogenesis of *P. aeruginosa* biofilms and that wrinkling itself is an adaptation that maximizes oxygen accessibility and thereby supports metabolic homeostasis. This type of redox-driven morphological change is reminiscent of developmental processes that occur in metazoans.

2-2 INTRODUCTION

The ubiquity of multicellularity—a property observed in all three domains of life—underscores the advantages conferred on organisms that assume this lifestyle (1, 2). Multicellularity allows division of labor, as well as protection from environmental insults, but also presents a significant challenge by exacerbating limitations for growth substrates. Eukaryotic macroorganisms alleviate this problem in part through (i) internal circulation that allows delivery of substrates to specific locations and (ii) metabolic differentiation. Although the significance of the multicellular lifestyle for metabolism and pathogenicity of microorganisms is well recognized (3–5), the mechanisms enabling microbial communities to cope with substrate limitation are poorly defined.

Pseudomonas aeruginosa is a leading causative agent of nosocomial infections that forms biofilms (i.e., surface-attached communities) on indwelling medical devices or tissues within the

host. It is also the primary cause of morbidity and mortality among people with cystic fibrosis, in whom it aggregates within accumulated mucus, causing chronic lung infections (6). The fact that *P. aeruginosa* forms biofilms in a variety of model laboratory systems has allowed researchers to identify mechanisms important for biofilm and aggregate formation. Our research has focused on the intricate structures formed by communities of *P. aeruginosa* as they grow on the surfaces of rich media solidified with agar ("colony biofilms"). Colony morphogenesis is highly dependent on the presence of endogenously produced redox-active small molecules called phenazines; colonies that produce phenazines are relatively smooth as they develop, while mutants that are unable to produce phenazines are more rugose and start wrinkling earlier in the incubation period (7) (Fig. 2-1A). Similar results have been obtained for flow cell biofilms (8). The phenazines produced by *P. aeruginosa* vary in structure and chemical properties (9, 10), but their redox potentials are such that they all can be reduced by the bacterial cell and react extracellularly with higher-potential oxidants, such as ferric iron and oxygen, acting as electron shuttles between the bacterium and an external substrate (11).

In the early 20th century, E. S. Guzman Barron, Ernst Friedheim, and others postulated that redox-cycling compounds such as phenazines are "accessory respiratory pigments" that can sustain bacterial "respiration" based on their ability to stimulate oxygen consumption in suspensions of many different types of cells (12–14). They speculated that these compounds can extend the depth of respiration for cells deprived of oxygen, such as those found in normal tissues and tumors (15, 16). This work was carried out before respiratory pathways were fully understood and well before the importance of microbial biofilms in nature and disease was widely recognized. In this regard, Barron, Friedheim, and their colleagues were both ahead of their time and handicapped by a lack of information. In the interval between these pioneering studies and the present work, attention shifted to exploring the roles of phenazines as virulence factors (17). Over a decade ago, we revived the "respiratory pigment" hypothesis in a biofilm context, speculating that the capacity for extracellular electron transfer might provide a physiological benefit for oxidant-limited cells (9, 18). While it has long been

appreciated that biofilms are metabolically heterogeneous and that oxygen avail- ability defines different metabolic zones (19, 20), to the best of our knowledge, no study has yet demonstrated that endogenous electron shuttles such as phenazines increase the habitability zone for biofilm cells. Evidence in support of this hypothesis, until now, has been indirect (21). Here, we test the hypothesis directly and go beyond it to demonstrate that the intracellular redox state, not phenazines per se, correlates with colony morphological development.

2-3 MATERIALS AND METHODS

2-3-1 Strains and growth conditions.

The strains used in this study are listed in Table 2-1. For routine liquid cultures, *P. aeruginosa* PA14 was grown in 3 ml lysogeny broth (LB) (22) in 12 by 100-mm tubes at 37°C with shaking at 250 rpm. Growth conditions for colonies are described below.

2-3-2 Construction of deletion and complementation plasmids.

Unmarked deletions were generated for the genes *napA* and *narG* in PA14 wild-type and Δ*phz* backgrounds. Deletion plasmids were generated using yeast gap repair cloning. Flanking regions (~1 kb in length) for *napA* and *narG* were generated using primers listed in Table 2-2. The flanking regions and the linearized allelic-replacement vector pMQ30 were assembled by gap repair cloning using the yeast strain InvSc1 (23). The resulting deletion plasmid was transformed into *Escherichia coli* BW29427 and mobilized into PA14 using biparental conjugation. PA14 single recombinants were selected on LB agar containing 100µg/ml gentamicin. Potential *napA* or *narG* deletion mutants were generated by selecting for double recombinants by identifying strains that grew in the presence of 10% sucrose. Strains with properties of double recombination were further analyzed by PCR for the desired deletion.

For construction of the *nap* operon complementation plasmid pAPW1, primers were designed using the *P. aeruginosa* PA14 genome sequence to anneal 490 bp upstream of *napE* and to

the last 19 bases of *napC*, yielding a PCR product including the *napEFDABC* operon and a putative promoter region. The amplified DNA was digested using restriction sites (HindIII and NheI) engineered within the primers. It was then ligated into plasmid pMQ72 digested with the same restriction enzymes and treated with calf intestinal phosphatase (Sigma). The resulting plasmid, pAPW1, contains the *napEFDABC* operon under the control of its native promoter.

2-3-3 Colony morphology assay.

Agar plates for colony morphology exper- iments were prepared as follows. A mixture of 1% agar (Teknova) and 1% tryptone (Teknova) was autoclaved and cooled to 60°C before 20 f..g/ml Coomassie blue (EMD) and 40µg/ml Congo red (EMD) were added. Sixty milliliters of medium was poured per 10-cm-square plate (Simport; D210-16) and allowed to dry with closed lids at room temperature for 24 h. For colony spotting and developmental studies, precultures were inoculated from single streak plate colonies and grown in LB medium for 12 h. Ten microliters of the preculture was spotted on plates and incubated for up to 6 days at 23 to 25°C. Colony images were taken daily with a digital microscope (Keyence; VHX-1000).

For colony development at different oxygen concentrations (15%, 21%, and 40%), we incubated plates in C-Chambers (BioSpherix; C274). Oxygen concentrations were regulated by mixing pure nitrogen and oxy- gen (TechAir) using the gas controller ProOx P110 (BioSpherix). Each chamber contained an open 10-cm round plate filled with 25 ml of water to keep the chambers humid. Humidity was monitored using an iButton Humidity Data Sensor (Maxim) and maintained at >90%. For colony growth under anoxic conditions, plates were stored in an anaerobic glove box filled with 80% N_2, 15% CO_2, and 5% H_2.

2-3-4 Preparation and imaging of colony thin sections.

Colonies were covered with 4% paraformaldehyde and allowed to fix for 10 min. The colonies were then lifted from the agar by gently shaking the plate and allowed to fix for an additional 10 min. Following this, the colonies were transferred into a wash basket, and the fixative was

removed by washing the colonies three times in phosphate-buffered saline (PBS). Excess PBS was removed by washing in 25%, 50%, and 75% Tissue-Tek OCT (Sakura; no. 4583) in PBS before the colonies were transferred to disposable embedding molds (Electron Microscopy Sciences; no. 70182) and overlaid with Tissue-Tek OCT. After flash freezing in a dry-ice– ethanol slurry, the samples were stored at -80°C. The frozen samples were cut into 10-μ.m-thick sections using a Leica CM1850 microtome at -16°C. The sections were collected on Thermo Superfrost Plus slides (no. 6776214) and stored at -80°C until imaging.

Thin sections were photographed using a Zeiss Axio Imager 2. All images were obtained at x10 magnification using a Zeiss EC-Plan Neofluar objective with differential interference contrast (DIC) and fluorescence optics. The images were taken at an exposure time of 328 ms, false colored, and processed in Photoshop CS4 (Adobe).

2-3-5 Oxygen measurements.

Oxygen profiles were taken using a miniaturized Clark-type oxygen sensor (Unisense; 10μm tip diameter). The electrode was connected to a picoampere amplifier multimeter (Unisense) and polarized with -0.8 V. The sensor was calibrated using a two-point calibration system. The atmospheric oxygen reading was obtained by placing the electrode in a calibration chamber (Unisense) that contained well-aerated deionized water. Complete aeration was achieved by constantly bubbling the water with air. The zero reading was obtained by bubbling water in the calibration chamber with ultra-high-purity nitrogen gas (TechAir). All calibration readings and profile measurements were obtained using SensorTrace pro 2.0 software (Unisense).

2-3-6 NADH/NAD+ assay.

Extraction and quantification of NADH and NAD^+ were carried out according to the methods described by San et al. (24) and Bernofsky and Swan (25). For cultures grown in LB, two 1-ml samples of culture were placed in two separate microcentrifuge tubes and centrifuged at 16,000 *xg* for 1 min. Colonies grown on 1% tryptone and 1% agar plates amended with 40μg/ml Congo

red and 20μg/ml Coomassie blue dyes were scraped off the agar plate at the indicated time points using sterile razor blades and resuspended in 1 ml of 1% tryptone. The colonies were disrupted using a pellet disrupter. For each resuspended colony, two 450 μL samples were placed into two separate microcentrifuge tubes. NADH and NAD^+ were then extracted from the liquid culture- or colony-derived samples, and relative or absolute quantification was carried out using an enzyme-cycling assay, as described by Price-Whelan et al. (26)

2-4 RESULTS AND DISCUSSION

In this study, we set out to characterize the relationship between redox metabolism/electron acceptor availability and *P. aeruginosa* biofilm development. This work supports the hypothesis that phenazine production and colony rugosity are adaptations that facilitate survival by mitigating electron acceptor limitation. In homogeneous liquid cultures of *P. aeruginosa*, phenazines affect gene expression and oxidize the intracellular redox state (26–28). Under conditions where no other oxidant is available, phenazine-dependent electron transfer between cells and an oxidizing electrode supports survival (21). Given that cells in biofilms experience steep gradients in oxygen availability, leading to hypoxia or anoxia at a distance from the surface (19, 20), we reasoned that the morphological switch observed in phenazine-deficient colonies is related to their limited ability to access oxidants.

To test this hypothesis, we first characterized the depth of oxygen penetration within our colony biofilm system. *P. aeruginosa* phenazine-null (Δ*phz*) biofilms characteristically increase their surface area relative to wild-type communities. Δ*phz* colonies also produce more exopolysaccharides than wild-type colonies (7). We therefore asked whether dissolved oxygen concentrations differed in the wild-type and Δ*phz* biofilms when they were grown under atmospheric (21%) oxygen on a nutrient-rich complex medium (1% tryptone, 1% agar containing 20μg/ml Coomassie blue and 40μg/ml Congo red). Measurements taken with a Clark oxygen electrode (10μm tip) revealed steep gradients, with oxygen becoming undetectable 60μm into the colony when the base area was profiled (Fig. 2-1B). Qualitatively, this is consistent

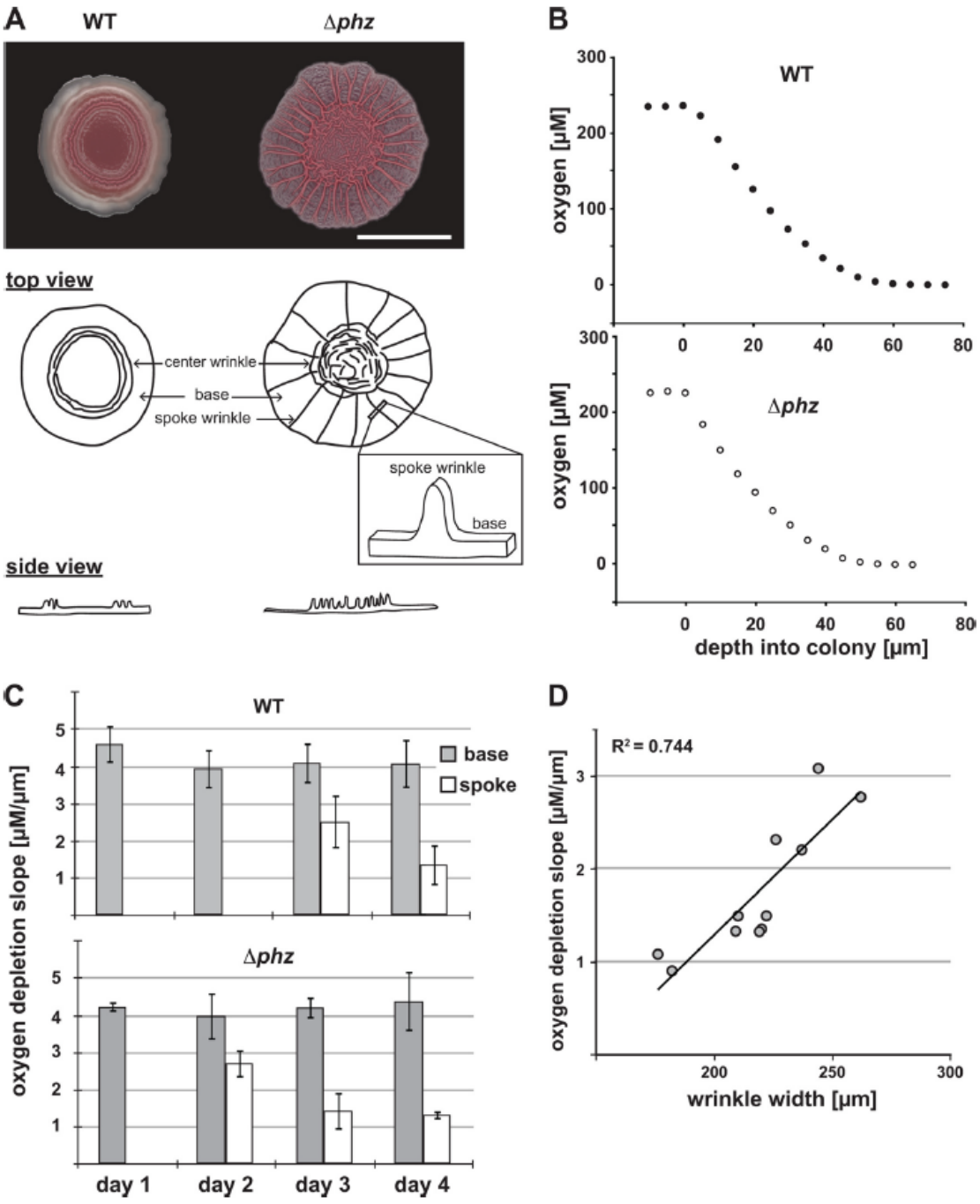

Figure 2-1. *P. aeruginosa* colony morphotypes and oxygen profiles. (A) Graphical representation of terms used to describe features within P. aeruginosa colonies. WT, wild type; Δ*phz*, phenazine-null mutant. The scale bar represents 1 cm, and the images were taken after 3 days of colony development. (B) Oxygen profiles in colony biofilms. Oxygen concentrations were measured in P. aeruginosa colonies on day 3 as a function of microelectrode depth in the colony. (C) Oxygen depletion (calculated as the initial slope, typically between 0- and 20- μm depth, of oxygen profiles over depth in the colony, as depicted in panel B) for the base and a wrinkle (spoke) during colony development. Wrinkles appear in Δ*phz* colonies 1 day earlier than in WT colonies. The error bars represent the standard deviations of this measurement in the bases or wrinkles of 5 independent colonies. (D) Oxygen depletion slopes from Δ*phz* colonies (representing data plotted in panel C) shown as a function of wrinkle thickness.

with oxygen microelectrode measurements of *P. aeruginosa* biofilms grown in flow cells showing oxygen depletion at depth due to the combined effects of consumption and diffusion limitation (20). The extent of oxygen depletion in the base remained constant over 4 days (Fig. 2-1C). When we measured oxygen depletion in emerging wrinkles, its slope was lower and decreased over time compared to the base. We found that wrinkle thickness correlated with oxygen abundance: thinner wrinkles were less oxygen depleted than thicker wrinkles (Fig. 2-1D).

While respiratory versatility is a hallmark of some bacterial species, *P. aeruginosa* is relatively limited in this regard. It can grow by aerobic respiration and denitrification and poorly by arginine fermentation (29); therefore, the major energy-generating metabolism contributing to growth of colonies on 1% tryptone is aerobic respiration. Moreover, it is generally believed that in the organic-rich environment of infections—such as the mucus that collects on the lungs of individuals with cystic fibrosis— growth and survival of *Pseudomonas* is not carbon/electron limited but constrained by oxygen availability (30). Microelectrode measurements showed oxygen depletion for both wild-type and Δ*phz* colonies 60μm from the surface (Fig. 2-1B), although wild-type colonies were 100μm tall. We asked if cell distributions in the colonies were comparable, expecting the cells to be confined to the region within 60μm from the colony surface, where oxygen was available. For these experiments, we generated versions of the wild type and the ∆*phz* mutant that constitutively expressed a stable yellow fluorescent protein (YFP). Colonies were fixed under oxic conditions with paraformaldehyde and embedded in Tissue-Tek OCT, frozen, and sectioned at a thickness of 10 μm (Fig. 2-2A to F). Because YFP can fully mature and fluoresce posttranslationally in the presence of oxygen (31, 32), our thin-section preparation method ensured that YFP could be seen even in regions of the sections that were previously anoxic.

In sections taken from ∆*phz* colonies, cells were found within 60μm from the surface, in the oxic zone (Fig. 2-2G). In sections taken from wild-type colonies, however, cells were found up to 100μm from the surface (Fig. 2-2G). Some of these cells, therefore, inhabited the 40μm-

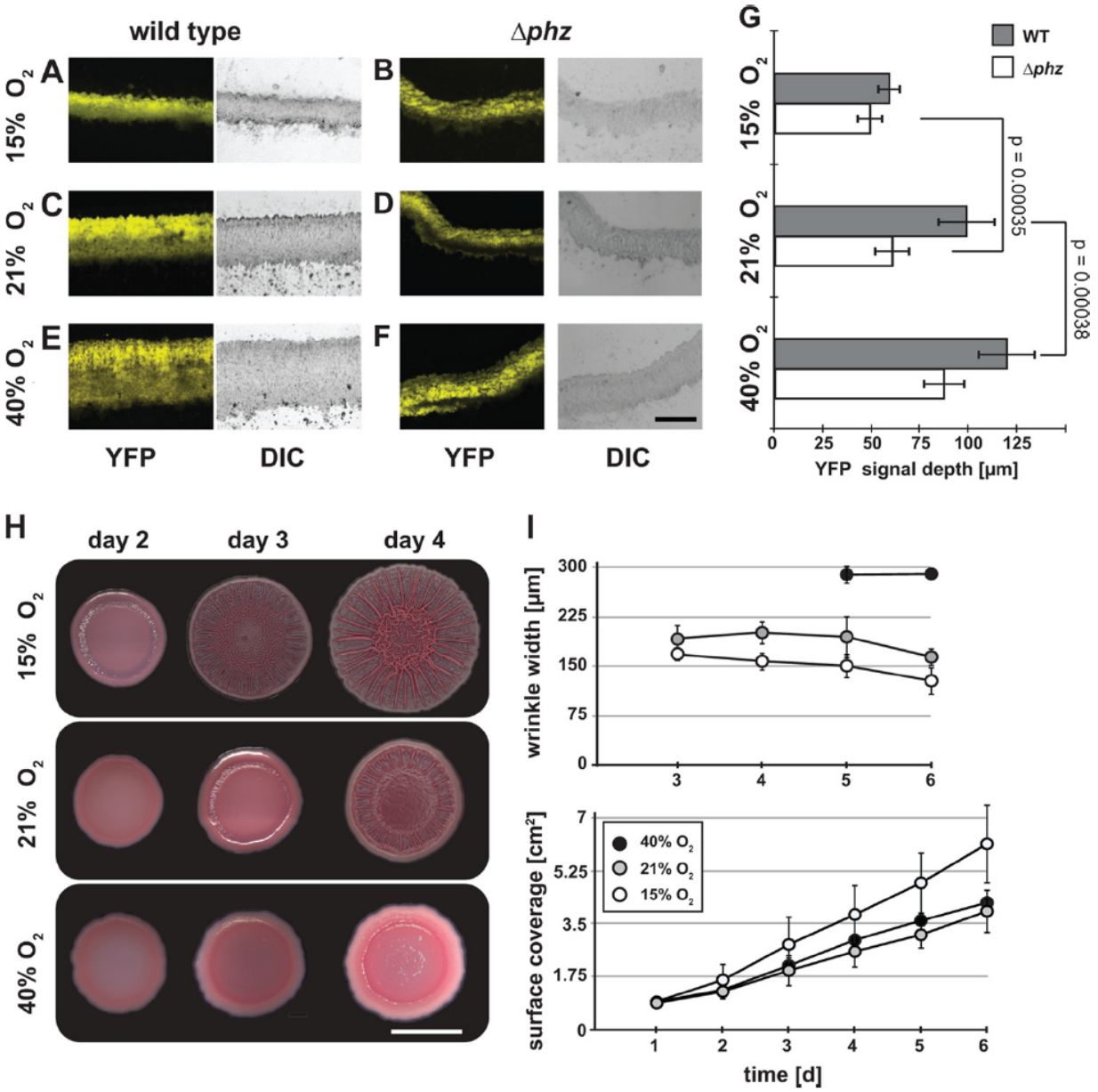

Figure 2-2. Oxygen and phenazine availability modulates colony morphology. (A to F) Oxygen and phenazines affect cell layer thickness in *P. aeruginosa* colonies. Colonies expressing constitutive ($P_{A1/04/03}$-driven [41]) YFP were grown at 15% (hypoxic), 21% (atmospheric), and 40% (hyperoxic) oxygen for 3 days and then embedded in Tissue-Tek OCT. The images were taken using fluorescence (YFP) and DIC microscopy. The scale bar represents 200 μm. (G) Depth at which the YFP signal was detected in the sample. The error bars represent standard deviations for the means of measurements for 15 bases or wrinkles from 3 colonies. P values were calculated using the one-tailed heteroscedastic Student's t test comparing YFP signal depth in WT or Δ*phz* colonies at different oxygen concentrations. The least significant differences are shown. (H) Colony morphology. Representative images of phz colonies grown at various atmospheric oxygen concentrations over 3 days. The scale bar represents 1 cm. (I) Colony wrinkle width (top) and surface coverage (bottom) for Δ*plz* colonies grown at various oxygen concentrations, with nitrogen comprising the atmospheric balance. The error bars represent the standard deviations of widths for 15 wrinkles from 3 colonies (top) or of measurements taken from 5 colonies (bottom).

thick anoxic zone. Reasoning that phenazines enable this survival by acting as alternate electron acceptors in the absence of oxygen, we altered the ambient oxygen concentration and predicted that the extent of the oxic zone within Δ*phz* colonies would determine the cell colonization depth (i.e., wider zones of habitation would correspond to higher atmospheric oxygen levels). We grew colonies under hyperoxic and hypoxic conditions (40% and 15% oxygen, respectively) and ob- served that the depth at which cells could be detected in both wild-type and Δ*phz* colonies correlated with the concentration of oxygen provided (Fig. 2-2A to F). Quantification of the cell layer thickness showed that under all conditions the Δ*phz* mutant was sig- nificantly thinner than the wild type, confirming that the presence of phenazines increases the habitable zone (Fig. 2-2G). We further probed this correlation using a mutant that overproduces the phenazine pyocyanin and found that the habitable zone increased beyond that of the wild type (Fig. 2-7).

We next evaluated whether oxygen accessibility affects other aspects of colony morphology by quantifying the surface coverage and wrinkle thickness of colonies grown with various concentrations of oxygen. As oxygen concentrations increased, the colonies spread less and formed fewer wrinkles. In addition, wrinkle thickness increased with increasing oxygen concentration (Fig. 2-2H and I). To further probe the link between oxidant availability and colony structure, we took advantage of *P. aeruginosa*'s ability to use nitrate instead of oxygen for respiration and redox homeostasis. Two *P. aeruginosa* nitrate reductase complexes, Nar and Nap, might be expected to affect the intracellular redox state under hypoxic conditions. While Nar is a cytoplasmic, membrane-associated complex that contributes to the production of a proton motive force and ATP generation, the Nap complex is periplasmic and is thought to balance the intracellular redox state without directly contributing to the generation of a transmembrane electrochemical gradient (33, 34). Both Nap and Nar catalyze the reduction of nitrate to nitrite. Three additional enzyme complexes, known as Nir (nitrite reductase), Nor (nitric

oxide reductase), and Nos (nitrous oxide reductase), allow *P. aeruginosa* to perform denitrification, the full reduction of nitrate to nitrogen gas (N_2)

We grew a Δ*phz* colony under atmospheric oxygen on medium amended with 40 mM

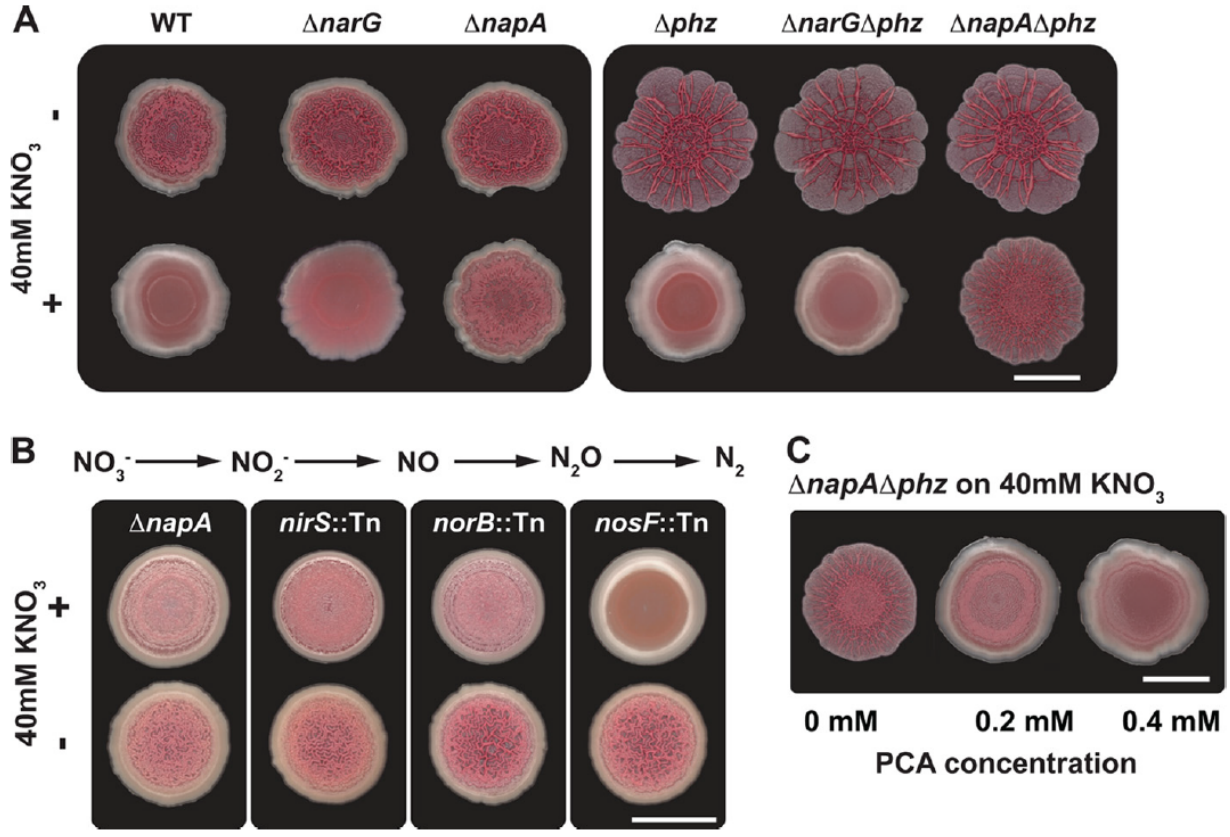

Figure 2-3. Nap-mediated nitrate reduction supports redox homeostasis for cells in colonies. (A) Nap-mediated nitrate reduction prevents colony wrinkling. Shown is the effect of medium amendment with 40mM potassium nitrate on colony morphology. The images are representative of 3 independent experiments. The scale bar represents 1 cm. (B) Colony morphology of denitrification mutants. Specific steps in the canonical denitrification pathway catalyzed by Nap, Nir, and Nor contribute to the nitrate-induced smoothness observed for wild-type colonies. The images shown are representative of 3 independent experiments. The scale bar represents 1 cm. (C) PCA rescues the Δ*napA* phenotype on nitrate; addition of exogenous PCA promotes smoothness in a Δ*napA*Δ*phz* mutant. The images are representative of 3 independent experiments. The scale bar represents 1 cm.

potassium nitrate and found that these conditions rendered the colony smooth (Fig. 2-3A). To determine whether this was due to nitrate reduction, we generated mutants lacking the nitrate reductase subunits NarG and NapA. The t,.*narG* mutant formed a smooth colony when grown on nitrate, suggesting that nitrate respiration is not required for the nitrate- dependent smooth-

colony phenotype. Strikingly, the Δ*napA* mutant wrinkled when grown on medium amended with nitrate (Fig. 2-3A) but reverted to smooth when complemented by the *nap* operon on a plasmid (Fig. 2-8). We then tested whether the downstream enzymes in the denitrification pathway were required for Nap-mediated colony smoothness. Mutants deficient in Nir and Nor also formed wrinkled colonies on 40 mM nitrate, while the mutant lacking functional Nos remained smooth, suggesting that reduction to nitrous oxide is required for NapA-dependent nitrate reduction (Fig. 2-3B). Furthermore, these results suggest that *P. aeruginosa* community structure is determined, at least in part, by the intracellular redox state. If both phenazine reduction and nitrate reduction contribute to oxidizing the intracellular redox state, one would predict that these two activities could complement each other to promote col- ony smoothness. Nitrate addition to a Δ*phz* mutant decreased wrinkling (Fig. 2-3A), and phenazine-1-carboxylic acid (PCA) addition to a ∆*napA* ∆*phz* mutant (grown in the presence of nitrate) also had this effect (Fig. 2-3C).

To further test the hypothesis that community structure and the intracellular redox state are linked, we set out to measure and manipulate the NADH-to-NAD^+ ratio in colony biofilms under different growth conditions. Building on previous results showing that phenazines and nitrate decreased NADH/NAD^+ ratios in liquid cultures (26), we first asked whether nitrate-dependent redox balancing required *napA*. We extracted NADH and NAD^+ from planktonically grown cells and measured their levels using an enzyme-based cycling assay (24, 25). We found that the Δ*napA* mutant showed a partial but significant defect in nitrate-dependent oxidation of the intracellular redox state relative to Δ*phz* and wild-type *P. aeruginosa* (Fig. 2-4A). We next adapted the NADH/NAD^+ extraction and quantification protocol for use with colony samples. This method revealed that the NADH/NAD^+ ratio of phenazine-null colonies reached a maximum that coincided with the induction of wrinkling, while the NADH/NAD^+ ratio of wild- type colonies remained relatively consistent throughout the time course (Fig. 2-4B). Absolute

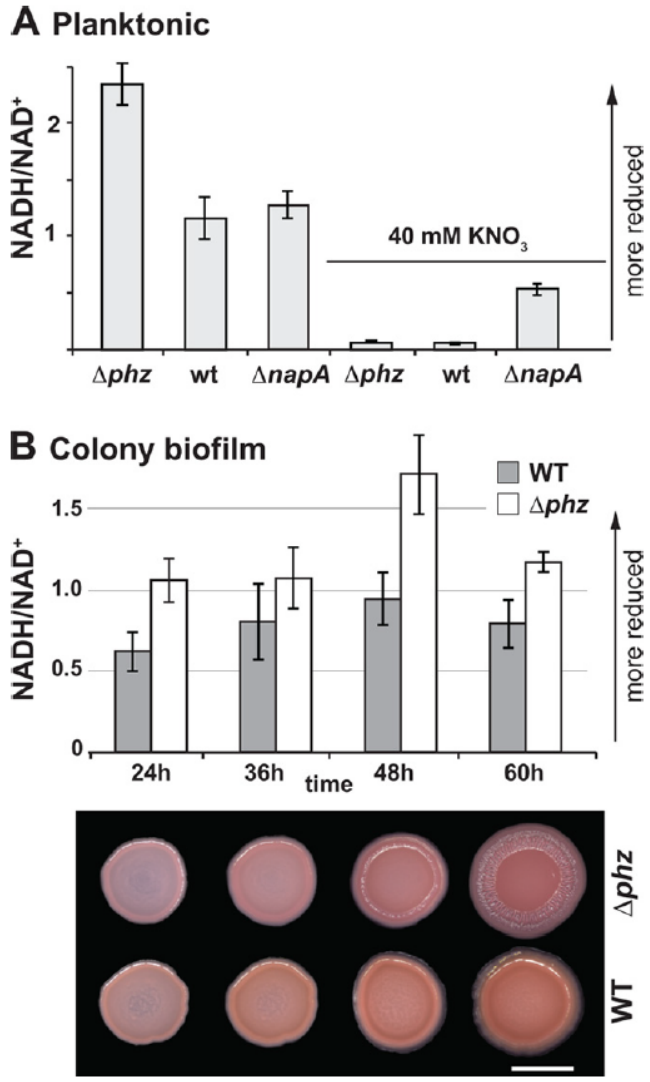

Figure 2-4. (A) NADH/NAD$^+$ ratios for liquid cultures grown for 16 h. For 40 mM KNO_3 cultures, potassium nitrate was added to the medium at the same time that blue pigmentation (pyocyanin production) was apparent in the wild-type cultures. The error bars represent the standard deviations of triplicate cultures. (B) (Top) NADH/NAD$^+$ for wild-type and Δ*phz* colonies. The error bars represent the standard deviations of measurements from triplicate colonies. (Bottom) Representative images of Δ*phz* and wild-type colonies at the time points for collection. The scale bar represents 0.5 cm. The images are representative of 3 independent experiments.

quantitation of the NADH and NAD$^+$ levels (Fig. 2-9) confirmed that the total NAD(H) pools of cells in wild-type and Δ*phz* colonies were approximately equivalent.

Rugosity appears to be induced when the cytoplasmic reducing potential reaches a threshold value, indicating that increased colony surface area is an adaptive response to oxidant limitation that promotes rebalancing of the intracellular redox state. To test this idea, we used a mutant defective in wrinkle formation. Previously, we observed a correlation between wrinkle formation and colony staining with Congo red, suggesting that production of the PEL polysaccharide is critical for rugose morphology (7). We therefore obtained Δ*pel* mutants lacking genes required for PEL biosynthesis to test in our colony biofilm assay (35). As expected, colony wrinkle

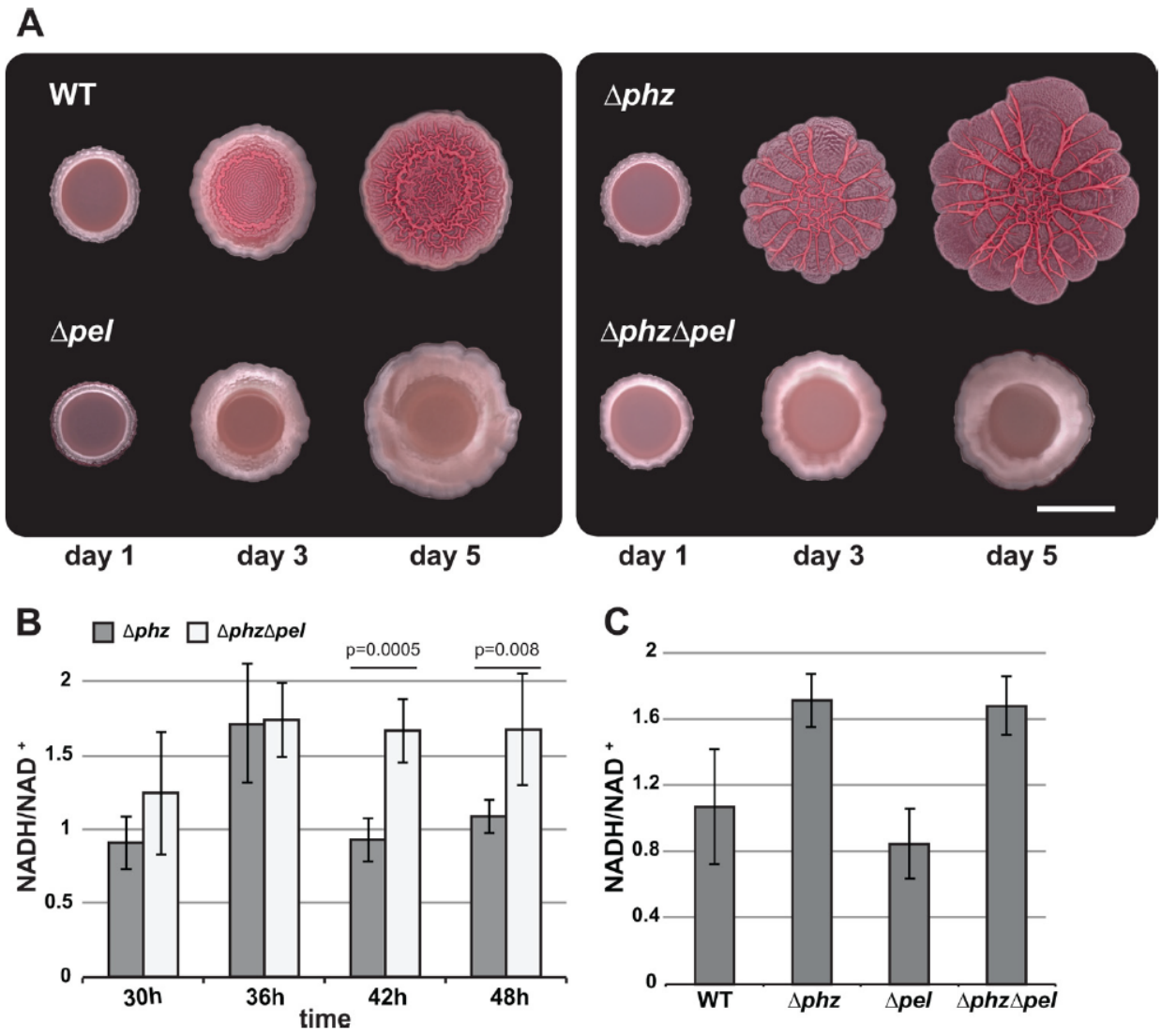

Figure 2-5. (A) PEL production is required for wrinkle formation. *pelB-pelG* were deleted in the wild-type and Δ*phz* backgrounds. Colonies were grown for 5 days on 1% tryptone,1%agar supplemented with 40μg/ml Congo red and 20μg/ml Coomassie blue. (B) NADH/NAD$^+$ ratios in colony biofilms for Δ*phz* and Δ*phz*Δ*pel* mutants. The error bars represent the standard deviations of measurements from triplicate colonies. P values were determined using the one-tailed heteroscedastic Student's t test comparing Δ*phz* and Δ*phz*Δ*pel* colonies at 42 and 48 h. (C) NADH/NAD$^+$ ratios in liquid culture (early stationary phase) for wild-type, Δ*phz*, Δ*pel*, and Δ*phz*Δ*pel* colonies grown in 1% tryptone to early stationary phase. The error bars represent the standard deviations of measurements from biological triplicates.

formation was abolished when this mutation was made in both wild-type and Δ*phz* backgrounds (Fig. 2-5A). We then measured NADH/NAD$^+$ ratios during colony maturation and found that the transient increased ratio that coincided with the onset of wrinkling in the t,.*phz* mutant persisted in the Δ*phz* Δ*pel* mutant (Fig. 2-5B). In contrast, the *pel* deletions had no

effect on the NADH/NAD^+ ratios of planktonically grown cells (Fig. 2-5C). This supports the hypothesis that wrinkling is a strategy for balancing the intracellular redox state of cells within a community. These results suggest that colony morphological development is an active process in which a critical redox state is sensed, leading to a biological response. We are in the process of identifying the circuitry responsible for this phenomenon and the extent to which wrinkling is an emergent property. We note that the specific time when the NADH/NAD^+ ratio peaks can vary from experiment to experiment as a function of slight differences in plate thickness, density of the initial inoculum, etc. However, occurrence of the peak just prior to colony wrinkling is highly reproducible.

All cells catalyze a repertoire of catabolic and anabolic reactions that must be balanced so that the cytoplasm remains a hospitable environment for protein function. In bacterial physiology, there has traditionally been a focus on the individual cell level, and redox reactions have been identified that appear to serve the sole purpose of modulating the intracellular redox state, i.e., they do not contribute directly to energy generation or the production of biomass. We have shown that *P. aeruginosa* can use endogenous phenazines and/or exogenous nitrate to balance the intracellular redox state when oxygen is limiting. The observation that mutants unable to produce phenazines form structurally more complex communities with increased surface area led us to propose that this morphogenetic switch is a response to a reduced cytoplasm. Similarly, we have observed that electron acceptor limitation elicits a community-wide response that maximizes oxygen accessibility—and thereby redox balance—in a bacterial system (Fig. 2-6). Furthermore, inhibiting this response disrupts redox balancing (Fig. 2-5B). Whether rugosity has a similar effect in other microbial species remains to be investigated. It would not be surprising if bacteria with different metabolic properties (e.g., with or without the ability to produce electron shuttles) have different mechanisms for growing and surviving in multicellular communities. Intriguingly, a recent study of patterning in *Bacillus subtilis* biofilms (36) suggested that localized cell death promotes wrinkle formation. Redox homeostasis may also play a role in this system, but to our knowledge, experiments have not yet been performed

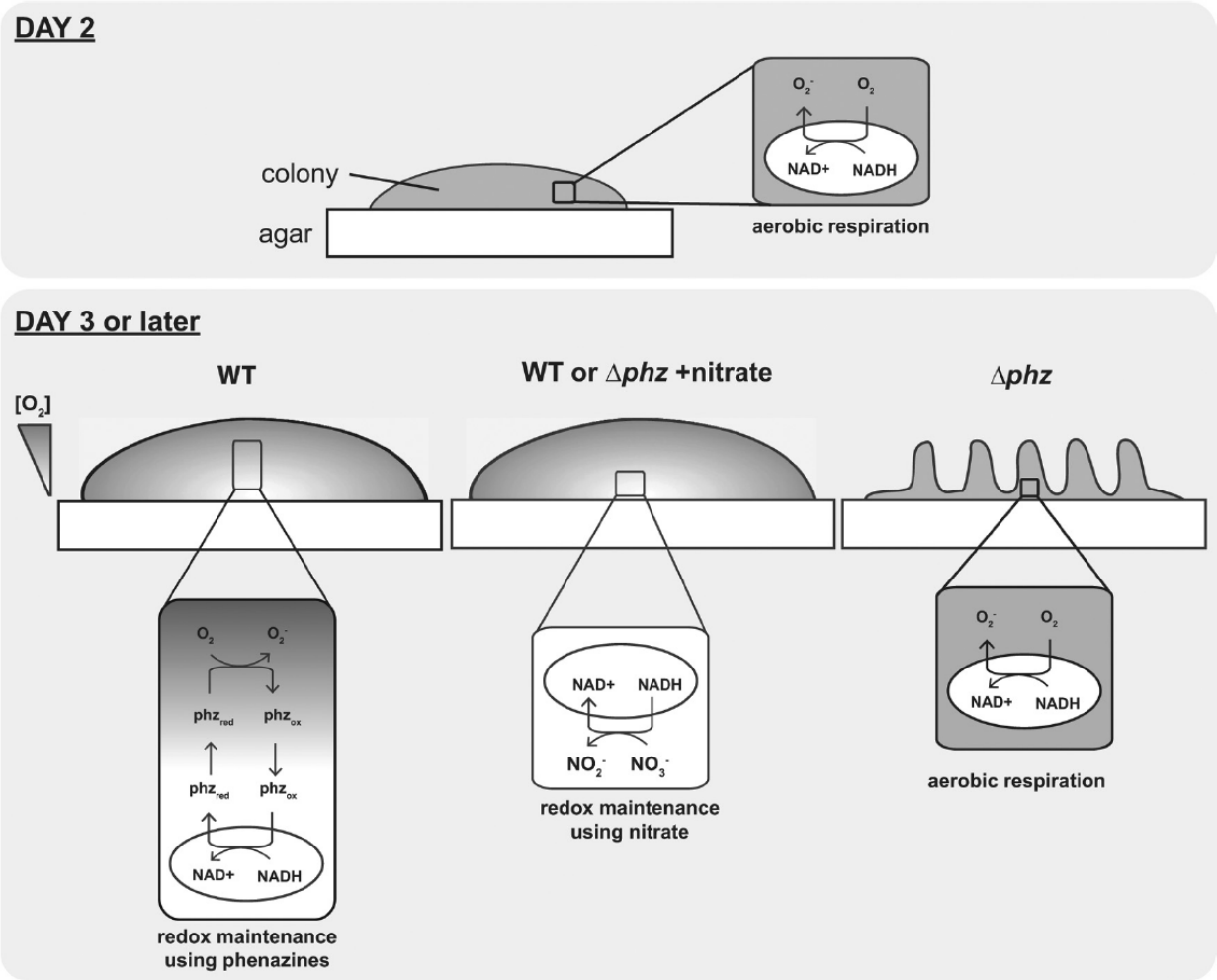

Figure 2-6. *P. aeruginosa* communities employ various strategies that enable access to electron acceptors. From inoculation to day 2, oxygen is detectable throughout the structure. By day 3, wild-type colonies and Δ*phz* colonies grown on nitrate-containing medium exceed the critical height that allows full oxygenation, and the lower portion of the colony becomes anoxic. Cells in the anoxic zone can maintain redox homeostasis by reducing phenazines or nitrate. In the absence of phenazines or nitrate, redox homeostasis can be mediated by a community-wide response: colony wrinkling increases the colony surface area and oxygen accessibility.

that enable a direct comparison. Understanding how active processes and passive physical effects interweave to achieve multicellular patterning in *Pseudomonas* is our long-term goal; it will be interesting to learn whether the mechanisms that underpin these patterns are generalizable. As has been well articulated by others (37), the complex interplay between physical, chemical, and biological processes in microbial communities provides a rich subject for future research.

In conclusion, as Friedheim recognized nearly a century ago (15), cellular aggregation leads to gradient formation due to limited diffusion and consumption of substrates by individual cells within a community. Whether they subsist in bacterial colonies or eukaryotic tissues, cells in multicellular environments likely em- ploy differing strategies to ensure substrate acquisition and survival, depending on the specific microenvironment they inhabit. This concept is well recognized in the biofilm field, and numerous reports have discussed the fact that oxygen defines metabolic zones in biofilms (19, 20, 38). Here, for the first time, we have demonstrated that it is not oxygen *per se* but rather changes in the intracellular redox state that correlate with biofilm morphological development. Mechanisms that aid in redox homeostasis at the cellular level have been characterized in diverse organisms. In metazoans, redox-balancing mechanisms that function at the multicellular level are also well known; for example, the development of the vascular system prevents oxygen starvation of the growing embryo (39). In multicellular aerobes, cells must cope with limited oxygen availability that leads to the formation of aerobic, microaerobic, and anaerobic zones. During processes such as tumor angiogenesis, relative oxygen concentrations act as cues that determine adaptive morphological features, facilitating oxygen delivery to cells within the macroscopic structure (40). Our findings suggest that, like metazoans, bacteria can also respond to electron acceptor limitation and balance intracellular redox levels through morphological changes at the community level. Morphological adaptation to redox imbalance thus appears to be a conserved biological strategy.

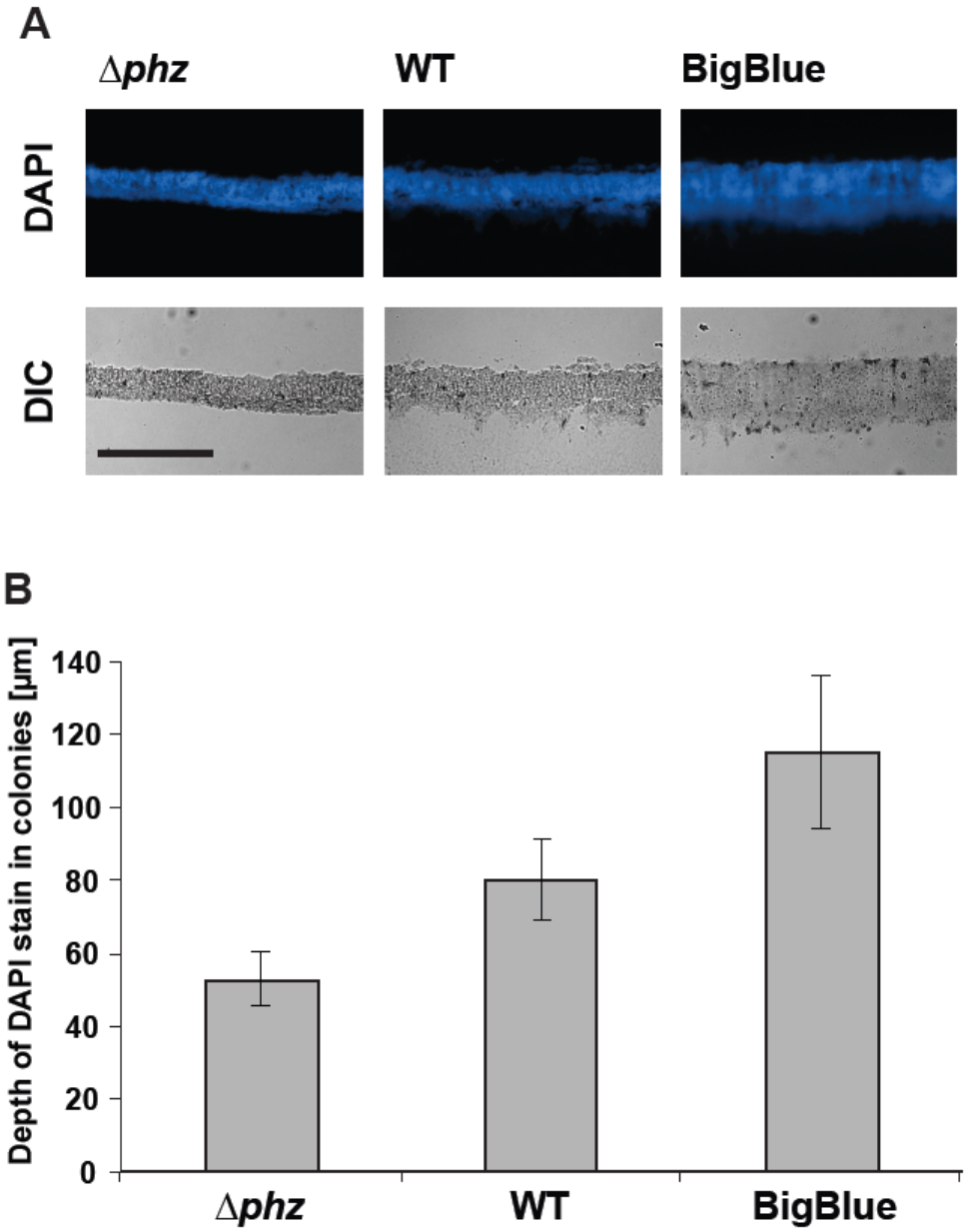

Figure 2-7. The pyocyanin-overproducer BigBlue forms a thicker cell layer in colony biofilms than wild type. BigBlue, wild type and Δ*phz* colonies were grown for 3 days on 1% agar and 1% tryptone (supplemented with 40 µg/ml Congo Red and 20 µg/ml Coomassie Blue), then fixed and sectioned. Cells were visualized by DAPI staining (A). Scale bar is 200 µm. Six sections from 3 different colonies each were measured (B). Error bars represent the standard deviation.

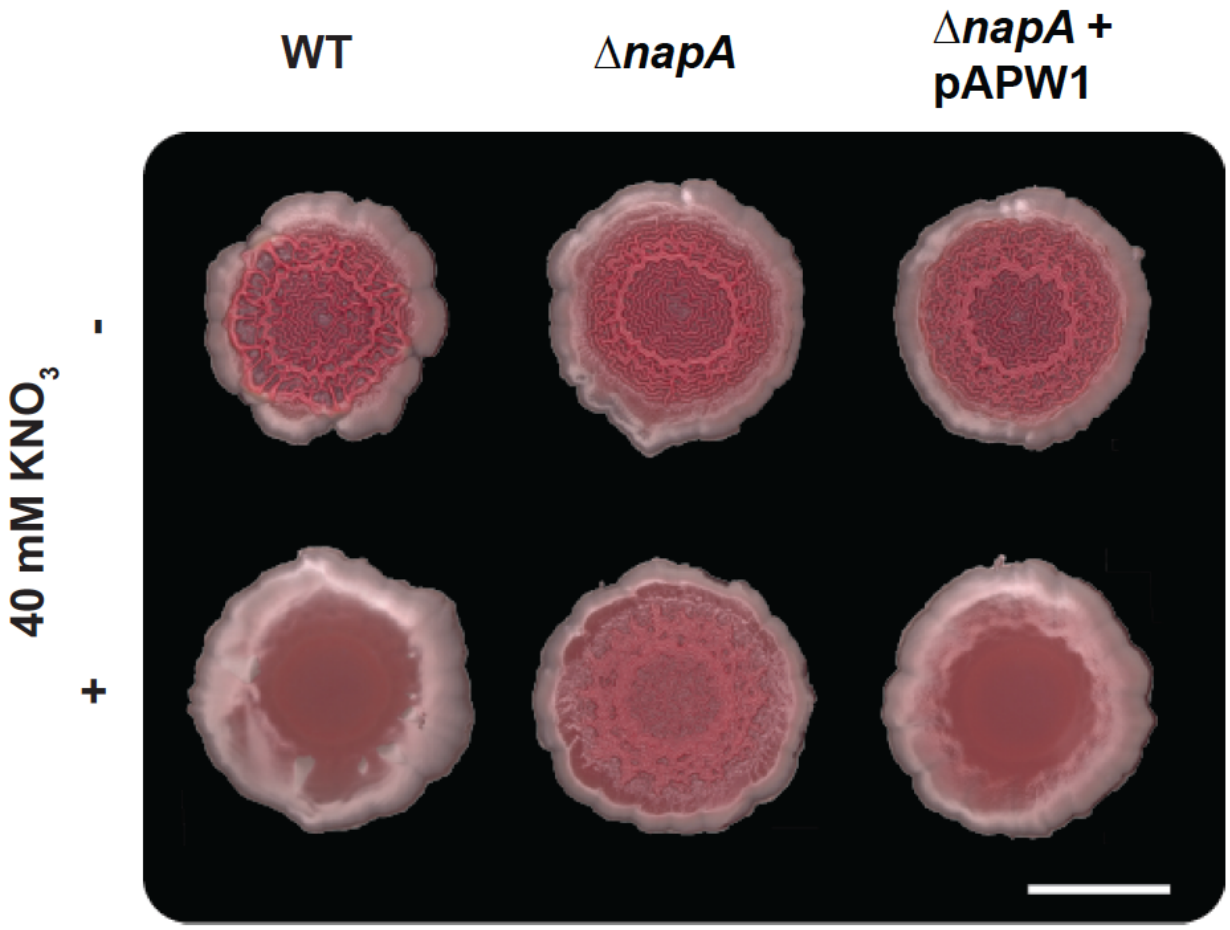

Figure 2-8. Complementation of Δ*napA*. Colonies were grown for 3 days on 1% agar, 1% tryptone and 40 mM potassium nitrate (supplemented with 40 µg/ml Congo Red and 20 µg/ml Coomassie Blue). In contrast to the wrinkled colony phenotype of Δ*napA*, cells complemented with the nap operon (pAPW1) exhibited a smooth colony morphotype. Scale bar is 1 cm.

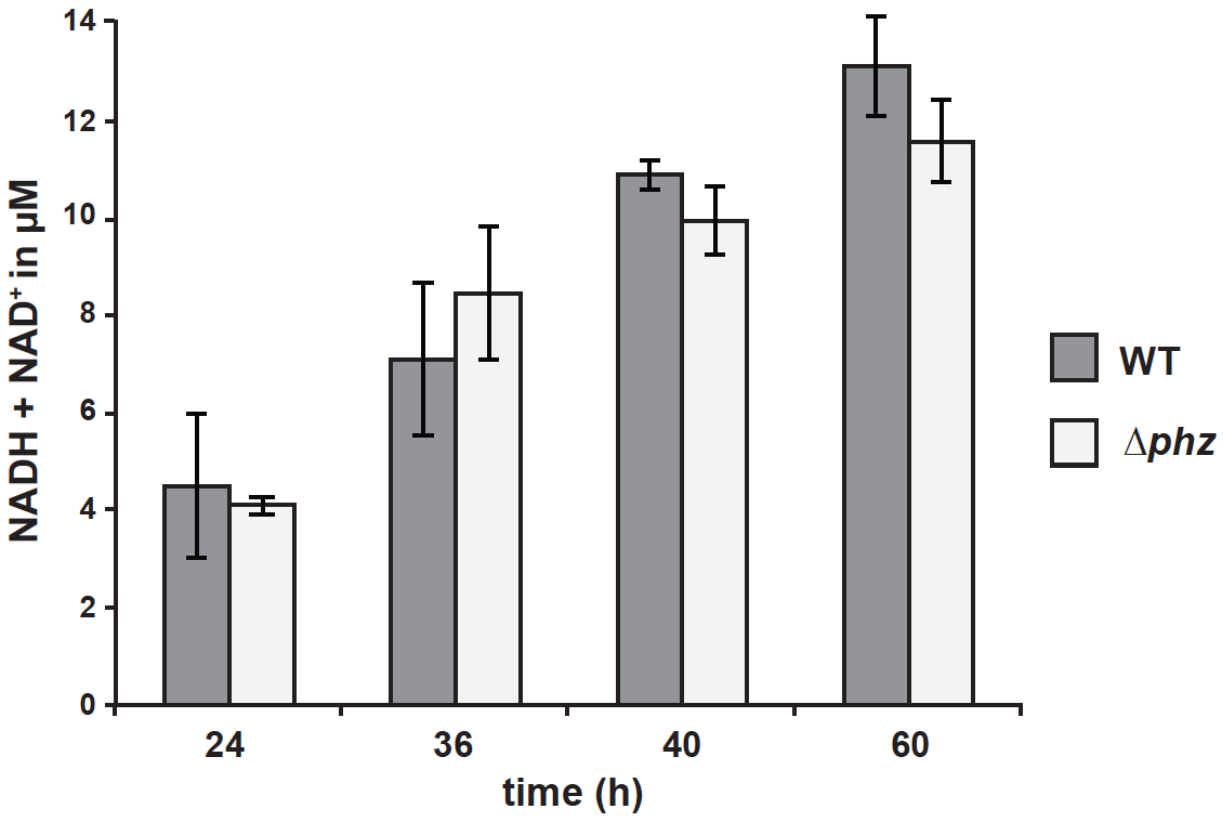

Figure 2-9. Total NAD(H) is comparable between wt and Δ*phz* colonies. Colonies were harvested at indicated times and then resuspendend in 1 ml of 1% tryptone buffer before extraction. Concentrations refer to the resuspension volume. These measurements accompany data presented in figure 2-4.

TABLE 2-1 Strains and plasmids used in this study[a]

Strains/plasmids	Characteristics	Source or reference
P. aeruginosa		
PA14	Clinical isolate UCBPP-PA14	42
PA14 Δ*phz*	PA14 with deletions of operons *phzA1-G1* and *phzA2-G2*	27
PA14 YFP	PA14 with chromosomally integrated constitutive eYFP	8
PA14 Δ*phz* YFP	PA14 Δ*phz* with chromosomally integrated constitutive eYFP	8
BigBlue	DKN370; PA14 containing two copies of *phzM*	26
Δ*pel*	PA14 with a deletion of *pelB-pelG*	G. Squyres
Δ*phz*Δ*pel*	PA14 Δ*phz* with a deletion of *pelB-pelG*	G. Squyres
Denitrification		
PA14 Δ*napA*	PA14 with a deletion of *napA*	This study
PA14 Δ*napA* Δ*phz*	PA14 with deletions of *napA*, *phzA1-phzG1*, and *phzA2-phzG2*	This study
PA14 Δ*narG*	PA14 with a deletion of *narG*	This study
PA14 Δ*narG* Δ*phz*	PA14 with deletions of *narG*, *phzA1-phzG1*, and *phzA2-phzG2*	This study
PA14 *nirS*::Tn	*nirS*::MAR2XT7; Gen^r	43
PA14 *norB*::Tn	*norB*::MAR2XT7; Gen^r	43
PA14 *nosF*::Tn	*nosF*::MAR2XT7; Gen^r	43
E. coli		
UQ950	*E. coli* DH5s λ(*pir*) host for cloning; F$^-$ Δ(*argF-lac*)*169* Φ80d*lacZ58*(ΔM15) *glnV44*(AS) *rfbD1 gyrA96*(Nal^r) *recA1 endA1 spoT1 thi-1 hsdR17 deoR* λ*pir*$^+$	D. Lies
BW29427	Donor strain for conjugation: *thrB1004 pro thi rpsL hsdS lacZ* ΔM15RP4–1360 Δ(*araBAD*)*567* Δ*dapA1341*::[*erm pir*(wt)]	B. Wanner
Saccharomyces cerevisiae		
InvSc1	*MAT*a/*MAT*α *leu2/leu2 trp1-289/trp1-289 ura3-52/ura3-52 his3-Δ1/his3-Δ1*	23; Invitrogen
Plasmids		
pMQ30	Yeast-based allelic-exchange vector; *sacB*[a] CEN/ARSH URA3$^+$ Gen^r	23
pMQ72	Yeast-based expression vector 2μm; URA3$^+$ Gen^r	23
pLD314	*napA* deletion fragments cloned into pMQ30	This study
pLD263	*narG* deletion fragments cloned into pMQ30	This study
pAPW1	pMQ72 with *napEFDABC* operon insert	This study

[a] Transposon mutants used in this study were confirmed by PCR or sequencing.

TABLE 2-2 Primers used in this study

Primer	Sequence (5= to 3=)
Transposon check	
nirS-1	ATTTGGCAAGCCACTGGT
nirS-2	GTCGTGCTGGGTGTTGTAGA
norB-1	AATGGCTCCCTGAAATTCG
norB-2	GGAAGCTCAGCAGGTAGGC
nosF-1	CCATGAGCCTGGTCGAGAT
nosF-2	ATGTGGTGGCGATAGAGGTC
Deletion plasmids	
pLD314	
ΔnapA 5= flank-1	GGAATTGTGAGCGGATAACAATTTCACACAGGAAACAGCTAAGCCAGGCTCTTCCTGTTC
ΔnapA 5= flank-2	CAGTCAGCAGAGGTTTCATGGATTCACGACGGGTGAGGTT
ΔnapA 3= flank-1	ACCTCACCCGTCGTGAATCCATGAAACCTCTGCTGACTG
ΔnapA 3= flank-2	CCAGGCAAATTCTGTTTTATCAGACCGCTTCTGCGTTCTGATACTCGAAGTTGTGGCAGTTG
pLD263	
ΔnarG 5= flank-1	GGAATTGTGAGCGGATAACAATTTCACACAGGAAACAGCTGATCTGGGTGCCGTTCATC
ΔnarG 5= flank-2	TCCAGTTCAGGGTGATCTCCGGCTCTCGTTGCTGGTCTC
ΔnarG 3= flank-1	GAGACCAGCAACGAGAGCCGGAGATCACCCTGAACTGGA
ΔnarG 3= flank-2	CCAGGCAAATTCTGTTTTATCAGACCGCTTCTGCGTTCTGATGGACCTGGTCGAAGTTCTTG
Complementation plasmid	
pAPW1	
napA-1	GAATTCTCCAAGCGCTTCAC
napA-2	CAGCACGTCGTAGAGGGTCT

2-5 REFERENCES

1. Grosberg RK, Strathmann RR. 2007. The evolution of multicellularity: a minor major transition? Annu. Rev. Ecol. Evol. Systematics 38:621– 654.
2. Orphan VJ, House CH, Hinrichs KU, McKeegan KD, DeLong EF. 2002. Multiple archaeal groups mediate methane oxidation in anoxic cold seep sediments. Proc. Natl. Acad. Sci. U. S. A. 99:7663–7668.
3. Lopez D, Vlamakis H, Kolter R. 2010. Biofilms. Cold Spring Harb. Perspect. Biol. 2:a000398. doi:10.1101/cshperspect.a000398.
4. Stewart PS, Franklin MJ. 2008. Physiological heterogeneity in biofilms. Nat. Rev. Microbiol. 6:199 –210.
5. Booth SC, Workentine ML, Wen J, Shaykhutdinov R, Vogel HJ, Ceri H, Turner RJ, Weljie AM. 2011. Differences in metabolism between the biofilm and planktonic response to metal stress. J. Proteome Res. 10:3190 –319
6. Hoiby N, Frederiksen B, Pressler T. 2005. Eradication of early Pseudomonas aeruginosa infection. J. Cyst. Fibros. 4(Suppl. 2):49 –54.
7. Dietrich LE, Teal TK, Price-Whelan A, Newman DK. 2008. Redox-active antibiotics control gene expression and community behavior in divergent bacteria. Science 321:1203–1206.
8. Ramos I, Dietrich LE, Price-Whelan A, Newman DK. 2010. Phenazines affect biofilm formation by Pseudomonas aeruginosa in similar ways at various scales. Res. Microbiol. 161:187–191.
9. Price-Whelan A, Dietrich LE, Newman DK. 2006. Rethinking 'secondary' metabolism: physiological roles for phenazine antibiotics. Nat. Chem.Biol. 2:71–78.
10. Mavrodi DV, Peever TL, Mavrodi OV, Parejko JA, Raaijmakers JM, Lemanceau P, Mazurier S, Heide L, Blankenfeldt W, Weller DM, Thomashow LS. 2010. Diversity and evolution of the phenazine biosyn- thesis pathway. Appl. Environ. Microbiol. 76:866 – 879.
11. Wang Y, Newman DK. 2008. Redox reactions of phenazine antibiotics with ferric (hydr)oxides and molecular oxygen. Environ. Sci. Technol. 42:2380 –2386.
12. Friedheim EA. 1931. Pyocyanine, an accessory respiratory enzyme. J. Exp. Med. 54:207–221.
13. Harrop GA, Barron ES. 1928. Studies on blood cell metabolism. I. The effect of methylene blue and other dyes upon the oxygen consumption of mammalian and avian erythrocytes. J. Exp. Med. 48:207–223.
14. Barron ES, Hoffman LA. 1930. The catalytic effect of dyes on the oxygen consumption of living cells. J. Gen. Physiol. 13:483– 494.

15. Friedheim EA. 1934. The effect of pyocyanine on the respiration of some normal tissues and tumours. Biochem. J. 28:173–179.

16. Barron ES. 1930. The catalytic effect of methylene blue on the oxygen consumption of tumors and normal tissues. J. Exp. Med. 52:447– 456.

17. Kerr JR. 2000. Phenazine pigments: antibiotics and virulence factors. Infect. Dis. Rev. 2:184 –194.

18. Hernandez ME, Newman DK. 2001. Extracellular electron transfer. Cell. Mol. Life Sci. 58:1562–1571.

19. Peters AC, Wimpenny JW, Coombs JP. 1987. Oxygen profiles in, and in the agar beneath, colonies of Bacillus cereus, Staphylococcus albus and Escherichia coli. J. Gen. Microbiol. 133:1257–1263.

20. Xu KD, Stewart PS, Xia F, Huang CT, McFeters GA. 1998. Spatial physiological heterogeneity in Pseudomonas aeruginosa biofilm is determined by oxygen availability. Appl. Environ. Microbiol. 64:4035– 4039.

21. Wang Y, Kern SE, Newman DK. 2010. Endogenous phenazine antibiotics promote anaerobic survival of Pseudomonas aeruginosa via extracellular electron transfer. J. Bacteriol. 192:365–369.

22. Bertani G. 2004. Lysogeny at mid-twentieth century: P1, P2, and other experimental systems. J. Bacteriol. 186:595– 600.

23. Shanks RM, Caiazza NC, Hinsa SM, Toutain CM, O'Toole GA. 2006. Saccharomyces cerevisiae-based molecular tool kit for manipulation of genes from gram-negative bacteria. Appl. Environ. Microbiol. 72:5027–5036.

24. San KY, Bennett GN, Berrios-Rivera SJ, Vadali RV, Yang YT, Horton E, Rudolph FB, Sariyar B, Blackwood K. 2002. Metabolic engineering through cofactor manipulation and its effects on metabolic flux redistribution in Escherichia coli. Metab. Eng. 4:182–192.

25. Bernofsky C, Swan M. 1973. An improved cycling assay for nicotinamide adenine dinucleotide. Anal. Biochem. 53:452– 458.

26. Price-Whelan A, Dietrich LE, Newman DK. 2007. Pyocyanin alters redox homeostasis and carbon flux through central metabolic pathways in Pseudomonas aeruginosa PA14. J. Bacteriol. 189:6372– 6381.

27. Dietrich LE, Price-Whelan A, Petersen A, Whiteley M, Newman DK. 2006. The phenazine pyocyanin is a terminal signalling factor in the quorum sensing network of Pseudomonas aeruginosa. Mol. Microbiol. 61:1308 –1321.

28. Sullivan NL, Tzeranis DS, Wang Y, So PT, Newman D. 2011. Quantifying the dynamics of bacterial secondary metabolites by spectral multiphoton microscopy. ACS Chem. Biol. 6:893– 899.

29. Vander Wauven C, Pierard A, Kley-Raymann M, Haas D. 1984. Pseudomonas aeruginosa mutants affected in anaerobic growth on arginine: evidence for a four-gene cluster encoding the arginine deiminase pathway. J. Bacteriol. 160:928 –934.

30. Worlitzsch D, Tarran R, Ulrich M, Schwab U, Cekici A, Meyer KC, Birrer P, Bellon G, Berger J, Weiss T, Botzenhart K, Yankaskas JR, Randell S, Boucher RC, Doring G. 2002. Effects of reduced mucus oxygen concentration in airway Pseudomonas infections of cystic fibrosis patients. J. Clin. Invest. 109:317–325.

31. Heim R, Prasher DC, Tsien RY. 1994. Wavelength mutations and posttranslational autoxidation of green fluorescent protein. Proc. Natl. Acad. Sci. U. S. A. 91:12501–12504.

32. Zhang C, Xing X-H, Lou K. 2005. Rapid detection of a GFP-marked Enterobacter aerogenes under anaerobic conditions by aerobic fluorescence recovery. FEMS Microbiol. Lett. 249:211–218.

33. Williams HD, Zlosnik JE, Ryall B. 2007. Oxygen, cyanide and energy generation in the cystic fibrosis pathogen Pseudomonas aeruginosa. Adv. Microb. Physiol. 52:1–71.

34. Richardson DJ, Berks BC, Russell DA, Spiro S, Taylor CJ. 2001. Functional, biochemical and genetic diversity of prokaryotic nitrate reductases. Cell. Mol. Life Sci. 58:165–178.

35. Friedman L, Kolter R. 2004. Genes involved in matrix formation in Pseudomonas aeruginosa PA14 biofilms. Mol. Microbiol. 51:675– 690.

36. Asally M, Kittisopikul M, Rue P, Du Y, Hu Z, Cagatay T, Robinson AB, Lu H, Garcia-Ojalvo J, Suel GM. 2012. Localized cell death focuses mechanical forces during 3D patterning in a biofilm. Proc. Natl. Acad. Sci. U. S. A. 109:18891–18896.

37. Klapper I, Dockery J. 2010. Mathematical description of microbial biofilms. Siam Rev. 52:221–265.

38. Xavier JB, Foster KR. 2007. Cooperation and conflict in microbial biofilms. Proc. Natl. Acad. Sci. U. S. A. 104:876 – 881.

39. Simon MC, Keith B. 2008. The role of oxygen availability in embryonic development and stem cell function. Nat. Rev. Mol. Cell Biol. 9:285–296.

40. Giaccia AJ, Simon MC, Johnson R. 2004. The biology of hypoxia: the role of oxygen sensing in development, normal function, and disease. Genes Dev. 18:2183–2194.

41. Lambertsen L, Sternberg C, Molin S. 2004. Mini-Tn7 transposons for site-specific tagging of bacteria with fluorescent proteins. Environ. Micro- biol. 6:726 –732.

42. Rahme LG, Stevens EJ, Wolfort SF, Shao J, Tompkins RG, Ausubel FM. 1995. Common virulence factors for bacterial pathogenicity in plants and animals. Science 268:1899 –1902.

43. Liberati NT, Urbach JM, Miyata S, Lee DG, Drenkard E, Wu G, Villanueva J, Wei T, Ausubel FM. 2006. An ordered, non redundant library of Pseudomonas aeruginosa strain PA14 transposon insertion mutants. Proc. Natl. Acad. Sci. U. S. A. 103:2833–2838.

Chapter 3

The phosphodiesterase RmcA (PA0575) mediates the *Pseudomonas aeruginosa* community response to oxidant limitation

Chinweike Okegbe[1], Blanche L. Fields[1], Stephanie J. Cole[2], Vincent T. Lee[2], Lars E.P. Dietrich[1]*

This chapter is adapted from the above-titled manuscript that was submitted for publication in Nature Microbiology

Author contributions:

B.F. contributed the *roeA*, *sadC* and *bifA* clean deletions in Figure 3-1a as well as the cyclic di-GMP quantification experiment in Figure 3-5. S.J.C and V.T.L. contributed the *in vitro* experiments in Figure 3-3d. C.O contributed all remaining experiments.

3-1 ABSTRACT

Diverse bacteria form three-dimensional multicellular structures by producing an extracellular matrix scaffold. While the signaling pathways that control this behavior have been extensively characterized in several species, the cues and mechanisms that activate these pathways, thereby enabling multicellular responses to environmental conditions, are not well understood. In colonies of the opportunistic pathogen *Pseudomonas aeruginosa* PA14, defects in the production of electron-shuttling antibiotics called phenazines stimulate matrix production and the development of wrinkle features that increase the colony surface area-to-volume ratio. Prior to wrinkling, phenazine-null colonies exhibit a transient accumulation of cellular reducing power, suggesting that electron acceptor limitation is a signal that triggers the multicellular response. PA14 matrix production is stimulated by the intracellular signal bis-(3',5')-cyclic-dimeric-guanosine (c-di-GMP). Here, we describe the molecular and physiological characterization of RmcA, a c-di-GMP phosphodiesterase containing 4 Per-Arnt-Sim (PAS) domains. Our results suggest that RmcA is activated by oxidized phenazines and/or cytoplasmic conditions to degrade c-di-GMP and thereby inhibit matrix production. RmcA thus acts as a mechanistic link between environmental redox conditions and the morphogenetic output of PA14 communities, playing a role similar to those of PAS-domain-containing regulatory proteins found in complex eukaryotes.

3-2 INTRODUCTION

Diverse species of microbes form colonies with intricate wrinkle patterns [1]. Detailed studies in a handful of organisms have revealed commonalities to this behavior, which requires secretion of aggregating proteins and/or polysaccharides and appears to be influenced by the availability of electron acceptors for ATP generation [2-7]. This latter property is intriguing due to its parallels in complex eukaryotic model systems such as embryos and tumors, where mechanisms that control development in response to the environmental or intracellular redox state have been described [8,9]. For bacterial species, however, the molecular links between

the redox environment or cellular energy metabolism and community morphogenesis remain largely uncharacterized.

The opportunistic pathogen *Pseudomonas aeruginosa* PA14 forms intricate wrinkle patterns in a simple model of colony development amenable to characterization using a variety of techniques. We have used this standardized colony morphology assay to show that structure formation is influenced by the production of endogenous redox-active antibiotics called phenazines. While wild-type (phenazine-producing) PA14 colonies initially exhibit a smooth surface and develop concentric ring structures after ~60 hours of incubation in this assay, a mutant unable to produce phenazines (Δ*phz*) begins to form a pronounced wrinkle pattern at ~37 hours that is characterized by a central ring surrounded by radial spokes. Phenazines can act as alternate electron acceptors to support ATP generation when O_2 is not available [10,11]. We have therefore proposed that colony wrinkling and its associated increase in the colony surface area-to-volume ratio is an adaptive response that maximizes access to O_2 for cells that would otherwise experience a redox imbalance due to electron acceptor limitation [12]. Measurements of intracellular NAD(H) extracted from colonies support this hypothesis [7].

PA14 colony wrinkling requires secretion of a polysaccharide called Pel, which is stimulated by high levels of the intracellular signal Bis-(3',5')-cyclic-dimeric-guanosine (c-di-GMP) [13-15]. A suite of enzymes encoded by the PA14 genome contain domains with the potential to modulate c-di-GMP levels through diguanylate cyclase (DGC) or phosphodiesterase (PDE) activity, and genetic screening has identified a subset of these that qualitatively affect Pel production [16]. However, the specific players that mediate the effects of extra- or intracellular redox state on Pel production and thus colony development have not yet been defined. Here, we describe identification and characterization of PA0575, a compelling candidate mediator of redox-driven community morphogenesis. We have named this protein RmcA for redox modulator of c-di-GMP.

3-3 RESULTS AND DISCUSSION

To identify sensors that act as mechanistic links between redox conditions and community behavior, we amassed a collection of transposon-insertion and deletion mutants representing each of the PA14 proteins predicted to produce or degrade c-di-GMP (i.e, those that contain “GGDEF”, “EAL”, and/or “HD-GYP” domains) and screened for mutations that influence biofilm morphogenesis using our colony morphology assay [7]. Of the 40 mutants tested, we found 8 with phenotypes that differed from that of wild-type PA14 (Supplmentary Fig 3-1). For brevity, we refer to PA14 genes of interest using the ORF numbers of homologous genes in strain PAO1. Four mutants, with disruptions in *PA0290*, *PA1107* (*roeA*), *PA3702* (*wspR*) and *PA4332* (*sadC*) (*roeA*: [17], *wspR*: [18], *sadC*: [19]), showed delayed wrinkling or smooth phenotypes (Fig. 3-1a), suggesting that their corresponding encoded proteins are DGCs. We also found 4 mutants, with disruptions in *PA0575* (*rmcA*), *PA4367* (*bifA*), *PA5017* (*dipA*/*pch*) and *PA5295* (*bifA*: [20], *dipA*/*pch*: [21,22]), that displayed early wrinkling or hyperwrinkled phenotypes (Fig. 3-1a). Though all 4 of the proteins represented by these mutants harbor both GGDEF and EAL domains, their associated colony phenotypes suggest that these proteins have PDE activity. Quantification of cellular c-di-GMP and CR binding (Supplmentary Fig. 3-3) by colonies representing a subset of DGC and PDE mutants produced results that generally correlated with colony phenotypes.

Several of our screen hits have previously been implicated in PA14 colony Pel production (*roeA*: [17]; *sadC*: [19]; *bifA*: [20]; *wspR*, *dipA* and *PA5295*: [16]). Although the conditions of our colony assay differ from those used in studies by other groups, the phenotypes we observed for these mutants were generally consistent with those that have been described previously. An exception to this is the enhanced-wrinkling phenotype we observed for Δ*PA0575* (*rmcA*), which contradicts the CR-binding defect previously reported for a similar mutant [16]. We engineered a complemented version of our Δ*PA0575* (rmcA) strain and found that it displayed a wild-type colony phenotype (Supplmentary Fig. 3-2), confirming that the Δ*PA0575* (*rmcA*) phenotype we

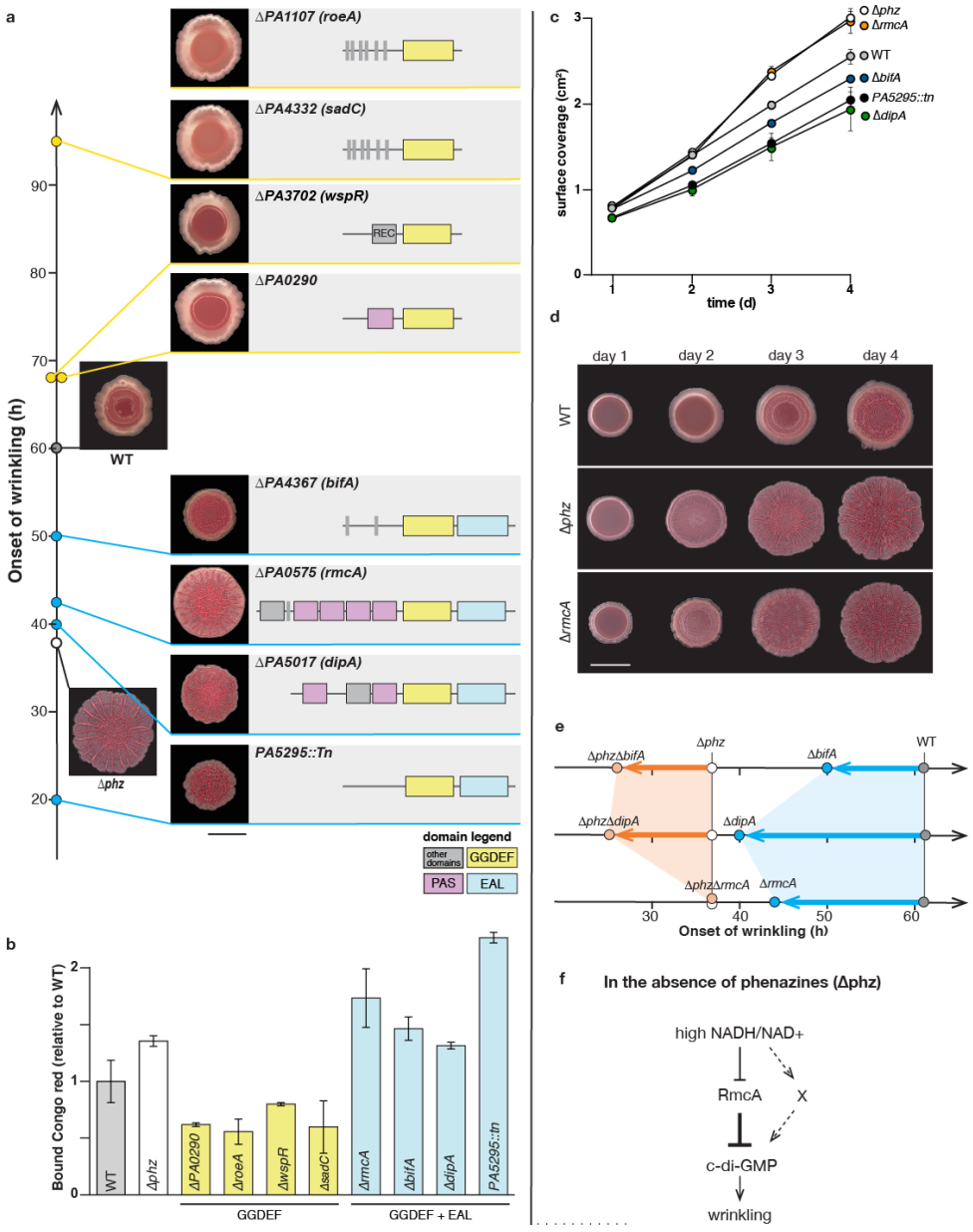

Figure 3-1. GGDEF- and GGDEF+EAL-domain-containing proteins modulate *P. aeruginosa* PA14 colony morphogenesis and are differentially affected by phenazine production. (a) Representative images of PA14 wild type (WT), Δ*phz*, and strains containing disruptions in the indicated genes, designated by PAO1 ORF number. Colony images are arranged according to the timing of the onset of wrinkling, with the time of inoculation represented by the start of the timeline at the left. Cartoons shown next to each colony depict the domain organization of each disrupted protein. (b) Pel content, quantified using the Congo red binding assay, in colonies grown for 2 days on 1% tryptone, 1% agar medium with no added dyes. Error bars represent SD and n≥3. (c) Surface coverage over time for WT and for mutants with early-onset wrinkling. Error bars represent SD and n=3. (d) Colony development over time for the indicated strains grown in the colony morphology assay. (e) Timing of the onset of wrinkling for the indicated strains. Orange and teal shading represent the shift in the onset brought about by the indicated mutations made in the Δ*phz* and WT parent strains, respectively. (f) Graphical representation of the effect of high NADH/NAD+ levels on signaling and morphological output in PA14 colonies. Each scale bar=1 cm.

observe can be attributed to the function of this locus.

We were struck by the phenotypic similarity between colonies formed by Δ*PA0575* (rmcA) and Δ*phz* [23]. PA0575 (*RmcA*) contains 4 PAS (Per-Arnt-Sim) domains (Fig. 3-1d). PAS domains function to sense environmental signals such as oxygen, nitrate and redox state [24-26] and control regulatory processes in diverse organisms. As we have been interested in identifying regulatory proteins with the potential to control Pel production in response to redox cues and therefore mediate the switch between Δ*phz* and wild-type colony morphotypes, PA0575 (RmcA) caught our attention as one such potential mediator. We propose a model in which PA0575 (RmcA) is active in the presence of phenazines and lowers c-di-GMP levels during the early stages of colony development in the wild type, thereby inhibiting Pel production and delaying colony wrinkling. Conversely, in the absence of phenazine, we propose that RmcA is inactive due to high NADH/NAD^+. This raises c-di-GMP levels which leads to colony wrinkling (Fig. 3-1f). We created combinatorial mutants with deletions in either *PA0575* (*rmcA*) or *PA4367* (*bifA*) in the Δ*phz* background and monitored the timing of colony wrinkling for these mutants relative to their phenazine-producing counterparts. Deleting PA4367 (*bifA*) in the Δ*phz* background moved the onset of wrinkling to a much earlier time point (26 h) than that observed for the individual Δ*PA4367* (*bifA*) or Δ*phz* mutants (50 h and 37 h, respectively) (Fig. 3-1e). In contrast, deleting *PA0575* (*rmcA*) in the Δ*phz* background gave rise to a mutant colony with an onset of wrinkling at 37 h and therefore had a negligible effect on the timing of wrinkling for the Δ*phz* mutant (Fig 3-1e). These results are consistent with a scenario in which the effects of BifA and phenazines on colony development act independently to inhibit wrinkling, while the effects of PA0575 (RmcA) and phenazines may act via the same pathway.

We performed additional phenotypic characterization of Δ*PA0575* (*rmcA*) to compare it to Δ*phz*. Colony phenazine production and liquid-culture growth phenotypes for Δ*PA0575* (*rmcA*) did not differ from those of the wild type (Supplmentary Fig. 3-4a,b). We assessed the swarming capabilities of selected mutants and found that the Δ*PA0575* (*rmcA*) and *PA5295::tn* mutants

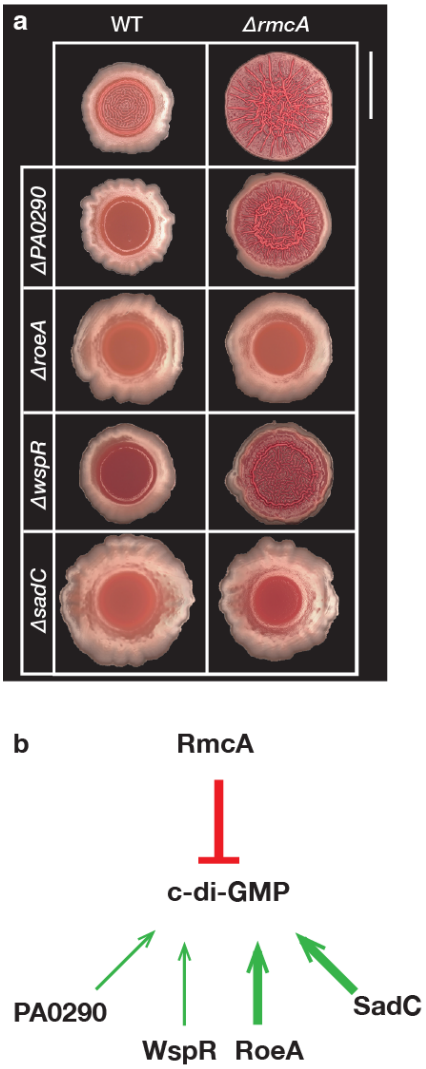

Figure 3-2. Specific GGDEF-domain proteins contribute to wrinkling upstream or downstream of RcmA-dependent effects on colony morphogenesis. (a) Representative images of PA14 WT, Δ*rcmA*, and deletion mutants made in the indicated parent backgrounds and grown on colony morphology assay medium for 3 days. Scale bar=1 cm. (b) Cartoon depicting the relative effects of RmcA and various GGDEF-domain proteins on c-di-GMP levels during PA14 colony development.

exhibited swarming motility (similar to Δ*phz* [27]), while Δ*PA4367* (*bifA*) and Δ*PA5017* (*dipA*) did not swarm (Fig. 3-3b). As hyperwrinkling phenotypes tend to be associated with swarming defects in mutants that have been described previously [21,28], the Δ*phz*, Δ*PA0575* (*rmcA*) and *PA5295::tn* mutants stand out as exceptions to this trend [17]. We also compared cellular NADH/NAD$^+$ levels from Δ*PA0575* (*rmcA*) colonies to those from Δ*phz* colonies. Consistent with previously published results, Δphz showed a spike in NADH/NAD$^+$ just prior to wrinkling [7],

while Δ*PA0575* (rmcA) did not exhibit elevated NADH/NAD^+ before wrinkling (Supplmentary Fig. 3-4c). This suggests that Δ*PA0575* (*rmcA*) hyperwrinkling is attributable not to a redox imbalance but rather to the "unnecessary" initiation of an adaptive wrinkling mechanism.

How does the PDE activity of PA0575 (RmcA) operate within the network of DGCs and PDEs that influence cellular c-di-GMP levels and colony development? We generated combinatorial mutants to investigate whether PA0575 (RmcA) degrades c-di-GMP produced by the DGCs identified in our screen (Fig. 3-1a). Deleting *PA1107* (*roeA*) and *PA4332* (*sadC*) in the Δ*PA0575* (*rmcA*) background yielded colonies that looked like the single *PA1107* (*roeA*) and *PA4332* (*sadC*) deletions (Fig. 3-2a). Deleting *PA0290* or *PA3702* (*wspR*) however, did not affect the Δ*PA0575* (*rmcA*) morphology drastically. This suggested that, under the conditions of our colony morphology assay, PA1107 (RoeA) and PA4332 (SadC) both lie upstream of PA0575 (RmcA) and likely produce the c-di-GMP that PA0575 (RmcA) then degrades to exert its inhibitory effects on colony structure formation while PA0290 and WspR likely fine tune c-di-GMP levels under certain conditions.

We continued our characterization of RmcA by generating a series of strains with mutations predicted to alter in vivo function. Strains in which the native *rmcA* promoter was replaced with a constitutive tac promoter, leading to a ~10-fold increase in protein levels, showed smooth colony morphology phenotypes. Colonies of the RmcA-overproduction ("RmcA+") strain (Supplmentary Fig. 3-5) also showed a ~2-fold reduction in c-di-GMP levels and CR binding compared to wild type (Fig. 3-3c). EAL domains have a canonical E(A/E/V)L motif that is required for PDE activity. We mutated the catalytic site of the RmcA EAL domain from EAL to AAA and found that this mutant phenocopied the Δ*rmcA* mutant in the colony morphology assay (Supplmentary Fig. 3-6). These results suggest that RmcA acts as a PDE to decrease c-di-GMP levels, and therefore Pel production, in colonies.

Next, we mutated the EAL motif in a strain that constitutively expresses RmcA and found that colonies formed by this RmcA+AAA strain displayed a distinct phenotype (Fig. 3-3c), with taller

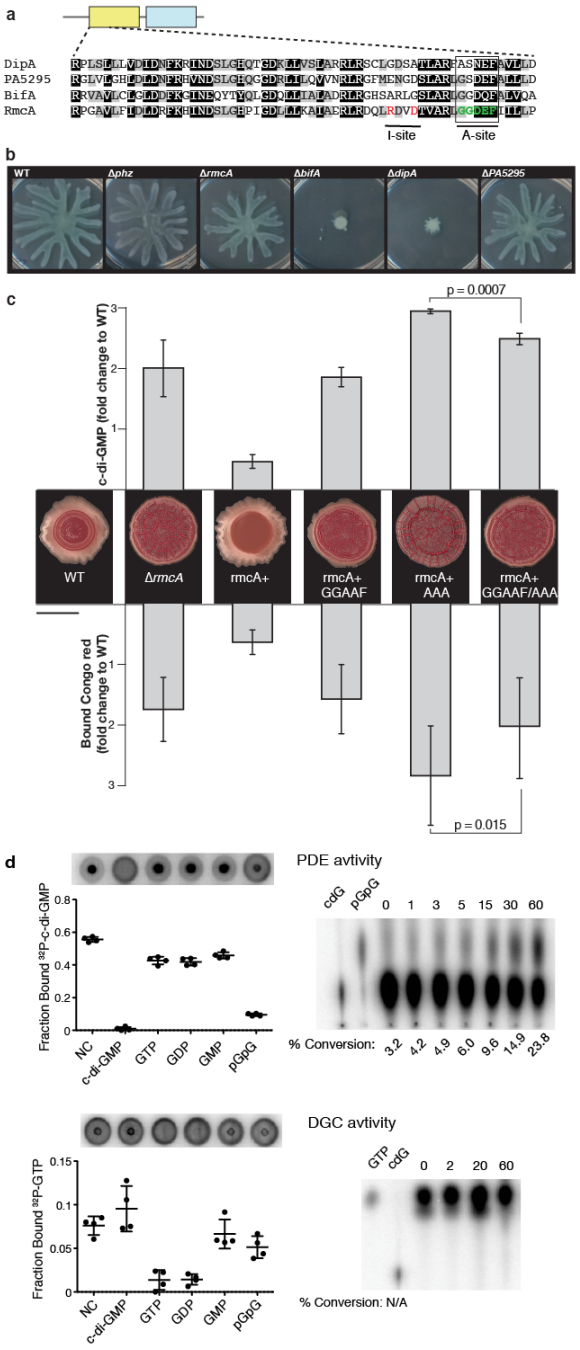

Figure 3-3. Characterization of *in vivo* functions of GGDEF+EAL-domain-containing proteins and *in vitro* function of RmcA. (a) Alignment highlighting the I-site (RxxD motif; in red) and A-site (GGDEF motif; in green) in RmcA and corresponding residues in other GGDEF+EAL-domain-containing proteins of interest. (b) Assessment of swarming capability for WT and selected mutants with altered colony phenotypes. (c) Relative Pel content, quantified using the Congo red binding assay after 2 days of growth, and c-di-GMP content, quantified after 3 days of growth, for colonies of the WT and indicated mutants. Error bars represent SD, n≥7, and p values were calculated using one-tailed heteroscedastic t-tests. Scale bar=1 cm. (d) Ligand binding and *in vitro* activities of the cytosolic portion of RmcA with a C-terminal 9xHis tag. Left-hand panels show cyclic-di-GMP (top left) and GTP (bottom left) binding. NC, no competitor. Right-hand panels show *in vitro* phosphodiesterase (top right) and diguanylate cyclase (bottom right) activity.

wrinkles forming the central ring and emanating spokes. RmcA+AAA mutant colonies also showed higher c-di-GMP levels and CR binding than those formed by Δ*rmcA* (Fig. 3-3c). These results were suggestive of a DGC activity for RmcA. RmcA has an intact GGDEF motif in the active site (A-site) that, when mutated to GGAAF in both wild-type and RmcA+ backgrounds, yielded colonies with wrinkling phenotypes similar to those of Δ*rmcA* (Fig. 3-4a). Colonies formed by the strain overexpressing the RmcA GGAAF mutant protein also exhibited c-di-GMP levels and CR binding that were similar to those measured for Δ*rmcA* colonies (i.e., higher than those found in wild-type colonies) (Fig. 3-3c). These results suggest that the GGDEF A-site in RmcA somehow acts to promote degradation of c-di-GMP and colony smoothness. These observations are similar to those reported for the mutational analysis of PA4367 (BifA), a PDE that also contains GGDEF and EAL domains; however, the A-site motif in the BifA GGDEF domain is degenerate [20].

Beyond its role in promoting the activity of the EAL domain, the higher c-di-GMP levels displayed by RmcA+AAA relative to Δ*rmcA* imply that the GGDEF domain also has a DGC activity that is only observable in the absence of a functional EAL domain (Fig. 3-3c). We investigated this by creating strain "RmcA+GGAAF;AAA," which constitutively expresses a version of RmcA that harbors mutations in both the GGDEF and the EAL domains. Adding the RmcA GGAAF mutation to RmcA+AAA decreased c-di-GMP to a level comparable to that observed for Δ*rmcA* (Fig. 3-3c) and produced a colony morphology similar to that of ΔrmcA (Fig. 3-3c).

In the context of the apparent PDE-promoting and DGC activities of the RmcA GGDEF domain, it is interesting to note that although all 4 of the hits from our screen with hyperwrinkled phenotypes represent proteins harboring both GGDEF and EAL domains, RmcA is the only one that contains an intact version of the GG(D/E)EF motif typically required for DGC activity; the corresponding sites in PA4367 (BifA), PA5017 (DipA) and PA5295 are degenerate. PA0575 (RmcA) is also the only one of these 4 represented proteins that contains an intact version of

the “I-site”, an RxxD motif that found in some GGDEF domains (Fig. 3-3a). In some DGCs, c-di-GMP binding to the I-site results in non-competitive allosteric inhibition, and the presence of an intact I-site tends to correlate with an intact GGDEF motif and DGC activity [29].

We next employed in vitro assays to test the ability of RmcA to bind c-di-GMP and other substrates associated with these domains, and to test RmcA for PDE and DGC activity. These studies were conducted using a His-tagged, truncated version of RmcA that lacks the domains predicted to localize to the periplasm and cytoplasmic membrane. Using a DRaCALA assay [30], we observed that the His-tagged cyotosolic truncation of RmcA is able to bind radiolabelled GTP and c-di-GMP (Fig. 3-3d), but that binding of c-di-GMP appeared to be much stronger than binding of GTP. We further tested the specificity of RmcA GTP and c-di-GMP binding by competition with other unlabeled substrates. RmcA binding to radiolabeled c-di-GMP was abolished by unlabeled c-di-GMP. GTP, GDP, and GMP caused modest decreases in c-di-GMP binding, while pGpG showed robust competition with c-di-GMP for binding. RmcA binding to radiolabeled GTP was abolished by unlabeled GTP and GDP. c-di-GMP, GMP and pGpG did not significantly affect GTP binding. The fact that GTP and GDP lead to similarly large decreases in the binding of radiolabeled GTP suggests that although RmcA may have modest DGC activity in vivo, its binding of GTP is not specific.

To investigate the in vitro kinetics of RmcA PDE and DGC activity, c-di-GMP or GTP was incubated with purified RmcA (His-tagged cytosolic truncation) and spotted on TLC plates. We observed a modest conversion of c-di-GMP to pGpG after 60 minutes, but no conversion of GTP during this time (Fig. 3-3d). The results of our assays for ligand binding and catalytic activities are consistent with RmcA functioning predominantly as a PDE. This is consistent with results from our mutational analyses of RmcA’s GGDEF and EAL domains, which suggest that, although this protein has both DGC and PDE activity, its PDE activity plays a dominant role in determining c-di-GMP levels, Pel production, and morphogenesis of PA14 colonies.

Finally, we shifted our attention to RmcA's PAS domains and tested the hypothesis that one or more of these is required for RmcA's role in colony development. We found that deleting PAS-B, PAS- C and PAS-D resulted in colonies that phenocopied Δ*rmcA* suggesting that they support RmcA PDE activity. Intriguingly, we found that deleting PAS-A in both the wild-type and Δ*phz* backgrounds yielded colonies that were smoother than those formed by their corresponding parent strains (Fig. 3-4a). This prompted us to hypothesize that PAS-A is involved in the modest DGC activity exhibited by RmcA in vivo, as the smoother phenotype of the PAS-A deletion indicates less Pel production and possibly less c-di-GMP produced. To test this, we took advantage of the RmcA+AAA mutant, which exhibited increased c-di-GMP levels and CR binding phenotypes that were attributed to DGC activity (Fig. 3-3c). When PAS-A was deleted in the RmcA+AAA background, the resulting colony phenocopied that formed by the RmcA+GGAAF;AAA mutant (Fig. 3-4b). This suggested that PAS-A might regulate the RmcA DGC activity that we observe in RmcA+AAA.

Sequence alignments using the PAS-D domain of RmcA revealed conserved residues that are involved in the binding of an FAD cofactor in other proteins (Fig. 3-4c). Indeed, when we expressed and purified a truncated form of RmcA composed of the 4 PAS domains, it exhibited a bright yellow color and an absorbance spectrum consistent with FAD binding (Supplementary Fig. 3-4e). If PAS-D does bind FAD, the redox state of this cofactor could be affected by that of the cytoplasm, providing a mechanism whereby RmcA activity--and therefore c-di-GMP levels, Pel production, and colony morphogenesis--could be modulated by redox conditions. Confirmation of this and identification of the cofactors associated with the other PAS domains of RmcA will likely require structural analysis, but the structural similarity of the pseudomonad phenazines to the isoalloxazine heterocycle of the flavin group raises the tantalizing possibility that RmcA binds phenazines directly and is influenced by their redox states. In addition to RmcA, the PDE PA5017 (DipA) and the DGC PA0290 also contain PAS domains with the potential to respond to changes in the redox environment. These various sensors could provide diverse avenues by which environmental influences ultimately determine the morphological

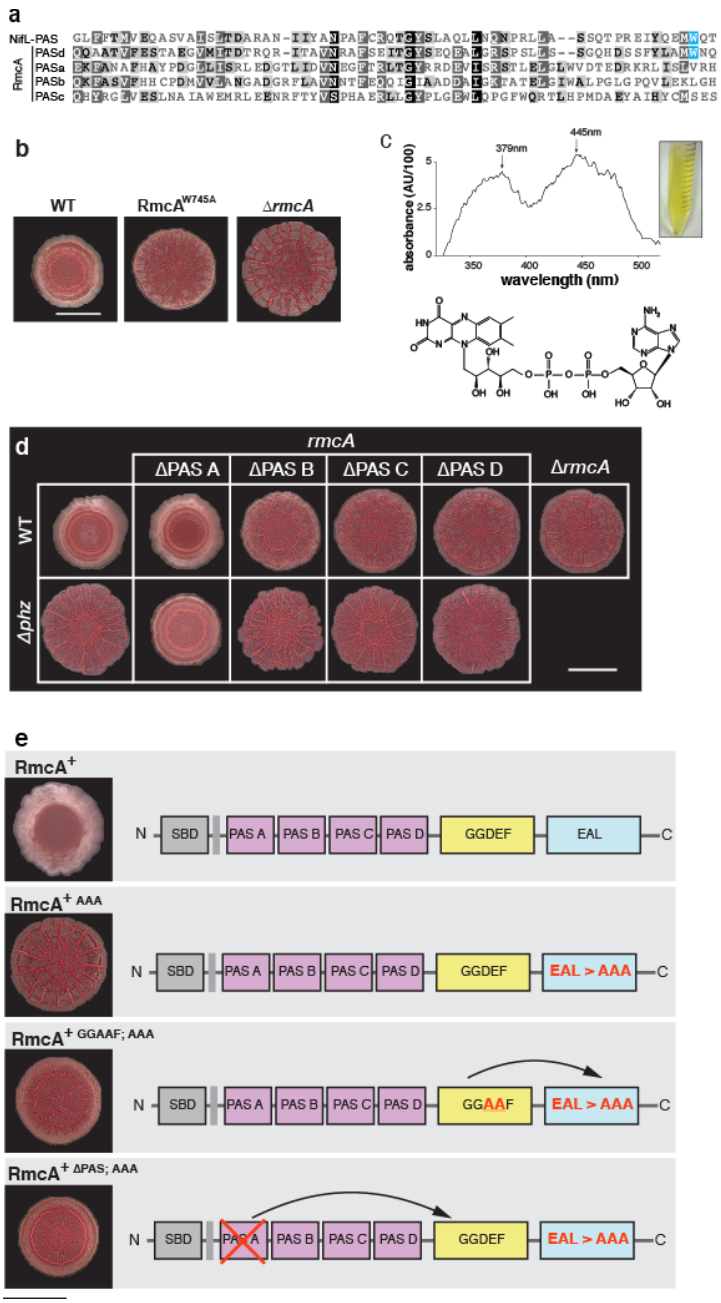

Figure 3-4. Roles of individual RmcA domains in cofactor binding and regulation of colony morphogenesis. (a) Alignment of the RmcA PAS domains with the PAS domain of *Azotobacter vinelandii* NifL shows that the PAS-D domain contains aa tryptophan required for covalent linkage to FAD (highlighted in teal). (b) Mutation of the residue implicated in FAD binding by RmcA leads to enhanced colony wrinkling. (c) Purification of a His-tagged RmcA truncation containing only the PAS domains yields a preparation that is bright yellow in color, and the UV visible spectrum for this preparation shows peaks corresponding to oxidized FAD. (d) Representative colony images for mutational analysis of the roles of individual PAS domains in RmcA function *in vivo*. Colonies were grown for 3 days. (e) Representative colony images for mutants testing the roles of specific motifs and potential interdomain crosstalk in RmcA. Cartoons depict hypothesized interactions between RcmA domains involved in c-di-GMP metabolism. Colonies were grown for 3 days. Scale bars each =1 cm.

output of PA14 communities.

3-4 MATERIALS AND METHODS

3-4-1 Strains and growth conditions

Strains used in this study are listed in Table 3-1. Unless otherwise stated, liquid cultures of *Pseudomonas aeruginosa* UCBPP-PA14 were grown in lysogeny broth (LB) (Miller) (Bertani 2004) at 37˚C, with shaking at 250 rpm. For genetic manipulation, strains were routinely plated on LB + 1.5% agar. For selection purposes, gentamicin was added to the medium at 100 µg/mL and 15 µg/mL for P. aeruginosa and E. coli, respectively. Growth conditions for colony biofilms are described below.

3-4-2 Phenazine quantification

Ten technical replicates (10 µL each) of overnight pre-cultures were spotted on 10-cm round petri dishes containing 40 mL of solidified 1% agar, 1% tryptone medium. Colonies were incubated for 3 days at 25 °C and 80-90% humidity, then scraped from the plate. Half of the solidified medium containing released phenazines was transferred to 50-mL conical tube containing 3 mL of water and nutated overnight in the dark at room temperature to extract phenazines. Extract was filtered using 0.22 µm Spin-X filter tubes (Costar) and loaded directly onto a Waters Symmetry C18 reverse-phase column (4.6 x 250 mm; 5 mm particle size) in a Beckman SystemGold HPLC with a photodiode array detector. Phenazines were separated following a previously described protocol (Dietrich 2006). Conversion factors used for PYO, PCA and PCN were 8 x 10^{-6} mM/AU, 9.5 x 10^{-6} mM/AU and 9.5 x 10^{-6} mM/AU respectively.

3-4-3 Colony morphology assay

Colony morphology assay medium was prepared by autoclaving a mixture of 1% tryptone (Teknova) and 1% agar (Teknova). Mixture was cooled to 60˚C and 20 mg/L Coomassie blue (EMD) and 40 mg/L Congo red (EMD) dyes were added. Sixty mL of medium was poured into 10 cm x 10 cm x 1.5 cm square plates (LDP) and allowed to solidify and dry for 16 - 24 hours.

Ten µL of overnight pre-cultures were spotted on dried plates and colonies were grown at 25 °C and 80-90% humidity. Images of colonies were taken daily using a Keyence VHX-1000 digital microscope.

3-4-4 Quantification of c-di-GMP from colonies

Ten µL of overnight pre-cultures were spotted in biological triplicates on colony morphology assay agar plates (prepared as described above) and grown for 2.5 days in conditions used for the colony morphology assay. Each colony was scraped from the plate, transferred to 1 mL PBS, and homogenized using a BeadBug (Benchmark Scientific) for 3 minutes. Homogenized colonies were transferred to pre-weighed MicroTubes (Sarstedt) and pelleted by centrifugation at 16,873 rcf. The supernatant was removed and cyclic di-GMP was extracted with methanol/ acetonitrile/water (40:40:20) with 0.1 N formic acid at -20°C for 1h. The extract was then centrifuged at 14,549 rcf for 5 min at 4°C. Two hundred µL of supernatant was transferred to a fresh tube and neutralized with 8 µl of 15% NH_4HCO_3, dried with a speed vacuum, and resuspended in 200 µl 10mM tributylamine +15mM Acetic acid. Samples were quantified at the Mass Spectrometry Facility of Michigan State University by electrospray ionization (ESI) analysis with Quattro Premier XE LC/MS/MS. The pellet from the extraction step was dried using a speed a vacuum and weighed. The final concentration of cyclic di-GMP was normalized to cell dry weight.

3-4-5 Pel polysaccharide quantification

Congo red binding was used to determine the amount of Pel polysaccharide produced by colonies. Ten µL of overnight pre-cultures were spotted in biological triplicates on 1% tryptone ,1% agar solidified medium and spots were grown for 2 days at 25˚C. Colonies were scraped from the plate into a 1 mL solution of PBS + 40mg/L Congo red dye. The resuspension was incubated at 37˚C for 1 hour, then transferred to clear 96-well plate (Grenier bio-one) for measurement of absorbance at 490 nm using a plate reader (Biotek Synergy 4). PBS + 40 mg/L

Congo red was used as a standard to determine to amount of Congo red bound by the colony and removed from the solution.

3-4-6 Initiation of colony wrinkling

Ten µL of overnight pre-cultures were spotted on colony morphology assay plates (as described above). After growth for 24 hours at room temperature, images of the developing colony were taken every 15 minutes over a 4-day period using a customized recording system (Logitech HD Webcam C525) under LED illumination. Lighting and image capture were synchronized with LabView (National Instruments).

3-4-7 Swarming assay

Overnight precultures were washed once in PBS and resuspended at an OD500 of 1.0. Two µL of this suspension was spotted at the center of a plate containing 20 mL of swarming assay medium (M9 salts medium amended with 0.2% glucose and 0.5% casamino acids, solidified with 0.5% agar) that had been dried for 45 minutes in a laminar flow hood. Plates were sealed with parafilm and incubated in an inverted position for 16 hours at 37˚C [31]. Plates were imaged with a Canon CanoScan 5600F scanner.

3-4-8 NADH/NAD^+ assay

Extraction of NADH and NAD^+ was performed as described previously [7,32] Ten µL of pre-cultures were spotted in biological triplicates on colony morphology assay agar plates (prepared as described above) and grown for the specified time. At the indicated time point, the colony was scraped off the plate into 1 mL 1% tryptone using a sterile 1 mL pipette tip and homogenized using a pellet disruptor. For each colony, two 450 µL samples were transferred to separate MicroTubes (Sarstedt) for NADH and NAD^+ extractions. NADH and NAD^+ were qunatified using an enzyme-cycling assay as described previously [32].

3-4-9 Western blot

Two mL cultures of strains with and without the N-terminal histidine tag on Rom were grown overnight with shaking at 37˚C, then used to seed 1 L cultures. The 1 L cultures were grown overnight at 37˚C with shaking. Cells were pelleted by centrifugation at 3,250 rpm for 30 minutes (Beckman J6-MI) and were resuspended in 50 mL of lysis buffer [50 mM Tris-HCl, pH 7.5, 0.5 M NaCl, 10% (v/v) glycerol, 1 mM $MgCl_2$, 1 mg/mL lysozyme (Sigma), 13.2 µg/mL dnase (Sigma) and 1 complete EDTA-free protease inhibitor tablet (Roche)]. Lysis buffer components that were degassed and chilled at 4˚C prior to cell lysis.

Cells were lysed by four passages through an Avestin Emulsiflex C-3 cell disrupter at an operating pressure of 15,000 psi. Cell lysate was centrifuged at 4,500 rpm for 15 minutes (Beckman Coulter, SX4750 rotor) at 4˚C to remove cell debris and unlysed cells; the supernatant was then ultracentrifuged at 45,000 rpm for 1 hour (Beckman, L8-70M). The pellet was rinsed by swirling lysis buffer over pellet twice and then resuspended in 10 mL of resuspension buffer [0.5 M NaCl, 50 mM Tris-HCl, pH 7.5, 0.3% (w/v) n-Dodecyl β-D-maltoside, 1 mM tris(2-carboxyethyl)phosphine (TCEP) and 30% (v/v) glycerol]. The resuspended pellet was incubated overnight with slow rotation at 4˚C and then ultracentrifuged at 45,000 rpm for 1 hour (Beckman, L8-70M). Protein concentration in supernatant was determined using the Bio-Rad protein assay with bovine serum albumin (BSA) as the standard.

Protein samples were separated on 4 - 12% NuPage Bis-Tris gels (Life Technologies) and blotted on to a 0.45 µM-pore size nitrocellulose membrane (GE Water and Process Technologies). The membrane were stained using Ponceau S stain (0.1%) (G Biosciences) and destained with 0.1 M NaOH according manufacturer's protocol. The membrane was incubated overnight in blocking solution [1X Tris buffered saline with 1% (v/v) Tween-20 (TBST) and 5% (w/v) non-fat dry milk powder]. The membrane was then probed with anti-6X His tag (HIS.H8; abcam) at a 1:2000 dilution in 50% (v/v) blocking solution (diluted with 1X TBST) for 1 hour at room temperature. Blots were washed and probed with goat anti-mouse horseradish

peroxidase (HRP)-conjugated secondary antibody (Sigma) and developed using Amersham ECL Plus Western Blotting Detection kit (GE Healthcare).

3-4-10 Construction of deletion, complementation, point mutation, and constitutive expression plasmids

Deletion, complementation, point mutation and constitutive expression plasmids were generated using yeast gap repair cloning. The strains generated from these plasmids are listed in Table 3-1 and the primers used to construct the plasmids are listed in Table 3.-3

To construct the deletion and point mutation plasmids, flanking regions ~1 kilobase in length for the genes to be deleted and residues to be mutated were amplified using PCR. For point mutation plasmids, the intended mutation sequence to be inserted into the genome was added at the 5' end of both flanking regions. To construct the *PA14_07500* complementation plasmid, *PA14_07500* with ~1 kilobase on both sides of the gene was amplified using PCR. A "promoter swap" plasmid was used to generate the constitutively expressing *PA14_07500* mutant. The regions flanking the native *PA14_07500* promoter and the constitutive $PA_{1/04/03}$ promoter were amplified using PCR.

Where applicable, the constitutive $PA_{1/04/03}$ promoter (constitutively expressing mutant only), the flanking regions and the linearized allelic-replacement vector pMQ30 were assembled by gap repair cloning using the yeast strain *InvSc1* (Invitrogen) (Shanks 2006). The resulting plasmid was transformed into *Escherichia coli* BW29427 and transformed into PA14 using biparental conjugation. PA14 single recombinants were selected on LB agar containing 100 μg/ml gentamicin. Potential complemented strains, deletion and point mutants were generated by selecting for double recombinants by identifying strains that grew in the presence of 10% (w/v) sucrose. Strains with properties of double recombination were further analyzed by PCR.

3-4-11 Construction of His-tag plasmids

The his-tag plasmid was designed to insert a N-terminal 9x Histidine tag 72 base pairs into PA14_07500. Flanking regions ~1 kilobase to this point in the gene were amplified using PCR. Each flanking region had a 9x Histidine residue sequence at the 5' end. The flanking regions and the linearized allelic-replacement vector pMQ30 were assembled by gap repair cloning using the yeast strain *InvSc1* (Invitrogen) (Shanks 2006). The resulting plasmid was transformed into *Escherichia coli* BW29427 and transformed into PA14 using biparental conjugation. PA14 single recombinants were selected on LB agar containing 100 μg/ml gentamicin. Potential his-tagged strains were generated by selecting for double recombinants by identifying strains that grew in the presence of 10% (w/v) sucrose. Strains with properties of double recombination were further analyzed by PCR.

3-4-12 Liquid-culture growth curves

Overnight pre-cultures were grown in LB at 37˚C with shaking at 250rpm. Pre-cultures were diluted in 1% (w/v) tryptone to a starting OD_{500} of 0.01 into 96-well plates (Greiner Bio-one). Cultures were shaken at "medium" speed and absorbance at 500nm was taken every 30 minutes using a plate reader (Biotek Synergy 4).

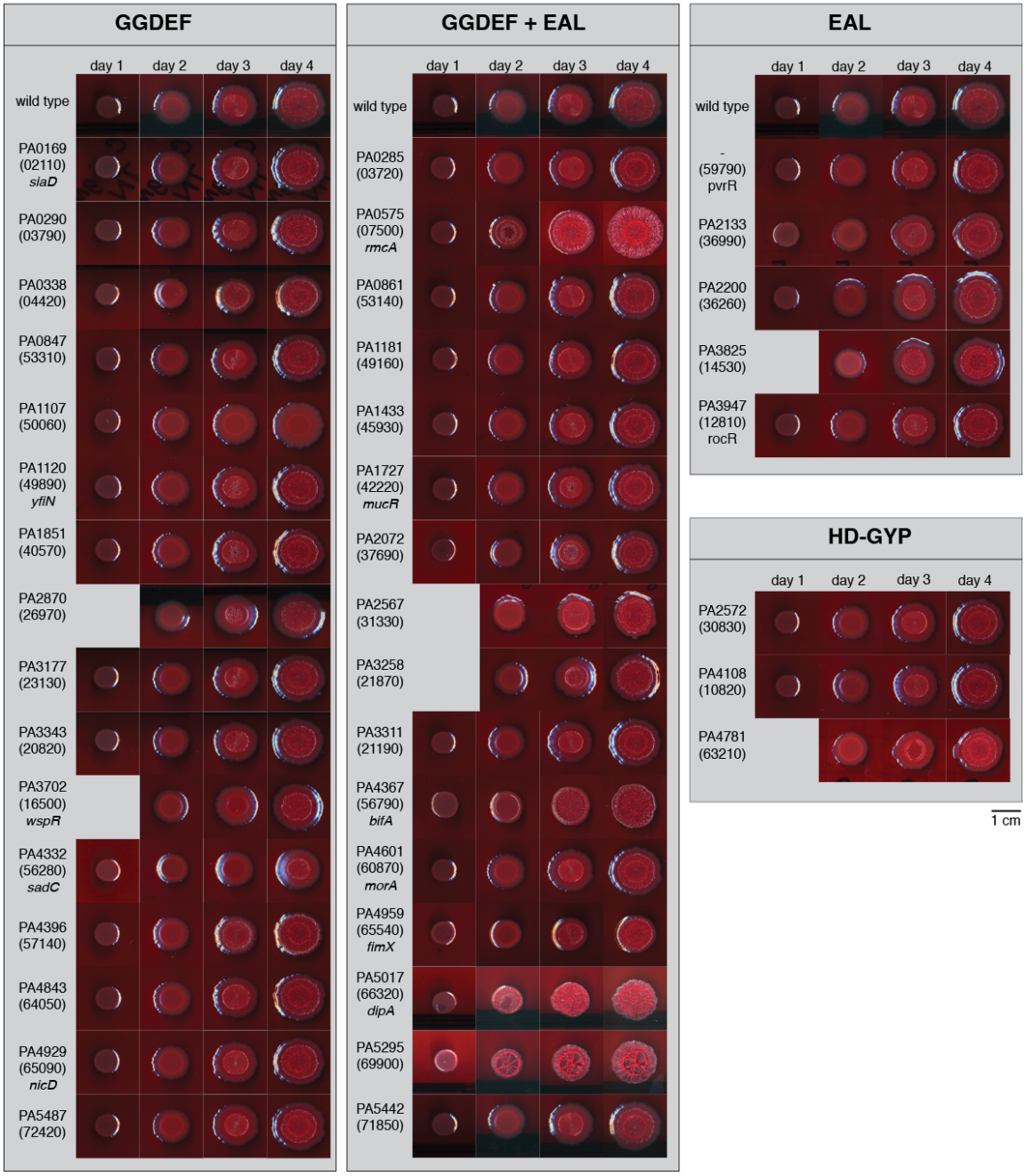

Supplementary Figure 3-1. Screen for proteins that modulate c-di-GMP levels during *P. aeruginosa* PA14 colony development. Representative images of mutants grown for 4 days in the colony morphology assay. All mutants shown contain transposon insertions or in-frame markerless deletions in genes predicted to encode GGDEF, EAL, and/or HD-GYP domains. Mutants are arranged according to the domain content of their disrupted proteins, then by number of the PAO1 ORF homologous to that of the disrupted protein. The corresponding PA14 ORF number for each protein is shown in parentheses.

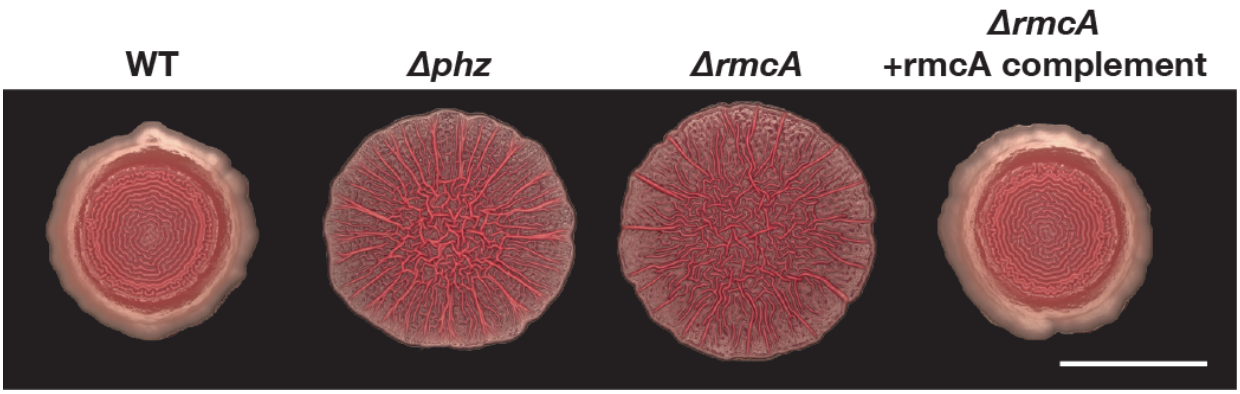

Supplementary Figure 3-2. Complementation of Δ*rmcA* restores the wild-type colony phenotype. Representative images of colonies grown for 3 days in the colony morphology assay. Scale bar=1 cm.

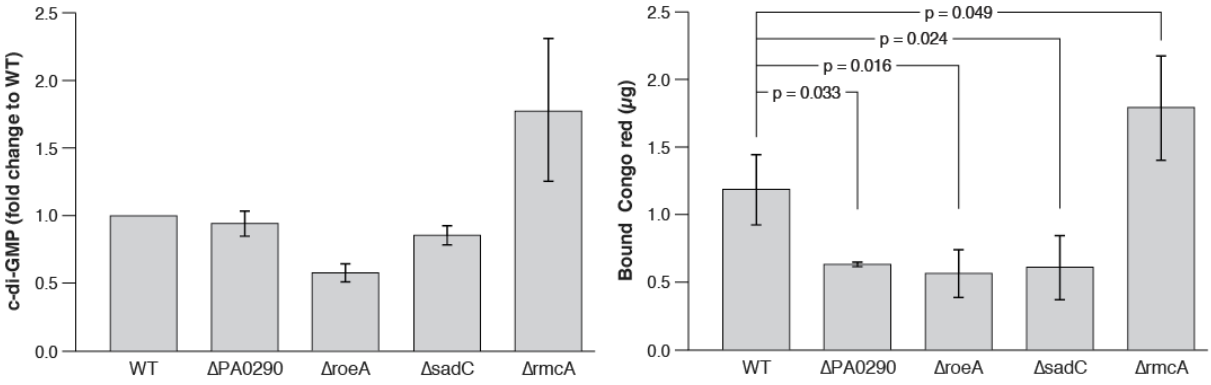

Supplementary Figure 3-3. Quantification of c-di-GMP and Pel production for selected mutants with altered colony phenotypes. Left: Relative cyclic-di-GMP (c-dI-GMP) levels in colonies grown for 3 days on colony morphology assay medium Right: Pel content, quantified using the Congo red binding assay, in colonies grown for 2 days on 1% tryptone, 1% agar medium with no added dyes. p values were calculated using one-tailed heteroscedastic t-tests. Error bars represent SD and n=3.

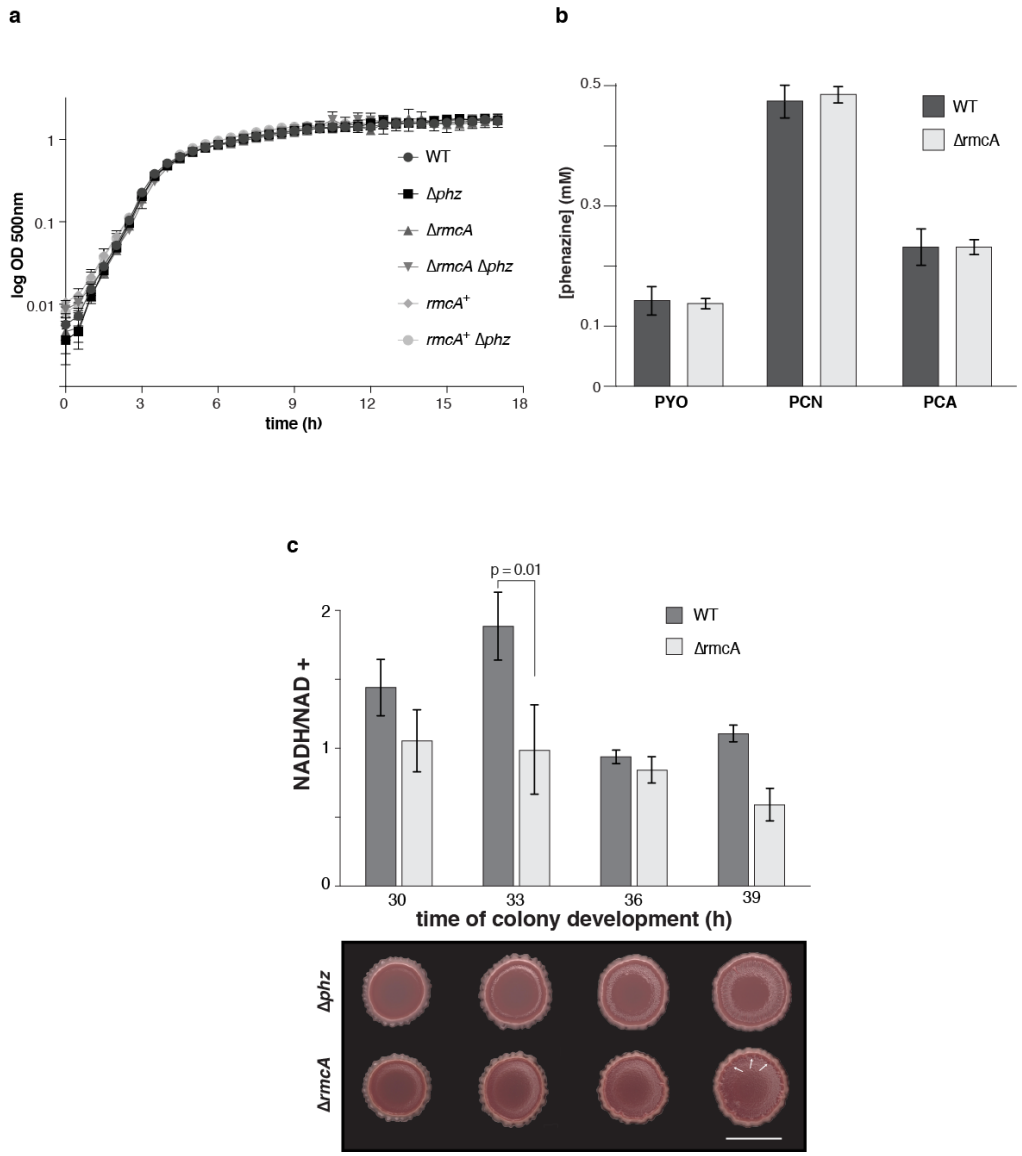

Supplementary Figure 3-4. Characterization of Δ*rmcA* liquid-culture growth, colony phenazine production, and cellular redox state. (a) Growth of shaken liquid cultures of WT, Δ*phz*, and related mutants in LB at 37°C. Error bars represent SD and n=4. (b) Quantification of pyocyanin (PYO), phenazine-1-carboxamide (PCN), and phenazine-1-carboxylic acid (PCA) in extracts of medium that supported the growth of PA14 WT and Δ*rmcA* colony biofilms. Colonies were grown on 1% tryptone, 1% agar for 3 days, then removed with a razor blade. Aqueous extract prepared from the agar was analyzed by HPLC. Error bars represent SD and n=3. (c) Top, time course showing differences in the intracellular redox state for Δ*phz* and Δ*rmcA*, two mutants with similar colony phenotypes (bottom). Colonies were grown on colony morphology assay medium. Scale bar=1 cm. Error bars represent SD, n=3, and p value was calculated using a one-tailed heteroscedastic t-test.White arrows indicate initiation of wrinkling Δ*rmcA* colony at 39 h

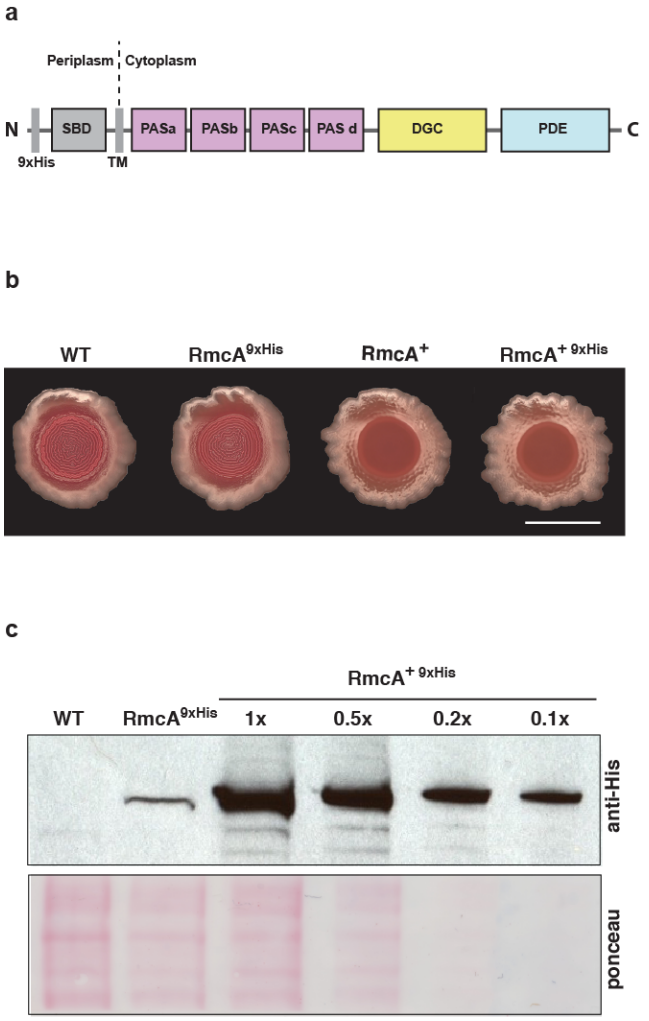

Supplementary Figure 3-5. Phenotypic characterization and expression analysis of RmcA with an N-terminal 9xHis tag. (a) Cartoon depicting the domain architecture of RmcA and the location of the N-terminal tag. (b) Addition of an N-terminal 9xHis tag does not affect *in vivo* function of RmcA. Colonies were grown on colony morphology assay medium for 3 days. Scale bar=1cm. (c) Overproduction of the His-tagged protein was confirmed by Western blot using membrane fractions from whole-cell lysates.

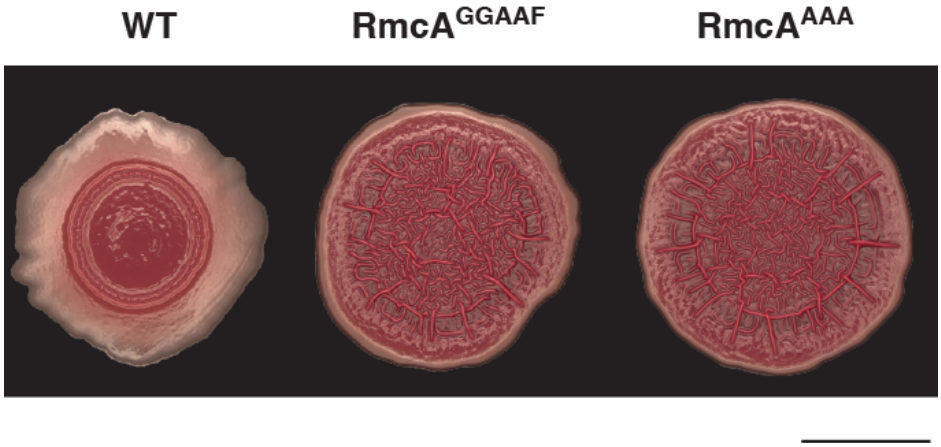

Supplementary Figure 3-6. Mutations in RmcA's EAL but not GGDEF motifaffect colony morphology. Representative images of colonies grown for 3 days on colony morphology assay medium. Scale bar=1 cm.

Table 3-1. Bacterial and fungal strains used in this study.

Strain	Relevant characteristics	Source
Pseudomonas aeruginosa		
UCBPP-PA14	Clinical isolate UCBPP-PA14	Rahme, *et al.* 1995
PA14 Δ*phz*	PA14 with deletions in *phzA1-G1* and *phzA2-G2* operons	Dietrich, *et al.* 2006
PA14 Δ*0575*	PA14 with deletion in PA14_07500	Dietrich *et al.* 2008
PA14 Δ*0290*	PA14 with deletion in PA14_03790	This study
PA14 Δ*4332*	PA14 with deletion in PA14_56280	This study
PA14 Δ*1107*	PA14 with deletions in PA14_50060	This study
PA14 Δ*3702*	PA14 with deletion in PA14_16500	This study
PA14 Δ*2870*	PA14 with deletion in PA14_26970	This study
PA14 Δ*3825*	PA14 with deletion in PA14_14530	This study
PA14 Δ*2133*	PA14 with deletion in PA14_36990	This study
PA14 Δ*2200*	PA14 with deletion in PA14_36260	This study
PA14 Δ*3258*	PA14 with deletion in PA14_21870	This study
PA14 Δ*bifA*	PA14 with deletion in PA14_56790	This study
PA14 Δ*4396*	PA14 with deletion in PA14_57140	This study
PA14 Δ*4781*	PA14 with deletion in PA14_63210	This study
PA14 Δ*2567*	PA14 with deletion in PA14_31330	This study

PA14 Δ*1107*Δ*bifA*	PA14 with deletions in PA14_50060 and PA14_56790	This study
PA14 Δ*4332*Δ*bifA*	PA14 with deletions in PA14_56280 and PA14_56790	This study
PA14 Δ*0575*Δ*1107*	PA14 with deletions in PA14_07500 and PA14_50060	This study
PA14 Δ*0575*Δ*4332*	PA14 with deletions in PA14_07500 and PA14_56280	This study
Escherichia coli		
UQ950	*E. coli* DH5 λ(pir) strain for cloning. F-Δ(*argF-lac*)169ϕ*80 dlacZ58*(ΔM15) *glnV44(*AS) *rfbD1 gyrA96*(NaI^R) *recA1 endA1 spoT thi-1 hsdR17 deoR* λ *pir*$^+$	D. Lies, Caltech
BW29427	Donor strain for conjugation. *thrB1004 pro thi rpsL hsdS lacZ* ΔM15RP4-1360 Δ(*araBAD*)*567* Δ*dapA1314::*[*erm pir*(wt)]	W. Metcalf, University of Illinois
Saccharomyces cerevisiae		
InvSc1	*MATa/MATalpha leu2/leu2 trp1-289/ trp1-289 ura3-52/ ura3-52 his3-Δ1/ his3-Δ1*	Invitrogen

Table 3-2. Plasmids used in this study.

Plasmids	Description	Source
pMQ30	7.5 kb mobilizable vector *oriT*, *sacB*, Gm^R	Shanks *et al.* 2006

Table 3-3. Primers used in this study.

Δ0575 **deletion strain**	
Δ0575 yeast-1	ccaggcaaattctgttttatcagaccgcttctgcgtt ctgTGTTCCAACCCCTATCCAGA
Δ0575 yeast-2	**gagttccgcgacgaacag**TGTTCGCCA GCAAATTCCTC
Δ0575 yeast-3	**gaggaatttgctggcgaaca**CTGTTCGTC GCGGAACTC
Δ0575 yeast-4	ggaattgtgagcggataacaatttcacacaggaa acagctCCATCGCCAAGAAGTACACC
Δ0290 **deletion strain**	
Δ0290 yeast-1	ccaggcaaattctgttttatcagaccgcttctgcgtt ctgatGGCCTGTTCAGCGACATC
Δ0290 yeast-2	**gctgtagagggcaccgag**GTCGTAGGC CCAGAGCAC
Δ0290 yeast-3	**gtgctctgggcctacgac**CTCGGTGCCC TCTACAGC
Δ0290 yeast-4	ggaattgtgagcggataacaatttcacacaggaa acagctGCTCACCGTTGCTTTCCAG
Δ*4332* **deletion strain**	
Δ4332 yeast-1	ccaggcaaattctgttttatcagaccgcttctgcgtt ctgatGGTTGGCCGCAGAGTAAG
Δ4332 yeast-2	**cacttacctgctcggcctg**GGCATGACCC TGCTGTATG
Δ4332 yeast-3	**catacagcagggtcatgcc**CAGGCCGAG CAGGTAAGTG
Δ4332 yeast-4	ggaattgtgagcggataacaatttcacacaggaa acagctAGGACTTCCTTCGCCATCAC
Δ*1107* **deletion strain**	
Δ1107 yeast-1	ccaggcaaattctgttttatcagaccgcttctgcgtt ctgatGGCGTTGATGAGCTATTTCG
Δ1107 yeast-2	**cggtagagagcctggtcgcg**GGTCAGAC GCGAGAGATT
Δ1107 yeast-3	**aatctctcgcgtctgacc**CGCGACCAGG CTCTCTACCG
Δ1107 yeast-4	ggaattgtgagcggataacaatttcacacaggaa acagctTCGCAGTAGCTGTTGTGTCC
Δ*3702* **deletion strain**	

Δ3702 yeast-1	ccaggcaaattctgttttatcagaccgcttctgcgtt ctgAGAATGTGCACCGGGTTTTC
Δ3702 yeast-2	tgttcttggcctggtagagCATGGCCTGATC ATCGACA
Δ3702 yeast-3	tgtcgatgatcaggccatgCTCTACCAGGC CAAGAACA
Δ3702 yeast-4	ggaattgtgagcggataacaatttcacacaggaa acagctGTGTTCACGTGCTGACCG
Δ*2870* deletion strain	
Δ2870 yeast-1	ccaggcaaattctgttttatcagaccgcttctgcgtt ctgatCGATTGCAGCATTCCCGG
Δ2870 yeast-2	agatcatggggctgttgctcCGCTCTACCA GGCCAAGAG
Δ2870 yeast-3	ctcttggcctggtagagcgGAGCAACAGCC CCATGATCT
Δ2870 yeast-4	ggaattgtgagcggataacaatttcacacaggaa acagctCTATGCCGCCAACCACCG
Δ*3825* deletion strain	
Δ3825 yeast-1	ccaggcaaattctgttttatcagaccgcttctgcgtt ctgaCAGCCTGGTGTTCGACTTC
Δ3825 yeast-2	aaagcagactctccagcggGATGAGCAGC CCCAGGAC
Δ3825 yeast-3	gtcctggggctgctcatcCCGCTGGAGAG TCTGCTTT
Δ3825 yeast-4	ggaattgtgagcggataacaatttcacacaggaa acagctTCAGCACAGACAGAAAACG C
Δ*2133* deletion strain	
Δ2133 yeast-1	ccaggcaaattctgttttatcagaccgcttctgcgtt ctgatGTGTTCGAACCAGCCGCT

Δ2133 yeast-2	cagaatgggagccgctctaGGACGTCTAT CTCCAGGGC
Δ2133 yeast-3	gccctggagatagacgtccTAGAGCGGCT CCCATTCTG
Δ2133 yeast-4	ggaattgtgagcggataacaatttcacacaggaa acagctATCGACCTGTACCGCGAAA
Δ*2200* deletion strain	
Δ2200 yeast-1	ccaggcaaattctgttttatcagaccgcttctgcgtt ctgGGGGAAAGCTGGAAGAACTC
Δ2200 yeast-2	atactgctcaccacgtcgtAAGGGATCGAG ACACAGGC
Δ2200 yeast-3	gcctgtgtctcgatcccttACGACGTGGTGA GCAGTAT
Δ2200 yeast-4	ggaattgtgagcggataacaatttcacacaggaa acagctCGAAGTGACGCTGTGGAAC
Δ*3258* deletion strain	
Δ3258 yeast-1	ccaggcaaattctgttttatcagaccgcttctgcgtt ctgAAACACTGGGATAGCCTGCT
Δ3258 yeast-2	gtcaccgagcagttgagcCTGCTGTCATT GTCCGTCG
Δ3258 yeast-3	cgacggacaatgacagcagGCTCAACTG CTCGGTGAC
Δ3258 yeast-4	ggaattgtgagcggataacaatttcacacaggaa acagctGCCGAATTGCAGAAGGACA A
Δ*bifA* deletion strain	
ΔbifA yeast-1	ccaggcaaattctgttttatcagaccgcttctgcgtt ctgACAGTTGCTGCGTGGATATG

ΔbifA yeast-2	ctgcttgaggtactgggtcagGCTGTGTCG GGAGTCCAGTT
ΔbifA yeast-3	aactggactcccgacacagcCTGACCCAG TACCTCAAGCAG
ΔbifA yeast-4	ggaattgtgagcggataacaatttcacacaggaa acagctCTGCGCTGGCTGTTCATC
Δ*4396* deletion strain	
Δ4396 yeast-1	ccaggcaaattctgttttatcagaccgcttctgcgtt ctgAAAAACACCCCTCCCTTCC
Δ4396 yeast-2	tttcaggctgatgaagccttcGACGACCAGG ATGCTGAGAT
Δ4396 yeast-3	atctcagcatcctggtcgtcGAAGGCTTCAT CAGCCTGAAA
Δ4396 yeast-4	ggaattgtgagcggataacaatttcacacaggaa acagctATGCATCGAGGAATAGTTGG
Δ*4781* deletion strain	
Δ4781 yeast-1	ccaggcaaattctgttttatcagaccgcttctgcgtt ctgGAAAACTTCAGGCCACGCTA
Δ4781 yeast-2	ggacaacctgctgctgatgTGGACGTGGA GATGCAGC
Δ4781 yeast-3	gctgcatctccacgtccaCATCAGCAGCA GGTTGTCC
Δ4781 yeast-4	ggaattgtgagcggataacaatttcacacaggaa acagctCTGTTCAGCCAGTTGTTCGG
Δ*2567* strain deletion	
Δ2567 yeast-1	ccaggcaaattctgttttatcagaccgcttctgcgtt ctgTCGGTCTGAACGGGAATATC
Δ2567 yeast-2	acaatccctatgtgcaaggcGAGGGCCAG GGCTATCTG
Δ2567 yeast-3	cagatagccctggccctcGCCTTGCACAT AGGGATTGT

Δ2567 yeast-4	ggaattgtgagcggataacaatttcacacaggaa acagctGGTAGAGCCGGACGACCA
PA0169/PA14_02110 transposon insertion check	
PA0169 in-check 1	GACCACGCGCTGCTCAAG
PA0169 in-check 2	AGGATTGCAGCTTCCCCTTC
PA0338/PA14_04420 transposon insertion check	
PA0338 in-check 1	CAAGGTGAAGTGGCTGCTG
PA0338 in-check 2	CTCTCCAGCGTGTTCATCG
PA3343/PA14_20820 transposon insertion check	
PA3343 in-check 1	GAGGAGCGTTTCGGCAAG
PA3343 in-check 2	GGGAAGATGCCGTAGTGC
PA3177/PA14_23130 transposon insertion check	
PA3177 in-check 1	GCGACTTCGTTACTGTCTACAA
PA3177 in-check 2	GGTTCATCAACGCCTTCAGT
PA1851/PA14_40570 transposon insertion check	
PA1851 in-check 1	GCTCCGCCTACTCCGATC
PA1851 in-check 2	AGTTGGCCCACGGATCTTG
PA1120/PA14_49890 transposon insertion check	
PA1120 in-check 1	CATCCGGTCCTGTCCATCA
PA1120 in-check 2	GAGACGGTCGAGATTGTTGC
PA0847/PA14_53310 transposon insertion check	
PA0847 in-check 1	GCTGGAAGGCATCGACGAT
PA0847 in-check 2	CAGCAGGTTGAGGGTCAGG
PA4396/PA14_57140 transposon insertion check	

PA4396 in-check 1	GGCGATCCAGTTCCTTGATG
PA4396 in-check 2	CTGGCCGTCTTCCACCAG
PA4843/PA14_64050 transposon insertion check	
PA4843 in-check 1	CATAAGCATGCCGTAGTCCG
PA4843 in-check 2	CTGGTCGAGCAACTGGAAC
PA4929/PA14_65090 transposon insertion check	
PA4929 in-check 1	TACTCATAGGCAGGAAGGGC
PA4929 in-check 2	TCTCGATGGACATGCTGGC
PA5487/PA14_72420 transposon insertion check	
PA5487 in-check 1	GAGGAACACGGCGATGTTG
PA5487 in-check 2	AATCTCGACCACATCCTGCT
PA0285/PA14_03720 transposon insertion check	
PA0285 in-check 1	CTCATGGGTCTCTGCTCCTG
PA0285 in-check 2	TCGAGAAAACCGTTGAACCAC
PA3311/PA14_21190 transposon insertion check	
PA3311 in-check 1	GTTACGAGCCGGTCAAGTG
PA3311 in-check 2	CCACCCATTGAAGCAACTCC
PA2567/PA14_31330 transposon insertion check	
PA2567 in-check 1	CAGCCTCGTCGTGGTCTG
PA2567 in-check 2	TACGTCCTACTTCCAGACGC
PA2072/PA14_37690 transposon insertion check	
PA2072 in-check 1	AAACTCCAGGTCGTAGCAGA

PA2072 in-check 2	GTCCGCTATGCCGAGGTAC
PA1727/PA14_42220 transposon insertion check	
PA1727 in-check 1	CAAAGCGCTGTACAAAAGGC
PA1727 in-check 2	AGAAGCCCCAGTACACACAG
PA1433/PA14_45930 transposon insertion check	
PA1433 in-check 1	CGACCTGTTGCCGGTGTA
PA1433 in-check 2	CCTTGCGCATCGAACTCAAT
PA1181/PA14_49160 transposon insertion check	
PA1181 in-check 1	TTCCAGCAACTCAAGGACCA
PA1181 in-check 2	ATCATCGAGAGCTACGACGG
PA0861/PA14_53140 transposon insertion check	
PA0861 in-check 1	TGGCAGTCGACGATCAGTT
PA0861 in-check 2	AAACGCTGTCTGTTCCGC
PA4367/PA14_56790 transposon insertion check	
PA4367 in-check 1	CAACTGGGACTTCGTAGCGA
PA4367 in-check 2	CGAATGGAACCGGGTGCG
PA4601/PA14_60870 transposon insertion check	
PA4601 in-check 1	CAGTTGCAATGGGTGGACAG
PA4601 in-check 2	CCGAACTGATGCCGAAGAG
PA4959/PA14_65540 transposon insertion check	
PA4959 in-check 1	GCAGAGCAGCCACTACCT
PA4959 in-check 2	AACGAGTTGCAGATCGTCGA

PA5295/PA14_69900 transposon insertion check	
PA5295 in-check 1	CCTGGCCTTCGAGTGGAA
PA5295 in-check 2	GCGTATTCTAACAGGCTGGC
PA5442/PA14_71850 transposon insertion check	
PA5442 in-check 1	AATCGGGATAGCAGGAGTCG
PA5442 in-check 2	GGGAGAGGTCGTCGTTCATC
PA3947/PA14_12810 transposon insertion check	
PA3947 in-check 1	CGAGATCGCCGTCCAGAATA
PA3947 in-check 2	GACGGATGCGCTTCGATG
PA14_59790 transposon insertion check	
PA14_59790 in-check 1	AACAGCAATACGGTCAGCAC
PA14_59790 in-check 2	CTACGGCGCCAAGGGTTC
PA4108/PA14_10820 transposon insertion check	
PA4108 in-check 1	CCATTTCTGCTGCGCTCTTC
PA4108 in-check 2	GTCGGCGGAGGGATTTGTAT
PA2572/PA14_30830 transposon insertion check	
PA2572 in-check 1	AAATTTCCCAGACCATCCGC
PA2572 in-check 2	CTCATCGATCACCAGCAAGC
PA0290/PA14_03790 transposon insertion check	
PA0290 in-check 1	ATCGCTACCCTGGTCTTCAG
PA0290 in-check 2	GTGTGCATGGGTGTACTCGT
PA3702/PA14_16500 transposon insertion check	
PA3702 in-check 1	CGCGGTGCAGATCCTTTC

PA3702 in-check 2	AATGGTCTGGGTGCGCTC
PA2870/PA14_26970 transposon insertion check	
PA2870 in-check 1	AGCTCGCTGACCTGGACC
PA2870 in-check 2	CAGCCCATCCTCGCCTATC

3-5 REFERENCES

1. Okegbe C, Price-Whelan A, Dietrich LEP: Redox-driven regulation of microbial community morphogenesis. Current Opinion in Microbiology 2014, 18:39–45.

2. Romero D, Aguilar C, Losick R, Kolter R: Amyloid fibers provide structural integrity to Bacillus subtilis biofilms. Proceedings of the National Academy of Sciences 2010, 107:2230–2234.

3. Yildiz FH, Schoolnik GK: Vibrio cholerae O1 El Tor: identification of a gene cluster required for the rugose colony type, exopolysaccharide production, chlorine resistance, and biofilm formation. Proc. Natl. Acad. Sci. U.S.A. 1999, 96:4028–4033.

4. Gerstel U, Römling U: Oxygen tension and nutrient starvation are major signals that regulate agfD promoter activity and expression of the multicellular morphotype in Salmonella typhimurium. Environmental Microbiology 2001, 3:638–648.

5. Serra DO, Richter AM, Hengge R: Cellulose as an Architectural Element in Spatially Structured Escherichia coli Biofilms. Journal of Bacteriology 2013, 195:5540–5554.

6. Kolodkin-Gal I, Elsholz AKW, Muth C, Girguis PR, Kolter R, Losick R: Respiration control of multicellularity in Bacillus subtilis by a complex of the cytochrome chain with a membrane-embedded histidine kinase. Genes Dev. 2013, 27:887–899.

7. Dietrich LEP, Okegbe C, Price-Whelan A, Sakhtah H, Hunter RC, Newman DK: Bacterial community morphogenesis is intimately linked to the intracellular redox state. Journal of Bacteriology 2013, doi:10.1128/JB.02273-12.

8. Yun Z, Maecker HL, Johnson RS, Giaccia AJ: Inhibition of PPAR gamma 2 gene expression by the HIF-1-regulated gene DEC1/Stra13: a mechanism for regulation of adipogenesis by hypoxia. Dev. Cell 2002, 2:331–341.

9. Giaccia AJ, Simon MC, Johnson R: The biology of hypoxia: the role of oxygen sensing in development, normal function, and disease. 2004:2183–2194.

10. Wang Y, Kern SE, Newman DK: Endogenous phenazine antibiotics promote anaerobic survival of Pseudomonas aeruginosa via extracellular electron transfer. Journal of Bacteriology 2010, 192:365–369.

11. Glasser NR, Kern SE, Newman DK: Phenazine redox cycling enhances anaerobic survival in Pseudomonas aeruginosa by facilitating generation of ATP and a proton-motive force. Mol Microbiol 2014, 92:399–412.

12. Kempes CP, Okegbe C, Mears-Clarke Z, Follows MJ, Dietrich LEP: Morphological optimization for access to dual oxidants in biofilms. Proceedings of the National Academy of Sciences 2014, 111:208–213.

13. Lee VT, Matewish JM, Kessler JL, Hyodo M, Hayakawa Y, Lory S: A cyclic-di-GMP receptor required for bacterial exopolysaccharide production. Mol Microbiol 2007, 65:1474–1484.

14. Hickman JW, Harwood CS: Identification of FleQ from Pseudomonas aeruginosa as a c-di-GMP-responsive transcription factor. Mol Microbiol 2008, 69:376–389.

15. Baraquet C, Murakami K, Parsek MR, Harwood CS: The FleQ protein from Pseudomonas aeruginosa functions as both a repressor and an activator to control gene expression from the pel operon promoter in response to c-di-GMP. Nucleic Acids Res. 2012, 40:7207–7218.

16. Ha D-G, Richman ME, O'Toole GA: Deletion mutant library for investigation of functional outputs of cyclic diguanylate metabolism in Pseudomonas aeruginosa PA14. Applied and Environmental Microbiology 2014, 80:3384–3393.

17. Merritt JH, Ha D-G, Cowles KN, Lu W, Morales DK, Rabinowitz J, Gitai Z, O'Toole GA: Specific control of Pseudomonas aeruginosa surface-associated behaviors by two c-di-GMP diguanylate cyclases. MBio 2010, 1.

18. D'Argenio DA, Calfee MW, Rainey PB, Pesci EC: Autolysis and autoaggregation in Pseudomonas aeruginosa colony morphology mutants. Journal of Bacteriology 2002, 184:6481–6489.

19. Merritt JH, Brothers KM, Kuchma SL, O'Toole GA: SadC reciprocally influences biofilm formation and swarming motility via modulation of exopolysaccharide production and flagellar function. Journal of Bacteriology 2007, 189:8154–8164.

20. Kuchma SL, Brothers KM, Merritt JH, Liberati NT, Ausubel FM, O'Toole GA: BifA, a cyclic-Di-GMP phosphodiesterase, inversely regulates biofilm formation and swarming motility by Pseudomonas aeruginosa PA14. Journal of Bacteriology 2007, 189:8165–8178.

21. Roy AB, Petrova OE, Sauer K: The phosphodiesterase DipA (PA5017) is essential for Pseudomonas aeruginosa biofilm dispersion. Journal of Bacteriology 2012, 194:2904–2915.

22. Kulasekara BR, Kamischke C, Kulasekara HD, Christen M, Wiggins PA, Miller SI: c-di-GMP heterogeneity is generated by the chemotaxis machinery to regulate flagellar motility. eLife 2013, 2:e01402.

23. Dietrich LEP, Teal TK, Price-Whelan A, Newman DK: Redox-active antibiotics control gene expression and community behavior in divergent bacteria. Science 2008, 321:1203–1206.

24. Taylor BL, Zhulin IB: PAS domains: internal sensors of oxygen, redox potential, and light. Microbiol. Mol. Biol. Rev. 1999, 63:479–506.

25. Zhulin IB, Taylor BL, Dixon R: PAS domain S-boxes in Archaea, Bacteria and sensors for oxygen and redox. Trends Biochem. Sci. 1997, 22:331–333.

26. Henry JT, Crosson S: Ligand-Binding PAS Domains in a Genomic, Cellular, and Structural Context. Annu. Rev. Microbiol. 2011, 65:261–286.

27. Ramos I, Dietrich LEP, Price-Whelan A, Newman DK: Phenazines affect biofilm formation by Pseudomonas aeruginosa in similar ways at various scales. Res. Microbiol. 2010, 161:187–191.

28. Caiazza NC, Merritt JH, Brothers KM, O'Toole GA: Inverse regulation of biofilm formation and swarming motility by Pseudomonas aeruginosa PA14. Journal of Bacteriology 2007, 189:3603–3612.

29. Merighi M, Lory S: Second Messenger c-di-GMP Signaling in Pseudomonas aeruginosa. In Pseudomonas. Springer Netherlands; 2010:97–138.

30. Roelofs KG, Wang J, Sintim HO, Lee VT: Differential radial capillary action of ligand assay for high-throughput detection of protein-metabolite interactions. Proceedings of the National Academy of Sciences 2011, 108:15528–15533.

31. Tremblay J, Déziel E: Improving the reproducibility of Pseudomonas aeruginosa swarming motility assays. J. Basic Microbiol. 2008, 48:509–515.

32. Kern SE, Price-Whelan A, Newman DK: Extraction and measurement of NAD(P)(+) and NAD(P)H. Methods Mol. Biol. 2014, 1149:311–323.

CHAPTER 4

Summary of Work and Future Directions

4-1 SUMMARY OF WORK

Most bacterial species show a tendency to form biofilms, communities of cells surrounded by self-produced matrices [1]. Biofilms, particularly those grown as colonies on agar-solidified media, often exhibit complex morphologies that are tuned by environmental conditions. In turn, community architecture influences the formation of internal microenvironments with unique conditions that influence bacterial physiology. Understanding biofilm-specific physiology is critical to efforts to promote or inhibit biofilm growth in clinical, industrial, and agricultural contexts. However, rigorous characterization of biofilm-specific metabolism and regulatory mechanisms has been hindered somewhat by technical challenges associated with popular laboratory biofilm models, as many of these are not amenable to high-throughput screening or metabolite analysis.

The work presented in this thesis leverages a simple, standardized model of colony biofilm development to investigate the relationship between electron acceptor availability and colony morphogenesis, and mechanisms underpinning the community response to redox conditions, in the opportunistic pathogen *Pseudomonas aeruginosa* PA14. This colony morphology assay can be used for high-throughput genetic screening and the generation of replicate samples for the investigation of the effects of environmental perturbations, profiling of chemical microecology, and metabolite analysis. I adapted protocols for the extraction and measurement of cellular metabolites and signals to enable quantitative descriptions of morphotypic responses, a significant technical advance over the status quo established for biofilm studies to date.

This work was initiated at a time when the importance of redox conditions in determining bacterial community behavior was garnering renewed attention in the field of microbiology. The colony morphology assay had revealed a dramatic effect for the production of phenazines, redox-active antibiotics that balance the intracellular redox state and support survival of anoxic

PA14 liquid cultures. Colonies of a PA14 mutant unable to make phenazines (Δ*phz*) show earlier and enhanced formation of wrinkle structures. This led to the hypothesis that wrinkle formation is an adaptive response that increases the surface area-to-volume ratio of the biofilm, and therefore increases access to oxygen for cells residing in the densely populated community (Chapter 1).

I began my thesis by characterizing relationships between redox conditions, utilization of electron acceptors for cellular redox balancing, changes in intracellular redox state, and colony morphogenesis in PA14 (Chapter 2). Colony oxygen profiling and thin sectioning paired with fluorescence microscopy showed that cells in wild-type colonies were distributed across the z-axis, including anoxic regions. Δ*phz* colonies were thinner than wild-type colonies and did not contain cells in anoxic zones, supporting a model in which phenazines support survival in anoxic subzones. NADH/NAD^+ measurements of samples obtained at time points over the course of development showed that Δ*phz* colonies exhibit spike in cellular reducing power just prior to the onset of wrinkling, corroborating the notion that colony wrinkle formation is an adaptive response to electron acceptor limitation. In further support of this, increased oxygen availability and the presence of an alternative electron acceptor, nitrate, decreased the extent of, or altogether abolished, wrinkling. Phenotypic analysis of mutants representing enzymes involved in *P. aeruginosa* nitrate metabolism indicated that nitrate reduction in PA14 colonies proceeds via a novel pathway that starts with a periplasmic nitrate reductase, which consumes reducing power but does not contribute to the proton motive force, and continues through the well-studied steps of *P. aeruginosa* denitrification. A modeling approach examining the effects of biofilm structure on the availabililty of a single oxidant (oxygen) or dual oxidants (oxygen and phenazines) for cellular redox balancing further supported the model that wild-type and Δ*phz* colonies assume structures that are optimal for cellular growth (Appendix B). Examination of the effects of phenazines on the morphogenesis of colony biofilms formed by the fungus *Candida albicans* revealed parallels in this system (Appendix C).

The transient elevation in NADH/NAD^+ exhibited by Δ*phz* colonies immediately before wrinkling prompts speculation that redox imbalance is the signal that triggers the community response. Therefore, for the next major phase of my thesis research, I identified and characterized sensor/regulators that serve as mechanistic links between redox conditions and PA14 biofilm morphogenesis (Chapter 3) As regulatory cascades controlling the stages of PA14 biofilm development have been studied in detail, I conducted a screen for potential redox-sensing proteins that could function in this context. PA14 colony wrinkling requires the excretion of a matrix polysaccharide called Pel, the production of which is stimulated by the bacterial secondary messenger cyclic di-GMP (c-di-GMP). We screened mutants representing proteins with the potential to modulate cellular levels of c-di-GMP for altered colony morphogenesis and identified the protein encoded by PA14 ORF 07500, which we named RmcA for redox modulator of cyclic-di-GMP. RmcA is a membrane bound protein with a periplasmic solute binding domain and four tandem PAS domains, a GGDEF domain and an EAL domain in the cytoplasm. Functional GGDEF and EAL have diguanylate cylclase (DGC) activity, which synthesizes c-di-GMP, and phosphodiesterase (PDE) activity, which hydrolyzes c-di-GMP, respectively [2]. PAS domains have been found in all domains of life and are involved in sensing environmental signals such as redox [3]. Colonies of the Δ*rmcA* mutant phenocopy Δ*phz* and detailed characterization of RmcA suggested that it posseses both DGC and PDE activity, but that PDE activity is dominant *in vivo*. Mutational analyses also provided clues regarding interdomain crosstalk in RmcA and suggested that one of the PAS domains binds FAD. We propose a model where RmcA PDE activity is inhibited by reducing intracellular conditions via redox sensitivity conferred by one or more of the PAS domains. This inhibition of RmcA PDE activity causes a buildup of c-di-GMP which leads to increased Pel production and colony wrinkling.

4-2 FUTURE DIRECTION

The findings presented in this thesis provide a foundation for understanding the molecular mechanisms underpinning redox-driven regulation of PA14 colony biofilm morphogenesis. They also raise several questions about the PA14 community response to environmental redox state, qualitative differences in community architecture, and the molecular mechanisms of redox sensing relevant for colony morphogenesis.

The colony morphology screen identified 8 proteins with the potential to modulate c-di-GMP levels that are required for wild-type colony development. Subsequent work focused on RmcA, which is a strong candidate sensor of intracellular redox state because it harbors 4 PAS domains and because the Δ*rmcA* mutant phenocopies the Δ*phz* mutant. However, two other proteins identified in the screen, the PDE DipA and the DGC PA0290, both contain PAS domains and therefore also have the potential to influence biofilm development in response to redox cues. Furthermore, whether specific electron donors (e.g., carbon sources) or acceptors (e.g., phenazines or nitrate) control the activities of individual DGCs and PDEs that operate within the PA14 c-di-GMP-dependent regulatory network remains to be investigated. In this context, it is interesting to note that, while preliminary observations suggest that one of the PAS domains of RmcA binds FAD, ligands or sensory motifs that influence the structures of the other RmcA PAS domains and potentially the activity of RmcA remain to be identified. Structural and additional mutational and biochemical analyses may ultimately reveal the molecular details that allow RmcA to control PA14 colony morphogenesis in a redox-depedent manner.

A further intriguing aspect of mutants with altered morphologies identified in the colony screen is that those with hyperwrinkled phenotypes showed qualitative differences in pattern formation. While the Δ*rmcA* mutant forms a spreading colony similar to that formed by Δ*phz*, the Δ*dipA*, Δ*bifA*, and Δ*PA5295* mutants form constrained colonies. The onset of wrinkling also varied between mutants. What is the biological significance of the different types of wrinkling

and the onset of wrinkling? A large colony morphology screen of mutants spanning the entire *P. aeruginosa* PA14 genome may provide clues as to what metabolic or signaling pathways govern certain types of wrinkling and what physiological benefits may be derived from different colony architectures.

4-3 REFERENCES

1. Shapiro J: Bacteria as multicellular organisms. Sci. Am. 1988.
2. Römling U, Gomelsky M, Galperin MY: C-di-GMP: the dawning of a novel bacterial signalling system. Mol Microbiol 2005, 57:629–639.
3. Taylor BL, Zhulin IB: PAS domains: internal sensors of oxygen, redox potential, and light. Microbiol. Mol. Biol. Rev. 1999, 63:479–506.

Appendix A. The Carbon Monoxide Releasing Molecule CORM-2 Attenuates *Pseudomonas aeruginosa* Biofilm Formation

This appendix is adapted from a manuscript that was published in PLoS ONE– Murray, Okegbe et al 2012. Here we show that that the carbon monoxide-releasing molecule CORM-2, prevents P. aeruginosa biofilm maturation and kills bacteria within an established biofilm. I contributed the experiments comparing the efficacy of CORM-2 against two P. aeruginosa strains PA14 and PAO1 in liquid culture and biofilms as well as under anaerobic conditions (Figures A-10 and A-11).

ABSTRACT

Chronic infections resulting from biofilm formation are difficult to eradicate with current antimicrobial agents and consequently new therapies are needed. This work demonstrates that the carbon monoxide-releasing molecule CORM-2, previously shown to kill planktonic bacteria, also attenuates surface-associated growth of the Gram-negative pathogen *Pseudomonas aeruginosa* by both preventing biofilm maturation and killing bacteria within the established biofilm. CORM-2 treatment has an additive effect when combined with tobramycin, a drug commonly used to treat *P. aeruginosa* lung infections. CORM-2 inhibited biofilm formation and planktonic growth of the majority of clinical *P. aeruginosa* isolates tested, for both mucoid and non-mucoid strains. While CORM-2 treatment increased the production of reactive oxygen species by *P. aeruginosa* biofilms, this increase did not correlate with bacterial death. These data demonstrate that CO-RMs possess potential novel therapeutic properties against a subset of *P. aeruginosa* biofilm related infections.

INTRODUCTION

Organized bacterial communities or biofilms are formed on both biotic and abiotic surfaces during infections by a wide variety of Gram-positive and Gram-negative pathogens [1]. The

bacteria are protected from both the immune system and antimicrobials by an extracellular matrix leading to prolonged colonization of the host [2]. Therefore, new approaches to biofilm eradication and the treatment of chronic biofilm-associated infections are needed. *P. aeruginosa* is an opportunistic Gram-negative pathogen that has served as a model organism to study the dynamics of biofilm assembly and maintenance [3]. Since *P. aeruginosa* causes chronic infection in patients with underlying lung disease such as cystic fibrosis (CF), therapies that disrupt or prevent P. aeruginosa biofilm formation are of critical clinical interest [4,5].

Carbon monoxide (CO) is a product of heme oxygenase activity that serves as an anti-inflammatory signaling molecule in mammalian cells [6,7] by binding, among others, divalent metals of heme-containing proteins such as guanylate cyclase, mitochondrial cytocrome c oxidase and NADPH oxidase [8,9,10]. CO selectively inhibits the expression of pro-inflammatory cytokines, increasing the anti-inflammatory cytokine IL-10 [11,12,13] and reducing neutrophil migration in septic lungs by suppressing transendothelial migration [14]. CO inhalation has been reported to exert an anti-inflammatory effect in patients with chronic obstructive pulmonary disease [15]. Exogenous administration of low concentrations of CO (10–500 ppm) by inhalation is currently in a phase I clinical trial to evaluate its potential to reduce acute airway inflammation (NCT00094406).

Due to concerns about delivering gaseous CO, which cannot be precisely controlled and could be toxic to tissue with prolonged exposure, chemical carriers of this gas known as CO-releasing molecules (CO-RMs) have been developed [6,16]. These carbonyl complexes contain a transition metal bound to CO that is released once in solution. Recent studies in bacteria, including *P. aeruginosa*, *Staphylococcus aureus*, and *Escherichia coli*, show that CO liberated from CO-RMs binds primarily to the heme moieties of proteins in the electron transport chain resulting in decreased oxygen consumption and rapid cell death [17,18,19]. Exposure of *E. coli* to CO-RMs also increases intracellular reactive oxygen species (ROS) resulting in bacterial DNA damage and death [20]. Thus, in addition to their anti-inflammatory properties, CO-RMs

potentially represent a novel class of antimicrobials. While the water-soluble CORM-3 efficiently kills planktonic *P. aeruginosa* at concentrations as low as 1 μM [18], the effect of CO-RMs on biofilms, where bacterial metabolism and respiration is likely to be altered, is poorly understood. Biofilm formation by *E. coli* is enhanced after exposure to CO-RMs but whether this is also true for other bacteria is unknown and has implications for developing these drugs as antimicrobials [21]. The purpose of this study was to evaluate the effects of CORM-2, a ruthenium-containing CORM soluble in dimethyl sulfoxide (DMSO), on *P. aeruginosa* biofilm formation and surface colonization. Our study demonstrates that CORM-2 attenuates *P. aeruginosa* formation at concentrations that are not toxic for mammalian cells, and that the CORM-2 bactericidal efficiency varies with the *P. aeruginosa* genetic background and growth conditions.

RESULTS

CORM-2 kills *P. aeruginosa* PAO1 during planktonic growth and biofilm formation.

Recent studies have shown that CORM-2, CORM-3 and, to a lesser extent, CORM-371 have previously been shown to kill planktonic *P. aeruginosa* [18,22]. All these CO-RMs contain a transition metal, either ruthenium (CORM-2 and CORM-3) or manganese (CORM-371). Our data confirm that CORM-2, but not its inactive counterpart iCORM, kills planktonic PAO1 in M9 medium supplemented with glucose. The effect was dose-dependent with a minimal inhibitory concentration of 10 μM (Fig. A-1). The vehicle alone (DMSO) did not affect growth of PAO1 (data not shown). Colony counts of viable bacteria determined that this killing was rapid with a three-log drop in recovered bacteria at 20 min and no viable bacteria recovered after 30 min (data not shown).

We next assessed whether CORM-2 can impact surface associated *P. aeruginosa*. Crystal violet (CV) staining of PAO1 biofilms formed in plastic wells demonstrated that a 6 h exposure to CORM-2 decreased CV biofilm staining with exposure to concentrations ≥25 μM of CORM-2

showing a statistically significant effect (ANOVA $p<0.001$) (Fig. A-2A). Post-test Dunnett's analysis demonstrated that CV staining levels for all samples treated with ≥25 μM CORM-2 were different from the control but not different from each other. The effect of CORM-2 on biofilm formation compared with vehicle was observed as early as 60 min after treatment and was statistically significant at 4 h ($p<0.007$, paired t-test) (Fig. A-2B). We next performed colony counts from sonicated biofilms +/- 100 μM iCORM or 100 μM CORM-2 to determine if bacterial cell death contributed to changes in CV of the biofilm. The data demonstrate that there is a statistically significant two-log drop in the number of viable bacteria recovered from the CORM-2 treated biofilm when compared with the initial viable cell counts and 100 μM iCORM (Fig. A-2C) (ANOVA<0.001, Dunnett's post-test analysis). Cell death is observed as early as 30 min after drug treatment and persists up to 6 h.

CORM-2 prevents maturation of PAO1 biofilms.

We next examined the dynamics of biofilm formation after addition of CORM-2, iCORM or tobramycin, a known antibiotic used for P. aeruginosa therapy. PAO1-YFP bacteria were incubated in glass bottom dishes for 16 h, then gently washed. Fresh medium with iCORM, DMSO, CORM-2 (50 μM) or tobramycin (100 μg/ml) was added to surface attached bacteria. Fluorescence microscopy was used to image the biofilm at a single location over time. We observed that PAO1 biofilms do not continue to mature in the presence of CORM-2 compared with biofilms formed in absence of the drug (compare Fig.s A-3A–D and A-3I–L). CORM-2 is as effective as tobramycin (100 μg/ml) in preventing bacterial growth, thus maturation of PAO1 biofilms (compare Figs. A-3I–L to M–P).

No effect on biofilm maturation was observed in the presence of the iCORM vehicle control (Fig. A-3E–H) or DMSO (data not shown). These data suggest that the release of CO mediated by CORM-2 prevents further biofilm development, similar to the growth inhibition observed during planktonic growth.

CORM-2 attenuates PAO1 microcolony formation on human bronchial epithelial cells.

We observed that CORM-2 prevents the development of mature biofilms on plastic and glass. We next decided to examine the effect of CORM-2 on bacterial colonization of human bronchial epithelial cells. PAO1-GFP bacteria attached to 16HBE14o- cells were treated with 50 μM of CORM-2 or DMSO and microcolony formation was followed for 6 h with time-lapse microscopy. The addition of 50 μM CORM-2 inhibited bacterial growth resulting in reduced microcolony formation and less damage to the epithelial cells when compared with DMSO addition (Fig. A-4A–H) or iCORM (data not shown). Epithelial cell integrity was continuously assessed by differential interference contrast.

Previous work has shown that CO-RM molecules are not toxic to mammalian cells [16,23] or when used intravenously in animal models [7]. We tested whether CORM-2 has a cytotoxic effect on airway epithelial cells. 16HBE14o- cells were treated with 50 μM, 100 μM and 200 μM of CORM-2 for 6 h or 12 h. Control cells were treated with vehicle alone (DMSO). CORM-2 was not associated with any cell toxicity at the doses tested either after 6 h or 12 h exposure (Fig. A-5A, B). These data reveal that at bactericidal concentrations (50 μM – 200 μM) CORM-2 is effective in disrupting *P. aeruginosa* surface colonization of biotic surfaces at doses that are not toxic for human bronchial epithelial cells.

CORM-2- and tobramycin-mediated antimicrobial activities are additive.

Given the difficulty in treating bacterial biofilms, we next sought to determine if CORM-2 would work as an adjuvant therapeutic agent with currently available antimicrobials. Tobramycin is an aminoglycoside antibiotic commonly given by nebulizer to patients with chronic pulmonary *P. aeruginosa* infection. One hundred μM CORM-2 is as effective as 1 mg/mL tobramycin at decreasing biofilm biomass as measured by CV staining (Fig. A-6A). The addition of CORM-2 (100 μM) and tobramycin (1 mg/ml) in combination for 6 h resulted in decreased CV staining of PAO1 biofilms compared with either no drug or either drug alone with no recovery of viable bacteria (Fig. A-6A) ($p<0.05$ ANOVA, Dunnett's post-test analysis). To determine whether there was a difference in the recovery of viable bacteria comparing single and combination

treatments, we lowered the dose of tobramycin to 100 μg/ml. Exposure to 100 μg/ml tobramycin resulted in a one-log drop in bacterial viability by 60 min, while exposure to CORM-2 led to a two-log drop at 60 min (Fig. A-6B). Exposure to both drugs resulted in an additive effect with a four-log drop in recovered viable bacteria at 60 min (Fig. A-6B), as assessed by colony forming units assay. Bacterial recoveries from all treatments except the 30-minute tobramycin group were significantly different than the number of bacteria recovered at t_0 (ANOVA<0.001, Dunnett's post-test analysis).

Antioxidants protect PAO1 biofilms from CORM-2 inhibition.

Previous work on planktonic *P. aeruginosa* demonstrated that multiple reducing agents (NAC, L-cysteine, and reduced glutathione) prevent *P. aeruginosa* killing by CO-RMs [18]. Our initial studies of planktonic *P. aeruginosa* and CORM-2 with NAC or L-cysteine confirmed this protection (data not shown). We next added NAC or L-cysteine in combination with CORM-2 during biofilm formation in M9 medium to determine whether the treated biofilms were protected against CORM-2 induced cell death. Indeed, CV staining of PAO1 biofilms formed in 96-well plates exposed to either NAC or L-cysteine in the presence of CORM-2 was similar to untreated biofilm formation (Fig. A-6A). CORM-2 treatment alone showed a significant decrease in CV staining compared with controls (no drug or DMSO) (Fig. A-7A) ($p<0.01$ ANOVA, Dunnett's post-test analysis).

Published reports have suggested multiple mechanisms of the bactericidal action of CO-RMs including ROS-mediated activity for CORM-2 [18,20,21]. ROS production by PAO1 biofilms increased after CORM-2 exposure >10 μM as assessed by DCF fluorescence intensity compared with untreated biofilms (Fig. A-7B, ANOVA $p<0.001$, Dunnett's post test analysis). Interestingly, while the addition of NAC to PAO1 biofilms prevented ROS production, the addition of L-cysteine only reduced ROS production to levels seen when 25 μM CORM-2 alone is added (Fig. A-7B). At this concentration, CORM-2 was sufficient to reduce CV staining (Fig. A-2A). L-cysteine with 100 μM CORM-2 resulted in no statistical significant decrease in biofilm

formation compared with control samples despite similar levels of ROS production (Fig. A-7A) (N.S. by ANOVA). Therefore, our data support the previous observations that ROS production is not the major mechanism by which CORM-2 disrupts *P. aeruginosa* growth in M9 medium with glucose and an alternative mechanism such as binding of CO to *P. aeruginosa* respiratory chain is more likely [22].

Rich medium protects against CORM-2-dependent PAO1 death.

We next examined biofilm formation in rich medium, where an increase in biofilm formation has been observed for *E. coli* after CORM-2 addition [21]. In contrast to *E. coli*, PAO1 biofilm formation in LB does not change significantly after addition of CORM-2 (Fig. A-8A). Planktonic PAO1 grown in shaking LB were also protected from CORM-2-dependent cell death (Fig. A-8B). ROS production by PAO1 biofilms grown in LB was slightly increased after exposure to 100 μM CORM-2 but not to the same extent as biofilms grown in minimal media (data not shown). The nutritional conditions and composition of the growth medium are therefore critically important in determining the activity of CORM-2 during both liquid and surface associated growth and this likely has implications [20] for *in vivo* efficacy.

CORM-2 has differential effects on biofilm formation and planktonic growth of clinical isolates and PA14.

CORM-2 prevents PAO1 planktonic growth and biofilm maturation. Given the genetic and phenotypic diversity of *P. aeruginosa* [24] we next tested the effect of CORM-2 on liquid growth and the biofilm formation of a number of previously characterized clinical isolates from respiratory specimens of non- CF patients [25]. Two of twelve respiratory isolates grew poorly in liquid M9 minimal medium (isolates #5 and #8) (Fig. A-9A, left panel). Of the remaining ten, growth of all strains was inhibited by the presence of 100 μM CORM-2 (Fig. A-9, right panel). Ten of the twelve (83%) strains grown overnight in plastic wells displayed statistically significant reduced CV staining of the biofilm after 6 h incubation with 100 μM CORM-2

compared with no treatment (Fig. A-9B) ($p<0.05$, paired t-tests). Three isolates (#3, #4, #10) formed poor biofilms both in the absence of CORM-2 and when CORM-2 was added. For these three isolates, the CV staining of the CORM-2 treated biofilms was similar to the un-inoculated blank. Two strains unaffected by CORM-2 (#1, #8) formed robust biofilms compared with PAO1 during standing growth in M9 with glucose (Fig. A-9B). These data suggest that while the majority of respiratory isolates are susceptible to CORM-2 treatment, isolates with robust biofilm formation are less likely to be affected by CORM-2 treatment. Interestingly, isolate #8 had poor planktonic growth but robust biofilm formation in M9 with glucose. These data highlight the role of biofilm formation in the process of *P. aeruginosa* strain adaptation to unfavorable metabolic conditions.

The above strains were from patients without CF and more likely represent environmental strains and not strains from patients with chronic infection. Chronic pulmonary *P. aeruginosa* infection often results in the selection of alginate producing mucoid strains [26]. We next examined whether CORM-2 alters the biofilm formation of isolates recovered from CF patients. We included both mucoid and non-mucoid clinical isolates from CF patients along with PDO351(mucA:aac+;alg+), a mucoid strain that is otherwise isogenic to PAO1 [27] (Fig. A-9C). Similar to the results for the non-CF *P. aeruginosa* isolates we found that CORM-2 reduced biofilm formation in some strains but not all (Fig. A-9C) ($p<0.012$, paired t-test). The efficacy of CORM-2 did not correlate with the mucoid status of the isolate; for example, CORM-2 had the same effects on mucoid PDO351 compared with non-mucoid wild type PAO1 while the biofilm formation of other mucoid clinical strains were unaffected by the addition of CORM-2 (Fig. A-9C). Given that biofilms may form under anaerobic conditions during chronic pulmonary infection, we assayed anaerobic planktonic growth in M9 glucose or LB medium using 40 mM potassium nitrate as an electron acceptor. Addition of 100 μM CORM-2 inhibited growth of PAO1 in M9 medium but not LB (as observed for aerobic conditions), demonstrating CORM-2 activity at different oxygen tensions (Fig. A-11).

Given the heterogeneity of the effects of CORM-2 on clinical isolates we next tested the effect of CORM-2 on another commonly used laboratory strain, PA14 (Fig. A-10). Similarly to clinical isolates #5 and #8, PA14 displayed poor planktonic growth in M9 glucose medium when compared with PAO1 (data not shown). PA14 was relatively resistant to CORM-2 and to prevent planktonic PA14 growth 200 μM CORM-2 was required; iCORM did not have any effect on PA14 growth at any concentration (Fig. A-10A). Interestingly, while planktonic PA14 growth was poor in M9, PA14 formed strong biofilms after overnight growth in M9 similarly to what observed for PAO1 (Fig. A-10B). Thus, PA14 displays adaptation to unfavorable metabolic conditions as also observed for clinical isolates #5 and #8. PA14 biofilms were insensitive to low doses of CORM-2 (10 – 200 μM) (as also observed for clinical isolated #8), and required much higher doses of CORM-2 (400–600 μM) to inhibit biofilm formation compared with PAO1 (Fig. A-10C). These data suggest that intrinsic differences in *P. aeruginosa* strains affect their susceptibility to CORM-2. Since we observed different growth rates between PAO1 and PA14 stains in minimal M9 medium supplemented with glucose, we hypothesized that the susceptibility to CORM-2 is related to the strain-related capability of using different carbon sources for energy. Our finding that CORM-2 becomes ineffective when either PAO1 or PA14 is grown in rich LB media (Fig. A-8) also supports this hypothesis.

DISCUSSION

In patients with CF, there is a chronic hyper-inflammatory state within the infected lung that fails to eradicate colonization with pathogens such as S. aureus and *P. aeruginosa* leading to clinical symptoms and frequent hospitalizations [5]. Chronic colonization is initiated with surface attachment followed by microcolony formation, the precursors to the mature, antibiotic-resistant biofilm [4,5]. Since mature biofilms are difficult to eradicate, an alternative approach to therapy is to generate novel antimicrobial agents to prevent these early stages of biofilm formation enhancing the efficacy of the immune response. CO is an appealing therapeutic agent because it has the potential to reduce both host pulmonary inflammation and bacterial

viability [15]. CO-RMs were developed to improve and maximize the effects of CO delivery to tissues and CORM-2, used in this study, can efficiently release controlled amount of CO with the same cytoprotective activities that are described by exogenous administration of CO gas without any cytotoxic effect on mammalian cells [16].

We demonstrate that, in addition to killing planktonic *P. aeruginosa*, CORM-2 also prevents microcolony formation on human bronchial epithelial cells while maintaining the integrity of the epithelium (Fig. A-4). Importantly, CORM-2 concentrations required for *P. aeruginosa* killing were not toxic to human airway epithelial cells even after a 12 hours exposure (Fig. A-5). We cannot exclude that CORM-2 prevented epithelial cells disruption not only by impairing bactericidal growth, but also by enhancing the antimicrobial activity of mammalian cells. This is an area of active investigation.

CORM-2 also attenuates *P. aeruginosa* biofilm formation on abiotic surfaces confirming the antimicrobial effect beyond that previously shown for planktonic bacteria [17,18] (Fig. A-2). Together, these data suggest CORM-2 can inhibit biofilm formation regardless of the surface used for bacterial attachment. Despite the genetic and phenotypic diversity of *P. aeruginosa*, the majority of clinical isolates from non-CF patients tested had decreased biofilm formation after exposure to CORM-2 (Fig. A-7). Importantly, pulmonary infections in CF patients are usually initiated by environmental *P. aeruginosa* strains that often cause other types of human infection. The two clinical isolates resistant to CORM-2 formed robust biofilms rapidly when compared with the other isolates, suggesting that the earlier CORM-2 is applied the more effective it is likely to be. CORM-2 also attenuated the biofilm formation of a subset of isolates from CF patients, including both non-mucoid and mucoid strains. While mucoid and non-mucoid strains have multiple phenotypic and genetic differences, mucoidy did not predict failure of CORM-2 treatment [28]. Interestingly, the commonly used laboratory strain PA14 showed increased resistance to CORM-2 exposure. We hypothesize this is due to its slow growth rate in the presence of glucose and its ability to adapt to unfavorable metabolic

conditions. Additional studies are required to determine whether metabolic differences between PA14 and PAO1 are responsible for their different susceptibility to CORM-2 treatment.

The combination of CORM-2 with tobramycin, an antibiotic currently used in therapy for *P. aeruginosa* pulmonary infection in CF patients, was more effective at killing bacteria and reducing biomass than either drug alone (Fig. 6). To our knowledge this is the first example of an added benefit when combining CORM-2 with another antimicrobial agent suggesting CORM-2may have a role as an adjunct therapy with currently available antimicrobials. This may be particularly helpful during chronic infections where subpopulations of antibiotic resistant bacteria persist after treatment.

Exposure of *E. coli* to CORM-2 results in increased ROS production, DNA damage and intracellular iron levels of iron [20], suggesting that ROS generation is the primary mechanism of cell death [20]. ROS production does not appear to be the mechanism of CORM-2 dependent PAO1 cell death in liquid growth [22]. Interestingly, while ROS production is increased from *P. aeruginosa* biofilms after CORM-2 exposure, the addition of L-cysteine only partially inhibits ROS production but completely protects *P. aeruginosa* biofilm formation from the effects of CORM-2 (Fig. A-7). This suggests that ROS do not cause cell death in CORM-2 treated biofilms. The mechanism of protection provided by reducing agents to *P. aeruginosa* observed by us and others remains unknown [20]. Microarray analysis of *E. coli* exposed to CO-RMs also demonstrate a global effect with transcriptional changes in a wide variety of metabolic pathways and transcriptional regulators, including those involved in carbohydrate production, energy metabolism, and stress response [19,21]. Whether any of the above transcriptional changes occur in *P. aeruginosa* and contribute to CORM-dependent cell death is unclear.

Exposure to CO-RMs has been shown to result in CO binding to components of the respiratory chain in both *E. coli* and *P. aeruginosa* [18,19]. The *P. aeruginosa* respiratory chain is complex and involves a large number of respiratory oxidases [29]. At least two cytochrome oxidases

interact with CORM-3 as assayed via dual wave spectrophotometry [18]. Exposure of planktonic cultures to CORM-3 results in a temporal decrease in oxygen consumption consistent with the hypothesis that interference of CO with the respiratory chain kills *P. aeruginosa* [18]. CORM-2 inhibits *E.coli*, *Camplyobacter jejuni* and *P. aeruginosa* PAO1 also under anaerobic conditions [19,30], suggesting that oxygen is not required as the terminal electron acceptor for CORM-2 activity.

In LB-rich medium *P. aeruginosa* planktonic growth and biofilm formation are unaffected by CORM-2. This is in contrast to *E. coli* where CO-RMs increase both oxidative stress and biofilm formation [21]. The reason CORM-2 is not effective during growth in rich medium is unknown. One hypothesis currently being tested is that the active energy pathways used by *P. aeruginosa* determine its susceptibility to CORM-2 and are dependent on the nutritional environment and bacterial growth rate. Given the genetic and phenotypic variability of *P. aeruginosa*, these observations are of particular importance since intrinsic differences in metabolism amongst *P. aeruginosa* strains may limit the effectiveness of therapies that target energy production.

In conclusion, this report demonstrates that, in addition to infections that likely involve planktonic bacteria such as bacteremia, CO-RMs are a potential therapeutic option for *P. aeruginosa* surface-associated infections with a biofilm component such as pulmonary and perhaps burn infections [18]. Since CORM-2 demonstrated activity against mucoid strains and under anaerobic conditions it has the potential to have an effect on chronic *P. aeruginosa* pulmonary infections as observed in patients with long-standing lung disease such as CF. However, as several clinical isolates and PA14 were resistant to CORM-2 dependent killing, this compound will not work for all infections and the emergence of resistant strains is possible. We hypothesize that the nutrients available and the energy pathways used by *P. aeruginosa* in the host during infection will be critical in determine the potential for CO-RMs as *in vivo* therapeutics. This is an important area for additional studies.

Importantly, a single dose of CORM-2 achieved significant bacterial killing for most isolates. If CORM-2 were dosed more frequently, we hypothesize it will result in additional bacterial death within the biofilm. Current efforts are underway to improve CORM-2-dependent biofilm disruption and better understand the mechanisms of both CORM-2 action within *P. aeruginosa* and CORM-2 resistance in non-susceptible strains or in different metabolic conditions.

METHODS

Drugs. CORM-2, which contains a ruthenium metal surrounded by six carbonyl (CO) groups, was dissolved in DMSO (stock solution 10 mM) (Sigma-Aldrich, St Louis MO). As a negative control for CORM-2, an inactive compound, here referred to as iCORM, was used (stock solution 10 mM). This compound [$Ru(DMSO)_4Cl_2$) consists of a ruthenium metal where the CO groups have been replaced by DMSO [11]. Both drugs were diluted to final concentrations of 10–600 μM, depending on the experiment. Stocks were prepared fresh for each experiment. Tobramycin (stock solution 100 mg/ml) (MP Biomedicals, Solon OH) was used at final concentrations ranging from 100 μg to 1 mg/ml, depending on the experiment. N-acetyl cysteine (NAC) was added at a final concentration of 1 mM and L-cysteine was used at 100 μM [18].

Strains and Growth Conditions. PAO1 is the reference laboratory strain used in all experiments except where described. In some experiments, the mucoid PDO351(mucA:aac +;alg+) strain, derived from PAO1, was used [27]. The effect of CORM-2 on clinical isolates was determined using previously characterized *P. aeruginosa* respiratory isolates from patients without CF [25] and isolates from patients with CF. M9 salts growth medium was supplemented with 0.4% glucose. Vogel Bonner Medium (VBM) agar plates selective for *P. aeruginosa* were made as described [25]. The expression of the yellow fluorescent protein (YFP) from the plasmid pMQ72 in PAO1 was induced by supplementing the media with arabinose (0.02%) [31]. PAO1 expressing green fluorescent protein (GFP) from the high copy plasmid pUCPSK was grown overnight in the presence of carbenicillin (200 μg/ml). The PAO1-GFP bacteria were

washed and resuspended in M9 medium without carbenicillin prior to incubation with respiratory epithelial cells. For growth experiments, overnight cultures of PAO1 were diluted into fresh medium to an optical density (OD) at 600 nm of 0.05, the CORM-2, iCORM, or DMSO added, and the OD followed over time. At specified intervals, aliquots were removed from the cultures, diluted to VBM agar plates, and incubated overnight at 37˚C to determine the number of viable bacteria. In some growth experiments, another laboratory strain, PA14, was used. PA14 was also diluted to an OD (600 nm) of 0.05 from overnight cultures grown aerobically at 37˚C in Luria-Bertani broth (EMD) or M9 salts growth medium was supplemented with 0.4% glucose. The CORM-2, iCORM or DMSO treatment was added and the OD at 600 nm was followed over time using a Biotek Synergy 4 spectrophotometer.

The effect of CORM-2 on PAO1 growth in anaerobic conditions was also tested. Luria-Bertani broth (EMD) and M9 medium with 0.4% glucose as the carbon source both supplemented with 40 mM KNO3 were autoclaved and moved into a Coy anaerobic chamber (80% / 15% / 5% N2 / CO2 / H2 atmosphere) 16 hours before inoculation. Pre-cultures were grown aerobically overnight and moved into the anaerobic chamber for use as inocula. Anaerobic media were dispensed 5 mL per 18X150 mm anaerobic Balch tube (Bellco) and inoculated to a final OD (600 nm) of 0.05. Cultures were stoppered and crimp-sealed in the chamber, then incubated at 37˚C with shaking at 250 rpm. OD at 600 nm was followed using a Thermo Spectronic 20D+ spectrophotometer.

Ethics Statement. Clinical *P. aeruginosa* isolates were taken from de-identified frozen stocks conserved at 280uC as part of a previous study approved by the Human Investigations Committee at Yale. These bacteria were recovered from pediatric and adult patients hospitalized at Yale-New Haven Hospital and identified by the clinical microbiology laboratory, as described in previously in detail [25]. All patients or their legal guardians provided informed consent.

Static biofilm formation and analysis. PAO1 static biofilms were formed in either 24-well plastic dishes (Corning, Lowell MA) or 96-well plastic dishes (Grenier bio-one, Germany). PA14 static biofilms were formed in 96-well plastic dishes (Grenier bio-one, Germany); the bacteria were inoculated from an overnight shaking culture to an OD (600 nm) of 0.05 and then incubated as a static (non-shaking) culture from 18 to 24 hours at 37°C [32]. Under these conditions, a biofilm forms around the edge of the miniscus against the wall of the well. CORM-2, iCORM, DMSO, and/or tobramycin were added directly without removing planktonic cells after biofilm formation. In a different set of experiments, the planktonic cells were removed and the remaining biofilm was gently washed before adding fresh medium with CORM-2 or controls (DMSO or iCORM). At selected times, the biofilm was washed in water, stained with 0.05% crystal violet (CV) and absorption at 595 nm was recorded [32]. For a single experiment, the drug additions were tested in triplicate and all experiments were repeated at least three times.

To recover viable bacteria from mature biofilms, the planktonic culture was removed after overnight growth, the biofilms were gently washed, and fresh medium with drug was added for 30 min to 6 hours. Following this incubation, the biofilms were washed 4 times with fresh medium, then sonicated to release bacteria [32]. The medium containing the released bacteria was serially diluted and plated on VBM agar. In all experiments, 3 wells on each plate were initially washed and sonicated to determine the viable cell counts at time point t_0.

Analysis of biofilm formation in real time. For real-time imaging of the effects of CORM-2 on biofilm formation, PAO1-YFP was grown overnight in glass bottom polylysine coated dishes (MatTek, Ashland MA) [33] and then placed in a VivaView incubator fluorescent microscopy system (Olympus, Center Valley PA), and equilibrated at 37°C. CORM-2 (50 μM), iCORM (50 μM), tobramycin (100 μg/ml) or DMSO was added and images were collected every 15 minutes for 8 hours. The images from three fields for each sample were collected and analyzed with VivaView software.

Microcolony formation on respiratory epithelial cells. The static bacteria/bronchial epithelial cell co-culture system was established as described [33]. 16HBE14o- bronchial epithelial cells (a kind gift of Dr. Dieter Gruenert) were maintained in Minimum Essential Medium supplemented with 10% fetal bovine serum, L-glutamine and penicillin/streptomycin. For time-lapse microscopy experiments, $1X10^6$ cells were plated in collagen/fibronectin coated glass bottom 3 cm dishes (MatTek, Ashland MA) and cultured for 5–7 days, allowing for tight junction formation. Subsequently the epithelial cells were inoculated with *P. aeruginosa*-GFP at a ratio of 1:3 in media without antibiotics. After 40 minutes in culture, unattached planktonic *P. aeruginosa* were removed by rinsing and replaced with fresh M9 medium supplemented with glucose, L-glutamine and 0.04% L-arginine. CORM-2 (50 μM), iCORM (50 μM) or DMSO was added and images were collected by time-lapse microscopy (VivaView, Olympus) every 10 minutes for 6 hours (objective 20X). The epithelium integrity was assessed by differential interference contrast and remained intact for 7–8 hours of culture in the absence of bacteria. The images from three fields for each sample were collected and analyzed with VivaView software.

Cell Viability Assay. 16HBE14o- bronchial epithelial cells were seeded in 96-wells plate ($5X10^4$ cells/well). After 5 days of culture in Minimum Essential Medium supplemented with 10% fetal bovine serum, Lglutamine and penicillin/streptomycin, cells were treated with different doses of CORM-2 (50 μM, 100 μM and 200 μM) or with vehicle alone (DMSO) for 6 hours or 12 hours. The cell viability was then assessed using the MTT (3-(4,5-Dimethylthiazol-2-yl)-2,5-Diphenyltetrazolium Bromide) colorimetric assay, which measures cellular metabolic activity. As control for cell death, 16HBE14o- cells were treated with saponin for 10 minutes before proceeding with the MTT staining. The MTT staining and the colorimetric detection (Cell Biolabs, INC) were performed following the manufacturer's instructions. Each condition was performed in triplicate.

Measurement of ROS production in bacteria. To determine ROS production, static biofilms were grown in 96-well plastic dishes (Corning, Lowell MA) as described above [32]. Biofilms were washed gently and CORM-2 (25 μM or 100 μM) or DMSO in the absence or presence of NAC (1 mM) or L-cysteine (100 μM) were added to the biofilm for 2 hours at 37˚C. Biofilms were then washed in Phosphate Buffered Saline (PBS) and loaded with 10 μM 5-(and-6)-chloromethyl-29,79-dichlorodihydrofluorescein diacetate, acetyl ester (CMH2DCFDA; Molecular Probes) for 30 min at 37˚C. This was followed by two washes in PBS. In the presence of intracellular ROS and esterases, CM-H2DCFDA is oxidized and deacetylated yielding the fluorescent molecule 29,79-dichlorodihydrofluorescein diacetate (DCF). Fluorescence intensity was assessed using a fluorescence plate reader (arbitrary units).

Statistical analysis. Data was compiled in Excel and transferred to Minitab for statistical analysis. For data derived from biofilm analysis using the CV method, for analysis of ROS production and for the analysis of cell viability statistical comparison of paired means was done with a paired t-test. When required, multiple comparisons of means were done using a one-way ANOVA. Post-test analysis determining confidence intervals for individual means was done with Dunnett's analysis comparing treated samples to the control.

FIGURES

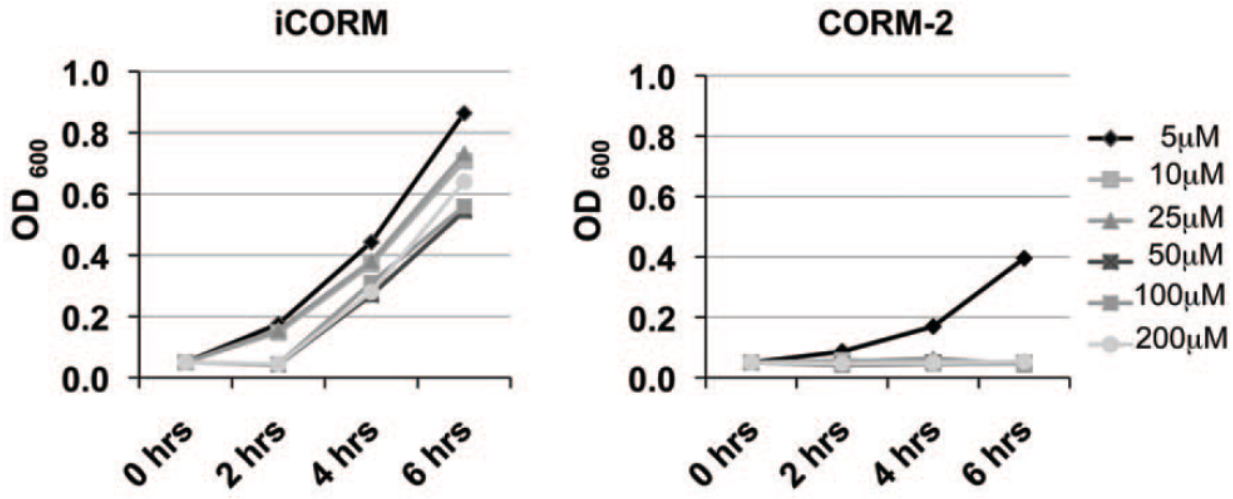

Figure A-1. CORM-2 kills planktonic *P. aeruginosa*. The control molecule iCORM has no effect on PAO1 growth in liquid M9 medium with glucose (left panel), while CORM-2 doses >5 μM prevent growth of PAO1 (right panel). doi:10.1371/journal.pone.0035499.g001

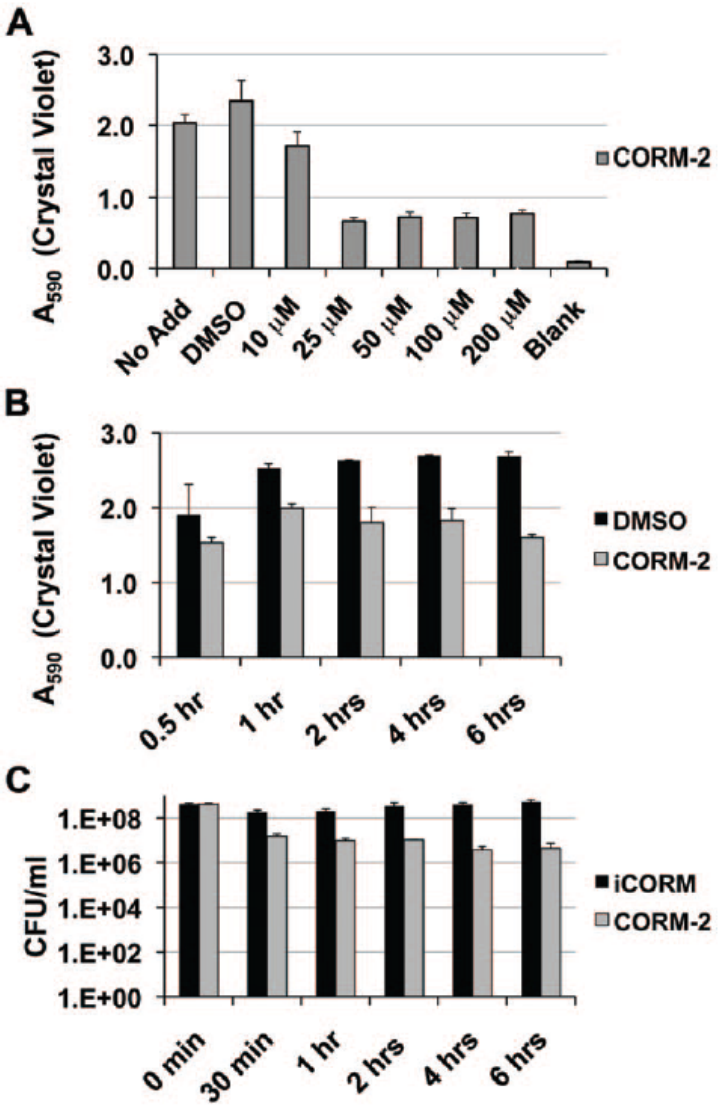

Figure A-2. CORM-2 attenuates *P. aeruginosa* biofilm formation. A) Crystal violet (CV) biomass staining decreases after CORM-2 exposure in a dose-dependent manner. Each condition was done in triplicate. B) CV staining of PAO1 biofilms treated with 100 μM CORM-2 demonstrates decreased staining of the biofilm after 2–6 hours of CORM-2 exposure compared with DMSO vehicle where the biofilm increases overtime. C) Colony counts of PAO1 released from the iCORM (100 μM) and CORM-2 (100 μM) treated biofilms demonstrate that there is a sustainable 2-log drop in bacterial viability. doi: 10.1371/journal.pone.0035499.g002

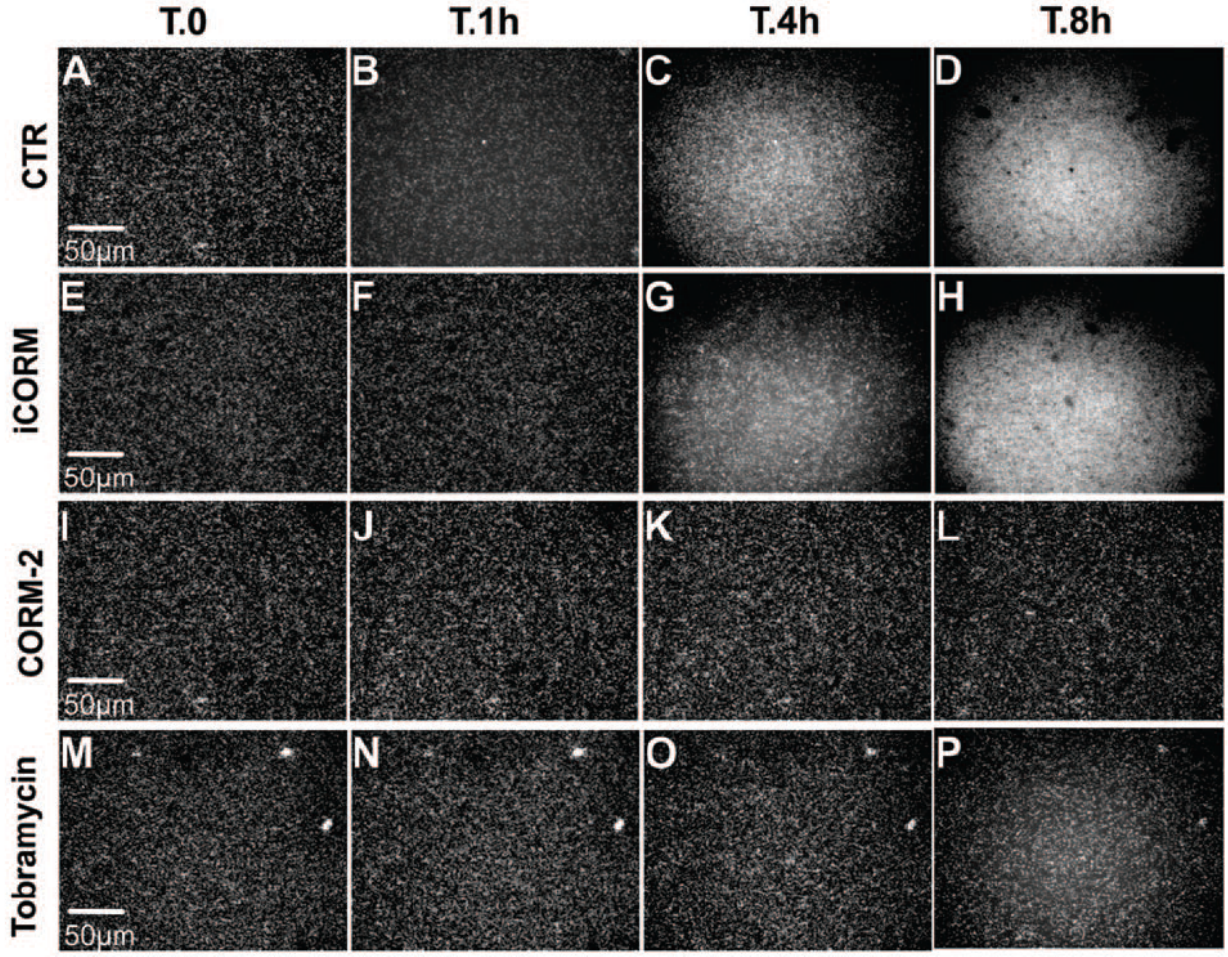

Figure A-3. CORM-2 attenuates PAO1 biofilm formation. YFP-*P. aeruginosa* were grown for 16 hours in a glass bottom dish and then visualized at selected locations for 12 additional hours using VivaView. A–D: control (CTR = no addition) biofilm formation; E-H: biofilm formation in presence of iCORM (50 μM); I–L: biofilm formation in presence of CORM2. The CORM-2 (50 μM) treated biofilm remains unchanged compared with the control biofilms that continue to mature; M–P: biofilm formation in presence of tobramycin. T indicates time; h indicates hours. Scale bars = 50 μm. doi:10.1371/journal.pone.0035499.g003

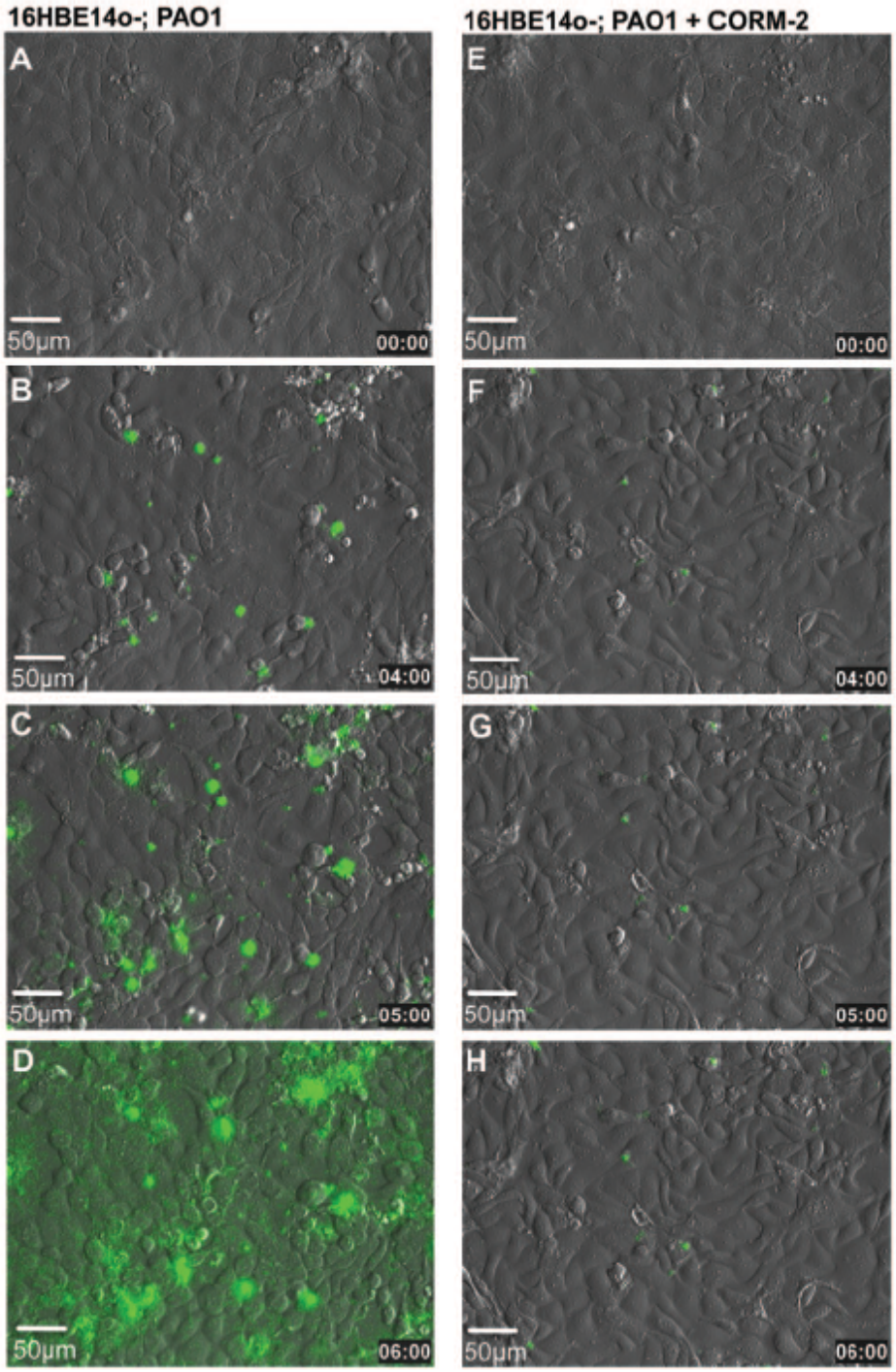

Figure A-4. CORM-2 attenuates *P. aeruginosa* colonization of respiratory epithelium. Time-lapse microscopy of bronchial epithelial cells cocultured with PAO1 (1:3 ratio) show that the addition of 50 μM of CORM-2 reduced microcolony formation. The time (hours) when the images were acquired is indicated at the bottom of each panel. Scale bars = 50 μm.doi:10.1371/journal.pone.0035499.g004

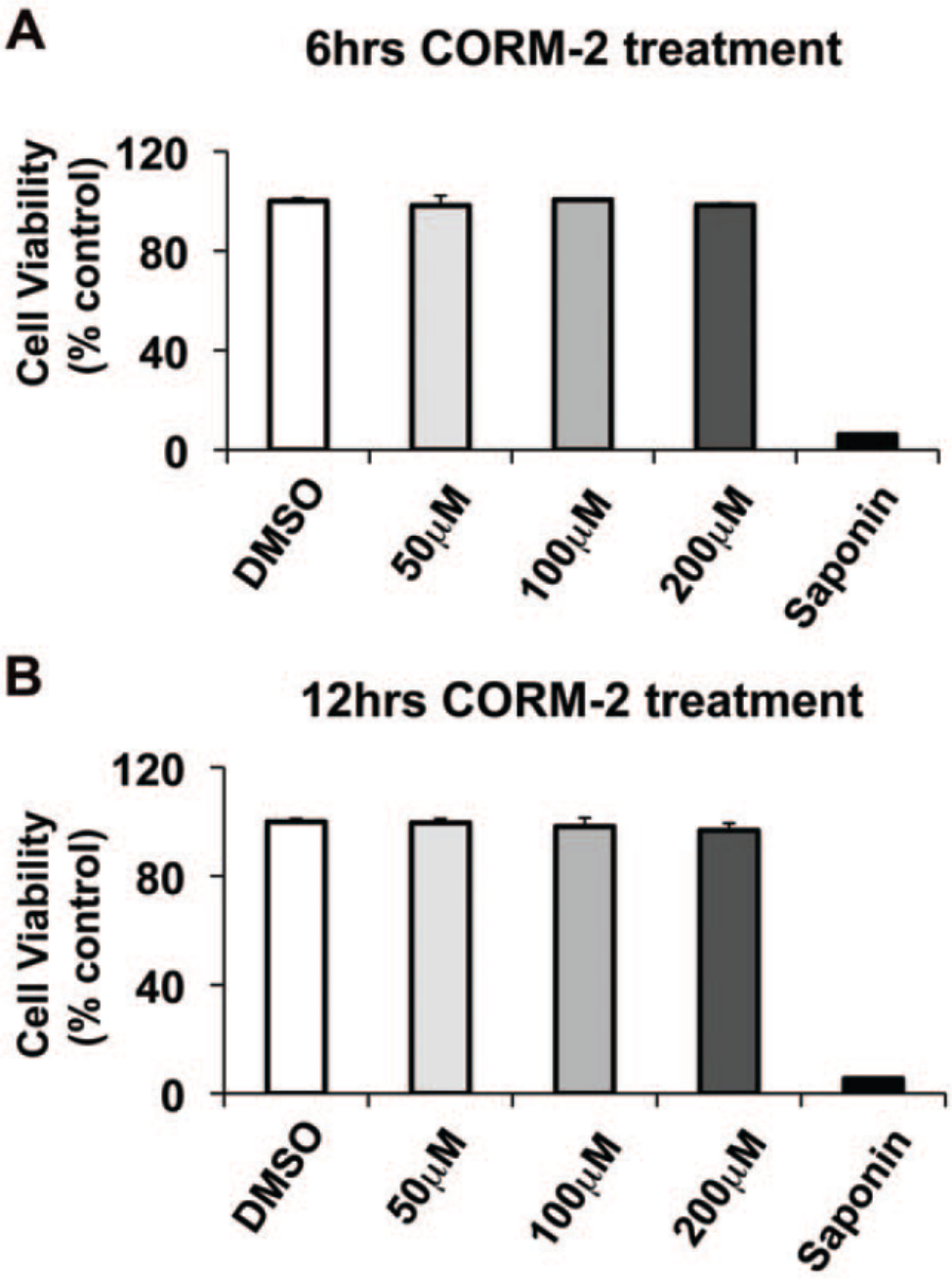

Figure A-5. CORM-2 does not affect airway epithelial cell viability. The MTT viability assay shows that 50–200 μM of CORM2 is not toxic to airway epithelial cells after 6 hours (A) or 12 hours (B) treatment. As a control for cell death, 16HBE14o- cells were treated with saponin for 10 minutes before proceeding with the MTT staining. CORM-2 viability is expressed as percentage of non-treated control cells (DMSO). doi:10.1371/journal.pone.0035499.g005

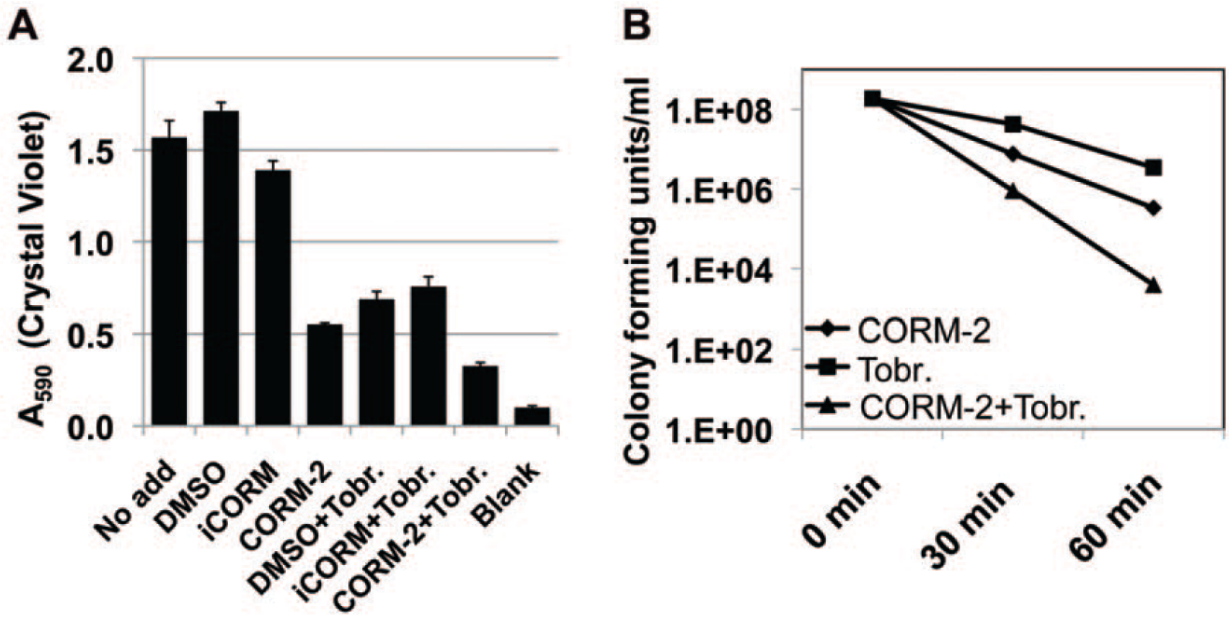

Figure A-6. CORM-2 and tobramycin have additive effects on PAO1 biofilm formation. A) CORM-2 (100 μM) is as effective as tobramycin (1 mg/ml) in decreasing the biomass of the bacterial biofilm after 6 hours treatment, as measured by CV staining and the combination is better than either alone. B) The combination of CORM-2 (100 μM) and tobramycin (Tobr.) results in increased PAO1 killing within the biofilm than either drug alone. doi:10.1371/journal.pone.0035499.g006

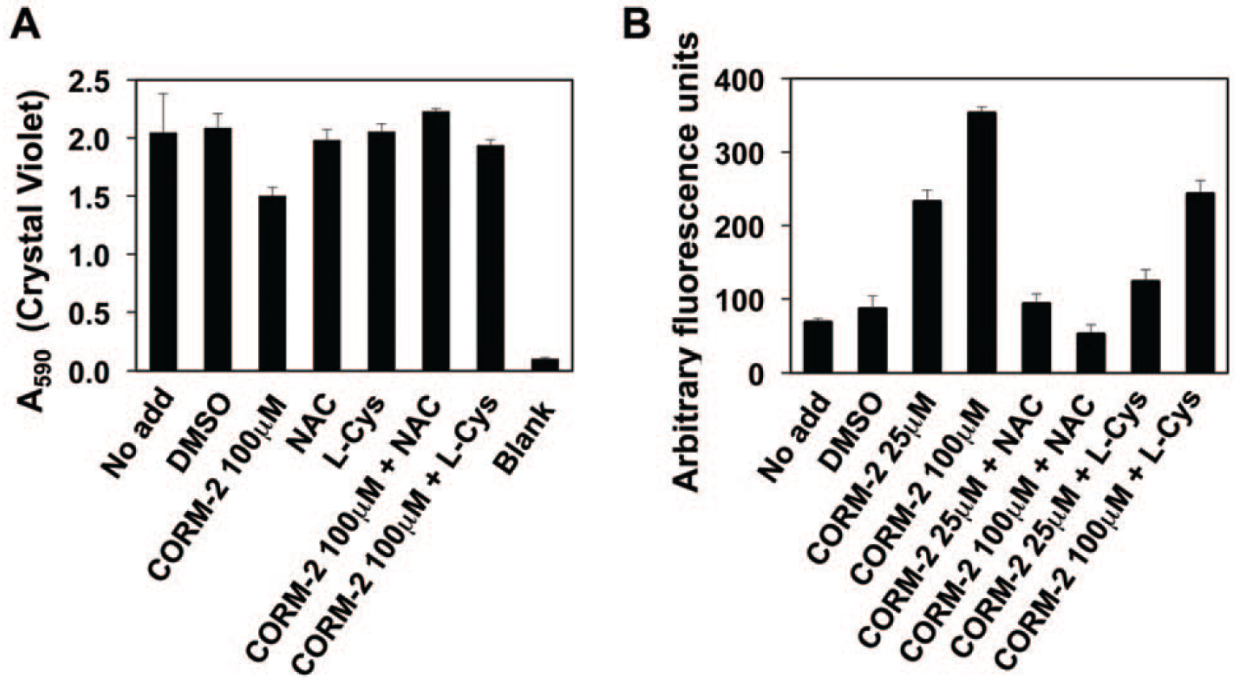

Figure A-7. Anti-oxidants protect *P. aeruginosa* biofilms from CORM-2 inhibition. A) The addition of NAC (1 mM) or L-cysteine (100 μM) to CORM-2 (100 μM) treated *P. aeruginosa* biofilms (6 hours) restores CV staining to levels comparable to untreated biofilms. B) Treatment with CORM-2 (25 μM and 100 μM) induces bacterial ROS formation; NAC (1 mM) prevents ROS production while the addition of L-cysteine (100 μM) did alter only partially ROS levels. doi:10.1371/journal.pone.0035499.g007

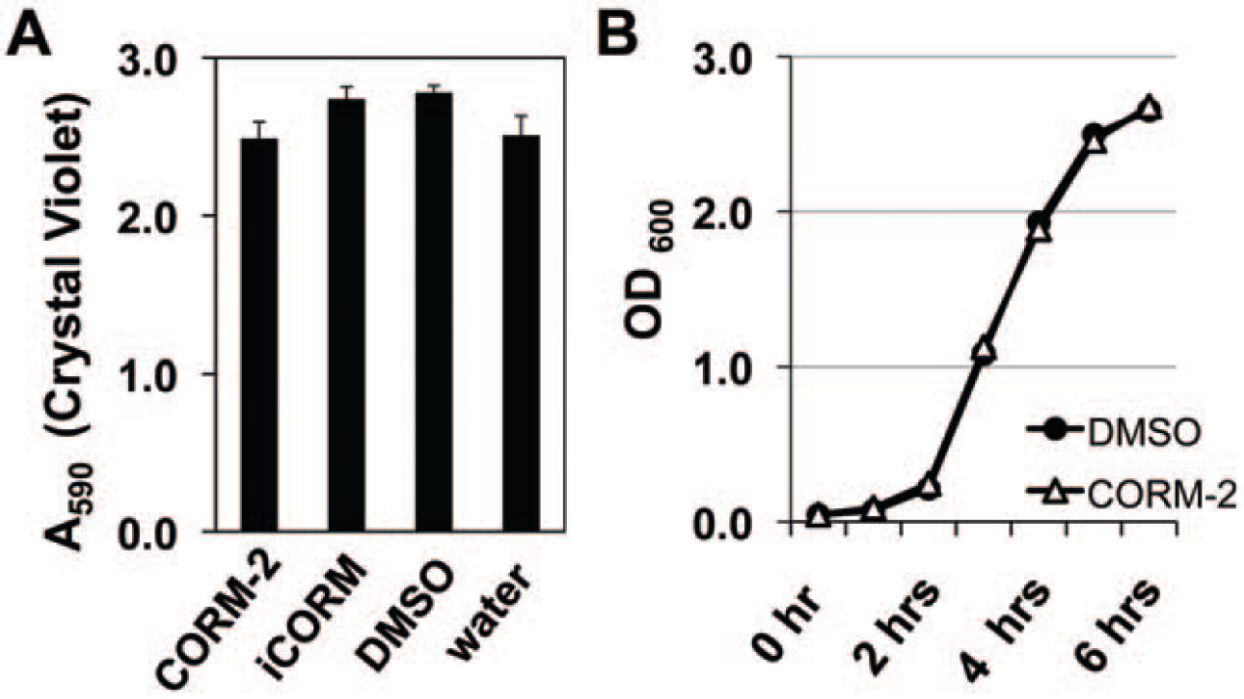

Figure A-8. Rich medium protects *P. aeruginosa* biofilms against CORM-2. A) Biofilm formation by *P. aeruginosa* treated with CORM-2 (100 μM) for 6 hours is similar to untreated controls when grown in LB. B) The addition of CORM-2 (100 μM) to *P. aeruginosa* growing in liquid LB medium does not result in cell death. doi:10.1371/journal.pone.0035499.g008

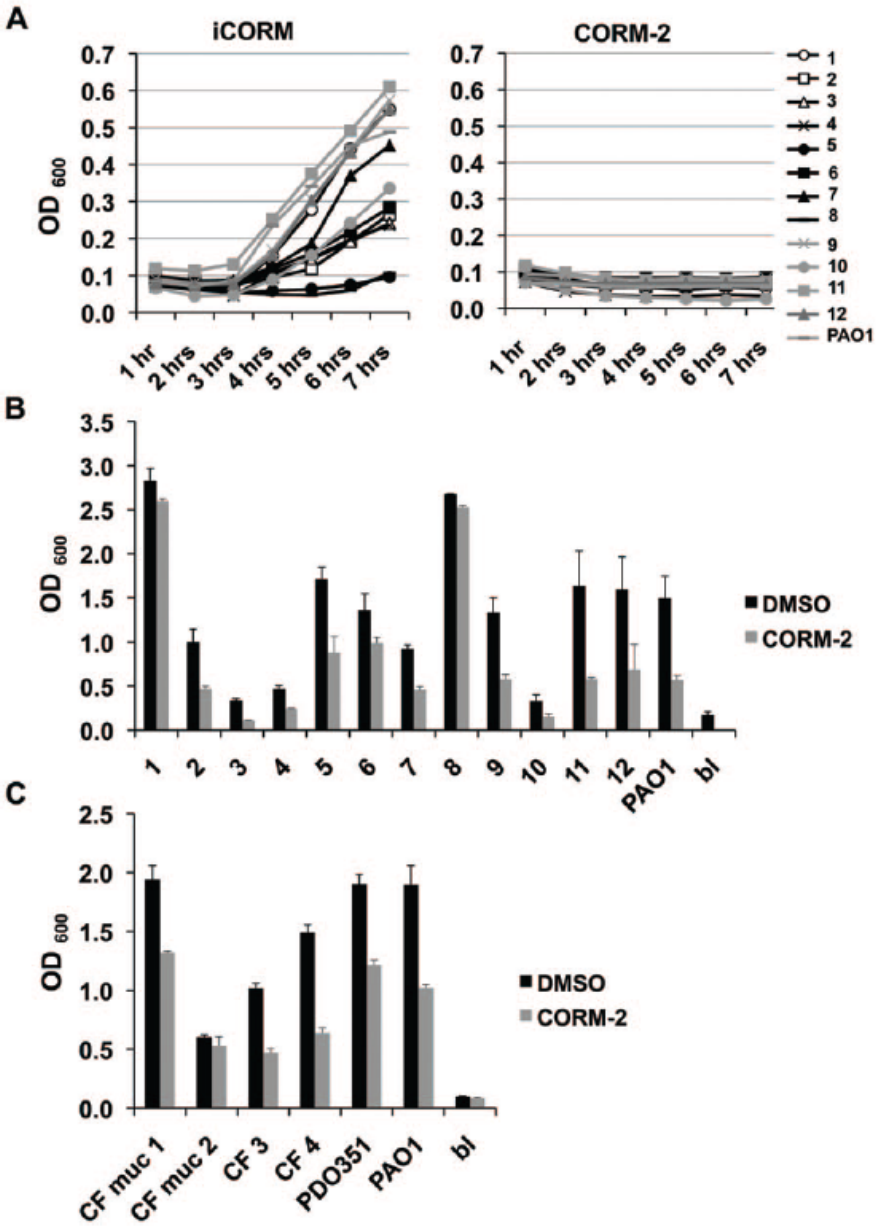

Figure A-9. The effect of CORM-2 on growth and biofilm formation of clinical, respiratory *P. aeruginosa* isolates. A) The addition of 100 μM CORM-2 to M9 liquid medium with glucose (left) prevents the growth of all clinical isolates compared with addition of DMSO alone (right). B) 6 hours exposure to 100 μM CORM-2 reduces the CV staining of 10/12 biofilms formed by respiratory isolates after overnight growth in plastic wells. C) 100 μM CORM-2 reduces the CV staining of 3 out of 4 biofilms formed by respiratory isolates from CF patients independently of the mucoid or non-mucoid after overnight growth in plastic wells. A similar effect was observed in mucoid-PAO1 laboratory strain PDO351 (mucA:aac+;alg+). doi:10.1371/journal.pone.0035499.g009

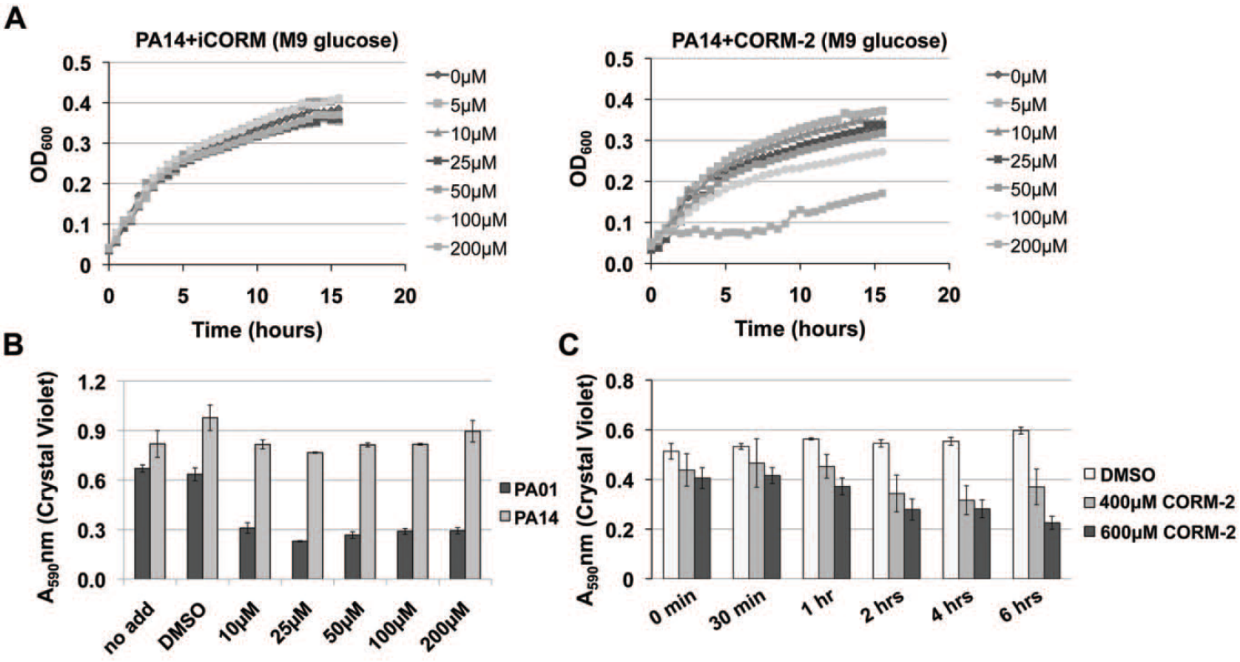

Figure A-10. High doses of CORM-2 are required to reduce growth and biofilm formation of PA14. A) CORM-2 doses .100 μM (right panel) but not iCORM (left panel) prevents PA14 growth in liquid M9 medium with glucose. B) As measured by CV staining, PA14 biofilms are resistant to the low doses of CORM2 treatment (10–200 μM) that reduce PAO1 biofilm formation. C) Higher doses of CORM-2 (400 μM and 600 μM) decreases CV staining of both PA14 and PAO1 biofilm formation. Each condition was tested in triplicate. doi:10.1371/journal.pone.0035499.g010

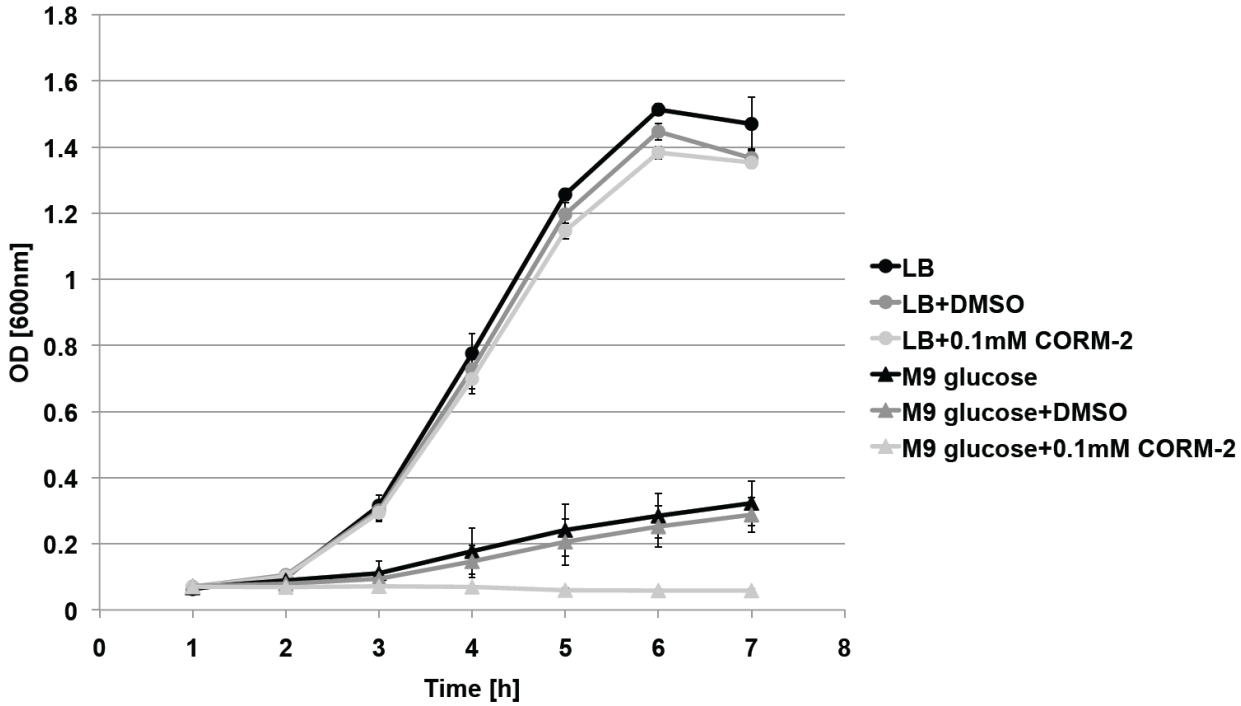

Figure A-11. CORM-2 inhibits anaerobic growth of PAO1 in M9 glucose medium. PAO1 was grown anaerobically in M9 glucose or LB medium in the presence of 40 mM nitrate. Addition of CORM-2 (100μM) inhibited planktonic growth of PAO1 in M9 but not in LB.

REFERENCES

1. Burmolle M, Thomsen TR, Fazli M, Dige I, Christensen L, et al. (2010) Biofilms in chronic infections - a matter of opportunity - monospecies biofilms in multispecies infections. FEMS Immunol Med Microbiol 59: 324–336.

2. Flemming HC, Wingender J (2010) The biofilm matrix. Nat Rev Microbiol 8: 623–633.

3. Monds RD, O'Toole GA (2009) The developmental model of microbial biofilms: ten years of a paradigm up for review. Trends Microbiol 17: 73–87.

4. Moreau-Marquis S, Stanton BA, O'Toole GA (2008) Pseudomonas aeruginosa biofilm formation in the cystic fibrosis airway. Pulm Pharmacol Ther 21: 595–599.

5. Hassett DJ, Korfhagen TR, Irvin RT, Schurr MJ, Sauer K, et al. (2010) Pseudomonas aeruginosa biofilm infections in cystic fibrosis: insights into pathogenic processes and treatment strategies. Expert Opin Ther Targets 14: 117–130.

6. Motterlini R, Mann BE, Foresti R (2005) Therapeutic applications of carbon monoxide-releasing molecules. Expert Opin Investig Drugs 14: 1305–1318.

7. Motterlini R, Otterbein LE (2010) The therapeutic potential of carbon monoxide. Nat Rev Drug Discov 9: 728–743.

8. Piantadosi CA (2008) Carbon monoxide, reactive oxygen signaling, and oxidative stress. Free Radic Biol Med 45: 562–569.

9. Bilban M, Haschemi A, Wegiel B, Chin BY, Wagner O, et al. (2008) Heme oxygenase and carbon monoxide initiate homeostatic signaling. J Mol Med 86: 267–279.

10. Desmard M, Boczkowski J, Poderoso J, Motterlini R (2007) Mitochondrial and cellular heme-dependent proteins as targets for the bioactive function of the heme oxygenase/carbon monoxide system. Antioxid Redox Signal 9: 2139–2155.

11. Sawle P, Foresti R, Mann BE, Johnson TR, Green CJ, et al. (2005) Carbon monoxide-releasing molecules (CO-RMs) attenuate the inflammatory response elicited by lipopolysaccharide in RAW264.7 murine macrophages. Br J Pharmacol 145: 800–810.

12. Chhikara M, Wang S, Kern SJ, Ferreyra GA, Barb JJ, et al. (2009) Carbon monoxide blocks lipopolysaccharide-induced gene expression by interfering with proximal TLR4 to NF-kappaB signal transduction in human monocytes. PLoS One 4: e8139.

13. Otterbein LE, Bach FH, Alam J, Soares M, Tao Lu H, et al. (2000) Carbon monoxide has anti-inflammatory effects involving the mitogen-activated protein kinase pathway. Nat Med 6: 422–428.

14. Mizuguchi S, Stephen J, Bihari R, Markovic N, Suehiro S, et al. (2009) CORM-3-derived CO modulates polymorphonuclear leukocyte migration across the vascular endothelium by reducing levels of cell surface-bound elastase. Am J Physiol Heart Circ Physiol 297: H920–929.

15. Bathoorn E, Slebos DJ, Postma DS, Koeter GH, van Oosterhout AJ, et al. (2007) Anti-inflammatory effects of inhaled carbon monoxide in patients with COPD: a pilot study. Eur Respir J 30: 1131–1137.

16. Motterlini R, Clark JE, Foresti R, Sarathchandra P, Mann BE, et al. (2002) Carbon monoxide-releasing molecules: characterization of biochemical and vascular activities. Circ Res 90: E17–24.

17. Nobre LS, Seixas JD, Romao CC, Saraiva LM (2007) Antimicrobial action of carbon monoxide-releasing compounds. Antimicrob Agents Chemother 51: 4303–4307.

18. Desmard M, Davidge KS, Bouvet O, Morin D, Roux D, et al. (2009) A carbon monoxide-releasing molecule (CORM-3) exerts bactericidal activity against Pseudomonas aeruginosa and improves survival in an animal model of bacteraemia. FASEB J 23: 1023–1031.

19. Davidge KS, Sanguinetti G, Yee CH, Cox AG, McLeod CW, et al. (2009) Carbon monoxide-releasing antibacterial molecules target respiration and global transcriptional regulators. J Biol Chem 284: 4516–4524.

20. Tavares AF, Teixeira M, Romao CC, Seixas JD, Nobre LS, et al. (2011) Reactive oxygen species mediate bactericidal killing elicited by carbon monoxide-releasing molecules. J Biol Chem.

21. Nobre LS, Al-Shahrour F, Dopazo J, Saraiva LM (2009) Exploring the antimicrobial action of a carbon monoxide-releasing compound through whole genome transcription profiling of Escherichia coli. Microbiology 155: 813–824.

22. Desmard M, Foresti R, Morin D, Dagouassat M, Berdeaux A, et al. (2011) Differential antibacterial activity against Pseudomonas aeruginosa by carbon monoxide-releasing molecules (CO-RMs). Antioxid Redox Signal.

23. Megias J, Busserolles J, Alcaraz MJ (2007) The carbon monoxide-releasing molecule CORM-2 inhibits the inflammatory response induced by cytokines in Caco-2 cells. Br J Pharmacol 150: 977–986.

24. Wiehlmann L, Wagner G, Cramer N, Siebert B, Gudowius P, et al. (2007) Population structure of Pseudomonas aeruginosa. Proc Natl Acad Sci U S A 104: 8101–8106.

25. Murray TS, Ledizet M, Kazmierczak BI (2010) Swarming motility, secretion of type 3 effectors and biofilm formation phenotypes exhibited within a large cohort of Pseudomonas aeruginosa clinical isolates. J Med Microbiol 59: 511–520.

26. Mathee K, Ciofu O, Sternberg C, Lindum PW, Campbell JI, et al. (1999) Mucoid conversion of Pseudomonas aeruginosa by hydrogen peroxide: a mechanism for virulence activation in the cystic fibrosis lung. Microbiology 145(Pt 6): 1349–1357.

27. Wood LF, Ohman DE (2006) Independent regulation of MucD, an HtrA-like protease in Pseudomonas aeruginosa, and the role of its proteolytic motif in alginate gene regulation. J Bacteriol 188: 3134–3137.

28. Rau MH, Hansen SK, Johansen HK, Thomsen LE, Workman CT, et al. (2010) Early adaptive developments of Pseudomonas aeruginosa after the transition from life in the environment to persistent colonization in the airways of human cystic fibrosis hosts. Environ Microbiol 12: 1643–1658.

29. Williams HD, Zlosnik JE, Ryall B (2007) Oxygen, cyanide and energy generation in the cystic fibrosis pathogen Pseudomonas aeruginosa. Adv Microb Physiol 52: 1–71.

30. Smith H, Mann BE, Motterlini R, Poole RK (2011) The carbon monoxide releasing molecule, CORM-3 (RU(CO)(3) CL(glycinate)), targets respiration and oxidases in Campylobacter jejuni, generating hydrogen peroxide. IUBMB Life 63: 363–371.

31. Shanks RM, Caiazza NC, Hinsa SM, Toutain CM, O'Toole GA (2006) Saccharomyces cerevisiae-based molecular tool kit for manipulation of genes from Gram-negative bacteria. Appl Environ Microbiol 72: 5027–5036.

32. Merritt JH, Kadouri DE, O'Toole GA (2005) Growing and analyzing static biofilms. Curr Protoc Microbiol Chapter 1: Unit 1B 1.

33. Moreau-Marquis S, O'Toole GA, Stanton BA (2009) Tobramycin and FDA approved iron chelators eliminate Pseudomonas aeruginosa biofilms on cystic fibrosis cells. Am J Respir Cell Mol Biol 41: 305–313.

Appendix B Morphological optimization for access to dual oxidants in biofilms

This appendix is adapted from a manuscript that was published in PNAS– Kempes, Okegbe et al 2014. Here we develop and apply a mathematical model, which incorporates empirical values, to show that the tall "ridges" produced by Pseudomonas aeruginosa colony biofilms maximize community growth via enhanced access to oxygen. I contributed all the experimental data that was used to develop the model.

ABSTRACT

A major theme driving research in biology is the relationship between form and function. In particular, a longstanding goal has been to understand how the evolution of multicellularity conferred fitness advantages. Here we show that biofilms of the bacterium *Pseudomonas aeruginosa* produce structures that maximize cellular reproduction. Specifically, we develop a mathematical model of resource availability and metabolic response within colony features. This analysis accurately predicts the measured distribution of two types of electron acceptors: oxygen, which is available from the atmosphere, and phenazines, redox-active antibiotics produced by the bacterium. Using this model, we demonstrate that the geometry of colony structures is optimal with respect to growth efficiency. Because our model is based on resource dynamics, we also can anticipate shifts in feature geometry based on changes to the availability of electron acceptors, including variations in the external availability of oxygen and genetic manipulation that renders the cells incapable of phenazine production.

INTRODUCTION

A desire to understand the relationship between form and function motivates many lines of inquiry in biology, including the study of multicellular morphologies and the evolution of these features. Cells grow and survive in populations in many types of natural systems. These multicellular populations include bacterial biofilms, such as Pseudomonas aeruginosa microcolonies in the lungs of cystic fibrosis patients (1) and cyanobacterial colonies and mats

in marshes, lakes, and oceans (2, 3), and complex eukaryotic macroorganisms, such as plants and animals. In many of these contexts, enhanced survival arises from advantages associated with multicellularity at multiple scales. Recent work demonstrated that simple cooperation within aqueous microbial biofilms allows groups of genetically similar cells to form tall mushroom-like structures that reach beyond local depletion zones into areas of fresh resources (4–12). Other work has shown that basic colonial growth (e.g., that of budding yeast) and the evolution of complex multicellular life are accompanied by enhanced growth efficiency and several energetic advantages (13–15).

The specific organization of and relationship between cells living within a population are important characteristics that determine whether organisms benefit from the multicellular lifestyle. For example, in mammals the metabolic rate of individual cells is regulated by the size of the whole organism, an effect that confers greater efficiency (15). Cells have dramatically elevated metabolic rates when living as individuals in culture compared with when they survive and grow as members of a multicellular organism (15). This regulation is considered a natural consequence of resource supply within hierarchical vascular networks (15–17) and highlights the importance of morphology and structure in dictating cellular physiology for multicellular systems. Variations in gross morphology also may provide information about how different species are adapted to their environments. For example, differences in leaf venation patterns among diverse species of plants are fundamentally related to tradeoffs associated with carbon assimilation and transpiration rates, water supply rates, and overall mass investment (18). This variation in venation network structure is affected by and may influence the mechanisms and efficiency with which resources are supplied to individual cells. Gradients of resources, particularly oxygen, are similarly important in modulating the development of embryos, lungs, hearts, and tumors (19–24).

Thus, one of the dominant effects of multicellularity is to alter the environment experienced by the individual cell. This raises questions such as (**i**) how are morphology, metabolism, and environmental conditions interconnected and (**ii**) how do these relationships govern the fundamental benefits and tradeoffs of multicellularity? Understanding these connections may help us understand the general trajectory by which simple and complex multicellular life evolved and allow us to better identify and quantify morphologically complex structures that may represent paleobiological populations (25).

Bacteria form structurally diverse biofilms in different environments and are well-suited for the study of relationships among the morphology, metabolism, and chemical heterogeneity of multicellular populations (26). Most laboratory studies addressing biofilm development are performed in flow-cell systems, in which bacteria are grown on a glass slide and exposed to a continuous flow of a liquid growth medium. In the regime of biofilms submersed in liquid, representative Gram-negative bacteria, including *P. aeruginosa,* form mushroom-like structures in response to external nutrient gradients (4–12). We grow *P. aeruginosa* biofilms on agar-solidified growth media in a controlled atmosphere. A standard protocol, the colony morphology assay, is used to generate these biofilms (27). Ten microliters of a cell suspension is pipetted onto an agar plate, and the development of the colony at room temperature and constant humidity is monitored over several days. In this model system, we can modify the environmental and biological conditions and examine the resulting shifts in structure and chemistry. Colony biofilms that form under these conditions exhibit spatial patterning (Fig. B-1A) and environmental sensitivity and constitute an ideal model system for exploring morphology as a metabolic adaptation (28).

Although numerous processes, including extracellular matrix production, osmotic pressure gradients, cellular motility, and spatially heterogeneous cellular death (e.g., refs. 4, 9, 12, 29, 30), have been shown to be involved in the production of biofilm patterning, it is not yet fully

understood why or how feature formation has evolved, especially in the context of air-exposed biofilms. We have reported that redox-active signaling molecules called phenazines have dramatic effects on population behavior. Whereas wild-type colonies remain smooth for the first 2 days of growth, phenazine-null mutant (*Δphz*) colonies undergo a major morphotypic transformation (31). At day 2, *Δphz* colonies begin to spread over the surface of the agar plate. Two types of wrinkle structures form: those within the area of the original droplet, which appear to be more "disorganized," at the colony center and those that radiate from the center toward the colony edge (referred to here as "ridges"). Both types of features are vertical structures (Fig. B-1). Wild-type colonies also form wrinkles in the center, but only after 3 days of growth, and a mutant that overproduces phenazines remains smooth when monitored for 6 days. These strains therefore demonstrate an inverse correlation between increased colony surface area and phenazine production (31).

More recently, we showed that *P. aeruginosa* colony wrinkling is a strategy to increase oxygen accessibility (28). We have proposed that phenazines attenuate this mechanism because they act as electron acceptors for cells in anoxic regions of the biofilm and shuttle electrons to the well-aerated regions, allowing cells to balance their internal redox state (28, 32, 33). We proposed that a reduced cellular redox status triggers a morphological change at the population level. Consistent with this model, adding nitrate (an alternate electron acceptor) to the agar, or increasing atmospheric oxygen concentrations (to 40%) prevents spreading of the *Δphz* colony and discourages wrinkle formation. Decreasing external oxygen availability (to 15%) increases wrinkle formation as well as spreading of the colony (28). Oxygen profiling of the colonies indicates that the *Δphz* mutant is well oxygenated within wrinkles, suggesting that its morphotype is an adaptation for enhanced oxygen uptake (28). It is noteworthy that wrinkles reach a final, static width while continuing to grow taller. The wrinkle width achieved is correlated with the concentration of oxygen provided in the atmosphere. Additionally,

eliminating the ability to wrinkle (by deleting the genes for extracellular matrix production) has been shown to lead to a redox imbalance, as indicated by an elevated $NADH/NAD_+$ ratio (28).

The sensitivity of colony morphogenesis to oxygen, nitrate, and phenazines suggests a significant role for oxidative capacity in modulating morphology. Here we develop a simple mathematical model, rooted in established physical laws and physiology, that demonstrates and confirms this significance. Combining this model with experimental verification enables us to make predictions and interpretations that would be infeasible using modeling or experimentation alone. The model incorporates the response of growth rate to oxygen availability and accurately predicts the measured oxygen distribution within colony features. Because it is based on resource dynamics, it also anticipates shifts in feature geometry based on external oxygen availability. Finally, quantitative experiments verify our methodology. We demonstrate that biofilms produce features with geometries optimal for the growth efficiency of the entire colony and sensitive to the redox environment, as determined by factors such as oxygen availability and phenazine production.

MODELING BIOFILM METABOLISM AND OXYGEN DYNAMICS

Several key features of the colony biofilm system inform our understanding of the processes governing morphology and form the foundation for our modeling framework. (**i**) Wrinkling in the colony system is a basic feature of the wild type that occurs late in development as a response to electron acceptor limitation (28). (**ii**) Overall colony wrinkling, as well as the geometry of individual features (width of wrinkles), can be modified easily by altering the redox conditions (e.g., increasing oxygen availability or knocking out the ability to produce phenazines) (see ref. 28 for *P. aeruginosa* and ref. 34 for similar results in *Bacillus subtilis*). (**iii**) Colony wrinkles reach a constant width early in development but continue to grow taller at a nearly linear rate. Taking these last two observations together, we assume that electron acceptor rather than nutrient supply is the primary limitation faced during colony development and is responsible for feature

geometry. If nutrient supply from the agar below a feature were controlling width, we would expect to see a decrease in the overall growth of a feature as the constant width is reached. We would not expect to observe the linear increase in ridge height; this would only increase nutrient limitation as chemicals are forced to diffuse over a narrow and increasingly long distance.

To study the basic dynamics of resources and geometric feature formation, we first empirically characterize and model colonies of the phenazine-deficient mutant (*Δphz*) in a context in which oxygen is the only available terminal electron acceptor. We later expand experiments and the model to consider wild-type colonies, which have the sole addition of redox-active phenazines produced by the cells.

We base our mathematical model on the simplest hypothesis for feature regulation: the dynamic feedback between metabolism, resource availability, and physical diffusion (e.g., refs. 6, 8, 35–43). We use the Pirt model, which interprets the linear relationship between population metabolism and growth rate as a metabolic partitioning between growth and maintenance (44) and is consistent with the physiology of a broad range of bacterial and eukaryotic species (see, e.g., refs. 13, 45 for a review). It is combined with the Monod model, which parameterizes population growth rate as a saturating function of the external concentration of a limiting resource (46). This combination of parameterizations has been used widely (e.g., refs. 6, 35, 41, 43) and here provides an equation for the oxygen consumption as a function of available oxygen:

$$Q = \frac{\mu_{max}}{Y}\frac{[O_2]}{k_s + [O_2]} + P, \qquad \textbf{[1]}$$

where Q is a consumption rate per unit mass of a limiting resource that provides energy and/or structural material to the population of cells (mol resources · s^{-1}·g $cells^{-1}$), **μ** is the specific growth rate (s^{-1}), Y is a yield coefficient (g cells · mol $resource^{-1}$), P is a maintenance term (mol

resource · s^{-1}·g $cells^{-1}$), μ_{max} is the maximum growth rate approached as the substrate concentration is taken to infinity, and k_s is the half-saturation constant.

Depletion of oxygen within the biofilm creates a gradient with the atmosphere and drives a diffusive flux of oxygen into the colony. The time-dependent spatial concentration of oxygen may be described by

$$\frac{\partial[O_2]}{\partial t} = D\nabla^2[O_2] - \left(\frac{\mu_{max}}{Y}\frac{[O_2]}{k_s + [O_2]} + P\right)a, \quad \textbf{[2]}$$

where a is the density of cells in the colony (g cells · m^{-3}). Similar models have been used widely in biofilm and broad ecological modeling (e.g., ref. 35). This equation can be conveniently non-dimensionalized:

$$\frac{\partial[O_2]^*}{\partial t^*} = \nabla^2[O_2]^* - \left(\frac{[O_2]^*}{1 + [O_2]^*} + g\right), \quad \textbf{[3]}$$

where the temporal and spatial scales, respectively, have been normalized by the factors

$$t_{fac} = \frac{a\mu_{max}}{k_s Y} \text{ and } x_{fac} = \left(\frac{a\mu_{max}}{k_s YD}\right)^{1/2}$$

Oxygen concentrations have been divided by k_s, and the nondimensional maintenance term is $g = YP/\mu_{max}$. For steady-state solutions, the model relies only on the concentration of oxygen at the colony surface, which is determined by the atmospheric mixing ratio and pressure, and the two parameters x_{fac} and k_s. We determined the value for both parameters by first compiling published measurements and then constructing the mean of every combination within this compilation. Here we use the Pirt–Monod diffusion model framework to interpret the community benefit of specific geometrical features of the colony and to interpret mechanisms underlying the architectural optimization within biofilms. We also model the dynamics and benefits associated with multiple oxidative resources and show that biogenic redox-active molecules are beneficial to community growth and survival.

RESULTS

Observations of Internal Oxygen Distribution. To investigate how these mechanisms regulate morphology, we study a single feature of a *P. aeruginosa* colony biofilm, i.e., the ridge (Fig. B-1), and its surrounding geometry. We take oxygen profiles of the colony **"**base**"** (Fig. B-1B), where biofilm geometry is simplest, and we use these profiles to examine our literature-based parameter estimates and calibrate our model. First, we measure oxygen availability with increasing depth (Fig. B-2). There is some variation in the decay rate and the depth at which oxygen no longer can be detected (Figs. B-4 and B-5). Most of this observed variation may be accounted for by rescaling the depth axis by a simple factor, after which the profiles share a similar shape. This normalization highlights common overall biological activity and variation in the physiological parameter values. We fit the observed variation in vertical 1D profiles by varying x_{fac} and solving for the steady-state oxygen concentration in our model for an isolated base geometry while keeping k_s fixed. Fig. B-2A shows that steady-state solutions of our model in the base capture the range of observed oxygen profiles. The variation in profiles also allows us to calibrate the range of x_{fac} to be bounded by 7.3 X 10^4 and 1.6 X 10^5 with a mean value of 9.1 X 10^4. This range compares well to our estimate from the literature of 7.7 X 10^4 μm. Given our definition of x_{fac} the observed variation could be due to differences in physiological parameters, such as maximum growth rate or substrate yield, or to differences in the physical parameters, such as density, wetness, and overall oxygen diffusivity of the colony. Experimentally, we find that oxygen availability decreases with increasing depth into the colony. However, this effect is much more dramatic in the base than in the ridge. This likely is the result of increased surface area for a reduced cellular mass. To interpret this phenomenon, we use the calibrated model to simulate the steady-state distribution of oxygen availability within a ridge and the surrounding base, and we do this for various geometries of the ridge (Fig. B-6A). Our model also captures the general decay rate and shape of these ridge profiles (Fig. B-2B). These profiles were created using the mean value of the parameter calibration and the general

variation in ridge width because it is experimentally challenging to measure the width and oxygen profile simultaneously. Our ability to anticipate the general shape and variation of oxygen profiles within the ridge gives us confidence in our calibration and the model's predictive capacity. It should be noted that once these calibrations have been made, all other results in this paper follow directly as predictions.

The Impact of Colony and Feature Geometry. The increased depth of oxygen penetration in the ridge region (Fig. B-2B) illustrates the importance of geometry in enhancing oxygen availability within the colony. The question then becomes how changes in this geometry affect oxygen availability within the colony. To explore this, we simulate the simplest geometric variation by preserving the overall shape of the ridge but varying the width of the ridge for a fixed height. Fig. B-6A shows the distribution of oxygen within ridges of different widths. From the internal oxygen distribution and Monod equation, we can calculate the local growth rate and we find that ridges generally have an enhanced growth rate relative to flatter regions of the colony (Fig. B-6B). This is because tall, thin features increase the total surface area for a relatively small amount of biomass, which enhances the oxygen flux per total consumption, resulting in increased oxygen penetration. However, we also see in Fig. B6 that as ridges grow wider, the effect of enhanced growth is diminished and the layer of growing cells within the ridge region becomes similar in thickness to that of the base regions. This effect implies a tradeoff for population metabolism: Although thin structures are entirely oxygenated, allowing cells to grow quickly, their relatively small size limits the number of cells they contain. Thick features house many more cells, but the region of enhanced oxygen penetration and growth is smaller. This tradeoff may be summarized using the total reproductive rate, **R**, of the colony, where the derivative of **R** with respect to mass describes how much added growth the colony will experience given an investment in additional mass. This derivative gives the growth efficiency of the colony in that it represents the return on mass investment in terms of total reproductive capacity. We calculate **R** for an ensemble of simulated features at a fixed height

but with different widths, and find that **R** reaches a maximum for ridges with a specific width. This represents the optimal width for efficient cell proliferation within the colony and also corresponds to the width at which all cells within a feature can at least meet their minimum metabolic maintenance requirements. More importantly, the optimal width found in our model accurately predicts the observed average width of colony features along with the observed variation in widths for colonies growing on an agar plate exposed to 21%external oxygen (Fig. B-3). This prediction is made by solving for the optimal width using the minimum, maximum, and average parameter values from our calibration to base profiles. Similarly, for simulations of the base, we find that **R** approaches a constant value when the height of the base reaches the maximum depth to which oxygen can penetrate. Thus, any additional base height does not produce additional growth for the colony. Experimentally, we find that the average base thickness corresponds to the average depth at which oxygen no longer is detectable. The observed colony features are such that if features grow wider (or taller in the case of the base) than this optimal size, the colony has invested a large amount of mass that will not grow quickly. If the features are smaller than this optimum, the colony has invested a small amount of mass, but there will be less overall growth as a consequence. We suggest that natural selection has favored cellular behavior that gives rise to features with emergent geometries that maximally benefit the population, as was proposed previously in similar contexts (e.g., ref. 26). It should be noted that we observe that during early colony growth, the ridges maintain a constant width while height continues to increase. This implies that nutrients are not limiting, and it then is surprising that in the outermost layer of cells, growth is arrested despite the abundance of oxygen and capacity for further growth. This raises the possibility that cellular growth within the ridges is regulated to optimize the growth efficiency of the population.

Morphological Response to Oxygen Availability. We have shown evidence of oxygen control driving the optimization of colony form. Feature geometry is important because of the impact it has on the availability of oxygen within the colony. Given this interconnection between

geometry and oxygen, we would expect that changes in the external availability of oxygen would result in shifts in colony form. To test this hypothesis, we exposed colonies to elevated concentrations of external oxygen (40% compared with the standard 21%). To quantify these shifts, we again calibrate the parameters of our model. We do not have the appropriate experimental setup to measure oxygen profiles in colonies grown in our hyperoxia chambers. As an alternative, we use colony base heights as proxies for oxygen penetration distances (base heights correspond to the depth at which oxygen is depleted). These measurements are sufficient for calibrating $\mathbf{x}_{fac}$ to the 40% external oxygen conditions. The observed widths in 40% external oxygen are wider than in 21%. Running our simulations with 40% external oxygen, and the calibrated range of parameter values, we again successfully predict the mean, upper bound, and lower bound on observed ridge widths (Fig. B-3). Through our model, we interpret the wider ridge width as the result of deeper oxygen penetration, which extends the width at which a diminishing return on mass investment occurs. We also predict, in good agreement with data, that in 15% external oxygen, ridge width will be reduced (Fig. B-7).

Morphological Response to Other Oxidants. Our observations and modeling thus far have concerned a *P. aeruginosa Δphz* mutant, which cannot produce phenazines. We can predict the significant effects of oxygen availability on feature development and the optimal ridge width in this scenario, in which oxygen is the only electron acceptor the bacteria can use to balance the intracellular redox state. However, it is important to test whether our conceptual framework may be used to determine the effects that phenazines, as endogenously produced oxidants, have on feature geometry (28). To address this challenge, we examine aspects of the wild-type colony in which we have developed a model that accounts for the dual use of oxygen and phenazines as electron acceptors. We have developed a mathematical model in which we allow both oxygen and phenazines to diffuse and be reduced within the colony. In this model, oxygen is consumed directly by cells and also is used for reoxidizing phenazines, and cells reduce both substrates to support their metabolic rate.

This model accurately predicts the decay of oxygen with increasing depth into the base region of the colony. Near the surface, this decay rate is observed to be nearly identical to that of the *Δphz* colonies. However, deep in wild-type colonies, cells cease to consume oxygen, which in the context of our model, may be interpreted as the point at which phenazines are used as alternate electron acceptors. Experimentally, cells expressing YFP from a constitutive promoter (suggesting metabolic activity) have been observed at a depth of 100 μm in wild-type colonies compared with a depth of only 60 μm in Δphz mutant colonies (28).

It appears that the presence of phenazines allows an oxidative potential to extend deeper into the colony. In our model, we see that this is the consequence of phenazines being oxidized in the surface layer and diffusing into the deep layers, where they are consumed when oxygen reaches a low enough level.

Using this model, we again can evaluate the effect of ridge width on colony growth and predict optimal ridge width when phenazines are present. Our predictions agree well with observations for the wild type growing in 21% oxygen (Fig. B-3C). The observed and predicted features are significantly wider than the *Δphz* ridges grown under the same conditions. The wild type is effectively a **Δ**phz mutant with phenazines added, and the effect of phenazine addition is qualitatively the same as that of increasing oxygen availability for the *Δphz* mutant. This highlights that the availability of oxidative resources strongly controls feature geometry and that these effects can be modeled predictably, provided that the redox chemistry and physiology of the colony are well defined.

DISCUSSION

The study of biofilms has diverse applications. For example, biofilms may act as model ecological systems to investigate the nature of cooperative and competitive behavior and dynamics (e.g., refs. 4, 12). To understand biofilm physiology in a variety of contexts, it is critical to define the connections between population structure and access to resources. We

have developed a mathematical model of substrate availability and cellular metabolism within colonies. The predicted oxygen distribution and its effects on colony morphology have been verified empirically using a standard biofilm assay. We have shown that standard physiological characterizations of biofilms may be combined with an analysis of community growth as a function of geometry to predict optimal biofilm morphology. Furthermore, we have illustrated that these optima are influenced greatly by external redox conditions and the ability of biofilms to produce redox-active molecules.

One of the major findings of this paper is that the shapes of biofilms may allow optimal interaction with the environment for resource availability and therefore optimal total growth and return on mass investment. The ridges of *P. aeruginosa* colonies maintain fairly uniform width even as they grow taller. Previous studies showed that steady-state biofilm feature shape results from external resource limitation and occurs when the environment no longer can supply substrates for further growth (e.g., refs. 4, 5, 7, 12, 47). In contrast to the model systems used for these studies, our colony biofilm is exposed to the open atmosphere, in which external resource gradients effectively are nonexistent. Thus, cells in the outermost layer of a colony are not resource limited, and they have the capacity for further growth, as evidenced by the oxygen profiles and the observation that they grow taller. The ridges have the capacity for horizontal growth, and the simplest passive model of the dynamics driven solely by growth rate would predict increasing ridge width over time. Therefore, unknown mechanisms must maintain the constant ridge width that apparently is advantageous to the overall colony.

Although wrinkling is a common response of the biofilm system, we have seen that ridge geometry is affected by both environmental (external oxygen availability) and physiological (the inability of the ***Δ****phz* mutant to produce phenazines) alterations. Furthermore, it has been observed that no wrinkling occurs in a mutant unable to produce the Pel polysaccharide [a critical component of matrix structure (27, 28)], and our experience with a wide variety of single

gene knockouts indicates that many physiological changes alter the details of spatial patterning and wrinkle formation. This suggests that wrinkling is the result of many physiological processes, as already highlighted by the variety of single mechanisms shown to be related to pattern formation in biofilms (4, 12, 29). Given the complexity of cellular physiology and response, there are countless systems of cellular behaviors, interactions, and feedbacks that conceivably might evolve to produce diverse biofilm structures. Many of these structures would not be optimal for the average reproductive success of cells within the colony. This suggests that the specific set of mechanisms in our biofilm system may have been selected to produce emergent patterns that we observe to be optimally beneficial to the colony. Studies recently indicated that biofilm structures are underpinned by diverse cell behaviors, including chemotaxis, extracellular matrix production, chemical signaling, and selective cellular death as an induction for mechanical buckling in thin films (4, 12, 29). Whether disruptions in these mechanisms produce suboptimal biofilm structures remains to be investigated. In addition, features may serve multiple roles in different contexts or species, implying a variety of selective pressures. For example, a recent study reported that the channels that form within wrinkles in *B. subtilis* biofilms facilitate liquid movement through the structure (48).

In considering the possibility that biofilm patterning has been selected for as a stable adaptive trait, it is important to recognize the tradeoffs faced by individual cells, including the potential for “cheaters” to disrupt patterning and the associated benefits to the population. For example, phenazines are a community resource produced at a cost. Once excreted, these compounds may be taken up and participate in repeated redox cycling by both phenazine-producing and nonproducing cells (32). In the biofilm context, strategies may be used to avoid the likely benefit experienced by cheaters that catalyze redox cycling without contributing to the phenazine pool. Recent work has shown that extracellular matrix formation is a strategy that allows only cooperating cells to gain the benefit of the tall structures built by the

community, so long as the cooperators exist in high enough local abundance and matrix properties (production rate and density) fall within a predictable range (4, 12).

Characterization of the relationships among metabolism, chemical gradients, and morphogenesis of bacterial biofilms provides information relevant to diverse fields. Bacterial biofilms may exhibit complex spatial patterning at scales comparable to those of putative microbial fossils (25, 47). Our biofilm system has allowed us to test the effects of different atmospheric oxygen concentrations directly and to demonstrate that the width of features changes predictably. These findings may provide a basis for verifying microbial fossils and using them as reporters of the ancient environment. For example, in aquatic environments, the diffusive boundary layer for oxygen that forms around the biofilm is what influences feature geometry (4–12) in contrast to the open-atmosphere biofilms studied here, in which the important oxidative gradients occur inside the biofilm. These differences provide avenues for interpreting which environments are capable of producing an observed morphology.

Biofilm development is a critical component of bacterial colonization of and persistence within human and other eukaryotic hosts. It contributes to the establishment and maintenance of various types of *P. aeruginosa* infections. Here we find that biofilms produce optimal structures to enhance growth and that the success of the colony depends on the ability to build these structures effectively. As we learn more about the complex set of cellular behaviors responsible for the emergent regulation of these features, we become better equipped to take new approaches toward controlling biofilms in clinical and industrial settings.

METHODS

Bacterial Strains and Growth Conditions. Wild-type *P. aeruginosa* PA14 and a mutant (*Δphz*) deficient in phenazine production were used in this study (49). Bacterial cultures were grown routinely at 37 °C in lysogeny broth, shaking at 250 rpm overnight. For all oxygen profiling experiments, colony biofilms were grown on 1% tryptone (Teknova)/1% agar (Teknova) plates

amended with 20 μg/mL Coomassie blue (EMD) and 40 μg/mL Congo red (EMD). Colony biofilms were grown at room temperature (22–25 °C) and at high humidity (>90%). Sixty milliliters of the medium was poured per 10-cm_2 plate (D210-16; Simport) and allowed to dry with closed lids at room temperature for 24 h. Ten microliters of the overnight culture was spotted on these agar plates, and colony biofilms were grown for 6 d. Colonies were grown under hypoxic (15% oxygen) or hyperoxic conditions (40% oxygen) as described earlier (28). Briefly, we incubated agar plates in C-Chambers (C274; BioSpherix). Oxygen concentrations were regulated by mixing pure nitrogen and oxygen (Tech Air), using the gas controller ProOx P110 (BioSpherix).

Colony Geometry Measurements. Width and height of ridges within colony biofilms were measured with a digital microscope (Keyence VHX-1000).

Oxygen Depth Profiles. Oxygen profiling was done using a miniaturized Clarktype oxygen sensor (Unisense; 10-μm tip diameter) on a motorized micromanipulator (Unisense) for depth control. The electrode was connected to a picoampere amplifier multimeter (Unisense) and polarized at –800 mV. The sensor was calibrated using a two-point calibration system at atmospheric oxygen and zero oxygen. The atmospheric oxygen reading was obtained by placing the electrode in a calibration chamber (Unisense) containing well-aerated deionized water. Complete aeration was achieved by constantly bubbling the water with air. The zero reading was obtained by bubbling water in the calibration chamber with ultra–high-purity nitrogen gas (Tech Air). All calibration readings and profile measurements were obtained using SensorTrace Pro 2.0 software (Unisense).

FIGURES

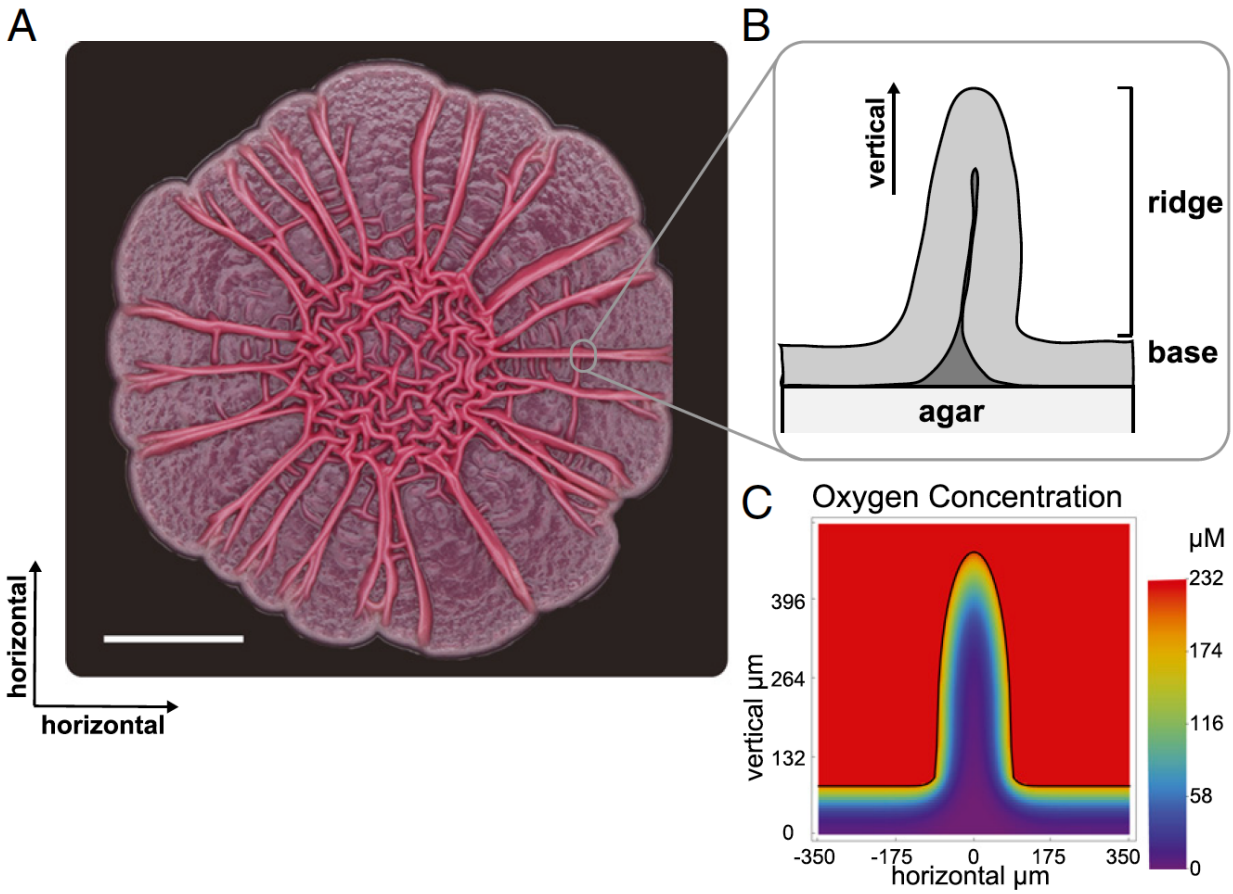

Figure B-1. Horizontal (**A**) and vertical (**B**) structures of *P. aeruginosa* colony biofilms. The colony was grown air-exposed on 1% tryptone, 1% agar for 5 d. The scale bar represents 0.5 cm. (**C**) The simulated concentration of oxygen within a ridge.

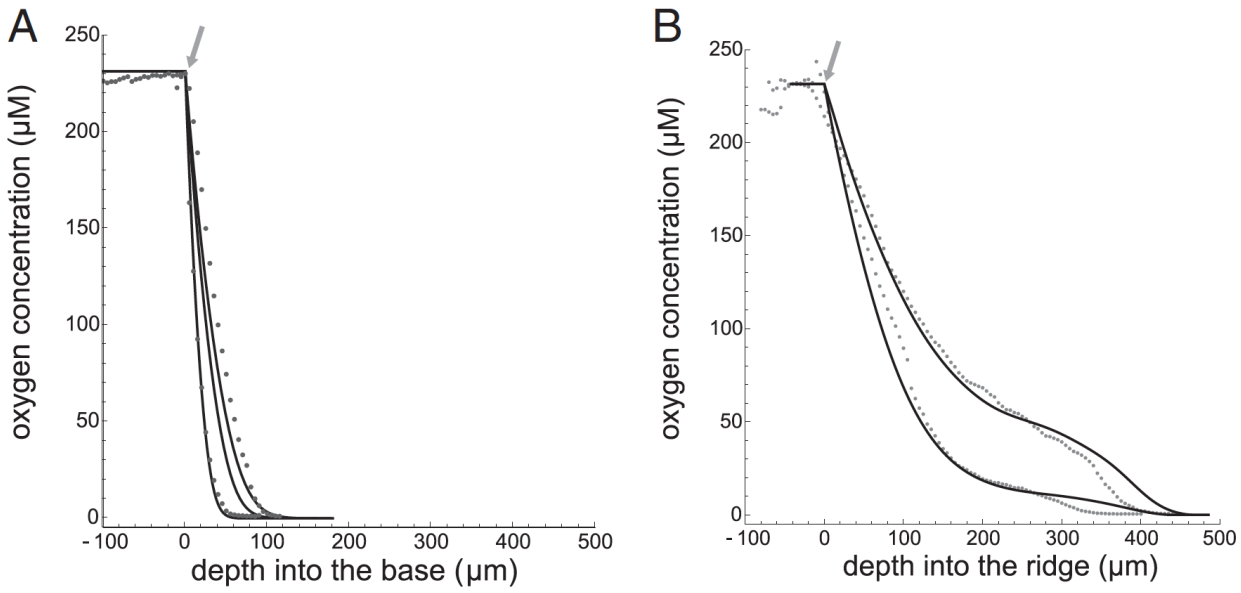

Figure B-2. Oxygen profiles of 4-d-old colony biofilms for (**A**) the base region and (**B**) the ridge. Measured values are given by points, and simulations are represented by the solid curves. We took measurements for 37 base profiles and 27 ridge profiles over 5 d of growth, and the data in **A** and **B** represent the variation within the observed profiles. Arrows indicate the top of the biofilm surface. Data from ref. 28

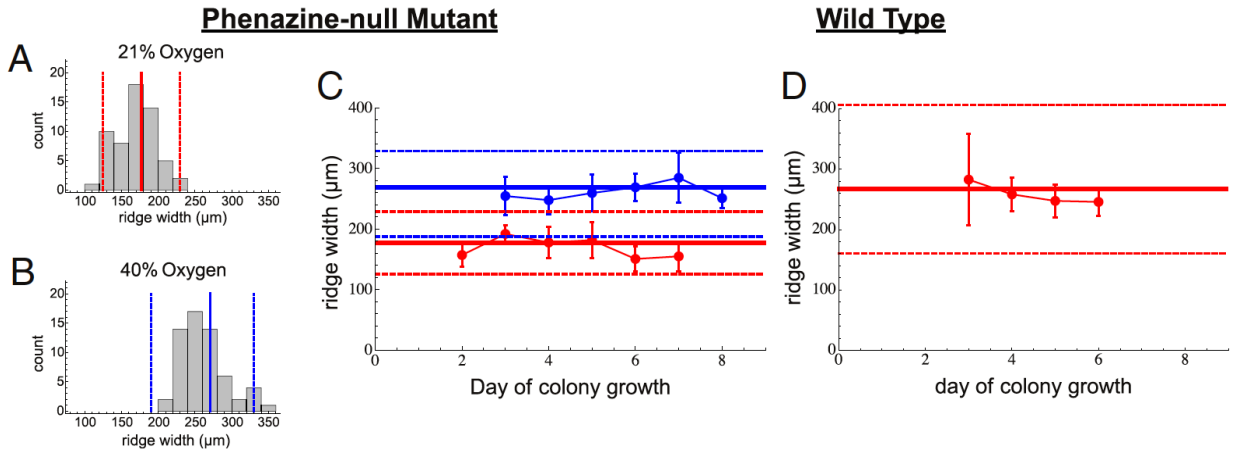

Figure B-3. The average width of colony ridges as a function of time for *Δphz* (A–C) and wild-type (D) colonies. (A and B) Histograms for all ridge width measurements at 21% and 40% oxygen. (A–D) The solid red (21% oxygen) and blue (40% oxygen) lines represent our predictions for optimal ridge width, and the dashed lines represent our predictions for the bounds of variation in ridge width.

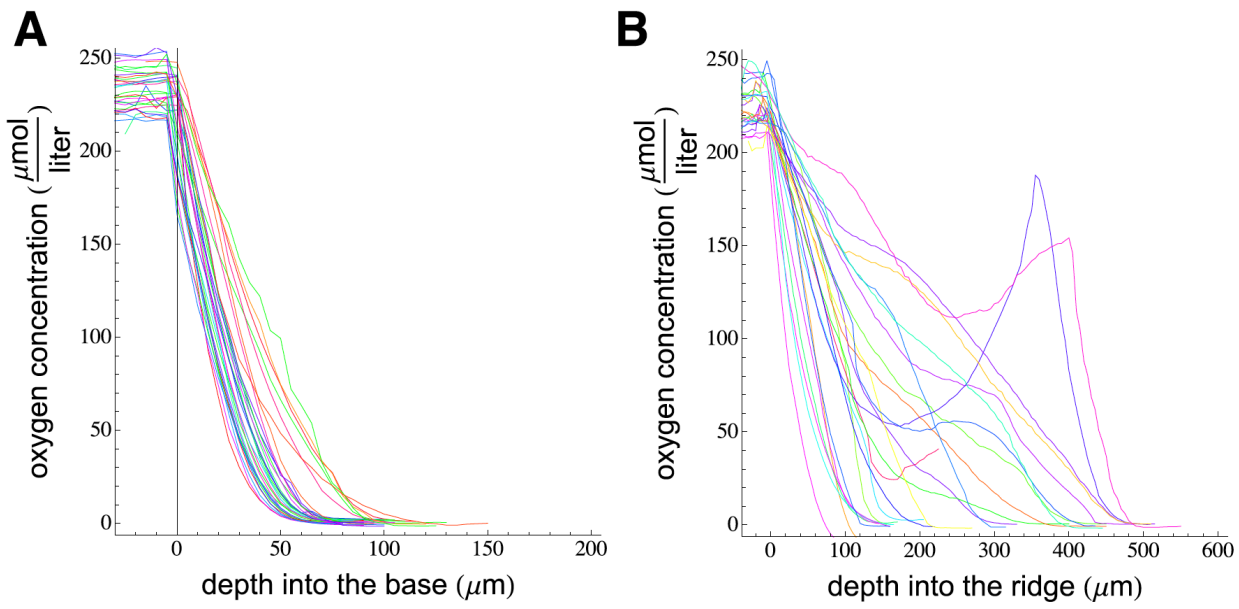

Figure B-4. All the measured oxygen profiles for the base region (**A**) and wrinkles (**B**) of *Δphz* colonies grown in 21% external oxygen. Note that the wide range of wrinkle profile decay rates, as well as the occasional increase in oxygen with increasing depth, is a result of the thin geometry of the wrinkle and the resulting experimental challenge of keeping the oxygen probe centered in the wrinkle as it moves deeper into the colony. Data from ref. 28

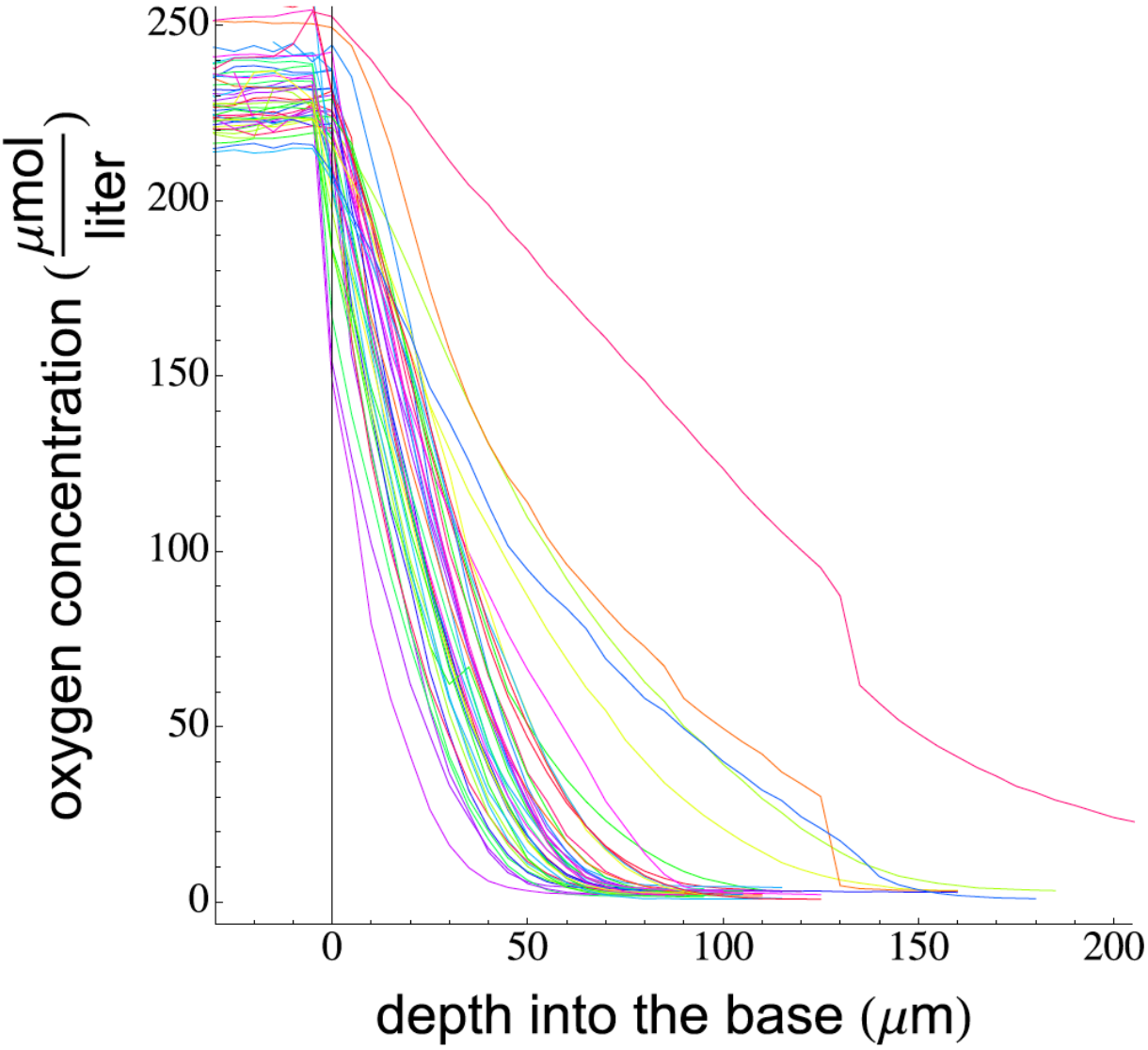

Figure B-5. All the measured oxygen profiles for the base region of wild-type colonies grown in 40% oxygen. Data from ref. 28.

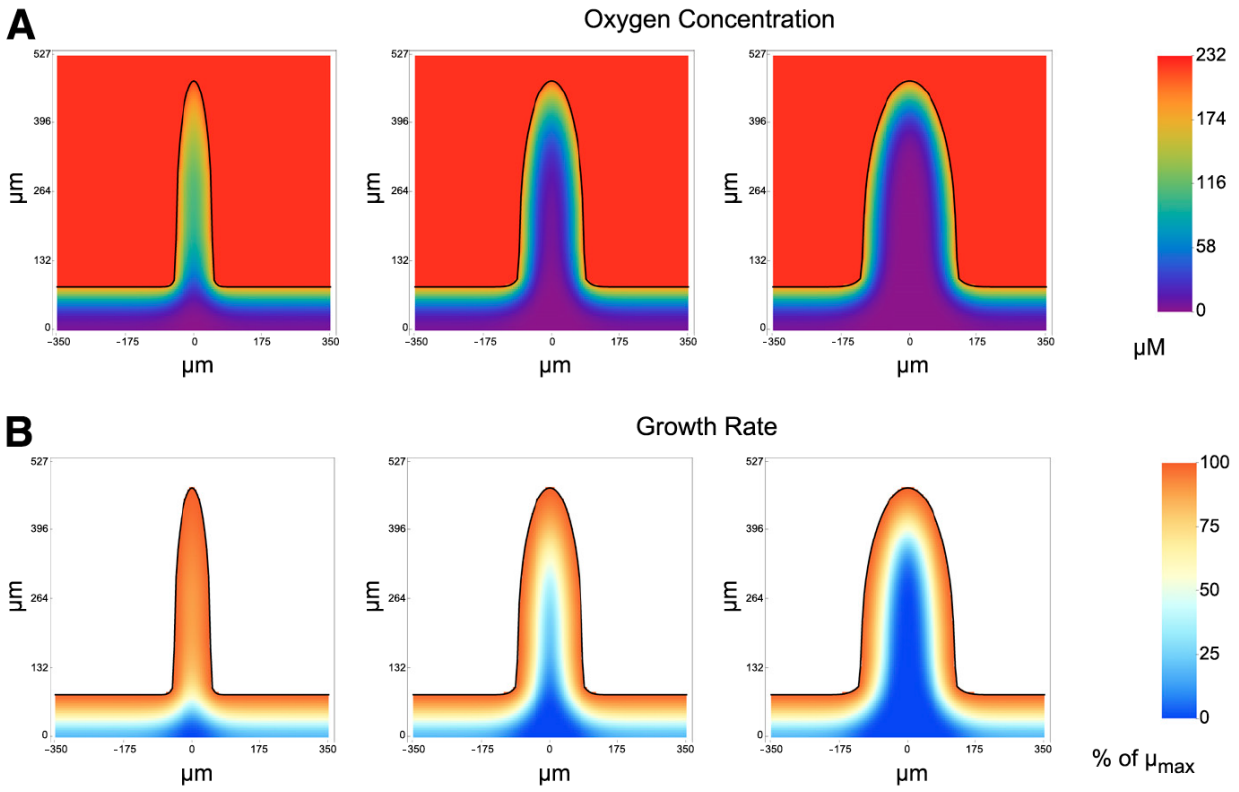

Figure B-6. The modeled internal availability of oxygen (**A**) along with the spatial distribution of growth rate (**B**) within a biofilm for features of different sizes.

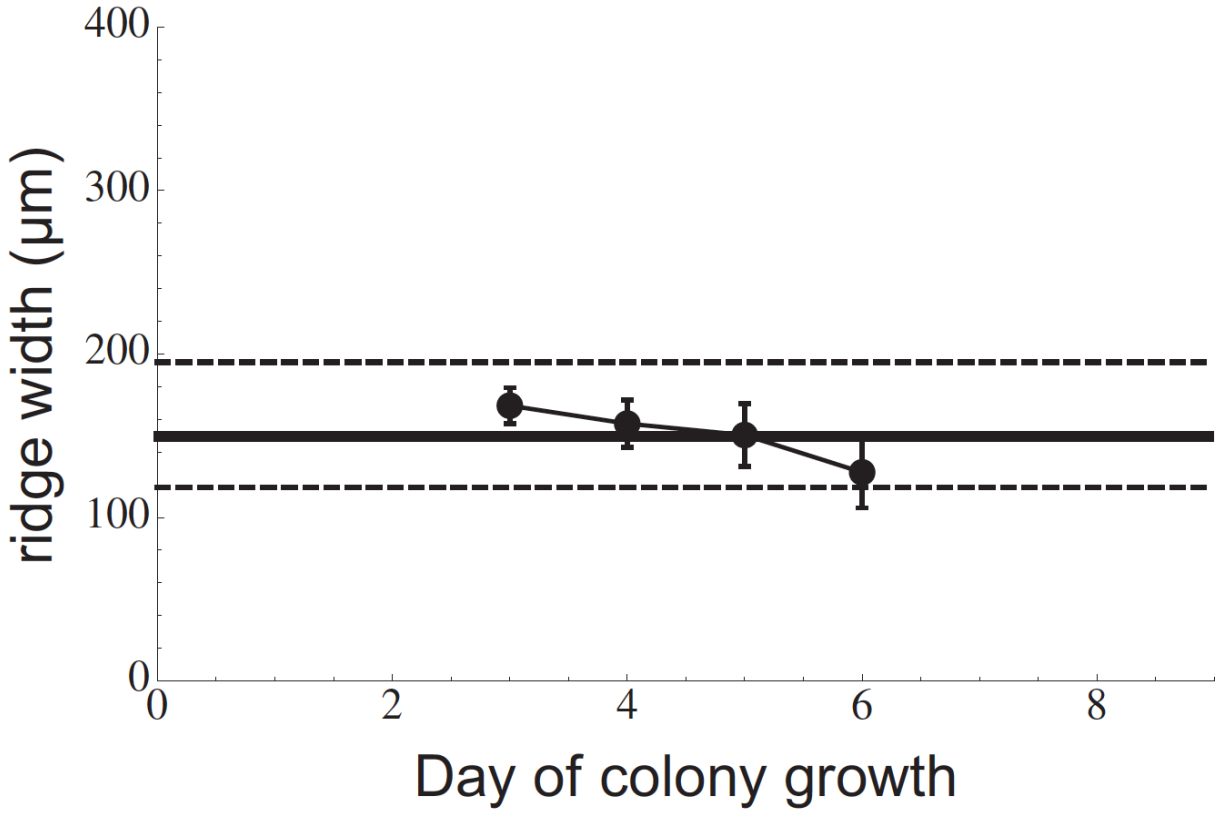

Figure B-7. The average width (points) of *Δphz* colony wrinkles grown in 15% external oxygen as a function of time. The solid line represents our predictions for optimal wrinkle width, and the dashed lines are our predictions for the bounds of variation in wrinkle width. The data were published previously in ref. 28.

REFERENCES

1. Worlitzsch D, et al. (2002) Effects of reduced mucus oxygen concentration in airway Pseudomonas infections of cystic fibrosis patients. J Clin Invest 109(3):317–325.
2. Stal L (1995) Physiological ecology of cyanobacteria in microbial mats and other communities. New Phytol 131(1):1–32.
3. Janson S, Bergman B, Carpenter E, Giovannoni S, Vergin K (1999) Genetic analysis of natural populations of the marine diazotrophic cyanobacterium Trichodesmium. FEMS Microbiol Ecol 30(1):57–65.
4. Xavier JB, Foster KR (2007) Cooperation and conflict in microbial biofilms. Proc Natl Acad Sci USA 104(3):876–881.
5. Picioreanu C, van Loosdrecht MC, Heijnen JJ (1998) Mathematical modeling of biofilm structure with a hybrid differential-discrete cellular automaton approach. Biotechnol Bioeng 58(1):101–116.
6. van Loosdrecht MC, Heijnen JJ, Eberl H, Kreft J, Picioreanu C (2002) Mathematical modelling of biofilm structures. Antonie van Leeuwenhoek 81(1-4):245–256.
7. Xavier JB, Picioreanu C, van Loosdrecht MC (2005) A framework for multidimensional modelling of activity and structure ofmultispecies biofilms. EnvironMicrobiol 7(8):1085–1103.
8. Kreft JU, Picioreanu C, Wimpenny JW, van Loosdrecht MC (2001) Individual-based modelling of biofilms. Microbiology 147(11):2897–2912.
9. Klausen M, et al. (2003) Biofilm formation by *Pseudomonas aeruginosa* wild type, flagella and type IV pili mutants. Mol Microbiol 48(6):1511–1524.
10. de Beer D, Stoodley P, Roe F, Lewandowski Z (1994) Effects of biofilm structures on oxygen distribution and mass transport. Biotechnol Bioeng 43(11):1131–1138.
11. Banin E, Brady KM, Greenberg EP (2006) Chelator-induced dispersal and killing of *Pseudomonas aeruginosa* cells in a biofilm. Appl Environ Microbiol 72(3):2064–2069.
12. Nadell CD, Foster KR, Xavier JB (2010) Emergence of spatial structure in cell groups and the evolution of cooperation. PLOS Comput Biol 6(3):e1000716.
13. Kempes CP, Dutkiewicz S, Follows MJ (2012) Growth, metabolic partitioning, and the size of microorganisms. Proc Natl Acad Sci USA 109(2):495–500.
14. Lane N, MartinW(2010) The energetics of genome complexity. Nature 467(7318):929–934.
15. West GB, Woodruff WH, Brown JH (2002) Allometric scaling of metabolic rate from molecules and mitochondria to cells andmammals. Proc Natl Acad SciUSA 99(Suppl 1): 2473–2478.

16. Banavar JR, Damuth J, Maritan A, Rinaldo A (2002) Supply-demand balance and metabolic scaling. Proc Natl Acad Sci USA 99(16):10506–10509.

17. Banavar JR, et al. (2010) A general basis for quarter-power scaling in animals. Proc Natl Acad Sci USA 107(36):15816–15820.

18. Blonder B, Violle C, Bentley LP, Enquist BJ (2011) Venation networks and the origin of the leaf economics spectrum. Ecol Lett 14(2):91–100.

19. Simon MC, Keith B (2008) The role of oxygen availability in embryonic development and stem cell function. Nat Rev Mol Cell Biol 9(4):285–296.

20. Bertout JA, Patel SA, Simon MC (2008) The impact of O2 availability on human cancer. Nat Rev Cancer 8(12):967–975.

21. Harris AL (2002) Hypoxia—a key regulatory factor in tumour growth. Nat Rev Cancer 2(1): 38–47.

22. Giordano FJ (2005) Oxygen, oxidative stress, hypoxia, and heart failure. J Clin Invest 115(3): 500–508.

23. Haworth SG, Hislop AA (2003) Lung development-the effects of chronic hypoxia. Semin Neonatol 8(1):1–8.

24. Chandel NS, Simon MC (2008) Hypoxia-inducible factor: roles in development, physiology, and disease. Cell Death Differ 15(4):619–620.

25. El Albani A, et al. (2010) Large colonial organisms with coordinated growth in oxygenated environments 2.1 Gyr ago. Nature 466(7302):100–104.

26. Davey ME, O'Toole GA (2000) Microbial biofilms: From ecology to molecular genetics. Microbiol Mol Biol Rev 64(4):847–867.

27. Friedman L, Kolter R (2004) Genes involved in matrix formation in *Pseudomonas aeruginosa* PA14 biofilms. Mol Microbiol 51(3):675–690.

28. Dietrich LE, et al. (2013) Bacterial community morphogenesis is intimately linked to the intracellular redox state. J Bacteriol 195(7):1371–1380.

29. Asally M, et al. (2012) Localized cell death focuses mechanical forces during 3D patterning in a biofilm. Proc Natl Acad Sci USA 109(46):18891–18896.

30. Seminara A, et al. (2012) Osmotic spreading of Bacillus subtilis biofilms driven by an extracellular matrix. Proc Natl Acad Sci USA 109(4):1116–1121.

31. Dietrich LE, Teal TK, Price-Whelan A, Newman DK (2008) Redox-active antibiotics control gene expression and community behavior in divergent bacteria. Science 321(5893):1203–1206.

32. Wang Y, Kern SE, Newman DK (2010) Endogenous phenazine antibiotics promote anaerobic survival of Pseudomonas aeruginosa via extracellular electron transfer. J Bacteriol 192(1):365–369.

33. Price-Whelan A, Dietrich LE, Newman DK (2007) Pyocyanin alters redox homeostasis and carbon flux through central metabolic pathways in *Pseudomonas aeruginosa* PA14. J Bacteriol 189(17):6372–6381.

34. Kolodkin-Gal I, et al. (2013) Respiration control of multicellularity in *Bacillus subtilis* by a complex of the cytochrome chain with a membrane-embedded histidine kinase.Genes Dev 27(8):887–899.

35. Sinsabaugh RL, Follstad Shah JJ (2012) Ecoenzymatic stoichiometry and ecological theory. Annu Rev Ecol Evol Syst 43:313–343.

36. Kondo S, Miura T (2010) Reaction-diffusion model as a framework for understanding biological pattern formation. Science 329(5999):1616–1620.

37. Murray J (2002) Mathematical Biology: An Introduction (Springer, Berlin).

38. Mimura M, Sakaguchi H, Matsushita M (2000) Reaction–diffusion modelling of bacterial colony patterns. Physica A 282(1):283–303.

39. Stewart PS (2003) Diffusion in biofilms. J Bacteriol 185(5):1485–1491.

40. Klapper I, Dockery J (2010) Mathematical description of microbial biofilms. SIAM Rev 52(2): 221–265.

41. Petroff AP, et al. (2011) Reaction-diffusion model of nutrient uptake in a biofilm: Theory and experiment. J Theor Biol 289:90–95.

42. Golding I, Kozlovsky Y, Cohen I, Ben-Jacob E (1998) Studies of bacterial branching growth using reaction–diffusion models for colonial development. Physica A 260(3):510–554.

43. Benefield L, Molz F (1985) Mathematical simulation of a biofilm process. Biotechnol Bioeng 27(7):921–931.

44. Pirt SJ (1965) The maintenance energy of bacteria in growing cultures. Proc R Soc Lond B Biol Sci 163(991):224–231.

45. Heijnen J, Roels J (1981) A macroscopic model describing yield and maintenance relationships in aerobic fermentation processes. Biotechnol Bioeng 23(4):739–763.

46. Monod J (1949) The growth of bacterial cultures. Annu Rev Microbiol 3(1):371–394.

47. Petroff AP, et al. (2010) Biophysical basis for the geometry of conical stromatolites. Proc Natl Acad Sci USA 107(22):9956–9961.

48. Wilking JN, et al. (2013) Liquid transport facilitated by channels in *Bacillus subtilis* biofilms. Proc Natl Acad Sci USA 110(3):848–852.

49. Dietrich LE, Price-Whelan A, Petersen A, Whiteley M, Newman DK (2006) The phenazine pyocyanin is a terminal signalling factor in the quorum sensing network of *Pseudomonas aeruginosa*. Mol Microbiol 61(5):1308–1321.

Appendix C. Control of *Candida albicans* Metabolism and Biofilm Formation by *Pseudomonas aeruginosa* phenazines

This appendix is adapted from a manuscript that was published in mBio– Morales, Grahl, Okegbe et al 2013. Here we show that phenazines produced by Pseudomonas aeruginosa modulate C. albicans metabolism and, through these metabolic effects, impact cellular morphology, cell-cell interactions, and biofilm formation. I contributed the experiments measuring oxygen profiles in C. albicans biofilms (Figure C-6).

ABSTRACT

Candida albicans has developmental programs that govern transitions between yeast and filamentous morphologies and between unattached and biofilm lifestyles. Here, we report that filamentation, intercellular adherence, and biofilm development were inhibited during interactions between *Candida albicans* and *Pseudomonas aeruginosa* through the action of *P. aeruginosa*-produced phenazines. While phenazines are toxic to *C. albicans* at millimolar concentrations, we found that lower concentrations of any of three different phenazines (pyocyanin, phenazine methosulfate, and phenazine-1-carboxylate) allowed growth but affected the development of *C. albicans* wrinkled colony biofilms and inhibited the fungal yeast-to-filament transition. Phenazines impaired *C. albicans* growth on nonfermentable carbon sources and led to increased production of fermentation products (ethanol, glycerol, and acetate) in glucose-containing medium, leading us to propose that phenazines specifically inhibited respiration. Methylene blue, another inhibitor of respiration, also prevented the formation of structured colony biofilms. The inhibition of filamentation and colony wrinkling was not solely due to lowered extracellular pH induced by fermentation. Compared to smooth, unstructured colonies, wrinkled colony biofilms had higher oxygen concentrations within the colony, and wrinkled regions of these colonies had higher levels of respiration. Together, our data suggest that the structure of the fungal biofilm promotes access to oxygen and enhances

respiratory metabolism and that the perturbation of respiration by bacterial molecules such as phenazines or compounds with similar activities disrupts these pathways. These findings may suggest new ways to limit fungal biofilms in the context of disease.

INTRODUCTION

Candida albicans, a commensal resident of mucosal surfaces, can overgrow under favorable conditions, leading to a wide range of diseases, referred to as candidiasis (1). *C. albicans* infections often involve more than one cellular morphology; yeast, pseudohyphal, and hyphal growth forms have all been associated with virulence (2). It has been proposed that filaments are responsible for tissue penetration, whereas yeasts play an important role in early dissemination and in less invasive disease infections (3). *C. albicans* infections are also associated with its formation of biofilms, which are dense single-species and mixed-species populations adhering to one another through the action of surface adhesins and extracellular polymers. Biofilms on implanted medical devices can serve as a source for infection, and dense *C. albicans* populations within the host may have properties in common with biofilms, such as high levels of drug resistance and resistance to host immune defenses (4, 5). Importantly, biofilm formation involves filamentation and adhesin-mediated aggregation of cells (6,7).

Many environmental cues impact fungal morphology and biofilm formation. Many conditions, such as hypoxia, elevated extracellular pH, N-acetylglucosamine (GlcNAc), amino acids, low concentrations of glucose, body temperature, and elevated CO_2 have been associated with C. albicans filamentation (8, 9). There have been a number of studies that also indicate that metabolic status can influence the decision to form hyphae (10–16). There are still many questions regarding how the fungus integrates these different signals and whether there are important links between known inducers of hyphal growth, biofilm formation, and metabolism.

C. albicans and bacteria can coexist within the host (17–19), where the nature of the interspecies interactions can determine the fate of the microbial populations (20) and thus

probably the outcome of polymicrobial diseases. *C. albicans* and *Pseudomonas aeruginosa*, two species commonly found together in mixed species, biofilm-related infections (21), interact in many different ways through physical association, killing by secreted factors and signaling events that modulate virulence properties (22–29). *P. aeruginosa* adheres to and forms biofilms on *C. albicans* filaments (23) and ultimately causes the death of the fungal hypha. A *P. aeruginosa* quorum-sensing molecule also induces a transition to yeast growth, and yeasts are more resistant to killing by P. aeruginosa (23). Redox-active phenazines produced by *P. aeruginosa* play a key role in controlling *C. albicans* when the two species are in close proximity (24, 29). We reported that *C. albicans* growth was antagonized by two *P. aeruginosa* phenazines, pyocyanin (PYO) and its biosynthetic precursor 5-methylphenazinium-1-carboxylate (5MPCA), as well as by a synthetic methylphenazinium analog phenazine methosulfate (PMS), which we have shown to be a surrogate for studying 5MPCA's antifungal activity (24, 29). Phenazines play important roles in bacterial interactions with fungi in which high concentrations of phenazines inhibit fungal growth (30).

Here, we demonstrate a new role for bacterial phenazines as modulators of *C. albicans* metabolism and community behavior. In the presence of phenazine-producing *P. aeruginosa* or low concentrations of purified phenazines, the fungus grew but no longer developed wrinkled colonies or robust biofilms on plastic surfaces. Phenazines markedly inhibited the yeast-to-filament transition. Consistent with published data indicating that phenazines can impact mitochondrial activity (31, 32), their presence led to increased production of fermentation products and decreased respiratory activity at concentrations that are found in clinical samples (33). Methylene blue (MB), which can also interact with the electron transport chain (ETC) (34, 35), inhibited the development of wrinkled *C. albicans* colony biofilms. These studies also revealed a link between wrinkles in colony biofilms and respiratory activity, and this finding was supported by the detection of higher oxygen concentrations in wrinkled colonies than in smooth and flat colonies comprised of yeast. Together, our data revealed a previously

unidentified role for phenazines as modulators of *C. albicans* metabolism and, through these effects, on cellular morphology, colony development, and biofilm formation on solid surfaces. Moreover, this work also provides new insights into the links between metabolism, morphogenesis, and community behaviors such as biofilm formation in *C. albicans*, and this may represent an emerging theme among the microbes.

RESULTS

***P. aeruginosa* phenazines repress *C. albicans* biofilm formation and hyphal growth**. When wild-type (WT) *P. aeruginosa* strain PA14 and WT *C. albicans* strain SC5314 were grown adjacent to one another, a striking change in *C. albicans* colony morphology occurred, with a smooth zone in the region adjacent to the bacterial colony and wrinkling in regions of the fungal streak that were more distant from the bacterial colony (Fig. C-1A). In contrast, *C. albicans* cocultured with a phenazine-deficient (Δ*phz*) *P. aeruginosa* strain wrinkled robustly up to the edge of the bacterial colony, suggesting that the soluble excreted phenazines played a role in this effect on *C. albicans* colony morphology (Fig. C-1A).

To determine if phenazines were directly responsible for the change in *C. albicans* colony morphology, we spot inoculated *C. albicans* onto medium with and without purified phenazines. Control cultures without phenazines formed wrinkled colony structures, while colonies grown in the presence of low concentrations of any of three phenazines, PYO, PMS, or PCA, were smooth, flat, and undifferentiated (Fig. C-1B). The effects of different concentrations of PMS and PYO were tested, and complete repression of colony wrinkling was apparent at concentrations as low as 5μM for PMS and 10μM for PYO, indicating that the concentrations required to inhibit wrinkled colony development were ~100-fold below those shown previously to be toxic to *C. albicans* (24, 29, 36).

C. albicans hyphal growth has been associated with both wrinkled colony morphology and biofilm formation on plastic surfaces (5, 37). We found that wrinkled colonies, formed upon

growth on medium with GlcNAc at 37°C, exhibited some biofilm-associated characteristics, including cells in hyphal, pseudohyphal, and yeast morphologies that remained associated with one another even upon suspension in liquid (Fig. C-1B). In contrast, smooth colonies formed in the presence of phenazines were comprised almost exclusively of yeast that dispersed easily upon transfer to liquid (Fig. C-1B). In addition to the change in cellular morphology, phenazines repressed expression of HWP1, a gene that is strongly correlated with hyphal growth and involved in biofilm formation (38, 39), as shown using a strain harboring a lacZ transcriptional reporter fused to the HWP1 promoter. A strain expressing an actin transcriptional reporter (ACT1::lacZ) did not show differences between colonies grown in the presence or absence of phenazines. Colonies grown at 30°C without GlcNAc (noninducing conditions) were smooth and contained only yeast (Fig. C-1B); no phenotypic changes in colony morphology were observed upon inclusion of phenazines in the agar medium under these conditions. The total numbers of CFUs in smooth colonies formed in the presence of either PMS or PYO were slightly but significantly ($P < 0.05$) lower than those in control colonies (Fig. C-1C).

Inhibition of extracellular alkalinization by phenazines prevents *C. albicans* filamentation and wrinkling. Previous studies demonstrated links between *C. albicans* morphological transitions and extracellular pH, with yeast growth dominating under acidic conditions and filamentation promoted at neutral pH (40). Seminal studies by Vylkova and colleagues (41) showed that *C. albicans* amino acid catabolism can raise the extracellular pH in environments that are initially acidic. Since our culture medium was rich in amino acids and had an initial pH of 5.0, we determined the role of alkalinization in the induction of filamentation and wrinkled colony morphology. As expected, alkalinization of the medium was evident only in the presence of amino acids, while medium containing only glucose as a carbon source remained acidic (Fig. C-2A). The addition of GlcNAc and incubation at 37°C (conditions that induce filamentation) promoted colony wrinkling on medium with amino acids that had increased pH (Fig. C-2A; control). However, GlcNAc and 37°C were not sufficient to support wrinkled colony formation in the absence of amino acids (Fig. C-2A). Concentrations of phenazines that inhibited colony

wrinkling also had striking effects on the pH changes in the medium. While the medium surrounding control colonies became red by 48 h, indicating a pH greater near 7, the medium surrounding PMS- and PYO-grown colonies remained acidic (Fig. C-2A). The addition of PMS or PYO did not change the pH of uninoculated media. These differences in extracellular pH led us to hypothesize that phenazines were impacting *C. albicans* metabolism.

Phenazine-induced fermentation correlates with *C. albicans* acidification of the extracellular milieu. In liquid culture conditions, as observed on agar (Fig. C-1C), PMS caused a small decrease in growth rate and final yield (Fig. C-2B), and the pH in the extracellular medium of cultures grown with PMS was lower (Fig. C-2C). Extracellular pH can increase upon ammonia release (41, 42), and acidic products can lower the pH. We first evaluated the effects of phenazines on ammonia release using an acid trap methodology (41). In control colonies, 138 ± 19 ppm NH_3 was detected in comparison to 290 ± 56 ppm NH_3 for colonies grown with PYO and 270 ± 69 ppm NH_3 for colonies grown with PMS. Thus, neither PMS nor PYO caused a decrease in ammonia release from colonies, suggesting that differences in amino acid catabolism were likely not the cause of the lower pH values in cultures with PMS or PYO.

To determine whether phenazines altered the production of acidic *C. albicans* products, we grew the fungus on filters floating on liquid medium with or without phenazines at 37°C (Fig. C-3A) and analyzed the culture supernatants. As on agar, the pH of the supernatants decreased in the presence of phenazines, as visualized by bromocresol green addition (Fig. C-3A, top). High-performance liquid chromatography (HPLC) analyses of the supernatants found 8- and 17-fold-higher levels of acetic acid produced per unit of optical density at 600 nm in the presence of PMS and PYO, respectively, at 24 h (Fig. C-3B) despite the fact that slightly less glucose was consumed compared to control cultures. Other fermentation products, such as ethanol, were also found at higher relative levels upon phenazine exposure. There was 5.5- and 3.4-fold more ethanol (mg/ml/OD_{600}) in cultures grown with PMS and PYO, respectively, than in 24-h supernatants from untreated cultures of *C. albicans* colonies (Fig. C-3B). HPLC

analyses of *C. albicans* supernatants in planktonic cultures at 8 h also showed higher levels of ethanol as well as glycerol, another *C. albicans* fermentation product, in PMS-containing cultures than in controls. Together, these data suggest a shift toward fermentation in the presence of phenazines.

Phenazines inhibit *C. albicans* growth on nonfermentable carbon sources. *C. albicans* can either ferment or respire glucose, whereas other substrates, like amino acids, alcohols, or organic acids, can be used only for energy generation via respiration (43). In light of the finding that phenazines increased production of *C. albicans* fermentation products (Fig. C-3B), we tested the hypothesis that phenazines inhibited respiration by assessing their effects on growth on non-fermentable carbon sources. Indeed, while growth on glucose was only slightly slower in the presence of PMS (Fig. C-4A), this phenazine caused a marked decrease in both growth rates and yield in cultures grown on amino acids (Fig. C-4B).

Phenazine-mediated *C. albicans* colony morphology changes are not due solely to altered extracellular pH. Phenazines repressed biofilm behaviors both on agar and in liquid medium with glucose (Fig. C-1) and caused acidification of the medium (Fig. C-2A and C). Because of the known role of extracellular pH in *C. albicans* morphological regulation (40, 41), we tested whether acidification of the extracellular milieu was required for phenazine-mediated inhibition of *C. albicans* filamentous growth and colony development. The fungus was spot inoculated on medium containing glucose and amino acids that was buffered at either pH 5 or pH 7 (Fig. C-5A). As previously described (44), a stable acidic extracellular milieu (pH 5.0) completely inhibited *C. albicans* filamentation and wrinkled colony formation (Fig. C-5A). Colonies formed on medium that was buffered at pH 7.0 were wrinkled in the absence of PMS or PYO. Interestingly, PYO and PMS still repressed filamentation and colony wrinkling on this buffered medium (Fig. C-5A). Therefore, our results demonstrate that while phenazine-mediated decreases in pH were sufficient to repress hyphal growth, this change in extracellular pH was not required to prevent inhibition of wrinkled colony morphology formation and filamentation.

Phenazines alter *C. albicans* respiratory activity. Our data led us to propose that phenazines altered *C. albicans* respiratory activity. To assess whether perturbation of respiratory activity was sufficient to repress colony biofilm development, we determined if methylene blue (MB), another well-known electron acceptor capable of altering mitochondrial activity and with structural similarity to phenazines (34, 35), also repressed colony wrinkling. Similar to the effects of PMS, PCA, and PYO (Fig. C-1B), micromolar concentrations of MB also caused *C. albicans* formation of smooth colonies on unbuffered medium (Fig. C-5B). Unlike phenazines, which promoted extracellular acidification (Fig. C-2A and C and C-3A), cultures with MB alkalinized the medium when it was at an initial pH of 5 and did not acidify the extracellular milieu when the initial pH was adjusted to 7 (Fig. C-5B). These data highlight that compounds that impact respiration can inhibit colony wrinkling and that extracellular pH changes were not required for the repression of hyphal growth and the development of wrinkled, structured colonies.

We next used TTC, a dye indicative of mitochondrial activity, in order to test the idea that phenazines could impair respiration directly. Reduction of TTC by the electron transport chain (ETC) leads to the formation of a red product that accumulates within cells (45). Colony biofilms formed without phenazines exhibited a high level of TTC reduction as evidenced by the strong red pigmentation (Fig. C-6A and B). However, PMS- or PYO-grown colonies showed decreased TTC conversion in this assay and, thus, were much less metabolically active (Fig. C-6A). To complement these studies, we used an electrode probe to measure the oxygen gradients as a function of depth from the top of the colony as an indicator of oxygen utilization within the colony interior. Under noninducing conditions, smooth colonies grown with PMS or PYO demonstrated higher concentrations of oxygen than control colonies when measured at comparable depths from the surface (Fig. C-6A). These data are consistent with oxygen utilization being repressed by phenazines. Together, these findings indicate that phenazines cause a disruption of the normal respiratory patterns in *C. albicans* cells.

The wrinkles of *C. albicans* colonies have elevated oxygen concentrations and exhibit a high respiratory metabolism. When TTC was added to *C. albicans* wrinkled colonies formed in inducing conditions in the absence of phenazines, stronger red pigmentation was observed than in colonies grown under noninducing conditions (Fig. C-6A and B), suggesting that wrinkled colony biofilms exhibited a more active respiratory metabolism than colonies with a smooth morphology. Consistent with this observation, phenazine-treated colonies grown under inducing conditions also showed decreased TTC-derived coloration than untreated wrinkled controls (data not shown). Strikingly, while there was even, red pigmentation from TTC conversion in smooth colonies (Fig. C-6A), wrinkled colonies had higher levels of pigmentation in the wrinkled areas (higher regions of the colony). The "valleys" appeared to have less respiratory activity (Fig. C-6B, inset). Based on these observations and in light of our previous results demonstrating that *C. albicans* wrinkled colony formation was repressed by phenazines and MB (Fig. C-1B and C-5B), we proposed that wrinkling was linked to respiration. To determine whether the topology of the wrinkles promoted access to oxygen within dense colonies, we used an electrode to quantify the oxygen concentration within the wrinkles of colonies grown under inducing conditions compared to non-inducing conditions at similar distances from the colony edge. Wrinkled colony areas had shallow oxygen gradients, and moderately high oxygen remained detectable throughout the structure (Fig. C-6B). In sharp contrast, the gradients for smooth yeast colonies formed in non inducing conditions were much steeper and showed significantly lower oxygen concentrations at all levels within the colony. Thus, our results suggest a model in which wrinkling promotes aerobic respiration as part of fungal colony biofilm development.

DISCUSSION

Our work reveals a new role for *P. aeruginosa* phenazines as modulators of *C. albicans* metabolism and biofilm development. We found that low, nonlethal concentrations of bacterial phenazines inhibited fungal morphogenesis and prevented the development of wrinkled colony

biofilms, and subsequent analyses indicated that these effects were due to alteration of *C. albicans* respiratory activity. Several lines of evidence indicated that phenazines inhibited normal fungal respiratory activity: (i) fermentation products were at higher concentrations in the presence of phenazines (Fig. C-3B), (ii) growth on non-fermentable carbon sources was severely impaired with only slight growth inhibition on glucose (Fig. C-4B), (iii) metabolic activity was lower in the presence of phenazines (Fig. C-6A), and (iv) oxygen concentrations were higher in yeast colonies grown with phenazines than in yeast colonies grown in their absence (Fig. C-6A). The increased secretion of acetic acid (Fig. C-3B) (46) in the presence of phenazines likely reduced the extracellular pH (Fig. C-2A and C); low pH was not the only mechanism responsible for the phenazine-mediated effects since buffering the medium at pH 7 did not ameliorate the effects of phenazines (Fig. C-5A). Importantly, MB, another compound that alters the cellular respiratory activity (34, 35), also repressed hyphal growth and colony biofilm formation but did not lead to a pH change, suggesting that a different spectrum of fermentation products may have been produced (Fig. C-5B). The different effects of MB and phenazines with respect to altering the extracellular pH may be explained by their respective redox properties (47), which could lead to different interactions with the ETC, or due to differences in other targets within the cell. Our data suggest that decreased ability to transfer electrons to oxygen led to decreased colony wrinkling and filamentation, and this model is supported by the fact that *C. albicans* wrinkled colony formation was inhibited (Fig. C-7) and biofilm formation on plastic in liquid medium does not occur in anoxic environments despite the fact that cells form hyphae (48, 49) (Fig. C-7).

Our observations that colony wrinkling was repressed under conditions that limit respiration suggest that these structures may allow cells to increase their access to oxygen in dense populations. Several findings support this model. First, while the absence of oxygen inhibited wrinkled colony formation (Fig. C-7), hypoxic conditions strongly promote colony wrinkling (10). Second, we found that wrinkled regions had higher rates of respiration than non-wrinkled regions of the colony (Fig. C-6B) and that wrinkled colonies had more respiratory activity than

colonies that lacked wrinkling (Fig. C-6). Lastly, mutants locked in a highly respiratory state, such as strains lacking Ace2 and Tye2, have increased colony wrinkling (10) and filamentation within biofilms (50). We speculate that the *C. albicans* wrinkled phenotype is related to biofilm phenotypes on submerged, plastic surfaces, as both structures involve spatially distributed filamemntation and cells that adhere tightly to one another. In multiple bacterial species, the study of colony wrinkling has led to the discovery of genes crucial for biofilm formation on solid surfaces (51–53).

Links between biofilm formation and oxygen availability may emerge as a common theme in diverse microbial species, including both fungi and bacteria. For example, wrinkled *P. aeruginosa* colonies have increased oxygen concentrations within the colony compared to smooth counterparts, and it has been hypothesized that biofilm structure enables access to oxygen by increasing surface area (54). In *P. aeruginosa*, endogenously produced phenazines serve as alternate electron acceptors, thereby facilitating *P. aeruginosa* survival in low-oxygen conditions (55, 56). Phenazines, likely in part through modulation of intracellular redox, led to decreased surface-to-volume ratios in both flow cell and colony biofilms (57, 58) in a manner that is reminiscent to what we observed with *C. albicans*. In addition, *C. albicans* biofilm development may also be influenced by ethanol, a metabolite that has been shown to inhibit submerged biofilm formation in this fungus (59).

Previous studies have also shown links between *C. albicans* respiratory metabolism and cellular and colony morphology. For instance, *C. albicans* strains that lack the mitochondrial NADH dehydrogenase were unable to filament (13), and other ETC inhibitors such as rotenone (13) and thenoyl trifluoro acetone (16) repressed *C. albicans* filamentation. However, it is important to note that antimycin A, another respiratory chain inhibitor, promoted filamentation (10), suggesting that the inhibition of filamentation in response to altered ETC activity is likely due to more than decreased energy generation, such as a response to a specific metabolic signal (10). Biochemical studies that have examined the interactions between phenazines and

respiratory electron transport systems in eukaryotic and bacterial cells have found that these compounds and related molecules can either inhibit or stimulate the flux of electrons through the ETC (31, 60, 61). Future work will determine what signal, such as ratios of intracellular electron carriers, the state of the ETC components, intracellular pH, or ATP levels, is sensed by the cell and which regulators respond to these important intracellular signals. Furthermore, additional studies will be required to explain the differences in respiration seen in the “folds” of wrinkled colonies compared to smooth regions. Possible explanations include regulated differences in metabolism or differences in cell density due to morphology or matrix production. While phenazines are likely too toxic for use as therapeutic agents, our findings with MB may have implications for antifungal therapy. MB is nontoxic in mammals and has been used as an antimalarial drug, a neurotoxin antidote, and a potentiating factor in photodynamic therapy (34, 35). Thus, there is potential for this or similar compounds to be used to inhibit *C. albicans* biofilm infections *in vivo*.

This work highlights that phenazines have different biological effects at different concentrations. Kerr and colleagues (27, 36) and our laboratory (24, 29) have demonstrated the anti-*Candida* properties of *P. aeruginosa* phenazines at high concentrations (> 500 μM). Here, we show that respiration is inhibited at concentrations that are 25- to 200-fold lower than those required to stop growth (29, 36) (Fig. C-1B). In the lungs of cystic fibrosis (CF) patients, where P. aeruginosa and C. albicans are often found together (21, 62), PYO and PCA were found to be between 5 and 80 μM (33). We show here that these concentrations repressed *C. albicans* filamentation and biofilm development but did not kill the fungus. A 1989 study by Bhargava et al. (63) that assessed fungal morphology in the CF lung suggests that this fungus exists as yeast in CF airways. Our findings also suggest the possibility that by releasing phenazines, *P. aeruginosa* causes *C. albicans* to secrete more fermentation products that are readily used by *P. aeruginosa* to enhance its own growth and survival.

MATERIALS AND METHODS

Strains, media, and culture conditions. See Table C-1 for strain descriptions. *C. albicans* and *P. aeruginosa* were inoculated from overnight cultures onto yeast nitrogen base synthetic medium (YNB salts with ammonium sulfate that was supplemented with 10 mM glucose [Glu], 0.2% [wt/vol] amino acids from yeast synthetic dropout medium supplement without tryptophan [AA] both Glu and AA, or succinate [10 mM]). Where stated, 40mMMOPS (morpholinepropanesulfonic acid; pH 7) or 100 mM citrate buffer (pH 5) was added. Non-inducing conditions that promoted growth as yeast and the formation of smooth colonies were defined as Glu or Glu-AA and incubation at 30°C. In inducing conditions that cause colony wrinkling and filamentation, 5 mM GlcNAc was added and cultures were incubated at 37°C. When indicated, media were supplemented with phenazines or methylene blue as described in the supplemental information. To monitor pH, bromocresol purple (0.01% [vol/vol]) was added to the agar medium. *C. albicans-P. aeruginosa* cocultures were performed on yeast extract-peptone-dextrose (YPD) agar.

Analysis of extracellular pH and ammonia production. *C. albicans* strains from stationary phase cultures with an adjusted absorbance (OD_{600}) of 8.0 in 5 ml of YPD were spot inoculated (10 µl) onto agar media. Extracellular alkalinization was qualitatively evaluated by adding 0.01 % of the pH indicator bromocresol purple in ethanol (Sigma) to the medium. To measure fermentation products from colony biofilms, *C. albicans* colonies grown in the liquid assay were cultured onto a 0.2 µm membrane (Millipore) that was floating on 600 µl of Glu+AA liquid medium with or without 5 µM PMS and 20 µM PYO in 24-well plates. 5 µl of a *C. albicans* was inoculated, and colonies were grown for 24 hours at 37°C. Acidification of the extracellular milieu was assessed by adding 0.01 % of the pH indicator bromocresol green (Sigma) in ethanol after the cells were cultured. Fermentation products were measured as described below.

To quantify the production of volatile ammonia by phenazine treated and untreated colonies, a previously described and slightly modified acid trap technique was used (41, 67). Briefly, individual colonies were grown under inducing conditions in 96-well plates with 150 µl of YNB Glu+AA agar alone or with 5 µM PMS or 20 PYO µM. Acid traps, with 100 µl of 10 % (w/v) citric acid per well of a 96-well plate, were situated directly on each well of inverted 96-well plates with growing colonies. After 24 hours at 37°C, the ammonia concentrations within the citric acid solution were determined. The solution was diluted 10-fold, and 20 µl was added to 80 µl of Nessler's reagent (Fisher). Samples were incubated at room temperature for 30 min prior to measurement of the absorbance at OD_{400}. Ammonia concentrations (ppm) were determined using an NH_4Cl standard curve (3-50 ppm).

To determine production of fermentation products, 500 µl of culture media were collected and centrifuged (10 min at 13,200 rpm) to pellet cells. Supernatants (450 µl) were filtered by using a HPLC Spin-X centrifuge tube filter (Costar) and then stored at -80°C until analysis. Filtered samples were acidified with 10% (w/w) H_2SO_4 and subsequently analyzed by HPLC with an Aminex-87H column (Bio-Rad Laboratories, Hercules, CA) operated at 60°C with 0.01 % (v/v) H_2SO_4 mobile phase using dual detection of refractive index and ultra violet (λ =210nm). Peak heights were measured and identified by comparison of retention times with authentic standards and their concentrations determined by the external standard method.

Respiratory activity analyses and oxygen tension analyses. To analyze the respiratory activity of colonies, we employed a TTC overlay technique (64) in which 2 ml of the TTC-agar solution was applied to 48-h-old spot-inoculated colonies. This method that was originally described by Lenhard in 1956 (70) has been broadly used to determine the ETC activity of microbial populations. Colorless 2,3,5 triphenyltetrazolium chloride (TTC) is able to pass through the plasma membrane and reach the mitochondria, where it is converted into reddish 1,3,5-triphenylformazan (TTF) by reducing equivalents and where the colored products then remain immobilized (64, 45). To assess metabolic activity in colonies, 2 ml of the TTC-agar

solution (55°C) was overlaid onto 55 mm plates containing spot-inoculated colonies grown as described in previous sections. Red color development was observed 24 hours after the addition of TTC at room temperature. The TTC-overlay agar solution consisted of 0.067 M potassium phosphate buffer at pH 7.0 and 0.1% TTC. Oxygen tensions within the colonies were measured at room temperature using an automated micro Clark-type oxygen sensor (Unisense) in three areas per colony from the top to bottom after growth for 72 h.

FIGURES

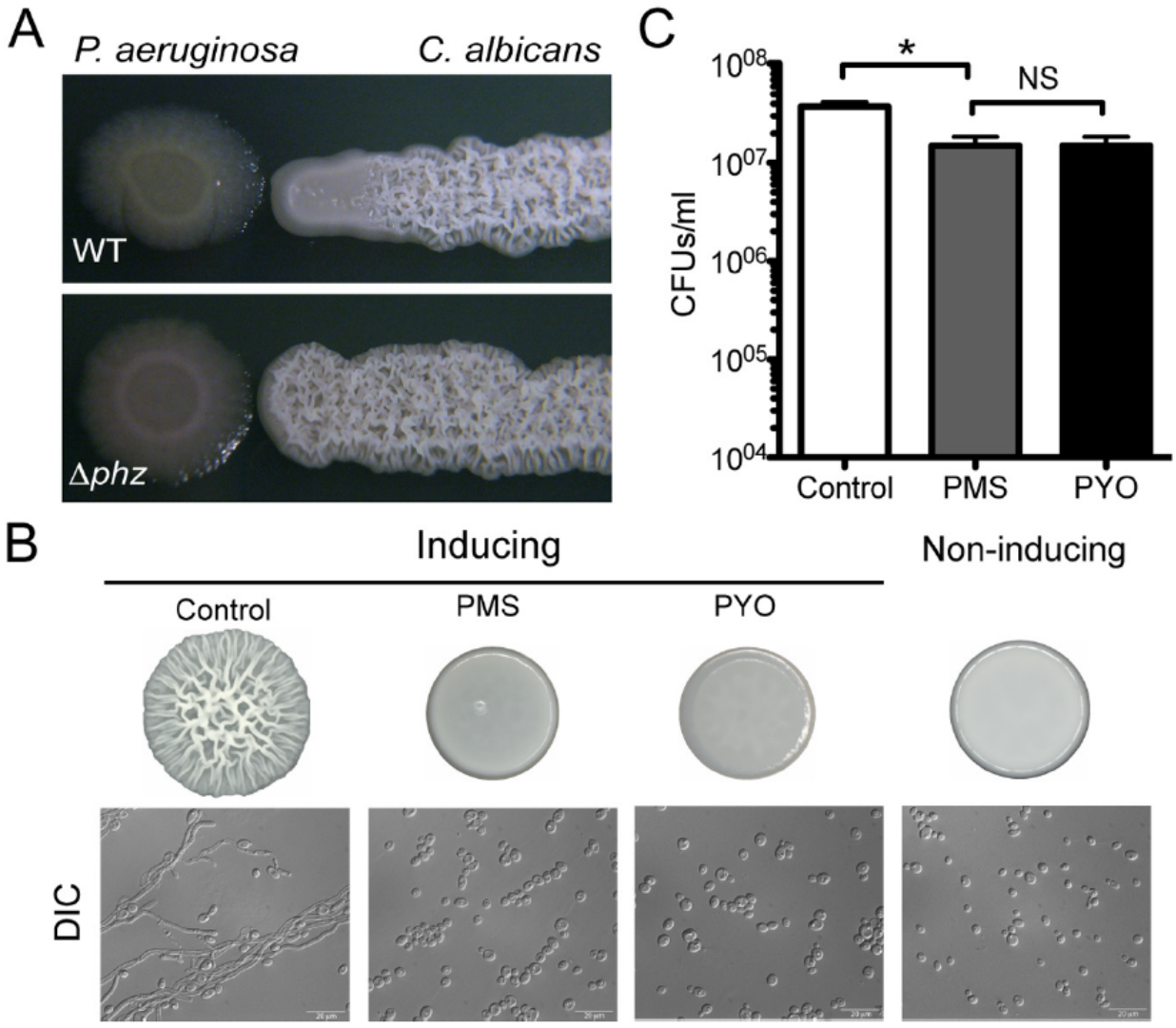

Figure C-1. Effects of phenazines on *C. albicans* colony development and cellular morphology. (A) *C. albicans* SC5314 colony morphology when near *P. aeruginosa* WT or the Δ*phz* strain. (B) Top, *C. albicans* colonies grown on Glu-AA-GlcNAc at 37°C (inducing conditions) or 30°C in the absence of GlcNAc (non-inducing conditions) for 48h in the absence or presence of 5 μM PMS or 20 μM PYO; bottom, microscopic view of cells from colonies, captured using differential interference contrast (DIC) microscopy. (C) Viable cell counts from *C. albicans* colonies exposed to phenazines. CFUs from colonies grown on Glu-AA at 30°C without or with 5 μM PMS or 20 μM PYO for 48h (*, $P < 0.05$; $n = 4$).

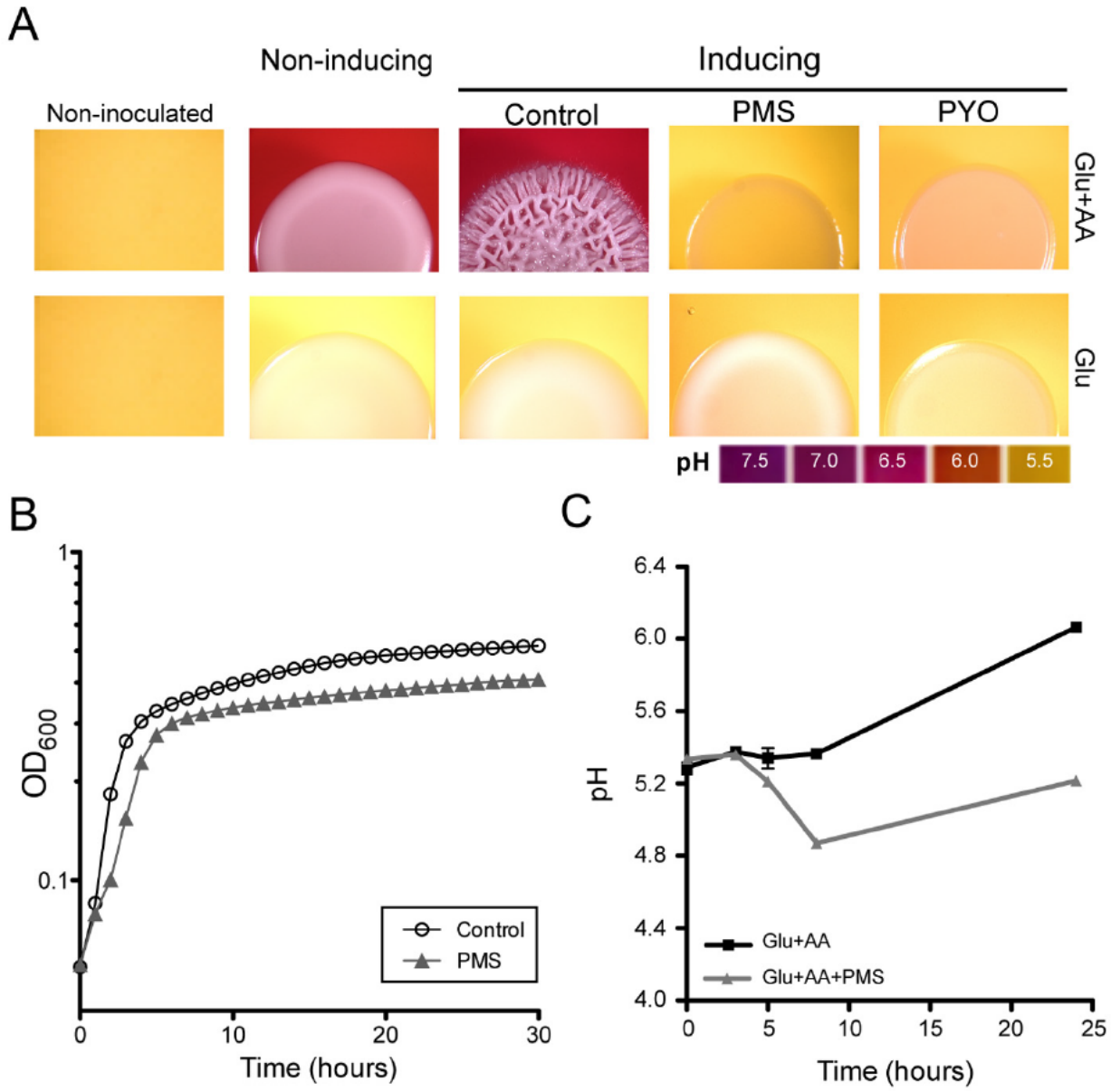

Figure C-2. Phenazines modulate *C. albicans* extracellular alkalinization and morphogenesis. (A) Fungal colonies grown on GluAA or Glu alone under filament-inducing and non-inducing conditions without or with 5 μM of PMS and 20 μM PYO for 48h; pH was monitored using bromocresol purple. The images were obtained by using a stereoscope (7.5X). (B and C) Growth (B) and pH (C) in liquid

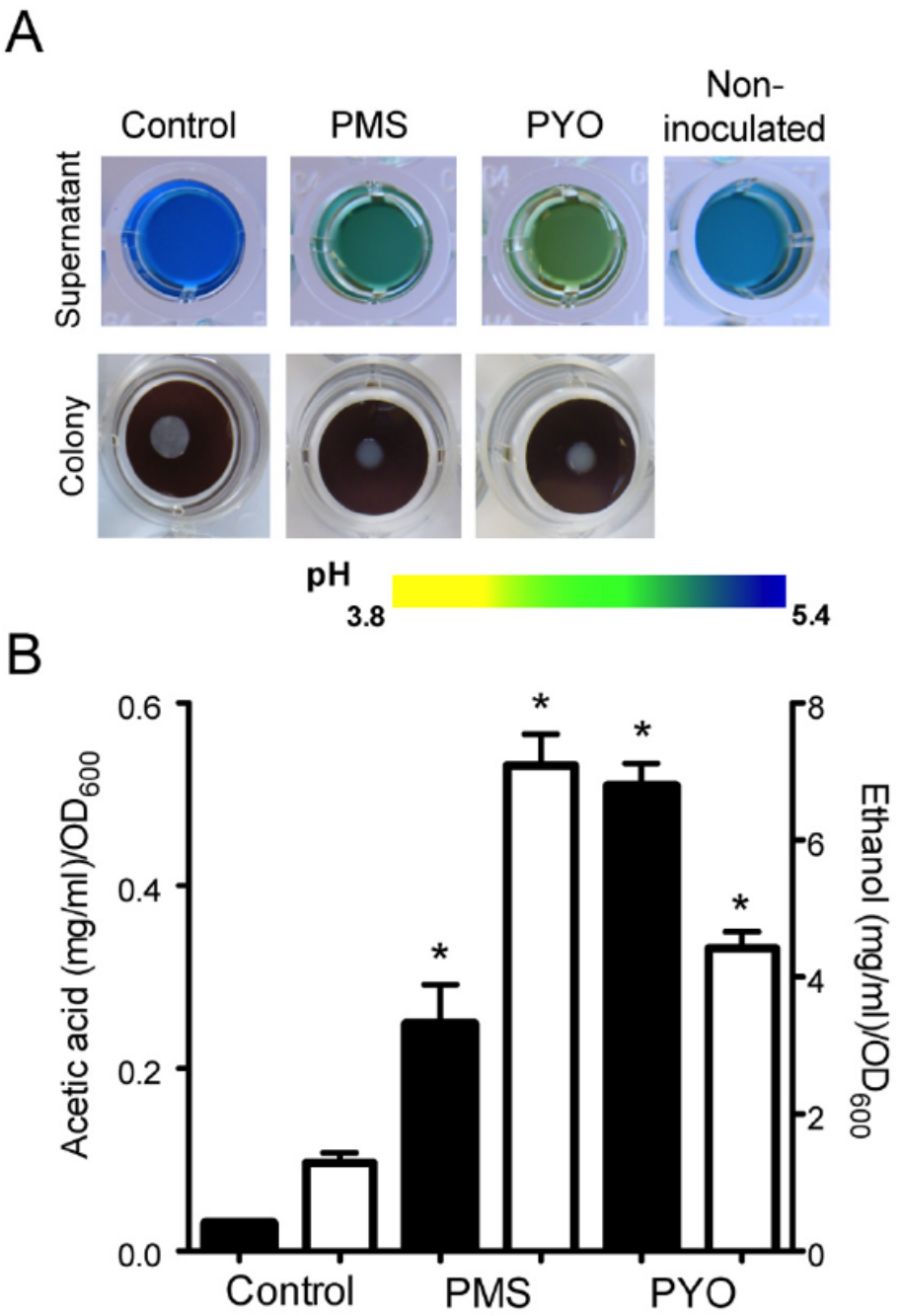

Figure C-3. Phenazines promote glucose fermentation. (A) Top, extracellular changes in pH were visualized by addition of bromocresol green; bottom, *C. albicans* colonies grown for 24h at 37°C on polycarbonate filters suspended on Glu-AA liquid medium in the presence or absence of 20 μM PYO and 5μM PMS without bromocresol green. (B) Quantification of acetic acid (black bars) and ethanol (white bars) in supernatants of colonies grown on filters (n = 3; *, $P < 0.05$).

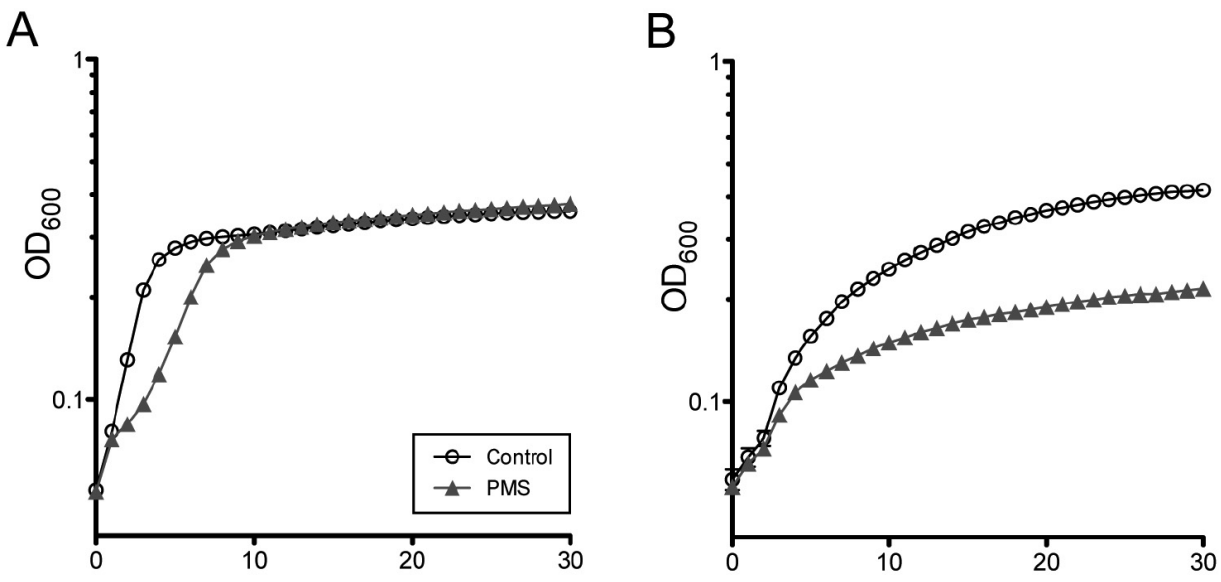

Figure C-4. Phenazines alter *C. albicans* growth in fermentable and non-fermentable carbon sources. Growth curves of liquid cultures on media containing only glucose (A) or amino acids (B) in the presence (triangles) or absence (open circles) of 5 M PMS at 37°C. The optical density (OD600) of each culture was monitored every hour.

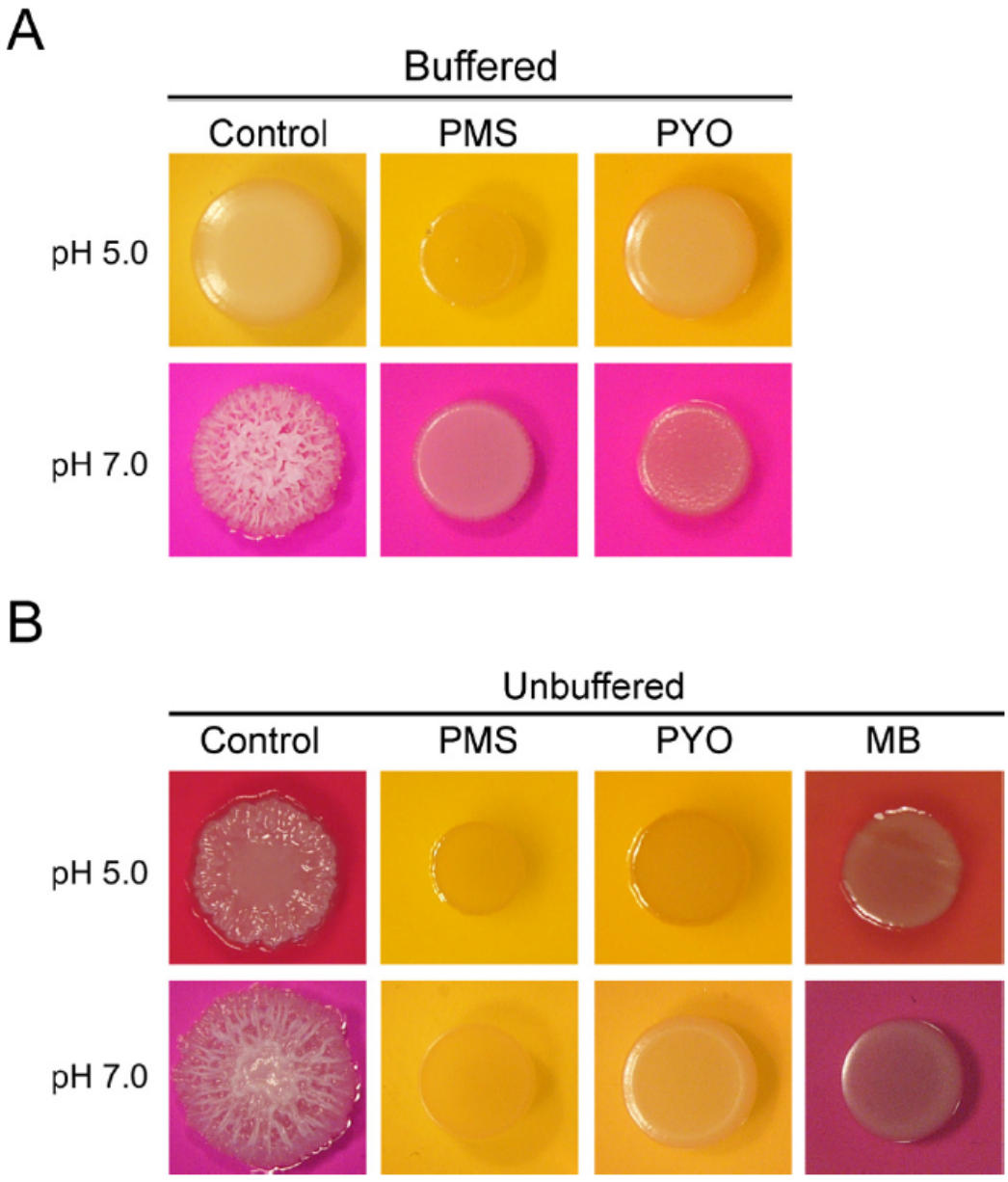

Figure C-5. Phenazine-modulated inhibition of C. albicans wrinkled colony morphology is not solely due to decreased extracellular pH. (A and B) *C. albicans* colonies grown on Glu-AA-GlcNAc with the pH adjusted to 7.0 or 5.0 prior to inoculation. A total of 5 μMof PMS, PYO, or methylene blue (MB) was added to the medium when specified, and the pH indicator bromocresol purple, which yields a red-purple color under alkaline conditions and a yellow-orange color under acidic conditions, was included. In panel A, the medium was buffered with 40 mM MOPS (pH 7) or 100 mM citrate (pH 5) as indicated. Colonies were incubated for 48h at 37°C.

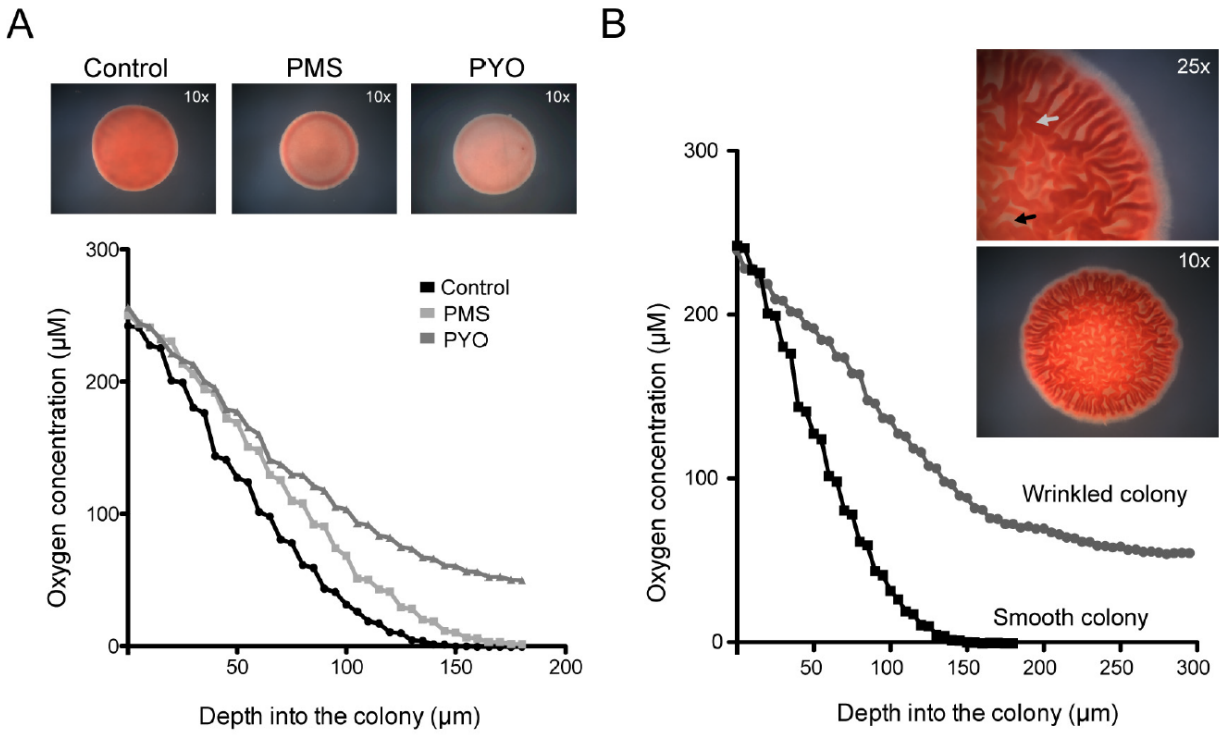

Figure C-6. Effects of phenazines on respiratory metabolism and oxygen consumption. (A) *C. albicans* colonies grown in Glu-AA medium alone or with 5 μM PMS or 20 μM PYO under non-inducing conditions. The respiratory activity of colonies was assessed using TTC, and images were captured using a stereoscope at 10X (top). Internal oxygen measurements in similarly grown colonies were made from the top to the bottom of control colonies (black), with PMS (light gray) or PYO (dark gray). (B) Oxygen gradients in colonies grown under noninducing (smooth) and inducing conditions (wrinkled) were measured at room temperature. The respiratory activity in wrinkled colonies was greater in wrinkles (gray arrow) than in valleys (black arrow) (inset).

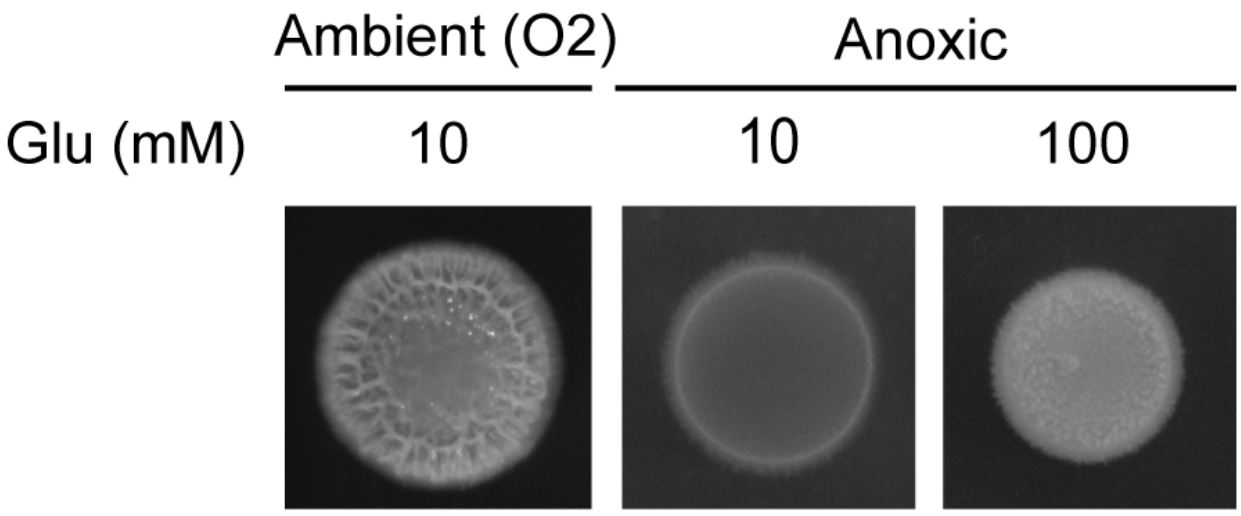

Figure C-7. *C. albicans* wrinkled colony development varies with oxygen availability and carbon source. Pictures of drop-inoculated fungal colonies grown in modified Glu-AA with 5 mM GlcNAc medium (with 20 μM oleic and 80 μM nicotinic acid) supplemented with 10 or 100 mM of Glu, incubated under anoxic conditions for 48 h at 37°C. For reference, a colony growth on YNB Glu-AA with 5 mM GlcNAc and 10 mM glucose at 48h is shown.

Table C-1. Bacterial and fungal strains used in this study

Strain	Description	DH # [a]	Source or reference
Pseudomonas aeruginosa strain			
PA14 WT	WT	123	(65)
PA14 Δ*phz*	In-frame deletion of *phzA1-G1* and *phzA2-G2* operons, phenazine negative	933	(57)
PA14 *phzM*::Tn*M*	Tn*M* mutant, 5MPCA negative	693	(66)
PA14 *phzS*::Tn*M*	Tn*M* mutant, PYO negative	698	(66)
Candida albicans strains			
SC5314	WT	35	(68)
HWP1-lacZ	CAI-4 derivative, Uri+. *HWP1* promoter fused to *lacZ* of *Streptococcus thermophilus*	119	(69)
ACT1-lacZ	CAI-4 derivative, Uri+. *HWP1* promoter fused to *lacZ* of *S. thermophilus*	146	(69)

[a] Lab collection number for reference.

REFERENCES

1. Odds FC. 1987. Candida infections: an overview. Crit. Rev. Microbiol. 15:1–5.

2. Sudbery PE. 2011. Growth of Candida albicans hyphae. Nat. Rev. Microbiol. 16:737–748.

3. Saville SP, Lazzell AL, Monteagudo C, Lopez-Ribot JL. 2003. Engineered control of cell morphology in vivo reveals distinct roles for yeast and filamentous forms of Candida albicans during infection. Eukaryot. Cell 2:1053–1060.

4. Xie Z, Thompson A, Sobue T, Kashleva H, Xu H, Vasilakos J, Dongari-Bagtzoglou A. 2012. Candida albicans biofilms do not trigger reactive oxygen species and evade neutrophil killing. J. Infect. Dis. 15:1936 –1945.

5. Nett J, Andes D. 2006. Candida albicans biofilm development, modeling a host-pathogen interaction. Curr. Opin. Microbiol. 9:340 –345.

6. Chandra J, Kuhn DM, Mukherjee PK, Hoyer LL, McCormick T, Ghannoum MA. 2001. Biofilm formation by the fungal pathogen Candida albicans: development, architecture, and drug resistance. J. Bacteriol. 183: 5385–5394.

7. Nobile CJ, Schneider HA, Nett JE, Sheppard DC, Filler SG, Andes DR, Mitchell AP. 2008. Complementary adhesin function in C. albicans biofilm formation. Curr. Biol. 18:1017–1024.

8. Kim J, Sudbery P. 2011. Candida albicans, a major human fungal pathogen. J. Microbiol. 49:171–177.

9. Whiteway M, Bachewich C. 2007. Morphogenesis in Candida albicans. Annu. Rev. Microbiol. 61:529 –553.

10. Mulhern SM, Logue ME, Butler G. 2006. Candida albicans transcription factor Ace2 regulates metabolism and is required for filamentation in hypoxic conditions. Eukaryot. Cell 5:2001–2013.

11. Kim SY, Kim J. 2010. Roles of dihydrolipoamide dehydrogenase Lpd1 in Candida albicans filamentation. Fungal Genet. Biol. 47:782–788.

12. Land GA, McDonald WC, Stjernholm RL, Friedman L. 1975. Factors affecting filamentation in Candida albicans: changes in respiratory activity of Candida albicans during filamentation. Infect. Immun. 12:119 –127.

13. McDonough JA, Bhattacherjee V, Sadlon T, Hostetter MK. 2002. Involvement of Candida albicans NADH dehydrogenase complex I in filamentation. Fungal Genet. Biol. 36:117–127.

14. Setiadi ER, Doedt T, Cottier F, Noffz C, Ernst JF. 2006. Transcriptional response of Candida albicans to hypoxia: linkage of oxygen sensing and Efg1p-regulatory networks. J. Mol. Biol. 361:399–411.

15. Vellucci VF, Gygax SE, Hostetter MK. 2007. Involvement of Candida albicans pyruvate dehydrogenase complex protein X (Pdx1) in filamentation. Fungal Genet. Biol. 44:979 –990.

16. Watanabe T, Ogasawara A, Mikami T, Matsumoto T. 2006. Hyphal formation of Candida albicans is controlled by electron transfer system. Biochem. Biophys. Res. Commun. 348:206 – 211.

17. Peleg AY, Hogan DA, Mylonakis E. 2010. Medically important bacterial-fungal interactions. Nat. Rev. Microbiol. 8:340 –349.

18. Morales DK, Hogan DA. 2010. Candida albicans interactions with bacteria in the context of human health and disease. PLoS Pathog. 6:e1000886.

19. Shirtliff ME, Peters BM, Jabra-Rizk MA. 2009. Cross-kingdom interactions: Candida albicans and bacteria. FEMS Microbiol. Lett. 299:1–8.

20. Lynch AS, Robertson GT. 2008. Bacterial and fungal biofilm infections. Annu. Rev. Med. 59:415– 428.

21. Leclair LW, Hogan DA. 2010. Mixed bacterial-fungal infections in the CF respiratory tract. Med. Mycol. 48:S125–S132.

22. Brand A, Barnes JD, Mackenzie KS, Odds FC, Gow NA. 2008. Cell wall glycans and soluble factors determine the interactions between the hyphae of Candida albicans and Pseudomonas aeruginosa. FEMS Microbiol. Lett. 287:48 –55.

23. Hogan DA, Kolter R. 2002. Pseudomonas-Candida interactions: an ecological role for virulence factors. Science 296:2229 –2232.

24. Gibson J, Sood A, Hogan DA. 2009. Pseudomonas aeruginosa-Candida albicans interactions: localization and fungal toxicity of a phenazine derivative. Appl. Environ. Microbiol. 75:504 –513.

25. Cugini C, Calfee MW, Farrow JM, III, Morales DK, Pesci EC, Hogan DA. 2007. Farnesol, a common sesquiterpene, inhibits PQS production in Pseudomonas aeruginosa. Mol. Microbiol. 65:896 –906.

26. Hogan DA, Vik A, Kolter R. 2004. A Pseudomonas aeruginosa quorum sensing molecule influences Candida albicans morphology. Mol. Microbiol. 54:1212–1223.

27. Kerr JR. 1994. Suppression of fungal growth exhibited by Pseudomonas aeruginosa. J. Clin. Microbiol. 32:525–527.

28. Cugini C, Morales DK, Hogan DA. 2010. Candida albicans-produced farnesol stimulates Pseudomonas quinolone signal production in LasR defective Pseudomonas aeruginosa strains. Microbiology 156:3096 –3107.

29. Morales DK, Jacobs N, Rajamani S, Krishnamurthy M, Cubillos-Ruiz J, Hogan D. 2010. Antifungal mechanisms by which a novel Pseudomonas aeruginosa phenazine toxin kills Candida albicans in biofilms. Mol. Microbiol. 78:1379 –1392.

30. Mavrodi DV, Parejko JA, Mavrodi OV, Kwak YS, Weller DM, Blankenfeldt W, Thomashow LS. 2012. Recent insights into the diversity, frequency and ecological roles of phenazines in

fluorescent Pseudomonas spp. Environ. Microbiol.http://dx.doi.org/10.1111/j.1462-2920.2012 . 02846.x.

31. O'Malley YQ, Abdalla MY, McCormick ML, Reszka KJ, Denning GM, Britigan BE. 2003. Subcellular localization of Pseudomonas pyocyanin cytotoxicity in human lung epithelial cells. Am. J. Physiol. Lung Cell. Mol. Physiol. 284:L420 –L430.

32. French SW, Palmer DS, Sim WA. 1973. Phenazine methosulfate uptake by rat liver mitochondria. Can. J. Biochem. 51:235–240.

33. Hunter RC, et al. 2012. Phenazine content in the cystic fibrosis respiratory tract negatively correlates with lung function and microbial complexity. Am. J. Respir. Cell Mol. Biol. 47:738 –745.

34. Kasozi DM, Gromer S, Adler H, Zocher K, Rahlfs S, Wittlin S, FritzWolf K, Schirmer RH, Becker K. 2011. The bacterial redox signaler pyocyanin as an antiplasmodial agent: comparisons with its thioanalog methylene blue. Redox Rep. 16:154 –165.

35. Schirmer RH, Adler H, Pickhardt M, Mandelkow E. 2011. Lest we forget you—methylene blue. Neurobiol. Aging 32:e7–16.

36. Kerr JR, et al. 1999. Pseudomonas aeruginosa pyocyanin and 1-hydroxyphenazine inhibit fungal growth. J. Clin. Pathol. 52:385–387.

37. Martinez JP, et al. 1990. Wall mannoproteins in cells from colonial phenotypic variants of Candida albicans. J. Gen. Microbiol. 136:2421–2432.

38. Ene IV, Bennett RJ. 2009. Hwp1 and related adhesins contribute to both mating and biofilm formation in Candida albicans. Eukaryot. Cell 8:1909 –1913.

39. Staab JF, Bradway SD, Fidel PL, Sundstrom P. 1999. Adhesive and mammalian transglutaminase substrate properties of Candida albicans Hwp1. Science 283:1535–1538.

40. El Barkani A, Kurzai O, Fonzi WA, Ramon A, Porta A, Frosch M, Muhlschlegel FA. 2000. Dominant active alleles of RIM101 (PRR2) bypass the pH restriction on filamentation of Candida albicans. Mol. Cell. Biol. 20:4635– 4647.

41. Vylkova S, Carman AJ, Danhof HA, Collette JR, Zhou H, Lorenz MC. 2011. The fungal pathogen Candida albicans autoinduces hyphal morphogenesis by raising extracellular pH. mBio 2:e00055-11.

42. Zikánová B, Kuthan M, Ricicová M, Forstová J, Palková Z. 2002. Amino acids control ammonia pulses in yeast colonies. Biochem. Biophys. Res. Commun. 294:962–967.

43. Brown AJ. 2006. Integration of metabolism with virulence in Candida albicans, p 185–203. In Brown AJ (ed), Fungal genomics. Mycota, vol XIII. Springer-Verlag, Heidelberg, Germany.

44. Davis D, Wilson RB, Mitchell AP. 2000. RIM101-dependent and independent pathways govern pH responses in Candida albicans. Mol. Cell. Biol. 20:971–978.

45. Rich PR, Mischis LA, Purton S, Wiskich JT. 2001. The sites of interaction of triphenyltetrazolium chloride with mitochondrial respiratory chains. FEMS Microbiol. Lett. 202:181–187.

46. Wolfe AJ. 2005. The acetate switch. Microbiol. Mol. Biol. Rev. 69:12–50.

47. Hassan HM, Fridovich I. 1979. Intracellular production of superoxide radical and of hydrogen peroxide by redox active compounds. Arch. Biochem. Biophys. 196:385–395.

48. Biswas SK, Chaffin WL. 2005. Anaerobic growth of Candida albicans does not support biofilm formation under similar conditions used for aerobic biofilm. Curr. Microbiol. 51:100 – 104.

49. Szawatkowski M, Hamilton-Miller J. 1978. Anaerobic growth and sensitivity of Candida albicans. Microbios Lett. 5:61– 66.

50. Bonhomme J, et al. 2011. Contribution of the glycolytic flux and hypoxia adaptation to efficient biofilm formation by Candida albicans. Mol. Microbiol.80:995–1013.

51. Römling U. 2005. Characterization of the rdar morphotype, a multicellular behaviour in Enterobacteriaceae. Cell. Mol. Life Sci. 62:1234 –1246.

52. Yildiz FH, Schoolnik GK. 1999. Vibrio cholerae O1 El Tor: identification of a gene cluster required for the rugose colony type, exopolysaccharide production, chlorine resistance, and biofilm formation. Proc. Natl. Acad. Sci. U. S. A. 96:4028–4033.

53. Friedman L, Kolter R. 2004. Two genetic loci produce distinct carbohydrate-rich structural components of the Pseudomonas aeruginosa biofilm matrix. J. Bacteriol. 186:4457– 4465.

54. Dietrich LE, Okegbe C, Price-Whelan A, Sakhtah H, Hunter RC, Newman DK. 2013. Bacterial community morphogenesis is intimately linked to the intracellular redox state. J. Bacteriol.http://dx.doi.org/10 .1128/JB.02273-12.

55. Wang Y, Kern SE, Newman DK. 2010. Endogenous phenazine antibiotics promote anaerobic survival of Pseudomonas aeruginosa via extracellular electron transfer. J. Bacteriol. 192:365–369.

56. Price-Whelan A, Dietrich LE, Newman DK. 2007. Pyocyanin alters redox homeostasis and carbon flux through central metabolic pathways in Pseudomonas aeruginosa PA14. J. Bacteriol. 189:6372– 6381.

57. Dietrich LE, Teal TK, Price-Whelan A, Newman DK. 2008. Redoxactive antibiotics control gene expression and community behavior in divergent bacteria. Science 321:1203–1206.

58. Ramos I, Dietrich LE, Price-Whelan A, Newman DK. 2010. Phenazines affect biofilm formation by Pseudomonas aeruginosa in similar ways at various scales. Res. Microbiol. 161:187–191.

59. Mukherjee PK, Mohamed S, Chandra J, Kuhn D, Liu S, Antar OS, Munyon R, Mitchell AP, Andes D, Chance MR, Rouabhia M, Ghannoum MA. 2006. Alcohol dehydrogenase restricts the

ability of the pathogen Candida albicans to form a biofilm on catheter surfaces through an ethanol-based mechanism. Infect. Immun. 74:3804 –3816.

60. Visarius TM, Stucki JW, Lauterburg BH. 1997. Stimulation of respiration by methylene blue in rat liver mitochondria. FEBS Lett. 412:157–160.

61. Hassan HM, Fridovich I. 1980. Mechanism of the antibiotic action pyocyanine. J. Bacteriol. 141:156 –163.

62. Chotirmall SH, O'Donoghue E, Bennett K, Gunaratnam C, O'Neill SJ, McElvaney NG. 2010. Sputum Candida albicans presages FEV1 decline and hospitalized exacerbations in cystic fibrosis. Chest 138:1186 –1195.

63. Bhargava V, Tomashefski JF, Jr, Stern RC, Abramowsky CR. 1989. The pathology of fungal infection and colonization in patients with cystic fibrosis. Hum. Pathol. 20:977–986.

64. Ogur M, St. John R, Nagai S. 1957. Tetrazolium overlay technique for population studies of respiration deficiency in yeast. Science 125:928 –92

65. Rahme, L. G., E. J. Stevens, S. F. Wolfort, J. Shao, R. G. Tompkins, and F. M. Ausubel. 1995. Common virulence factors for bacterial pathogenicity in plants and animals. Science 268:1899-1902.

66. Liberati, N. T., J. M. Urbach, S. Miyata, D. G. Lee, E. Drenkard, G. Wu, J. Villanueva, T. Wei, and F. M. Ausubel. 2006. An ordered, nonredundant library of Pseudomonas aeruginosa strain PA14 transposon insertion mutants. Proc. Natl. Acad. Sci. U S A 103:2833-2838.

67. Gori, K, H. D. Mortensen, N. Arneborg, L. Jespersen. 2007. Ammonia production and its possible role as a mediator of communication for Debaryomyces hansenii and other cheese-relevant yeast species. J. Dairy. Sci. 90:5032-5041.

68. Gillum, A.M., E. Y. Tsay, and D. R. Kirsch. 1984. Isolation of the Candida albicans gene for orotidine-5'-phosphate decarboxylase by complementation of S. cerevisiae ura3 and E. coli pyrF mutations. Mol. Gen. Genet. 198:179-182.

69. Uhl, M.A. and A.D. Johnson. 2001. Development of Streptococcus thermophilus lacZ as a reporter gene for Candida albicans. Microbiology 147:1189-1195.

Appendix D. Efforts to crystallize RmcA and PA0290

This appendix summarizes efforts to crystallize RmcA and PA0290 for the purposes of solving their structures. This work was done in collaboration with Drs. Farhad Forouhar, John Hunt, and Liang Tong. Victor Wong and Dr. Chi Wang also provided advice and technical assistance.

INTRODUCTION

Chapter 3 described roles for two PAS-domain-containing proteins in the modulation of c-di-GMP levels and colony morphology in PA14: the phosphodiesterase RmcA and the diguanylate cyclase PA0290. Genetic analysis and biochemical characterization suggested that RmcA is inactive or repressed, while PA0290 is induced or activated, under reducing conditions. These effects lead to increased c-di-GMP levels, which promote colony wrinkling as an adaptation to the redox imbalance. I sought to purify, crystallize, and solve the structures of these proteins to gain mechanistic insights into the links between PA14 redox sensing and modulation of c-di-GMP levels, including the identities of co-factors or ligands that bind to the RmcA and PA0290 PAS domains and how signals are propagated from sensory PAS domains to c-di-GMP output domains within these proteins. The experiments and data that follow show approaches employed and progress made in these efforts (See Fig. D-1 for overview of work flow).

MATERIALS AND METHODS

Materials. Plasmid pET28b was a generous gift from Momchil Kolev (NESG and Hunt lab, Columbia University). *Escherichia coli* C43 (DE3), which was used for protein expression, was a gift from Dr. Andreas Hartel (Shepard Lab, Columbia University). Unless otherwise stated, all enzymes were purchased from Thermo Scientific. Isopropyl-D-1-thiogalactopyranoside (IPTG) was purchased from VWR. Terrific Broth growth medium (11.8 g/L tryptone, 23.6 g/L yeast extract, 0.4% (v/v) glycerol, 9.4 g/L K_2HPO_4, 2.2 g/L KH_2PO_4) was used for all expression experiments. Lysis buffer, used to resuspend cells prior to sonication, contained 0.1% NP40 (Sigma), 500 mM NaCl, 50 mM Tris-Cl pH 7.5, 10mM imidazole, 2 tablets complete protease

inhibitor (Roche), 10% glycerol, and 10mM 2-mercaptoethanol (BME). For Ni-NTA gravity flow column purification, wash and elution buffers contained 500 mM NaCl, 50 mM Tris-Cl pH 7.5,, 10% glycerol, and 10 mM BME. Wash and elution buffers also contained 30 mM and 300 mM Imidazole, respectively, unless otherwise stated.

Cloning and purification of full-length and/or truncated RmcA and PA0290. Sequences for full-length and/or truncated versions of RmcA and PA0290 constructs were amplified from PA14 genomic DNA using primers listed in Table D-1. They were ligated into the pET28b vector using restriction sites NcoI and XhoI for PA0290 constructs and NdeI and HindIII for RmcA constructs. Table D-2 contains a list of engineered constructs.

To improve solubility of expressed proteins, I inserted an MBP (maltose-binding protein)-tag derived from a pMAL vector (New England Biolabs) downstream of the N-terminal hexahistidine (6xHis) tag in pET28b using BamHI and NdeI restriction sites, generating MBP-pET28b. A thrombin-cleavage site preceding MBP and a Factor Xa cleavage site downstream of MBP allow removal of the MBP and 6xHis-tags from the recombinant protein (Fig. D-2).

Protein expression and purification. Expression was carried out in *E. coli* C43 (DE3). Cultures were grown at 37˚C with shaking at 250 rpm in Terrific Broth medium with 35 µg/mL kanamycin to OD_{600} = 0.5. Expression was induced by the addition of 0.5 mM IPTG and cells were incubated for an additional 16-18 h at 16˚C with continued shaking at 250 rpm. Cells were harvested by spinning at 2700 g for 30 min and resuspended in 3x pellet volume of lysis buffer. Lysozyme was added at 25µg/mL to aid cell lysis. Cells were sonicated and lysate was centrifuged at 24,500 g for 60 min (RC5C, SA-600 rotor, Sorvall Instruments). Clarified lysate was applied to a gravity-flow column containing charged Ni-NTA resin and eluted with 300 mM Imidazole. Eluted protein was further purified using a Superdex 200 prep grade gel filtration column (GE Healthcare, Catalog # 151-1901) on an AKTA FPLC (GE Healthcare, Piscataway, NJ) equilibrated with 10 mM Tris, pH 7.5, 100 mM NaCl unless otherwise stated. Gel filtration

was done at 4˚C at a flow rate of 0.4mL/min. Protein purity of collected fractions was checked by SDS-PAGE.

Crystallization Screening. Pure protein fractions were pooled and concentrated using Amicon ultrafiltration cartridges (Millipore, Billerica, MA). Protein samples were concentrated to at least 8 mg/mL and stored at -80˚C after being flash-frozen in liquid nitrogen. A 460-µL aliquot was saved and flash frozen before being sent to Hauptman Woodward Medical Research Institute (Buffalo, NY) for high throughput crystal screening in 1536 conditions.

RESULTS AND DISCUSSION

The cytosolic portion of RmcA is soluble when expressed from pET28b or MBP-pET28b. All RmcA constructs described in this appendix are truncations that contain only the cytosolic portion (PAS, GGDEF and EAL domains) of the protein (see Fig. 3-1a, Chapter 3 for RmcA domain architecture) This truncation has 922 residues and is ~106kDa. RmcA was expressed according to methods listed above. Small scale solubility testing for the cytosolic portion of RmcA in both vectors (with or without the MBP fusion) was performed using 6mL cultures. For these small scale tests, preparation of lysate and protein purification was conducted as described above, except that centrifugation for collection of cells and clarified lysate was carried out at 4000 g and 16,000 g respectively. RmcA-pET28b and RmcA-MBP-pET28b were both expressed and soluble at 16˚C although RmcA-MBP-pET28b was more soluble (Fig. D-3). Nevertheless, for the *in vitro* assays discussed in Chapter 3 and crystallization studies, I proceeded with RmcA-pET28b to avoid any complications that could arise from the MBP tag.

Large scale protein expression and purification for the cytoplasmic porrtion of RmcA was carried out using two liters of culture and as described in the methods, except that 60 mM imidazole was used to obtain a cleaner elution when using the gravity flow column containing charged Ni-NTA resin. Eluted protein was immediately flash frozen in liquid nitrogen and stored at -80˚C.

Gel filtration traces showed three major peaks (Fig. D-4). Fractions 41, 51 and 67 were associated with peaks 1, 2 and 3 respectively. Given the size of RmcA (~106 kDa), we expected RmcA to elute in relatively late fractions, and SDS-PAGE analysis of the collected fractions showed that RmcA was only associated with the third peak (Fig. D-5). These fractions were concentrated to 1.2 mg/mL as described in methods using a 50kDa cutoff ultrafiltration cartridge (cat #UFC9050) before submission for crystal screening.

The construct for expression of full-length PA0290 yielded a soluble product. PA0290 is a 323-amino-acid protein with an N-terminal PAS domain followed by a GGDEF domain (Fig. 3-1a, Chapter 3). I designed 5 constructs for the expression of full-length PA0290 and various PA0290 truncations, which are listed in Table D-2. I tested the solubility of the constructs on a small scale using the method described for the RmcA constructs. Of the 5 protein products tested, only the full-length version was soluble (Fig. D-6) and this construct was used for subsequent large-scale expression and purification as described in the methods.

Gel filtration trace reveals a dominant dimeric state of PA0290. Following Ni-NTA column purification, the PA0290 elution was further purified using a gel filtration column as described in the Methods section above. In repeated purifications we observed peaks consistent with both dimeric and monomeric states for PA0290 (Fig. D-7). Interestingly, SDS-PAGE analysis of the collected fractions corresponding to these peaks both showed dominant bands at 36 kDa and 72 kDa, which match up with expected sizes of a PA0290 monomer and dimer respectively (Fig. D-8). The dimeric and monomeric fractions were concentrated as described in methods to 51 mg/mL and 42 mg/mL,respectively using a 10 kDa cutoff ultrafiltration cartridge (cat #UFC9010). Only the concentrated dimeric fractions were submitted for crystal screening.

Crystal screening yielded two hits for the cytoplasmic portion of RmcA and four hits for full-length PA0290. Protein samples were sent for crystal screening as described in the Methods section. The conditions that gave crystal hits for the cytoplasmic portion of RmcA and full-length PA0290 are shown in, and described in the legends of, Figs. D-9 and D-10,

respectively. These conditions were identified using UV and Second Harmonic Generation (SHG) imaging methods. The cytoplasmic portion of RmcA showed crystallization by UV imaging but not SHG imaging, while full-length PA0290 showed crystallization by both UV and SHG (Figs. D-9 and D-10). This difference could be attributed to the fact that the protein concentration of the cytoplasmic portion of RmcA used for the crystal screen was significantly lower than that used for full-length PA0290. As the next step, an additive screening method is being used to optimize the conditions that gave crystal hits in order to improve the size and quality of the crystals.

FIGURES

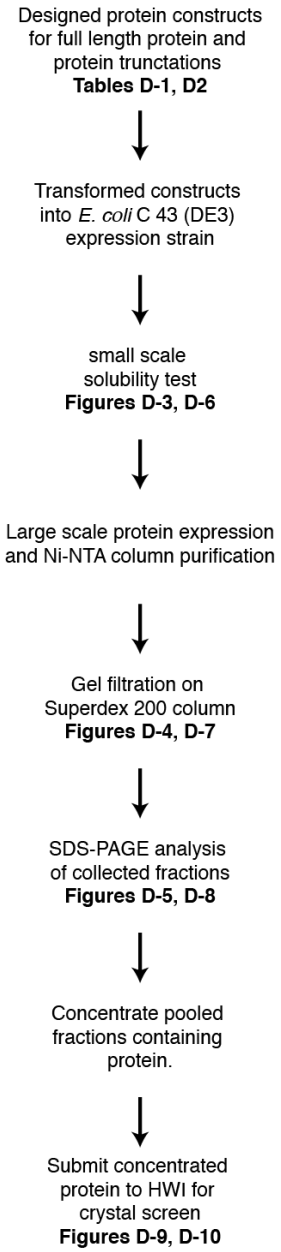

Figure D-1. Overview of work flow.

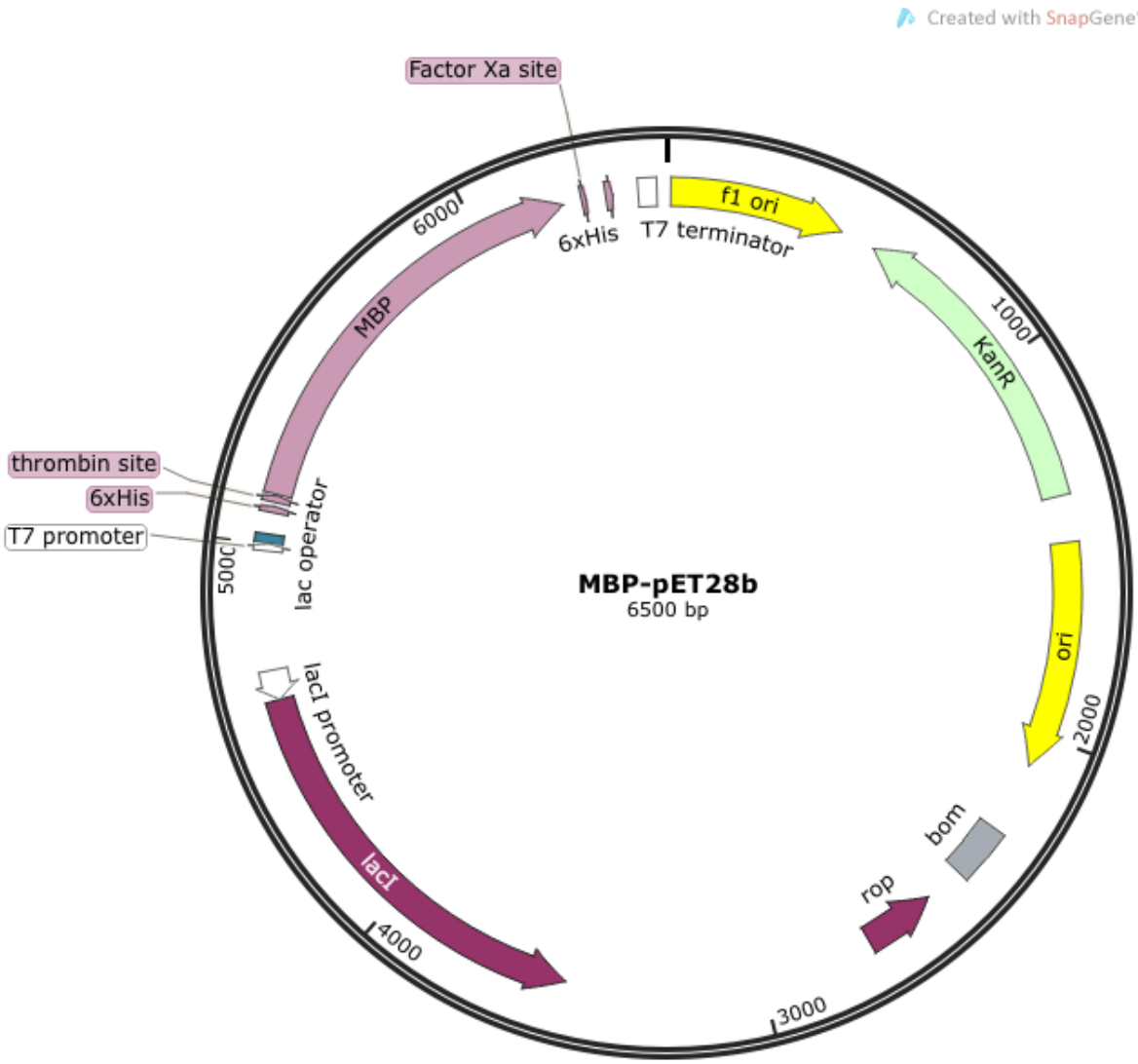

Figure D-2. Plasmid Map of MBP-pET28b. MBP from the pMAL vector (New England Biolabs) was inserted into pET28b.

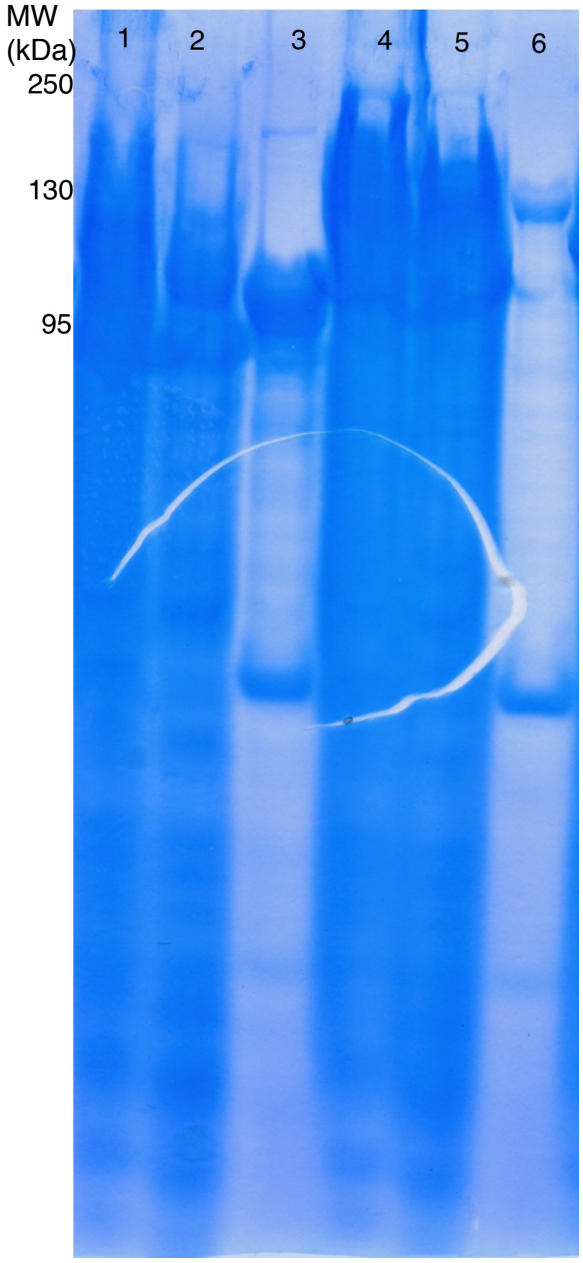

Figure D-3. Small scale solubility test for the cytoplasmic portion of RmcA. Lanes 1 and 4: total lysate; Lanes 2 and 5: supernatant (soluble) fraction; Lanes 3 and 6: pellet (insoluble) fraction for the cytoplasmic portion of RmcA expressed from pET28b (~106kDa; Lanes 1-3) and MBP-pET28b (~149kDa; Lanes 4-6).

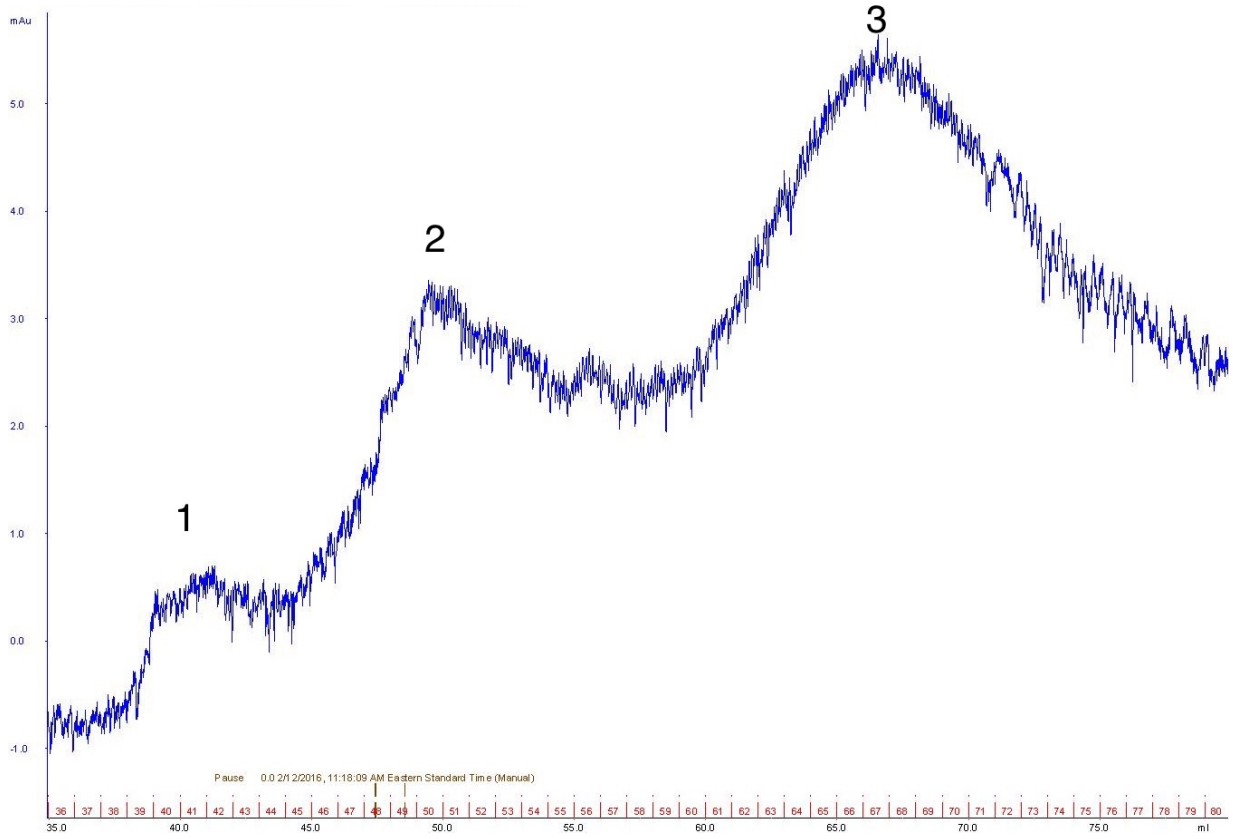

Figure D-4. Gel filtration of the cytoplasmic fraction of RmcA yields 3 peaks. Peak 1, 2 and 3 correspond to fractions 41, 51, and 67, respectively. Y-axis represents UV absorption (arbitary units) and X-axis represents fractions and elution volume (mL)

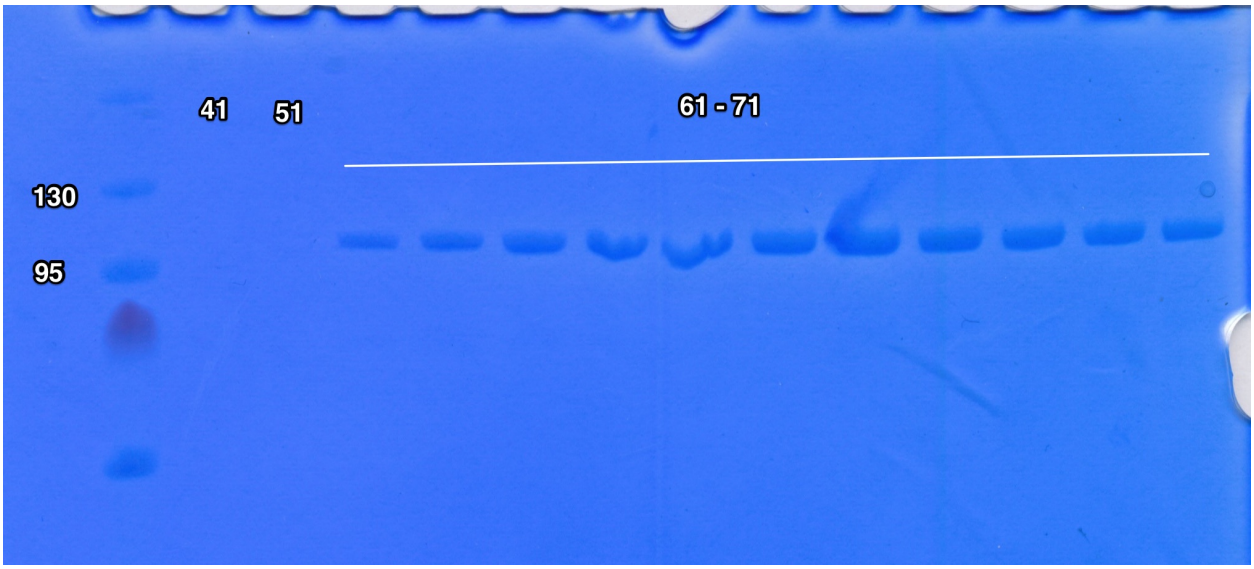

Figure D-5. Fractions 61-71 (peak 3) from gel filtration contain the cytoplasmic portion of RmcA. Fractions 41 and 51 under peaks 1 and 2 respectively did not contain the cytoplasmic portion of RmcA.

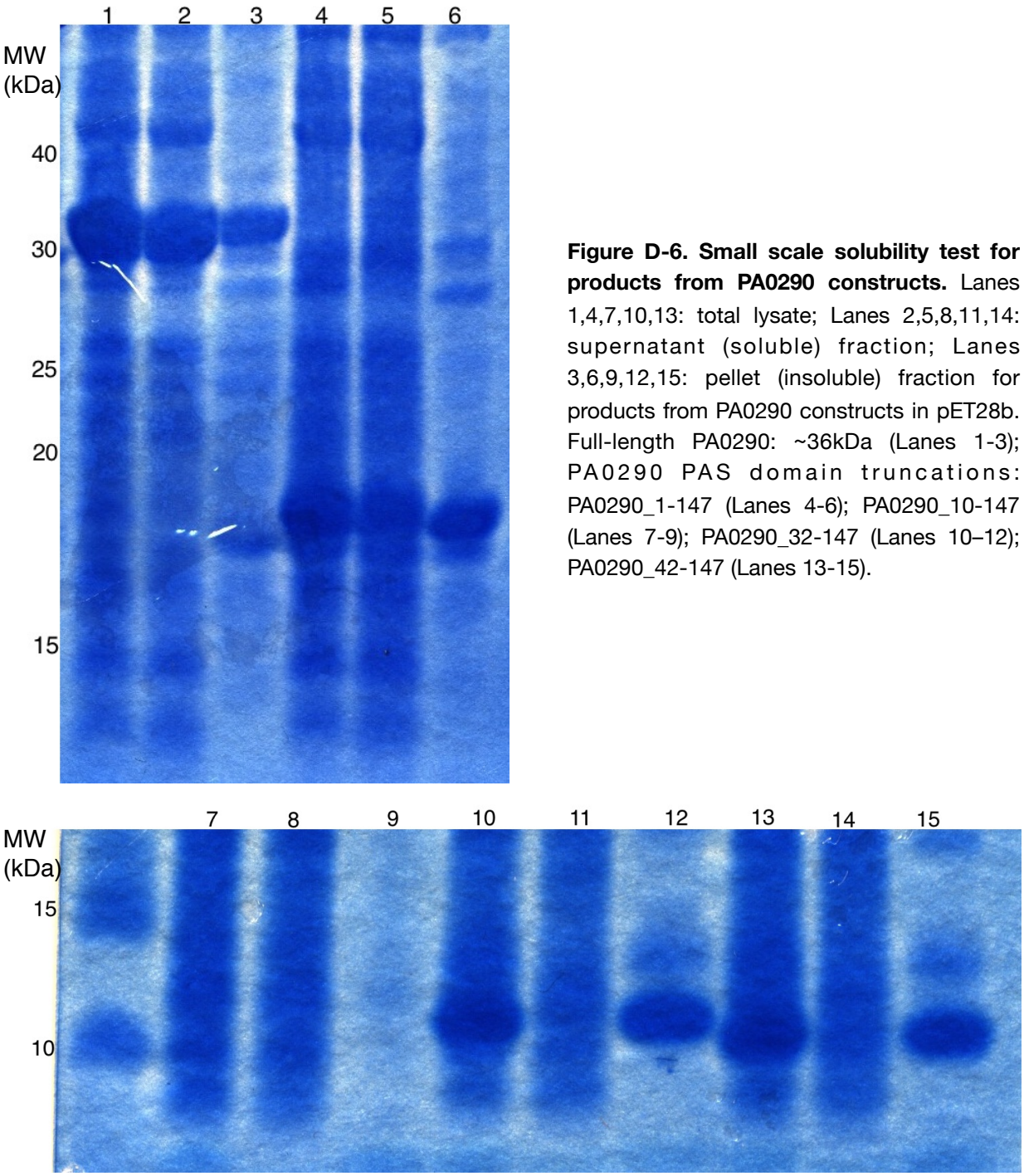

Figure D-6. Small scale solubility test for products from PA0290 constructs. Lanes 1,4,7,10,13: total lysate; Lanes 2,5,8,11,14: supernatant (soluble) fraction; Lanes 3,6,9,12,15: pellet (insoluble) fraction for products from PA0290 constructs in pET28b. Full-length PA0290: ~36kDa (Lanes 1-3); PA0290 PAS domain truncations: PA0290_1-147 (Lanes 4-6); PA0290_10-147 (Lanes 7-9); PA0290_32-147 (Lanes 10–12); PA0290_42-147 (Lanes 13-15).

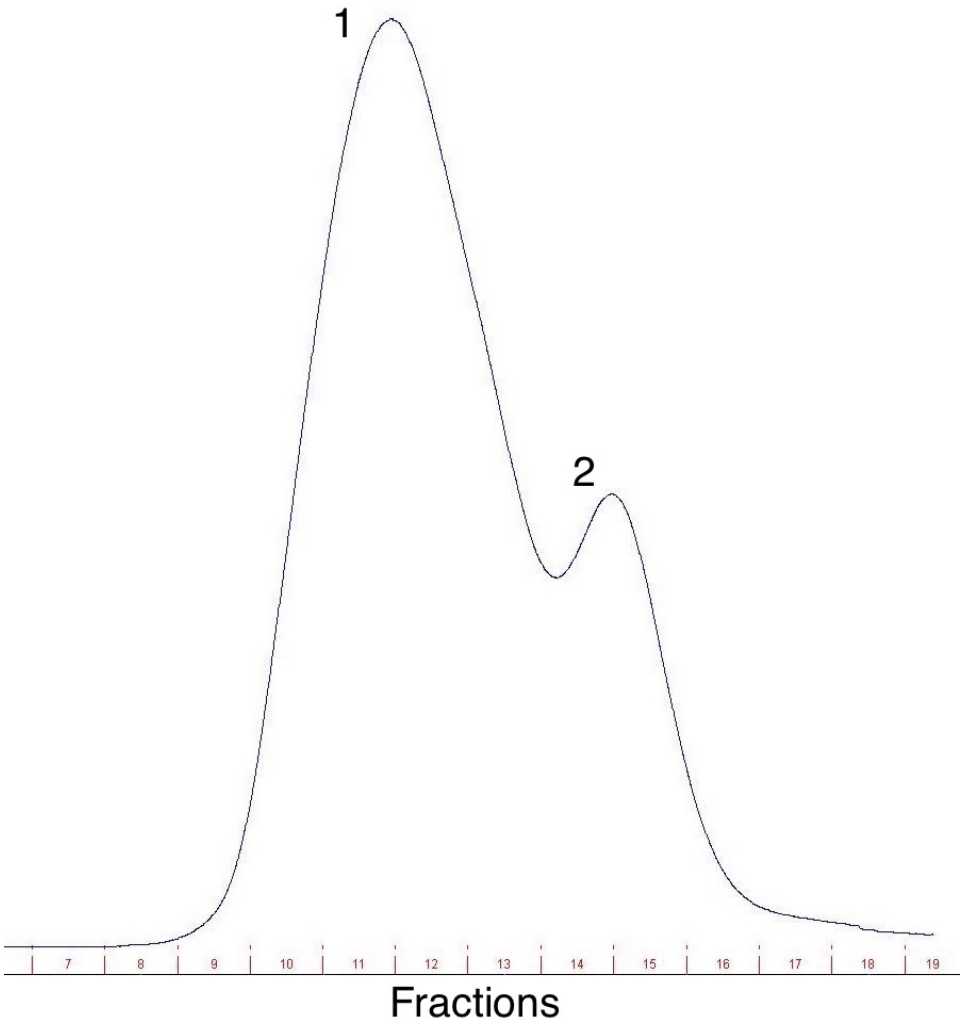

Figure D-7. Gel filtration of full-length PA0290 yields 2 peaks. X-axis represents fractions collected. Y-axis is relative UV absorption.

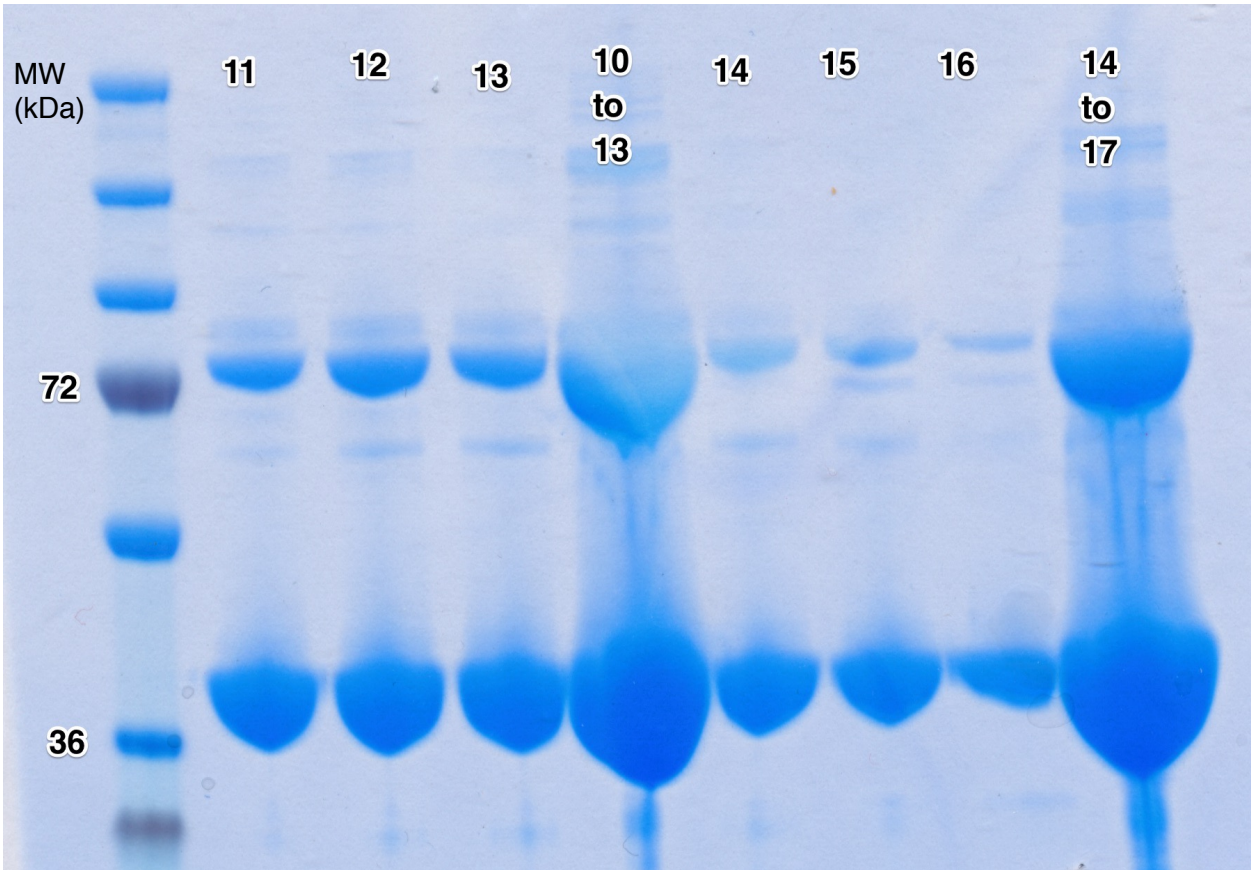

Figure D-8. Fractions from gel filtration of full-length PA0290 corresponding to peaks representing dimeric and monomeric states. Individual fractions 11-13 corresponding to the dominant dimeric peak from Figure D-7 show a ~72kDa band on SDS-PAGE. This band is also present in fractions 14-16, corresponding to the monomeric peak, but at a lower intensity. The band intensifies in pooled fractions ("10 to 13" and "14 to 17").

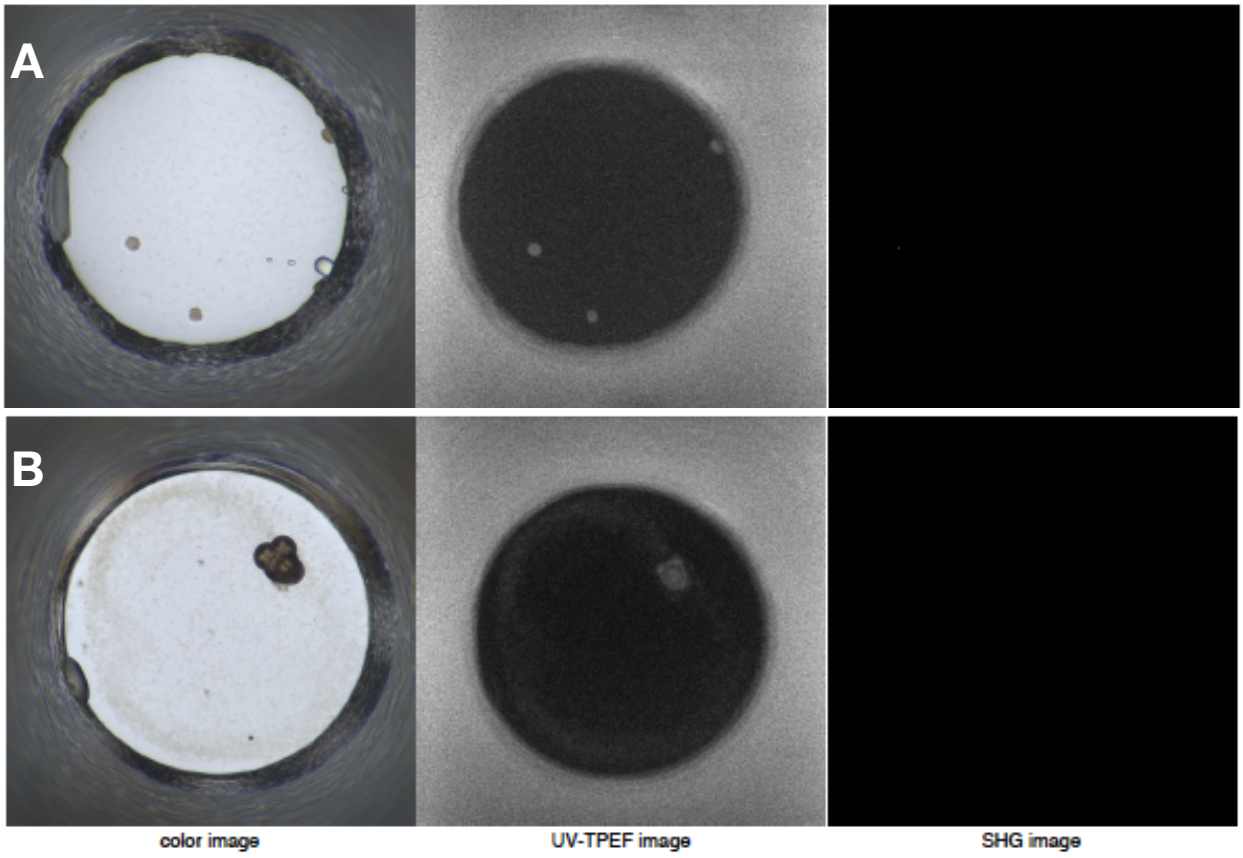

Figure D-9. Crystal screening hits for the cytoplasmic portion of RmcA. Color, UV and SHG images (left to right) for the following conditions: **(A)**"HR Index Screen HT F2": 0.2M Trimethylamine n-oxide dihydrate; 0.1M Tris pH: 8.5; 20%(w/v) PEG MME 2000. **(B)** "HR Index Screen HT H8": 0.10M magnesium formate-dihydrate; 15%(w/v) PEG 3350.

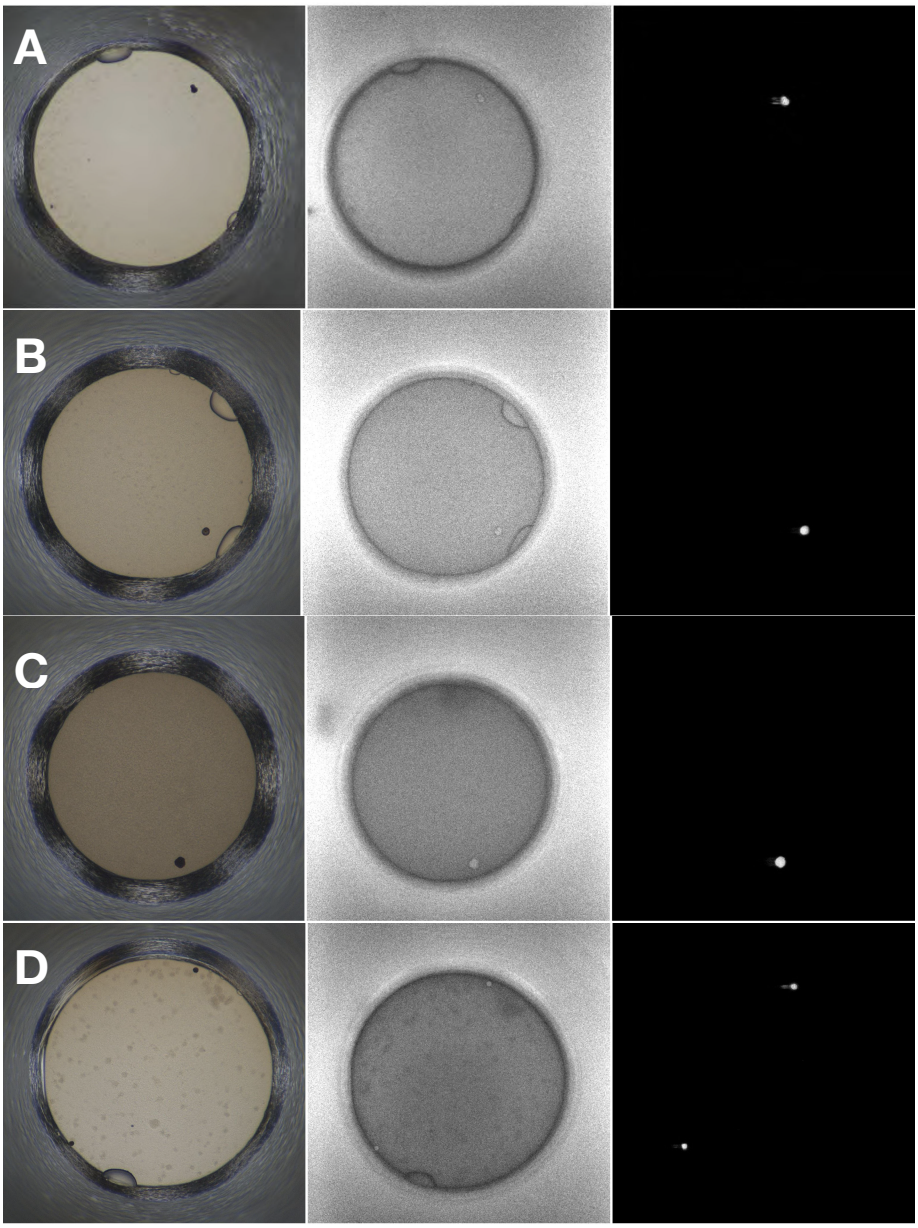

Figure D-10. Crystal screening hits for full-length PA0290. Color, UV and SHG images (left to right) for the following conditions: **(A)**"(1 :1) Silver Bullet A3 (HR2-096) + 30% PEG3350 pH 6.8"; Silver Bullet A3; 0.05M HEPES pH: 6.8; 15% (w/v) PEG 3350. **(B)**"(1 :1) Silver Bullet A11 (HR2-096) + 30% PEG3350 pH 6.8"; Silver Bullet A11; 0.05M HEPES pH: 6.8; 15% (w/v) PEG 3350. **(C)** "HR PEG/Ion HT-011"; 0.2M potassium citrate-tri basic-monohydrate pH: 8.3; 20%(w/v) PEG 3350. **(D)** "HR PEG/Ion HT-G11"; 2%(v/v) Tacsimate, pH 8.0; 0.1 M Tris pH: 8.5; 16%(w/v) PEG 3350.

Table D-1 Primers used in this study.

Primer name	primer#	Sequence (5' to 3')
0290 fwd(NcoI)	1053	ATATATccatggACGACCTACCCGGCATT
0290 rev(XhoI)	1054	ATATATctcgagGCCCACGACGATGCAGTCCTT
0290_10fwd(NcoI)	1055	ATATATccatggACCCGCAGGAGGCCGCG
0290_32fwd(NcoI)	1056	ATATATccatggAGCAACTCTTCAGCGCC
0290_42fwd(NcoI)	1057	ATATATccatggTCAACTCGGTGCTCTGG
0290_147rev(XhoI)	1058	ATATATctcgagGTCCTCGGCGATGCCCAC
MBP-pET28b fwd NdeI	1787	GGGAATTCcatATGAAAATCGAAGAAGGTAAA
MBP-pET28b rev BamHI	1788	ATATATATggatccTGAAATCCTTCCCTCGATCCC

Table D-2 Constructs used in this study.

Construct	Strain#	Description
pET28b-PA0290full	LD1902, LD1930	full-length PA0290 cloned into pET28b vector and transformed into *E. coli* Dh5α (LD1902) and *E. coli* C43 (LD1930)
pET28b-PA0290_1-147	LD1903, LD1939	PA0290 PAS domain truncation with residues 1 to 147 cloned into pET28b vector and transformed into *E. coli* Dh5α (LD1903) and *E. coli* C43 (LD1939)
pET28b-PA0290_10-147	LD1904	PA0290 PAS domain truncation with residues 10 to 147 cloned into pET28b vector and transformed into *E. coli* Dh5α (LD1904)
pET28b-PA0290_32-147	LD1905, LD1940	PA0290 PAS domain truncation with residues 32 to 147 cloned into pET28b vector and transformed into *E. coli* Dh5α (LD1905) and *E. coli* C43 (LD1940)
pET28b-PA0290_42-147	LD1906, LD1941	PA0290 PAS domain truncation with residues 42 to 147 cloned into pET28b vector and transformed into *E. coli* Dh5α (LD1906) and *E. coli* C43 (LD1941)
MBP-pET28b	LD2531	MBP inserted into pET28b protein expression vector
RmcA-pET28b	LD2532, LD2552	RmcA PAS+GGDEF+EAL domains cloned into pET28b vector and transformed into *E. coli* Dh5α (LD2532) and *E. coli* C43 (LD2552). Insert was derived from pMAL construct in LD1690 using NdeI and HindIII sites
RmcA-MBP-pET28b	LD2533, LD2553	RmcA PAS+GGDEF+EAL domains cloned into MBP-pET28b vector and and transformed into *E. coli* Dh5α (LD2533) and *E. coli* C43 (LD2553). Insert was derived from pMAL construct in LD1690 using BamHI and HindIII sites

Appendix E. Candida albicans Ethanol Stimulates Pseudomonas aeruginosa WspR-Controlled Biofilm Formation as Part of a Cyclic Relationship Involving Phenazines

This appendix is adapted from a manuscript that was published in PLOS Pathogens– Chen, Dolben, Okegbe et al 2014. Here we show that ethanol, such as that produced by C. albicans, causes increased levels of c-di-GMP in P. aeruginosa which promotes biofilm formation. This response is mediated through the WspR signaling cascade. I contributed the phenazine quantification and analyses in Figure E-9.

ABSTRACT

In chronic infections, pathogens are often in the presence of other microbial species. For example, *Pseudomonas aeruginosa* is a common and detrimental lung pathogen in individuals with cystic fibrosis (CF) and co-infections with *Candida albicans* are common. Here, we show that P. aeruginosa biofilm formation and phenazine production were strongly influenced by ethanol produced by the fungus *C. albicans*. Ethanol stimulated phenotypes that are indicative of increased levels of cyclic di-GMP (c-di-GMP), and levels of c-di-GMP were 2-fold higher in the presence of ethanol. Through a genetic screen, we found that the diguanylate cyclase WspR was required for ethanol stimulation of c-di-GMP. Multiple lines of evidence indicate that ethanol stimulates WspR signaling through its cognate sensor WspA, and promotes WspR-dependent activation of Pel exopolysaccharide production, which contributes to biofilm maturation. We also found that ethanol stimulation of WspR promoted *P. aeruginosa* colonization of CF airway epithelial cells. *P. aeruginosa* production of phenazines occurs both in the CF lung and in culture, and phenazines enhance ethanol production by *C. albicans*. Using a *C. albicans* adh1/adh1 mutant with decreased ethanol production, we found that fungal ethanol strongly altered the spectrum of *P. aeruginosa* phenazines in favor of those that are most effective against fungi. Thus, a feedback cycle comprised of ethanol and phenazines drives this polymicrobial interaction, and these relationships may provide insight into why co-infection

with both *P. aeruginosa* and *C. albicans* has been associated with worse outcomes in cystic fibrosis.

INTRODUCTION

Pseudomonas aeruginosa is an opportunistic pathogen capable of causing severe nosocomial infections and infections in immunocompromised patients. *P. aeruginosa* is a common pathogen of individuals with cystic fibrosis (CF), a genetic disease that is caused by a mutation in the gene coding for the CFTR ion transporter and strongly associated with chronic, recalcitrant lung infections. Altered CFTR function leads to a fluid imbalance that results in thick, sticky mucus in the lungs that is difficult to clear, thus creating a hospitable environment for microbial growth, biofilm formation, and persistence. While *P. aeruginosa* is a common microbe in the CF lung, it is rarely the only microbe present [1–5]. Co-infections of *P. aeruginosa* with other bacterial and fungal species are common, and there is a need to understand how these complex multi-species infections impact disease course and treatability. For example, the presence of the fungus *Candida albicans* correlates with more frequent exacerbations and a more rapid loss of lung function in CF patients [6,7]. Additional studies are needed to determine if the presence of the fungus contributes to more severe disease.

Published reports strongly suggest that in the CF lung, *P. aeruginosa* forms biofilms [8], described as hearty aggregations of cells in a sessile group lifestyle that includes extracellular matrix comprised of proteins, membrane vesicles, DNA, and exopolysaccharides. A biofilm existence provides many advantages to P. aeruginosa including increased antibiotic tolerance [9,10]. As with many Gram-negative species, *P. aeruginosa* biofilm formation is positively regulated by the secondary signaling molecule cyclic-di-GMP (c-di-GMP) [11]. C-di-GMP is formed from two molecules of GTP by diguanylate cyclases (DGCs) and its levels inversely correlate to motility. High levels of c-di-GMP promote biofilm formation in a number of ways including via increased matrix production and decreased flagellar motility [12–14].

P. aeruginosa also produces a class of redox-active virulence factors called phenazines. In CF sputum, the phenazines pyocyanin (PYO) and phenazine-1-carboxylate (PCA) are found in micromolar (5–80 mM) concentrations, and their levels are inversely correlated with lung function [15]. Phenazines play a role in the relationships between *P. aeruginosa* and eukaryotic cells. Several studies have shown how phenazines can negatively affect mammalian physiology [16,17]. In addition, phenazines impact different fungi, including *C. albicans*. At high concentrations, phenazines are toxic to *C. albicans*, and lower concentrations of phenazines reduce fungal respiration and impair growth as hyphae [18]. Phenazines figure prominently in shaping the chemical ecology within mixed-species communities. For example, when exposed to low concentrations of phenazines, *C. albicans* increases the production of fermentation products such as ethanol by 3 to 5 fold [18]. Furthermore, *P. aeruginosa-C. albicans* co-cultures form red derivatives of 5-methyl-phenazine-1-carboxylic acid (5MPCA) that accumulate within fungal cells [19].

In the present study, we show that ethanol produced by *C. albicans* stimulated *P. aeruginosa* biofilm formation and altered phenazine production. Ethanol caused a decrease in surface motility in both strains PA14 and PAO1 concomitant with a stimulation in levels of c-di-GMP, a second messenger nucleotide that promotes biofilm formation. Through a genetic screen, we found that the diguanylate cyclase WspR, a response regulator of the Wsp chemosensory system, was required for this response. Elements upstream and downstream of WspR signaling were required for the ethanol response. Ethanol no longer stimulated biofilm formation in a mutant lacking WspA, the membrane-localized sensor methyl-accepting chemotaxis protein (MCP) that is involved in the activation of WspR [20]. In addition, an intact Pel exopolysaccharide biosynthesis pathway, known to be stimulated by c-di-GMP derived from the Wsp pathway [21,22], was also required for ethanol stimulation of biofilm formation. The effects were observed on both abiotic surfaces and a cell culture model for *P. aeruginosa* and *P. aeruginosa-C. albicans* airway colonization. We found that both exogenous and fungally

produced ethanol enhanced the production of two phenazine derivatives known for their antifungal activity [19,23], 5MPCA and phenazine-1-carboxamide (PCN), through a Wsp-independent pathway and independent of ethanol catabolism. Because phenazines stimulate fungal ethanol production [18], we present evidence for a signaling cycle that helps drive this polymicrobial interaction.

RESULTS

Ethanol stimulates biofilm formation and suppresses swarming in *P. aeruginosa* strain PA14. Our previously reported findings show that *P. aeruginosa* produces higher levels of two phenazines, PYO and 5MPCA [24,25], when cultured with *C. albicans* and that phenazines stimulate *C. albicans* ethanol production [18]. Thus, we sought to determine how fungally-derived ethanol affects *P. aeruginosa*. A concentration of 1% ethanol (v/v) was chosen for these studies based on the detection of comparable levels of ethanol in *C. albicans* supernatants from cultures grown with phenazines [18]. The presence of 1% ethanol in the culture medium did not affect *P. aeruginosa* growth in minimal M63 medium with glucose or LB (doubling time of 36±2 min in LB versus 39±2 min in LB with ethanol), or on solid LB medium. When we performed a microscopic analysis of the effects of ethanol on *P. aeruginosa* strain PAO1, we observed a significant increase in attachment of cells to the bottom of a titer dish well within 1h (15±5 cells per field in vehicle treated compared to 31±6 cells per field in cultures with ethanol, $p < 0.01$) and development of microcolonies was strongly enhanced (Fig. E-1A). Ethanol also promoted an increase in the number of attached cells and microcolonies in cultures of another *P. aeruginosa* strain, PA14 (Fig. E-1B). Using two assays that assess biofilm-related phenotypes (swarming motility and twitching motility), we sought to gain additional insight into how ethanol impacted biofilm formation. Our initial studies focused on strain PA14. We found that ethanol repressed swarming motility, a behavior that is inversely correlated with biofilm formation (Fig. E-1C).

Ethanol increases c-di-GMP levels through WspR. Ethanol stimulated attachment and biofilm formation on plastic and inhibited swarming motility (Fig. E-1). These two phenotypes are positively and negatively regulated by levels of the second messenger molecule c-di-GMP [30]. Thus, we measured intracellular levels of this dinucleotide in P. aeruginosa strain PA14 cells grown on swarm plates with or without 1% ethanol for 16.5h as described previously. We found a 2.4-fold increase in c-di-GMP levels in cells exposed to ethanol (Fig. E-2).

To identify the enzyme(s) responsible for this increase, we screened a collection of 31 P. aeruginosa strain PA14 mutants [31] defective in different genes predicted to encode proteins that may modulate c-di-GMP levels based on the detection of a DGC and/or an EAL domain [22,31]. We found that one mutant, Δ*wspR*, was strikingly resistant to the repression of swarming by ethanol (Fig. E-3). As expected, this mutant also had a slight hyper swarming phenotype when compared to the wild type in control conditions [31], and both phenotypes were complemented by the wild-type wspR allele on an arabinose-inducible plasmid when grown in the presence of 0.02% arabinose (Fig. E-3). The empty vector (EV) control exhibited a swarming pattern comparable to that of the Δ*wspR* mutant.

WspR is a response regulator with a GGDEF domain [32], which is associated with diguanylate cyclase activity [20]. Consistent with the observation that Δ*wspR* continued to swarm on medium with ethanol, c-di-GMP levels were not different between cultures with and without ethanol in the Δ*wspR* background (Fig. E-2). These data suggest that WspR activity, and thus c-di-GMP levels, are enhanced by ethanol.

WspR is known to regulate the production of the Pel polysaccharide [21,22], and production of Pel is associated with colony wrinkling and biofilm formation [33]. After 72 hours on swarm plates, we also observed that ethanol strongly promoted colony wrinkling while the addition of equivalent amounts of other carbon sources, such as glycerol or choline, did not have this effect. Furthermore, the colony wrinkling induced by ethanol was less apparent in a Δ*wspR*

strain (not shown) and completely absent in a strain lacking *pelA*, an enzyme required for Pel biosynthesis (Fig. E-4). The Δ*pelA* mutant, like the Δ*wspR* mutant, continued to swarm in the presence of ethanol (Fig. E-4) suggesting that the repression of swarming in the presence of part, due to increased Pel production.

Ethanol induces c-di-GMP signaling in *P. aeruginosa* strain PAO1 through WspA and WspR. As we found that ethanol stimulated biofilm formation in *P. aeruginosa* wild-type strains PA14 and PAO1 (Fig. E-1) and that WspR mediated the ethanol effect in strain PA14, we also examined the role of WspR in the ethanol response in strain PAO1. As shown above, PAO1 wild-type cells had increased early attachment and subsequent microcolony formation on plastic when ethanol was added to the medium (Fig. E-5). Consistent with our model that ethanol is acting through WspR, ethanol did not stimulate surface colonization in the PAO1 Δ*wspR* mutant (Fig. E-5). We also examined the ethanol-responsive phenotype for *P. aeruginosa* strain PAO1 Δ*wspR*, which lacks the membrane bound receptor that is the most upstream element described in the Wsp system [20]. Like Δ*wspR*, Δ*wspA* did not show increased attachment to plastic upon the addition of ethanol (Fig. E-5) suggesting that both the MCP sensor and the WspR response regulator were required for the response to ethanol. Ethanol also promoted colony wrinkling in strain PAO1, as was observed in strain PA14, consistent with the prediction that increased WspR activity would lead to increased matrix production.

Ethanol promotes WspR clustering and a functional Wsp system is required for this effect. Previous studies have shown that the fluorescently-tagged WspR protein forms intracellular clusters when in its active phosphorylated form upon incubation of cells on an agar surface, and cluster formation is positively correlated with WspR activity [20]. To complement the mutant analyses, we determined if ethanol also promoted WspR-YFP clustering, and if known components of the WspR activation system were required for WspR stimulation by ethanol. To facilitate these analyses, we used the WspR variant $WspR_{E253A}$-YFP, which forms

larger clusters that are more easily visualized [34]. In these studies, we observed a two fold increase in WspR clustering in the presence of ethanol (Fig. E-5C). To determine if WspF, a methyl esterase that negatively regulates WspR activity [21], was involved in the regulation of WspR in response to ethanol, we also assessed WspR clustering in a Δ*wspF* background where WspR is constitutively active. In Δ*wspF*, WspR clustering was higher than in the *wspF*+ reference strain, and WspR clustering was not further stimulated by ethanol, lending support for the model that ethanol was acting through the Wsp system and not through an independent pathway for WspR activation.

***C. albicans* and ethanol promote airway epithelial cell monolayer colonization.** To understand the effects of ethanol on *P. aeruginosa* in a well-established CF-relevant disease model, we studied the effects of ethanol on *P. aeruginosa* strain PAO1 in the context of bronchial epithelial cells with the most common CF genotype (homozygous *CFTR*ΔF508) [35,36]. We cultured *P. aeruginosa* strain PAO1 with the epithelial cells in medium without and with 1% ethanol, and observed an obvious enhancement in the size of biofilm microcolonies (Fig. E-6A) and a 2.2-fold increase in colony forming units (CFUs) on the airway cells with ethanol (Fig. 6B). When the same experiment was performed with the Δ*wspR* or Δ*wspA* mutants, no stimulation by ethanol was observed. Ethanol alone did not impact epithelial cell viability as measured by an LDH release assay (9.44%±0.98 LDH release for control and 10.47%±1.2 LDH release with ethanol, N = 3) and other studies have also found these concentrations of ethanol to be well below those that cause overt toxicity to epithelial cells or disruption of epithelial barrier integrity [37,38].

When *P. aeruginosa* PAO1 and *C. albicans* were co-inoculated into epithelial cell co-cultures, 4.7-fold more *P. aeruginosa* CFUs were found to be associated with the monolayer after 6 h (Fig. E-7). To determine if C. albicans-derived ethanol contributed to the enhanced colonization by *P. aeruginosa* in the presence of *C. albicans*, we used a *C. albicans adh1*/*adh1* mutant that

produced lower levels of ethanol. We constructed the *adh1* null strain and its complemented derivative, and confirmed that the absence of *ADH1* caused a reduction in ethanol by HPLC analysis of culture supernatants, a finding consistent with previously [39]. When *P. aeruginosa* was co-cultured with the *C. albicans adh1*/*adh1* strain, there was a significant decrease in *P. aeruginosa* CFUs recovered, and this defect was corrected upon complementation with the *ADH1* gene in trans. These data strongly suggest that *C. albicans*-produced ethanol promotes *P. aeruginosa* colonization of both abiotic and biotic surfaces through activation of the Wsp system, which likely exerts these effects through promoting Pel production.

Exogenous and *C. albicans*-produced ethanol alters *P. aeruginosa* phenazine production through a WspR-independent pathway. In part, these studies were instigated by the finding that *P. aeruginosa* phenazines strongly stimulate *C. albicans* ethanol production [18]. Thus, we were intrigued by the observation that colonies on ethanol-containing swarm plates, but not control plates, contained abundant emerald green crystals, similar to those formed by reduced phenazine-1-carboxamide (PCN) [40] (Fig. E-8A, Fig. E-4 and Fig. E-9), which could indicate a reciprocal relationship between ethanol and phenazines. Phenazine concentrations were measured using HPLC in either extracts from *P. aeruginosa* strain PA14 colonies or extracts from the underlying agar. In extracts from wild type colonies, PCN and PCA concentrations were 24.2- and 5.8-fold higher, respectively, when ethanol was in the medium (Fig. E-9B); much smaller differences in PCN and PCA concentrations were found in extracts of the underlying agar (Fig. E-9C). Because PCA is the precursor for all other phenazine derivatives, including PCN (Fig. E-9A), we further explored the effect of ethanol on PCA production. For this, we measured levels of PCA in a strain lacking all of the PCA modifying enzymes (PhzH, PhzM, and PhzS; see Fig. E-9A for pathways) [41]. We found that Δ*phzHMS* colonies contained 1.7-fold more PCA (Fig. E-9D) and released 1.3-fold more PCA into the agar (Fig. E-9E) when grown in the presence of ethanol compared to control conditions. These data suggest that ethanol may cause a minor increase in PCA, and that it has greater effects on which species of phenazines

are formed. The differences in phenazine levels or profiles did not appear to be responsible for ethanol effects on swarming as the Δ*phz* mutant [42], which lacks *phzA1-G1* and *phzA2-G2*, was like the wild type in that its swarming was repressed in the presence of ethanol, but it swarmed robustly in its absence (Fig. E-9F).

To determine if there was a connection between ethanol effects on Wsp signaling and ethanol stimulation of PCN levels, we assessed PCN accumulation in mutants lacking *wspR* or *pelA*. We found that both strains responded like the wild type in terms of PCN crystal formation upon growth with ethanol (Fig. E-4).

Having observed alterations in the phenazine profile induced by ethanol, we examined the impact of ethanol in the production of a fourth phenazine derivative, 5MPCA, which we have previously shown to be released by *P. aeruginosa* when in the presence of *C. albicans* [19,24]. Because *P. aeruginosa*-produced 5MPCA is converted into a red pigment within *C. albicans* cells, 5MPCA accumulation can be followed by observing the formation of a red color where *P. aeruginosa* and *C. albicans* are cultured together [19,24]. To examine the effects of ethanol production on the accumulation of red 5MCPA derivatives, we again used the *C. albicans adh1*/*adh1* mutant and its complemented derivative. Strikingly, when *P. aeruginosa* was cultured on lawns of the *C. albicans adh1*/*adh1* strain, a strong decrease in red pigmentation was observed (Fig. E-8B). When *ADH1* was provided in trans to the *adh1*/*adh1* mutant, accumulation of the red pigment was restored (Fig. 8B).

Together, our data suggest that ethanol only slightly increases total phenazine production (Fig. E-9D and E) but more strongly affects the derivatization of phenazines in *P. aeruginosa* colonies (Fig. E-9B and C). Furthermore, *C. albicans*-produced ethanol stimulated *P. aeruginosa* 5MPCA production, and in turn, phenazines, including 5MPCA analogs, promote ethanol production [18]. Thus, it appears that *P. aeruginosa*-*C. albicans* interactions include a

positive feedback loop that promotes fungal ethanol production and *P. aeruginosa* Wsp-dependent biofilm formation when the two species are cultured together.

DISCUSSION

This paper reports new effects of ethanol on *P. aeruginosa* virulence-related traits, and illustrates that these effects occur through multiple pathways (Fig. E-10). We found that ethanol: i) promoted attachment to and colonization of plastic and airway epithelial cells, ii) decreased swarming, but not twitching motility, iii) increased Pel-dependent colony wrinkling, and iv) increased c-di-GMP levels. All of these responses to ethanol required the diguanylate cyclase WspR. WspR is part of the Wsp chemosensory system, which is a member of the "alternative cellular function" (ACF) chemotaxis family [20,21,43]. The Wsp chemosensory system is different from the chemotaxis systems in *P. aeruginosa* in terms of its localization and response to environmental signals [44]. The membrane-bound receptor WspA and the CheA homologue WspE are necessary for the Wsp system to function, and WspE activates WspR via phosphorylation [44]. Consistent with our hypothesis that the entire Wsp system is required for the response to ethanol, we found that a *wspA* mutant was also insensitive to the effects of ethanol on biofilm formation (Fig. E-5). The activation of WspR was independent of ethanol catabolism and independent of phenazine production. Ethanol and other alcohols can increase the rigidity of cell membranes by promoting an altered composition of fatty acids [45], and future studies will determine if the Wsp system, particularly the membrane localized WspA, can be activated by changes in the lipid composition or changes in the physical properties of P. aeruginosa membranes. Because the Wsp system is also activated upon contact with a surface [20], it is intriguing to consider how these stimuli might be similar.

C. albicans and other *Candida* spp. are commonly detected in the sputum of CF patients, and clinical studies suggest that the presence of both *P. aeruginosa* and *C. albicans* results in a worse prognosis for CF patients [6,46]. *In vivo* ethanol production by other fungi has been

documented [47,48], but a link between *Candida* spp. and ethanol production in the lung has not yet been made. It is important to note, however, that ethanol was one of two metabolites in exhaled breath condensate that differentiated CF from non-CF individuals [49]. Thus, regardless of the source of ethanol, be it fungal or bacterial, the effect of ethanol on pathogens such as *P. aeruginosa* is likely of biological and clinical relevance. We tested this interaction in the context of CF, but this polymicrobial interaction likely occurs in other contexts as well.

As shown above, ethanol promoted biofilm formation and likely concomitant increases in drug tolerance. In the airway epithelial cell system, *P. aeruginosa* CFU recovery was increased 3-fold by addition of ethanol (Fig. E-6B) and 4.7-fold by co-culture with *C. albicans* (Fig. E-7). A two-fold difference is comparable to the differences in colonization between wild-type *P. aeruginosa* strains and mutants lacking genes known to play a role in virulence in animal models. For example, a Δ*plcHR* mutant lacking hemolytic phospholipase C or a Δ*anr* strain defective in a global regulator have 1.3- to 2.6-fold fewer CFUs recovered from airway cells compared to wild type, and notable differences in animal models [50,51]. Hence the presence of ethanol may result in increased virulence of *P. aeruginosa* in the host. Ethanol has also been shown to promote *P. aeruginosa* conversion to a mucoid state [52], in which the exopolysaccharide alginate is overproduced; mucoidy is common in CF isolates and is correlated with a decline in lung function [53,54]. Ethanol has been shown to enhance virulence and biofilm formation by other lung pathogens such as *Staphylococcus aureus* [55] and *Acinetobacter baumanii* [56–59] via mechanisms that have not yet been described. Like in P. aeruginosa, ethanol caused a slight stimulation of growth in *A. baumanii* [58]. In addition to the effects of ethanol on *P. aeruginosa*, ethanol is an immunosuppressant that negatively influences the lung immune response [60–64]. In a mouse model, ethanol inhibits lung clearance of *P. aeruginosa* by inhibiting macrophage recruitment [65]. Together, these observations suggest that in mixed infections, *P. aeruginosa* may promote the production of ethanol by fungi, and

that fungally-produced ethanol may in turn enhance the virulence and persistence of co-existing pathogens, and thus may directly impact the host. It is not yet known how ethanol influences the spectrum of *P. aeruginosa* phenazines produced. In a previous study, we found evidence for increased production and release of 5MPCA when *P. aeruginosa* is grown in co-culture with *C. albicans*, and that live *C. albicans* is required for this effect [19]. More recent studies show that *C. albicans* ethanol production increased in the presence of even very low concentrations of the 5MPCA analog phenazine methosulfate [18], that the 5MPCA-like compounds were even more effective inhibitors of fungi than PCA and PYO, the two phenazines normally produced when *P. aeruginosa* is grown in mono-culture. Here, our findings suggest a feedback loop in which *C. albicans*-produced ethanol promoted the release of phenazines (Fig. E-7) that may promote further ethanol production [18]. It is also important to consider that some studies have reported that 5MPCA and PCN have enhanced antifungal activity when compared to PCA and PYO [19,23,24]. The ethanol-induced changes in PCA were not as dramatic when compared to the ethanol-induced changes in PCN and 5MPCA, suggesting that ethanol mainly affected the biosynthetic steps after the formation of PCA leading to its conversion to PCN, 5MPCA and PYO. In different settings, such as liquid cultures or in clinical isolates lacking activity of LasR, a transcriptional regulator for quorum sensing that controls phenazine production, the presence of *C. albicans* enhanced the production of 5MPCA and PYO [24,25]. Taken together, all these observations indicate that fungally-produced ethanol may enhance the conversion of PCA to end products such as PCN, 5MPCA and PYO. These studies indicate how microbial species can alter the behavior of one another and suggest that the nature of these dynamic interactions can change depending on the context. In the rhizosphere, where pseudomonad antagonism of fungi includes the colonization of fungal hyphae and phenazine production, the enhancement of fungally-produced ethanol by phenazines and stimulation of biofilm formation and phenazine production by ethanol may create a cycle that is relevant to biocontrol [23,66,67]. In chronic infections where these two species are found together, such as in chronic CF-associated lung disease, this molecular

interplay may be synergistic and promote long-term colonization of both species in the host. These findings indicate that the treatment of colonizing fungi may be beneficial due to their effects on other pathogens even if the fungi themselves are not acting as overt agents of host damage.

MATERIALS AND METHODS

Strains, media, and growth conditions. Bacterial and fungal strains and plasmids used in this study are listed in Table E-1. Bacteria and fungi were maintained on LB [68] and YPD (2% peptone, 1% yeast extract, and 2% glucose) media, respectively. When stated, ethanol (200-proof), choline chloride or glycerol was added to the medium (liquid or molten agar) to a final concentration of 1%. Control cultures received an equivalent volume of water. When ethanol was supplied as a sole carbon source, glucose and amino acids were omitted. Mutants from the PA14 Non-Redundant (NR) Library were grown on LB with 30 μg/mL gentamicin [29]. When strains for the NR library were used, the location of the transposon insertion was confirmed using sets of site-specific primers followed by sequencing of the amplicon. The primers are listed in Table E-2.

Growth curve analysis of *P. aeruginosa* in the presence of ethanol. For growth curves, overnight cultures were diluted into 5 ml fresh medium (LB or M63 with 0.2% glucose [69] with or without ethanol) to an OD600 nm of ~0.05 and incubated at 37˚C on a roller drum. Culture densities below 1.5 were measured directly inthe culture tubes using a Spectronic 20 spectrophotometer. At higher cell densities, diluted culture aliquots were measured using a Genesys 6 spectrophotometer.

Quantification of P. aeruginosa attachment to plastic and airway epithelial cells. To measure the attachment of cells to the plastic surface in 6-well or 12-well untreated polystyrene plates, wells were inoculated with a suspension of cells at an initial OD600 nm of 0.002 from overnight cultures. Every 90 minutes, the culture medium was removed and fresh medium was supplied. Pictures were taken using an inverted Zeiss Axiovert 200 microscope

with a long distance 63 X DIC objective at specified intervals. To quantify the number of cells or microcolonies in control cultures compared to cultures with ethanol, images were captured, randomized, and analyzed by a researcher who was blind to the identity of the sample at the time of analysis. In each experiment, more than 10 fields were counted for each strain. Microcolonies were defined as clusters of more than 5 cells in physical contact with one another. Biofilm formation on plastic microtiter dishes were performed and analyzed using the crystal violet assay as described in [55] and biofilm values were measured by quantification of dye as measured absorbance at 650 nm.

The analysis of P. aeruginosa colonization of airway epithelial cells was performed using CFBE human bronchial epithelial cells (CFBE410$^-$) with the *CFTR*ΔF508/ΔF508 genotype [70] as described previously [35,36]. For imaging, cells were grown in 6-well glass bottom dishes (MatTek). For quantification of attached cells, CFBEs were grown in 6 or 12 well plates. P. aeruginosa strain PAO1 cells were added at an MOI of 30:1, and the medium was exchanged every 1.5 hours. For experiments with *C. albicans*, PAO1 cells and *C.albicans* were added together to CFBE monolayers, where *C. albicans* was at an MOI of 10:1 with respect to the epithelial cells. Pictures were taken using a Zeiss Axiovert 200 microscope with a 63 X DIC objective at specified intervals. We performed multiple experiments with technical replicates (between three and six) on different days and analyzed the data with a one-way analysis of variance and Tukey's post hoc t-test using Graph Pad Prism 6. We observed that cells from different passages had differences in the mean attachment across all samples from that day. Thus, we normalized values to the mean across all samples from each experiment. LDH release was measured after six hours using the Promega CytoTox96 Non-Radioactive Cytotoxicity kit as described in the manufacturer's instructions.

Analysis of *P. aeruginosa* swarming and twitching motility. Swarming motility was tested by inoculating 2.5 mL of overnight cultures on fresh M8 (M8 salts without trace elements supplemented with 0.2% glucose, 0.5% casamino acids, and 1 mM MgSO4) containing 0.5%

agar as described previously [71]. Plates were incubated face up at 37˚C with 70–80% humidity in stacks of no more than 4 for 16.5 hrs. To quantify the degree of swarming, percent coverage of the plate was measured using ImageJ software [72]. Twitching motility was analyzed as described previously [26].

Cyclic-di-GMP measurements. Cells were collected from swarm plates after incubation at 37˚C for 16.5 h and placed in pre-weighed 1.5 mL Eppendorf tubes. Tubes were centrifuged at 5,000 rpm for 4 minutes. The pellets were then resuspended in 250 mL of extraction buffer by vigorous vortexing (extraction buffer: MeOH/acetonitrile/dH_2O 40:40:20+0.1 N formic acid stored at -20˚C). The extractions were incubated at -20˚C for 30 minutes in an upright position. The tubes were then centrifuged at 13,000 rpm for 5 minutes at 4˚C. 200 mL of the extraction were recovered into new Eppendorf tubes and neutralized with 4 mL of 15% NH_4HCO_3 per 100 mL of sample. The tubes with cell debris were left to dry and reweighed for normalization of cell numbers from swarm plates. 150 mL of samples were sent to the RTSF Mass Spectrometry and Metabolomics Core at Michigan State University for LC-MS analysis.

Microscopic analysis of WspR. Sample preparation and microscopy were performed as previously described [20,34]. To analyze liquid-grown cells, cultures were grown at 37˚C while shaking to an optical density at 600 nm (OD600) of 0.3 in M9 medium (16M9 salts pH 7.4, 2 mM MgSO4, 0.1 mM CaCl2, 0.2% glycerol, 0.2% casamino acids and 10 mg/ml thiamine HCl). induction of *wspR*, and 1% ethanol was added when comparing its effect on WspR clustering. From each culture, 3 ml were spotted onto a 0.8% agarose PBS pad on a microscope slide and then covered with a coverslip. More than 100 cells were counted for each condition.

P. aeruginosa-C. albicans co-cultures. Preformed lawns of *C. albicans* CAF2 and *adh1/adh1* were prepared by spreading 700 mL of a YPD-grown overnight culture onto a YPD 1.5% agar plate followed by incubation at 30˚C for 48 hr. Exponential phase *P. aeruginosa* liquid cultures were spotted (5–10 mL) onto the *C. albicans* lawns, then incubated at 30˚C for an additional 24 to 72 hours.

Analysis of phenazines. Overnight cultures of *P. aeruginosa* PA14 wild-type and Δ*phzH*Δ*phzM*Δ*phzS* strains were grown in LB at 37˚C (shaken at 250 rpm). Ten microliters of each culture were spotted onto a track-etched membrane (Whatman 110606; pore size 0.2 mm; diameter 2.5 cm) that was placed on a 1.5% agar M8 medium supplemented with either vehicle (water) or 1% v/v ethanol. Plates contained 3 ml of medium in a 35610 mm agar plate (Falcon). The colonies were incubated at 37˚C for 24 hours and then at room temperature for 72 hours, after which phenazines were extracted from the colonies and agar separately. Each track-etched membrane with a colony was lifted off the agar plates and nutated in 5 mL of 100% methanol overnight at room temperature. Similarly, the agar was nutated overnight in 5 mL of 100% methanol. Colony and agar extracts were filtered (0.2 mm pore) and phenazines in the extraction volume (5 mL) were quantified by high-performance liquid chromatography as previously described [41] at a flow rate of 0.4 mL/min.

Statistical analyses. All data were analyzed using Graph Pad Prism 6. The data represent the mean standard deviation of at least three independent experiments with multiple replicates unless stated otherwise. For normally distributed data, comparisons were tested with Student's t-test.

FIGURES

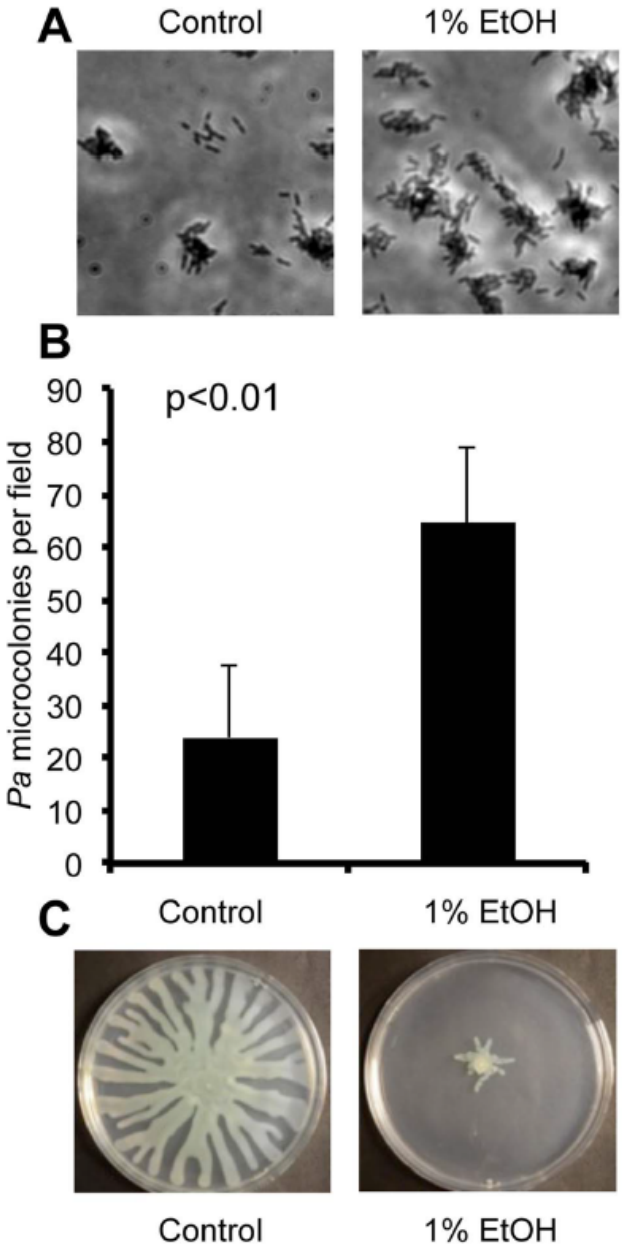

Figure E-1. Ethanol represses swarming and stimulates biofilm formation by *P. aeruginosa*. A. *P. aeruginosa* strain PAO1 attachment to the bottom of a polystyrene plastic well after 6 hours in medium with and without 1% ethanol (EtOH). **B.** *P. aeruginosa* strain PA14 attachment to plastic as assessed by quantification of microcolonies per field in wells containing medium with or without ethanol for 7 h. Error bars represent the standard deviation ($p < 0.01$ as determined by a student's t-test, N= 12). **C.** *P. aeruginosa* strain PA14 swarming in the absence and presence of 1% ethanol. Images are representative of results in more than ten independent experiments. doi:10.1371/journal.ppat.1004480.g001

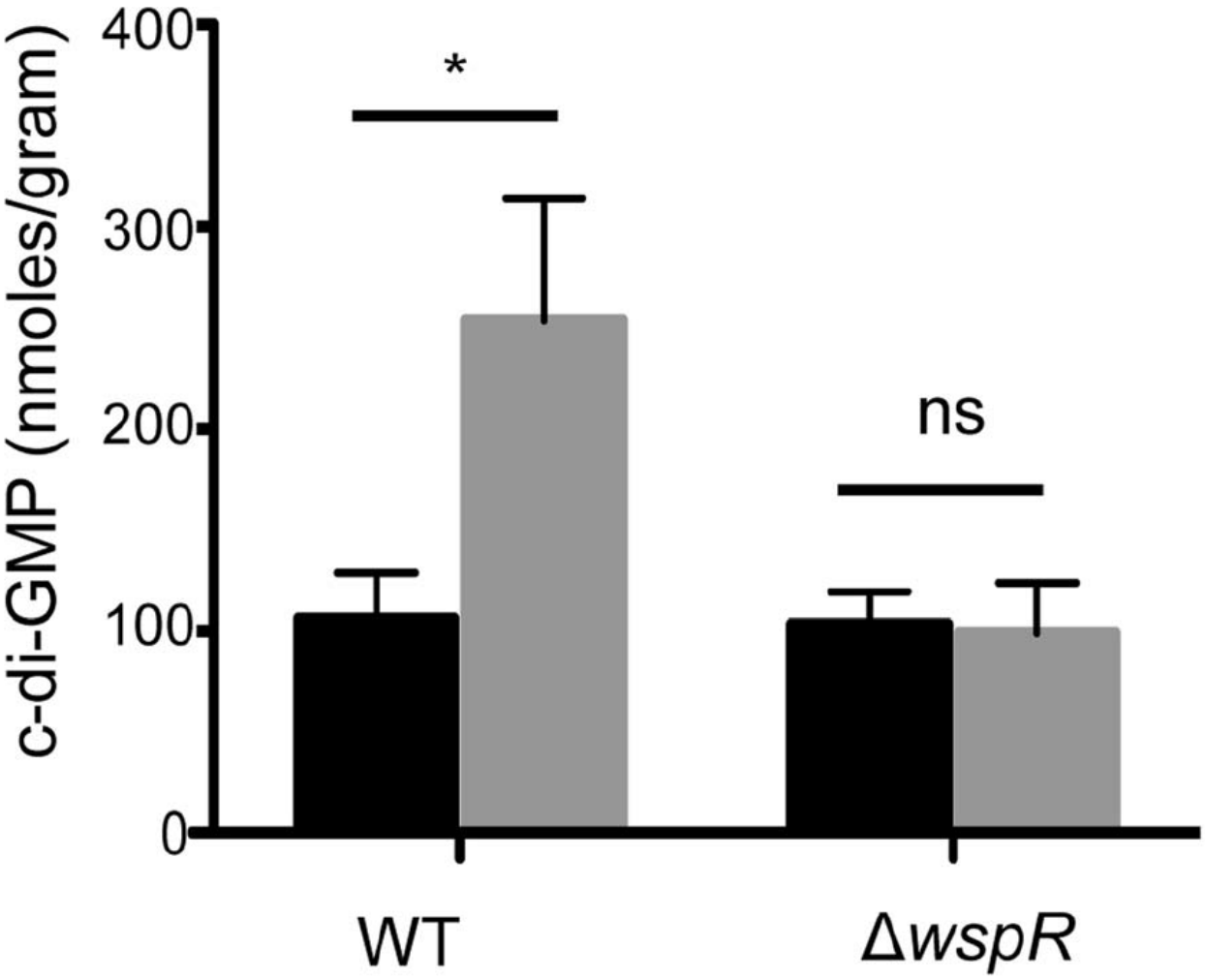

Figure E-2. Ethanol increases c-di-GMP levels in *P. aeruginosa* strain PA14 WT but not in a Δ*wspR* mutant. c-di-GMP levels from cultures grown on swarm plates without (black) or with 1% ethanol (grey) were measured by LC-MS. Error bars represent one standard deviation (*, $p < 0.05$, N= 5); ns, not significant). doi:10.1371/journal.ppat.1004480.g002

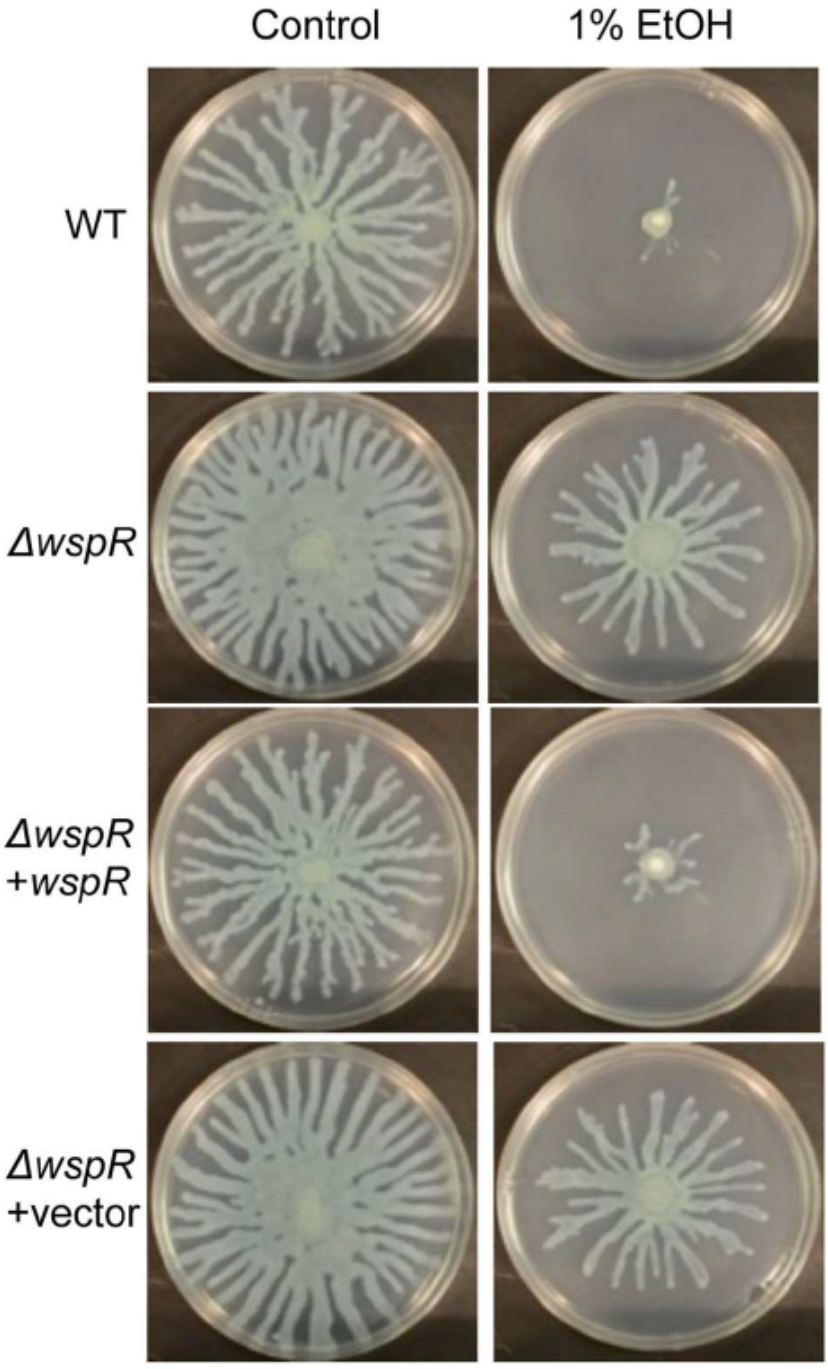

Figure E-3. *P. aeruginosa* Δ*wspR* shows loss of swarm repression in the presence of ethanol. *P. aeruginosa* strain PA14 WT, Δ*wspR*, and Δ*wspR* strains containing either plasmid-borne *wspR* or the empty vector were analyzed on swarm medium with and without 1% ethanol (EtOH) and with 0.02% arabinose (to induce *wspR* expression in the complemented strain). Images are representative of at least 5 experiments for each strain. doi:10.1371/journal.ppat.1004480.g003

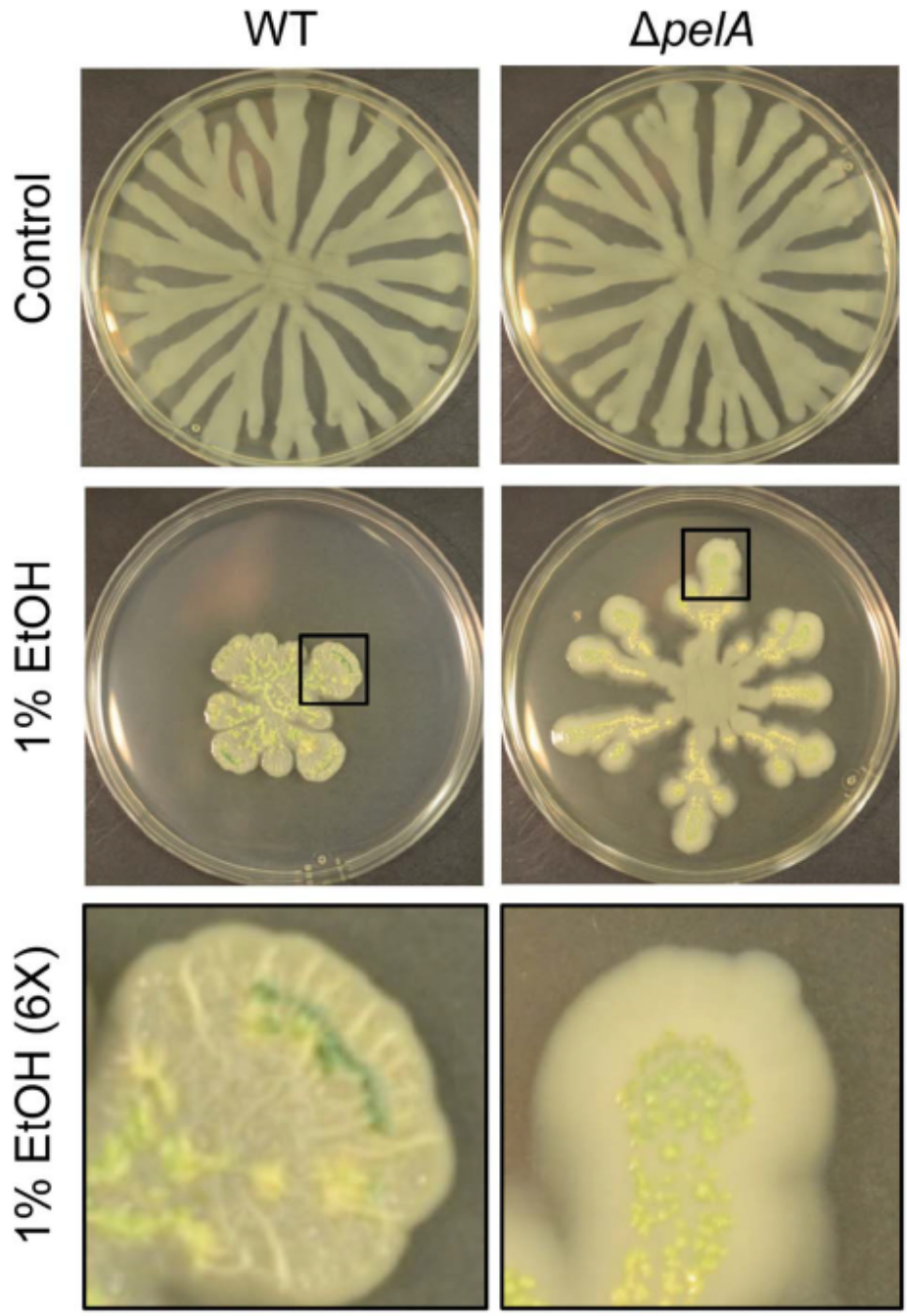

Figure E-4. Pel production in response to ethanol. *P. aeruginosa* strain PA14 WT and Δ*pelA* swarm colonies on medium with and without 1% ethanol (EtOH) after 72 h. The bottom panels show an enlarged view (6X) of swarm tendrils of the colonies grown with ethanol (indicated by a black box). Enlarged images demonstrate the yellow/green PCN crystals in both strains and colony wrinkles in the WT that form upon growth on ethanol. doi:10.1371/journal.ppat.1004480.g004

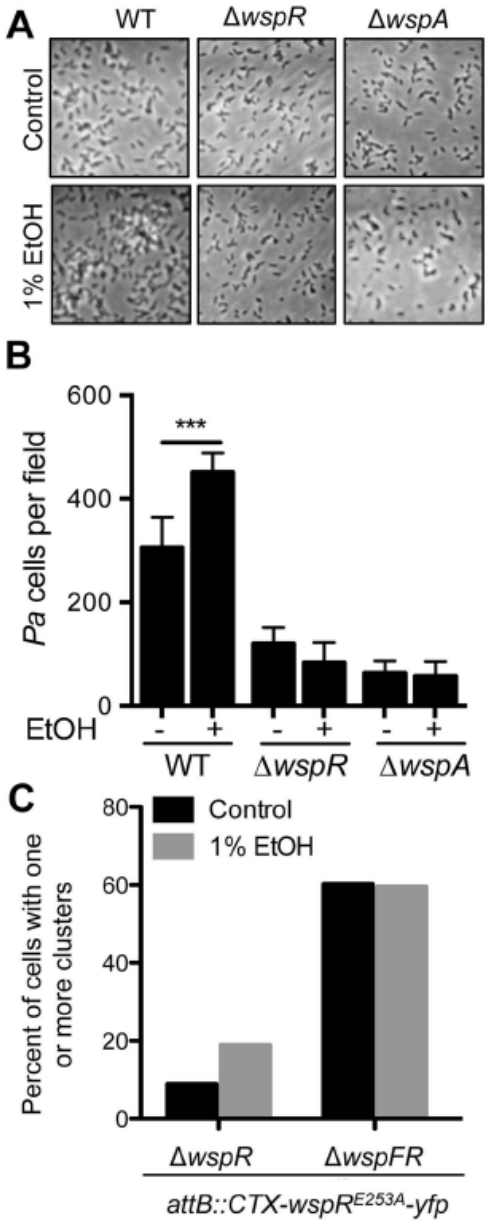

Figure E-5. Ethanol acts through the Wsp system. A. Attachment of *P. aeruginosa* strain PAO1 WT, Δ*wspR* and Δ*wspA* mutants to the bottom of a polystyrene dish during growth in M63 medium with glucose and casamino acids, and with vehicle (Control) or with 1% ethanol for 6 hours. **B.** The number of cells per field for each condition was enumerated. Images and data are representative of results from more than three separate experiments. Significance determination was based on an ordinary one-way ANOVA followed by Sidak's multiple comparisons test for each intrastrain comparison; ***, $P < 0.001$. **C.** Δ*wspR* and Δ*wspFR* strains expressing WspR-E253A-YFP were grown without and with 1% EtOH, and the number of cells with fluorescent clusters were counted out of a total of approximately 100 cells examined per condition across two experiments. doi:10.1371/journal.ppat.1004480.g005

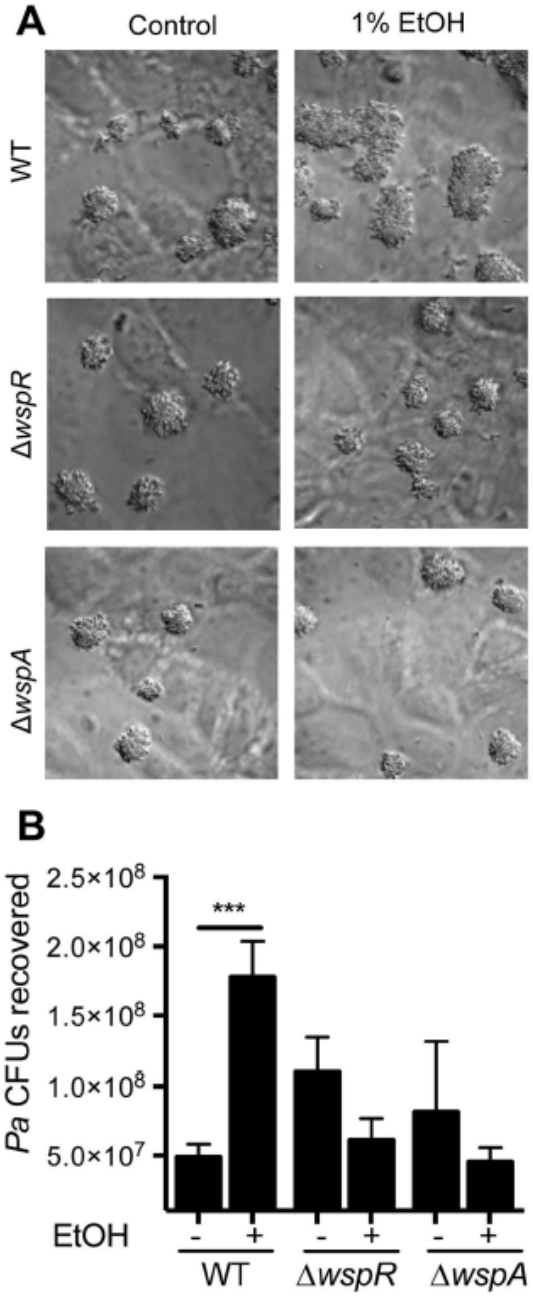

Figure E-6. Ethanol significantly increases *P. aeruginosa* strain PAO1 WT biofilm formation on airway cells. **A.** PAO1 WT, Δ*wspR* or Δ*wspA* were co-cultured with a monolayer of ΔF508 CFTR-CFBE cells at an MOI of 30:1 in medium with or without 1% ethanol and imaged after 6 h. Pictures are representative of at least 3 separate experiments with similar results. **B.** The number of CFUs from cultures determined as described above. Significance determination was based on an ordinary one-way ANOVA followed by Sidak's multiple comparisons test for each intrastrain comparison; ***, $P < 0.001$. Error bars represent one standard deviation. doi:10.1371/journal.ppat.1004480.g006

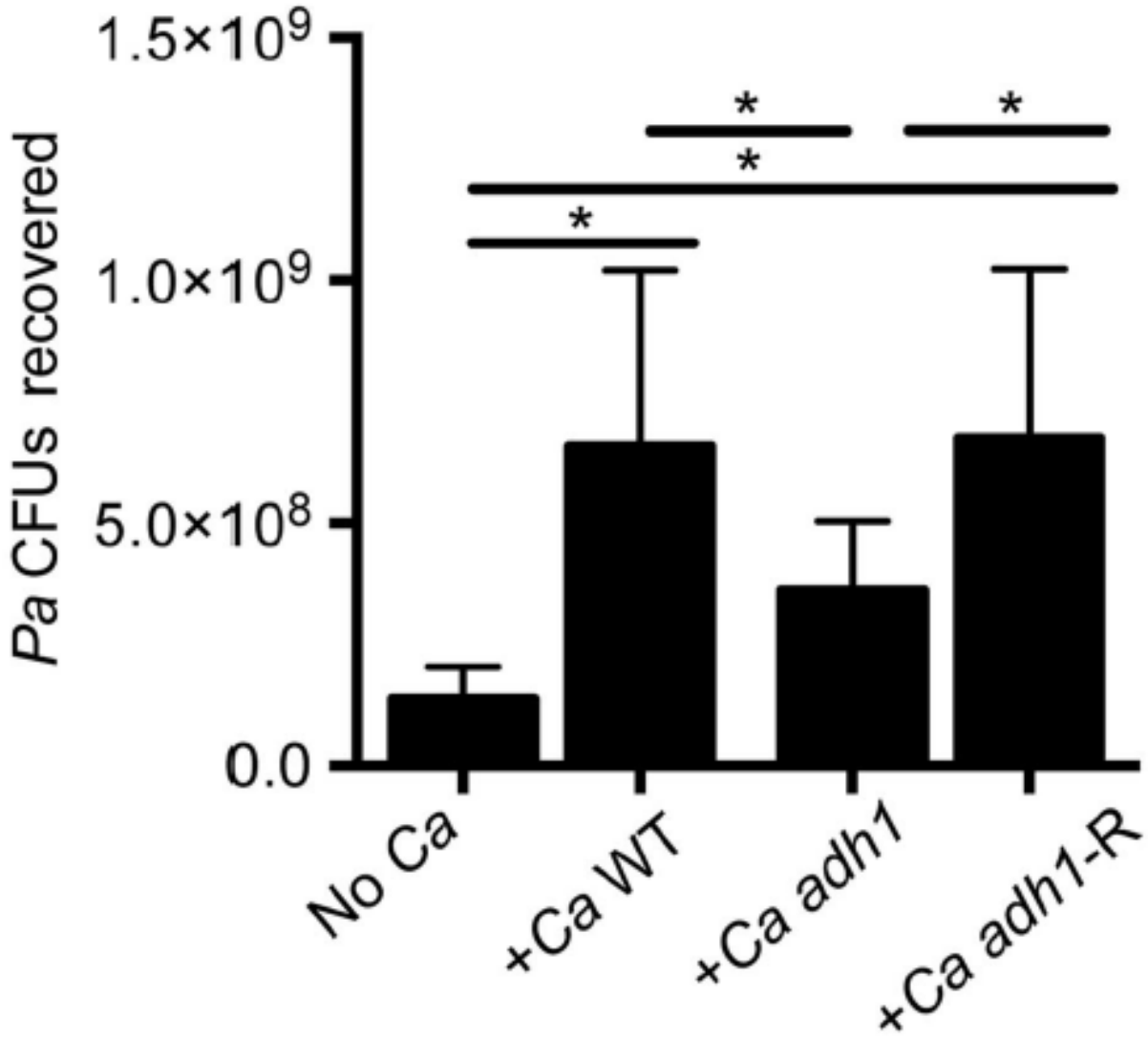

Figure E-7. *C. albicans* promotes *P. aeruginosa* strain PAO1 WT biofilm formation on airway epithelial cells in part through ethanol production. *P. aeruginosa* PAO1 WT was cultured with a monolayer of ΔF508 CFTR-CFBE cells alone or with *C. albicans* CAF2 (reference strain), the *C. albicans adh1/adh1* mutant (*adh1*), and its complemented derivative, *adh1/adh1+ADH1* (*adh1-R*). Data are combined from three independent experiments with 3–5 technical replicates per experiment, (* represents a statistically significant difference ($p < 0.05$) between indicated strains). Error bars represent one standard deviation. doi:10.1371/journal.ppat.1004480.g007

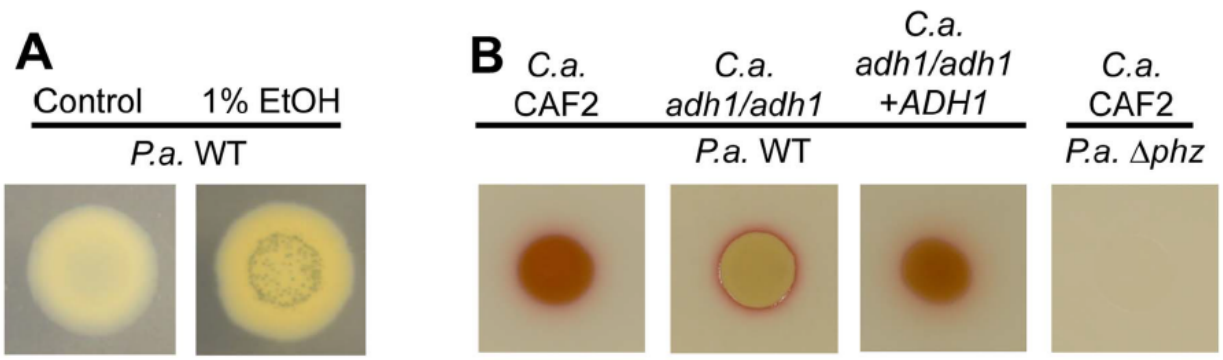

Figure E-8. Ethanol leads to higher levels of PCN crystal formation and 5MPCA derivatives. A. *P. aeruginosa* strain PA14 wild type (WT) was grown on medium without and with 1% ethanol. With ethanol, PCN crystals form and the colony has a yellowish color likely attributed to reduced PCN. **B.** *P. aeruginosa* strain PA14 WT was cultured on lawns of *C. albicans* CAF2 (WT reference strain), the *C. albicans adh1/adh1* mutant, and its complemented derivative (*adh1/adh1+ADH1*); the PA14 Δ*phz* mutant defective in phenazine production was plated on the *C. albicans* CAF2 for comparison. doi: 10.1371/journal.ppat.1004480.g008

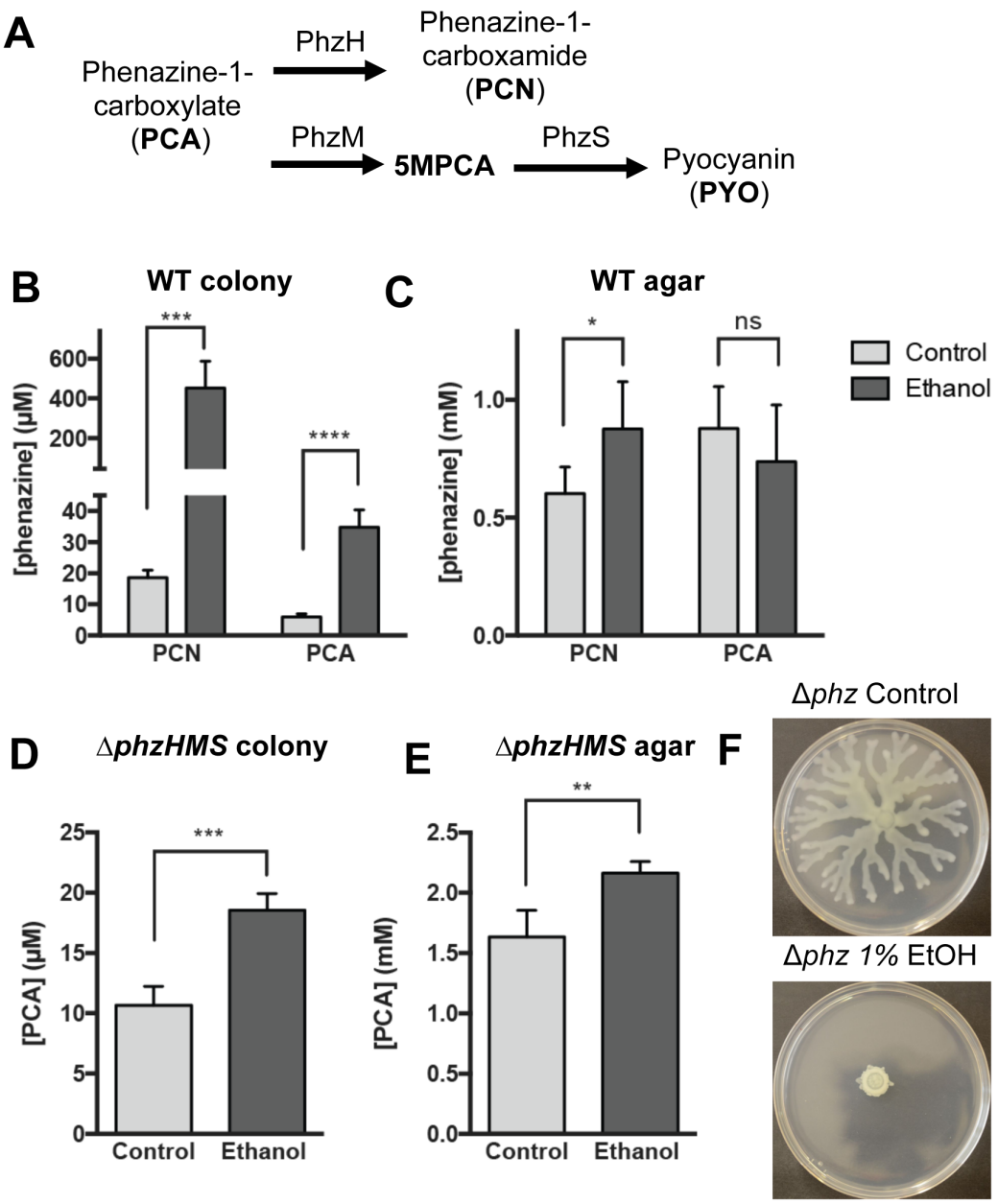

Figure E-9. Ethanol stimulates PCN production but not PCA production in *P. aeruginosa* strain PA14. A. Phenazine biosynthetic pathway and enzymes necessary for phenazine modifications. **B–E**. Concentrations of PCN and PCA in 5 ml extracts from the colony (**B**) or the underlying agar (**C**). In **B** and **C**, the wild type (WT) was grown without and with 1% ethanol. In **D** and **E**, PA14 Δ*phzHMS*, which lacks the ability to transform PCA into phenazine derivatives, was used. The error bars represent standard deviations for the phenazines extracted from 6 samples; *, $P > 0.05$; **, $P \leq 0.05$; ***, $P \leq 0.01$, ****, $P \leq 0.001$; ns, $P > 0.05$. **F**. Swarm phenotype of the Δ*phz* mutant without and with 1% ethanol. doi: 10.1371/journal.ppat.1004480.s007

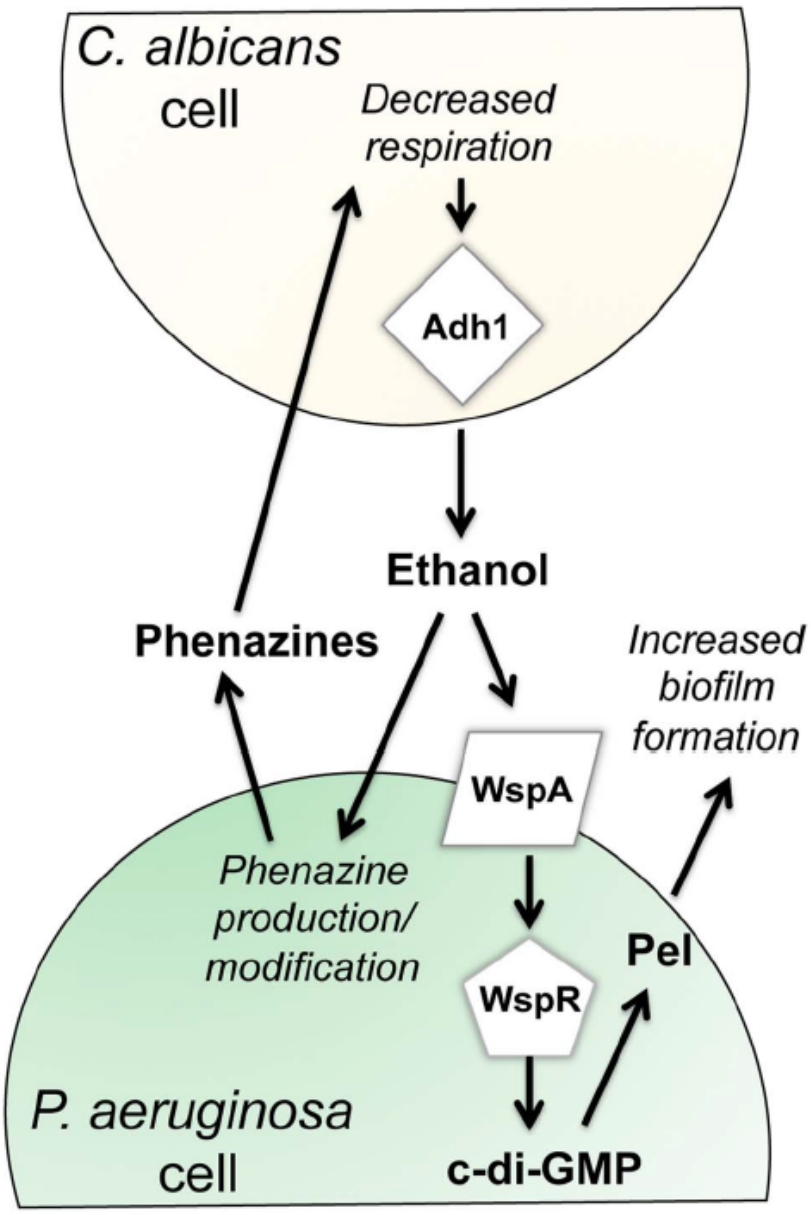

Figure E-10. Our proposed model for the impacts of fungally-produced ethanol on *P. aeruginosa* behaviors. Our previous work has shown that *P. aeruginosa* phenazines increase fungal ethanol production. Here, we show that ethanol stimulates the Wsp system, leading to a WspR-dependent increase in c-di-GMP levels and a concomitant increase in Pel production and biofilm formation on plastic and on airway epithelial cells. In addition, ethanol altered phenazine production by promoting 5MPCA release and the accumulation of PCN. doi:10.1371/journal.ppat.1004480.g009

Table E-1. Strain and plasmid list

Strains	Lab #	**Description**
P. aeruginosa		
PA14 wild type	DH123	Wild-type
PA14 *flgK*::Tn*5*	DH2	Deficient in swarming and swimming
PA14 Δ*pilA* SMC3782	DH2142	Deficient in twitching
PA14 Δ*phz*	DH933	In-frame deletions of *phzA1-phzG1* and *phzA2-phzG2*
PA14 Δ*phzHMS*		PA14 with deletions of the *phzM, phzH and phzS* genes
PA14 Δ*pelA*	DH97	In-frame deletion mutant of *pelA*
PA14 *exaA*::Tn*M*	DH2130	Tn*M* mutant, lacks ethanol dehydrogenase
PA14 *pqqB*::Tn*M*	DH2131	Tn*M* mutant, $PqqB^-$
PA14 *acsA*::Tn*M*	DH2132	Tn*M*, lacks acetaldehyde dehydrogenase
PA14 Δ*wspR*	DH2125	In-frame deletion mutant of *wspR*
PA14 Δ*wspR*+*wspR*	DH2144	DH2125 with arabinose-inducible *wspR* on plasmid pDPM73
PA14 Δ*wspR*+EV	DH2143	DH2125 containing the empty vector pDPM73
PAO1 wild type	DH1856	From lab of S. Dove
PAO1 *flgK*::Tn*5*	DH2136	From O'Toole Lab
PAO1 Δ*wspR*	PAO1103/ DH2117	In-frame deletion mutant
PAO1 Δ*wspA*	PAO1101/ DH2118	In-frame deletion mutant
PAO1 Δ*wspR* *attB::miniCTX-*$wspR^{E253A}$*-yfp*		In-frame deletion of *wspR* with $wspR^{E235A}$*-yfp*
PAO1 Δ*wspFR* *attB::miniCTX-*$wspR^{E253A}$*-yfp*		In-frame deletion of *wspF* and *wspR* with $wspR^{E235A}$*-yfp*
C. albicans		
C. albicans CAF2	DH331	Reference strain *URA3/ura3*
C. albicans adh1/adh1	DH2176	*adh1/adh1 URA3/ura3*
C. albicans adh1/adh1+ADH1	DH2177	*adh1/adh1 +ADH1*

Table E-2. Primers used in this study

Primer	Primer no.	Description
R2Tn*M*	P1043	5' TGTCAACTGGGTTCGTGCCTTCATCCG 3'
exaA Tn conf_FWD	558	5' ACA ACG TGT TCA AGC TGA C 3'
exaA Tn conf_REV	559	5' ACA CCT TGT CGC CAT AGA 3'
pqqB Tn conf_FWD	560	5' GGT TTC GAA GTG ACC CTC TAC 3'
pqqB Tn conf_REV	561	5' CAG GGC GAT GGA GGA TTG 3'
acsA Tn conf_FWD	562	5' CGA CCA CCA GGA AAT CAC 3'
acsA Tn conf_REV	563	5' GAT CAC CAC CTT CGA CTT G 3'

REFERENCES

1. Filkins LM, Hampton TH, Gifford AH, Gross MJ, Hogan DA, et al. (2012) Prevalence of streptococci and increased polymicrobial diversity associated with cystic fibrosis patient stability. J Bacteriol 194: 4709–4717.

2. Zhao J, Schloss PD, Kalikin LM, Carmody LA, Foster BK, et al. (2012) Decade long bacterial community dynamics in cystic fibrosis airways. Proc Natl Acad Sci U S A 109: 5809–5814.

3. Fodor AA, Klem ER, Gilpin DF, Elborn JS, Boucher RC, et al. (2012) The adult cystic fibrosis airway microbiota is stable over time and infection type, and highly resilient to antibiotic treatment of exacerbations. PLoS One 7: e45001.

4. Delhaes L, Monchy S, Frealle E, Hubans C, Salleron J, et al. (2012) The airway microbiota in cystic fibrosis: a complex fungal and bacterial community implications for therapeutic management. PLoS One 7: e36313.

5. Leclair LW, Hogan DA (2010) Mixed bacterial-fungal infections in the CF respiratory tract. Med Mycol 48: S125–S132.

6. Chotirmall SH, O'Donoghue E, Bennett K, Gunaratnam C, O'Neill SJ, et al. (2010) Sputum Candida albicans presages FEV1 decline and hospitalized exacerbations in cystic fibrosis. Chest 138: 1186–1195.

7. Navarro J, Rainisio M, Harms HK, Hodson ME, Koch C, et al. (2001) Factors associated with poor pulmonary function: cross-sectional analysis of data from the ERCF. European Epidemiologic Registry of Cystic Fibrosis. Eur Respir J 18: 298–305.

8. Parsek MR, Singh PK (2003) Bacterial biofilms: an emerging link to disease pathogenesis. Annu Rev Microbiol 57: 677–701.

9. Davey ME, O'Toole G A (2000) Microbial biofilms: from ecology to molecular genetics. Microbiol Mol Biol Rev 64: 847–867.Mah TF, O'Toole GA (2001) Mechanisms of biofilm resistance to antimicrobial agents. Trends Microbiol 9: 34–39.

11. Romling U, Galperin MY, Gomelsky M (2013) Cyclic di-GMP: the first 25 years of a universal bacterial second messenger. Microbiol Mol Biol Rev 77: 1–52.

12. Baraquet C, Harwood CS (2013) Cyclic diguanosine monophosphate represses bacterial flagella synthesis by interacting with the Walker A motif of the enhancer-binding protein FleQ. Proc Natl Acad Sci U S A 110: 18478–18483.

13. Irie Y, Borlee BR, O'Connor JR, Hill PJ, Harwood CS, et al. (2012) Selfproduced exopolysaccharide is a signal that stimulates biofilm formation in Pseudomonas aeruginosa. Proc Natl Acad Sci U S A 109: 20632–20636.

14. Kuchma SL, Griffin EF, O'Toole GA (2012) Minor pilins of the type IV plus system participate in the negative regulation of swarming motility. J Bacteriol 194: 5388–5403.

15. Hunter RC, Klepac-Ceraj V, Lorenzi MM, Grotzinger H, Martin TR, et al. (2012) Phenazine content in the cystic fibrosis respiratory tract negatively correlates with lung function and microbial complexity. Am J Respir Cell Mol Biol 47: 738–745.

16. Rada B, Leto TL (2013) Pyocyanin effects on respiratory epithelium: relevance in Pseudomonas aeruginosa airway infections. Trends Microbiol 21: 73–81.

17. Denning GM, Iyer SS, Reszka KJ, O'Malley Y, Rasmussen GT, et al. (2003) Phenazine-1-carboxylic acid, a secondary metabolite of Pseudomonas aeruginosa, alters expression of immunomodulatory proteins by human airway epithelial cells. Am J Physiol Lung Cell Mol Physiol 285: L584–592.

18. Morales DK, Grahl N, Okegbe C, Dietrich LE, Jacobs NJ, et al. (2013) Control of Candida albicans metabolism and biofilm formation by Pseudomonas aeruginosa phenazines. MBio 4: e00526-00512.

19. Morales DK, Jacobs NJ, Rajamani S, Krishnamurthy M, Cubillos-Ruiz JR, et al. (2010) Antifungal mechanisms by which a novel Pseudomonas aeruginosa phenazine toxin kills Candida albicans in biofilms. Mol Microbiol 78: 1379–1392.

20. Guvener ZT, Harwood CS (2007) Subcellular location characteristics of the Pseudomonas aeruginosa GGDEF protein, WspR, indicate that it produces cyclic-di-GMP in response to growth on surfaces. Mol Microbiol 66: 1459–1473.

21. Hickman JW, Tifrea DF, Harwood CS (2005) A chemosensory system that regulates biofilm formation through modulation of cyclic diguanylate levels. Proc Natl Acad Sci U S A 102: 14422–14427.

22. Kulasakara H, Lee V, Brencic A, Liberati N, Urbach J, et al. (2006) Analysis of Pseudomonas aeruginosa diguanylate cyclases and phosphodiesterases reveals a role for bis-(3**9**-5**9**)-cyclic-GMP in virulence. Proc Natl Acad Sci U S A 103: 2839–2844.

23. Chin AWTF, Thomas-Oates JE, Lugtenberg BJ, Bloemberg GV (2001) Introduction of the phzH gene of Pseudomonas chlororaphis PCL1391 extends the range of biocontrol ability of phenazine-1-carboxylic acid-producing Pseudomonas spp. strains. Mol Plant Microbe Interact 14: 1006–1015.

24. Gibson J, Sood A, Hogan DA (2009) Pseudomonas aeruginosa-Candida albicans interactions: localization and fungal toxicity of a phenazine derivative. Appl Environ Microbiol 75: 504–513.

25. Cugini C, Morales DK, Hogan DA (2010) Candida albicans-produced farnesol stimulates Pseudomonas quinolone signal production in LasR-defective Pseudomonas aeruginosa strains. Microbiology 156: 3096–3107.

26. O'Toole GA, Kolter R (1998) Flagellar and twitching motility are necessary for Pseudomonas aeruginosa biofilm development. Mol Microbiol 30: 295–304.

27. Mern DS, Ha SW, Khodaverdi V, Gliese N, Gorisch H (2010) A complex regulatory network controls aerobic ethanol oxidation in Pseudomonas aeruginosa: indication of four levels of sensor kinases and response regulators. Microbiology 156: 1505–1516.

28. Kretzschmar U, Schobert M, Gorisch H (2001) The Pseudomonas aeruginosa acsA gene, encoding an acetyl-CoA synthetase, is essential for growth on ethanol. Microbiology 147: 2671–2677.

29. Liberati NT, Urbach JM, Miyata S, Lee DG, Drenkard E, et al. (2006) An ordered, nonredundant library of Pseudomonas aeruginosa strain PA14 transposon insertion mutants. Proc Natl Acad Sci 103: 2833–2838.

30. Tamayo R, Pratt JT, Camilli A (2007) Roles of cyclic diguanylate in the regulation of bacterial pathogenesis. Annu Rev Microbiol 61: 131–148.

31. Ha DG, Richman ME, O'Toole GA (2014) Deletion mutant library for investigation of functional outputs of cyclic diguanylate metabolism in Pseudomonas aeruginosa PA14. Appl Environ Microbiol 80: 3384–3393.

32. D'Argenio DA, Calfee MW, Rainey PB, Pesci EC (2002) Autolysis and autoaggregation in Pseudomonas aeruginosa colony morphology mutants. J Bacteriol 184: 6481–6489.

33. Friedman L, Kolter R (2004) Genes involved in matrix formation in Pseudomonas aeruginosa PA14 biofilms. Mol Microbiol 51: 675–690.

34. Huangyutitham V, Guvener ZT, Harwood CS (2013) Subcellular clustering of the phosphorylated WspR response regulator protein stimulates its diguanylate cyclase activity. MBio 4: e00242-00213.

35. Anderson GG, Moreau-Marquis S, Stanton BA, O'Toole GA (2008) In vitro analysis of tobramycin-treated Pseudomonas aeruginosa biofilms on cystic fibrosis-derived airway epithelial cells. Infect Immun 76: 1423–1433.

36. Moreau-Marquis S, Bomberger JM, Anderson GG, Swiatecka-Urban A, Ye S, et al. (2008) The DeltaF508-CFTR mutation results in increased biofilm formation by Pseudomonas aeruginosa by increasing iron availability. Am J -Physiol Lung Cell Mol Physiol 295: L25–37.

37. Elamin E, Jonkers D, Juuti-Uusitalo K, van Ijzendoorn S, Troost F, et al. (2012) Effects of ethanol and acetaldehyde on tight junction integrity: in vitro study in a three dimensional intestinal epithelial cell culture model. PLoS One 7: e35008.

38. Ma TY, Nguyen D, Bui V, Nguyen H, Hoa N (1999) Ethanol modulation of intestinal epithelial tight junction barrier. Am J Physiol 276: G965–974.

39. Mukherjee PK, Mohamed S, Chandra J, Kuhn D, Liu S, et al. (2006) Alcohol dehydrogenase restricts the ability of the pathogen Candida albicans to form a biofilm on catheter surfaces through an ethanol-based mechanism. Infect Immun 74: 3804–3816.

40. Kanner D, Gerber NN, Bartha R (1978) Pattern of phenazine pigment production by a strain of Pseudomonas aeruginosa. J Bacteriol 134: 690–692.

41. Recinos DA, Sekedat MD, Hernandez A, Cohen TS, Sakhtah H, et al. (2012) Redundant phenazine operons in Pseudomonas aeruginosa exhibit environment-dependent expression and differential roles in pathogenicity. Proc Natl Acad Sci U S A 109: 19420–19425.

42. Dietrich LE, Price-Whelan A, Petersen A, Whiteley M, Newman DK (2006) The phenazine pyocyanin is a terminal signalling factor in the quorum sensing network of Pseudomonas aeruginosa. Mol Microbiol 61: 1308–1321.

43. Wuichet K, Alexander RP, Zhulin IB (2007) Comparative genomic and protein sequence analyses of a complex system controlling bacterial chemotaxis. Methods Enzymol 422: 1–31.

44. O'Connor JR, Kuwada NJ, Huangyutitham V, Wiggins PA, Harwood CS (2012) Surface sensing and lateral subcellular localization of WspA, the receptor in a chemosensory-like system leading to c-di-GMP production. Mol Microbiol 86: 720–729.

45. Ingram LO, Buttke TM (1984) Effects of alcohols on microorganisms. Adv Microb Physiol 25: 253–300.

46. Azoulay E, Timsit JF, Tafflet M, de Lassence A, Darmon M, et al. (2006) Candida colonization of the respiratory tract and subsequent pseudomonas ventilator-associated pneumonia. Chest 129: 110–117.

47. Himmelreich U, Allen C, Dowd S, Malik R, Shehan BP, et al. (2003) Identification of metabolites of importance in the pathogenesis of pulmonary cryptococcoma using nuclear magnetic resonance spectroscopy. Microbes Infect 5: 285–290.

48. Grahl N, Puttikamonkul S, Macdonald JM, Gamcsik MP, Ngo LY, et al. (2011) In vivo hypoxia and a fungal alcohol dehydrogenase influence the pathogenesis of invasive pulmonary aspergillosis. PLoS Pathog 7: e1002145.

49. Montuschi P, Paris D, Melck D, Lucidi V, Ciabattoni G, et al. (2012) NMR spectroscopy metabolomic profiling of exhaled breath condensate in patients with stable and unstable cystic fibrosis. Thorax 67: 222–228.

50. Jackson AA, Gross MJ, Daniels EF, Hampton TH, Hammond JH, et al. (2013) Anr and its activation by PlcH activity in Pseudomonas aeruginosa host colonization and virulence. J Bacteriol 195: 3093–3104.

51. Wargo MJ, Gross MJ, Rajamani S, Allard JL, Lundblad LK, et al. (2011) Hemolytic phospholipase C inhibition protects lung function during Pseudomonas aeruginosa infection. Am J Respir Crit Care Med 184: 345–354.

52. DeVault JD, Kimbara K, Chakrabarty AM (1990) Pulmonary dehydration and infection in cystic fibrosis: evidence that ethanol activates alginate gene expression and induction of mucoidy in Pseudomonas aeruginosa. Mol Microbiol 4: 737–745.

53. Deretic V, Govan JR, Konyecsni WM, Martin DW (1990) Mucoid Pseudomonas aeruginosa in cystic fibrosis: mutations in the muc loci affect transcription of the algR and algD genes in response to environmental stimuli. Mol Microbiol 4: 189–196.

54. Boucher JC, Yu H, Mudd MH, Deretic V (1997) Mucoid Pseudomonas aeruginosa in cystic fibrosis: characterization of muc mutations in clinical isolates and analysis of clearance in a mouse model of respiratory infection. Infect Immun 65: 3838–3846.

55. Korem M, Gov Y, Rosenberg M (2010) Global gene expression in Staphylococcus aureus following exposure to alcohol. Microb Pathog 48: 74–84.

56. Nwugo CC, Arivett BA, Zimbler DL, Gaddy JA, Richards AM, et al. (2012) Effect of ethanol on differential protein production and expression of potential virulence functions in the opportunistic pathogen Acinetobacter baumannii. PLoS One 7: e51936.

57. Camarena L, Bruno V, Euskirchen G, Poggio S, Snyder M (2010) Molecular mechanisms of ethanol-induced pathogenesis revealed by RNA-sequencing. PLoS Pathog 6: e1000834.

58. Smith MG, Des Etages SG, Snyder M (2004) Microbial synergy via an ethanol-triggered pathway. Mol Cell Biol 24: 3874–3884.

59. Smith MG, Gianoulis TA, Pukatzki S, Mekalanos JJ, Ornston LN, et al. (2007) New insights into Acinetobacter baumannii pathogenesis revealed by highdensity pyrosequencing and transposon mutagenesis. Genes Dev 21: 601–614.

60. Goral J, Karavitis J, Kovacs EJ (2008) Exposure-dependent effects of ethanol on the innate immune system. Alcohol 42: 237–247.

61. Szabo G, Mandrekar P (2009) A recent perspective on alcohol, immunity, and host defense. Alcohol Clin Exp Res 33: 220–232.

62. Karavitis J, Kovacs EJ (2011) Macrophage phagocytosis: effects of environmental pollutants, alcohol, cigarette smoke, and other external factors. J Leukoc Biol 90: 1065–1078.

63. Happel KI, Nelson S (2005) Alcohol, immunosuppression, and the lung. Proc Am Thorac Soc 2: 428–432.

64. Guidot DM, Hart CM (2005) Alcohol abuse and acute lung injury: epidemiology and pathophysiology of a recently recognized association. J Investig Med 53: 235–245.

65. Greenberg SS, Zhao X, Hua L, Wang JF, Nelson S, et al. (1999) Ethanol inhibits lung clearance of Pseudomonas aeruginosa by a neutrophil and nitric oxide-dependent mechanism, in vivo. Alcohol Clin Exp Res 23: 735–744.

66. Chin AWTF, Bloemberg GV, Mulders IH, Dekkers LC, Lugtenberg BJ (2000) Root colonization by phenazine-1-carboxamide-producing bacterium Pseudomonas chlororaphis PCL1391 is essential for biocontrol of tomato foot and rootrot. Mol Plant Microbe Interact 13: 1340–1345.

67. Bolwerk A, Lagopodi AL, Wijfjes AH, Lamers GE, Chin AWTF, et al. (2003) Interactions in the tomato rhizosphere of two Pseudomonas biocontrol strains with the phytopathogenic fungus Fusarium oxysporum f. sp. radicis-lycopersici. Mol Plant Microbe Interact 16: 983–993.

68. Bertani G (1951) Studies on lysogenesis. I. The mode of phage liberation by lysogenic Escherichia coli. J Bacteriol 62: 293–300.

69. Neidhardt FC, Bloch PL, Smith DF (1974) Culture medium for enterobacteria. J Bacteriol 119: 736–747.

70. Cozens AL, Yezzi MJ, Chin L, Simon EM, Finkbeiner WE, et al. (1992) Characterization of immortal cystic fibrosis tracheobronchial gland epithelial cells. Proc Natl Acad Sci U S A 89: 5171–5175.

71. Kohler T, Curty LK, Barja F, van Delden C, Pechere JC (2000) Swarming of Pseudomonas aeruginosa is dependent on cell-to-cell signaling and requires flagella and pili. J Bacteriol 182: 5990–5996.

72. Abramoff MD, Magelhaes P.J., Ram S.J (2004) Image Processing with ImageJ. Biophotonics International 11: 36–42.